Structure and Mechanical Properties of Elastomeric Block Copolymers

A DISSERTATION
SUBMITTED TO THE FACULTY OF THE GRADUATE SCHOOL
OF THE UNIVERSITY OF MINNESOTA
BY

Carlos Guillermo Alfonzo

IN PARTIAL FULFILLMENT OF THE REQUIREMENTS
FOR THE DEGREE OF
DOCTOR OF PHILOSOPHY

Frank S. Bates, Advisor

December 2010

Acknowledgments

First and foremost, I would like to thank my advisor, Prof. Frank Bates, for his support from the very first day I asked about his research to these last intensive days of writing. I am very grateful for the opportunity to work with him and for his guidance throughout these years. I would also like to express my most sincere gratitude to Dr. Kim Chaffin, who has also been a great mentor to me, as well as Medtronic at large for the financial support.

I am deeply grateful to several people in the Bates and other polymer groups. I'd like to especially acknowledge Dr. Feng Zuo and Dr. Guillaume Fleury, who have worked along me and made major contributions to this work. Similarly, Jihua Chen was a great friend and mentor in my first few years in the group. I want to recognise Sangwoo Lee, Mike Bluemle, Zach Thompson, Marc Rodwogin, Brad Jones, Louis Pitet and David Giles for their generous efforts in training me in experimental techniques. Many thanks to Ameara Mansour, Erica Redline and Dawud Tan for organizing group-wide initiatives and for helpful research discussions. I am appreciative to Soohyung Choi and Rajiv Taribagil for their advice and for being superb roommates both at Argonne and APS. Finally, thanks to Whitney Kruse, Carmelo Declet-Perez, Jingwen Zhang, Luca Martinetti, Intaek Lee, Brian Habersberger and Sangwon Kim for the great camaraderie.

I'd also like to thank my friends and family, who have been incredibly supportive. Special thanks to my roommates during graduate school, who were so generous and understanding, Vivek Kalihari, Ramiro Nandes and especially Alana Hedlund, whose support in the past year truly helped me to complete this work. I also thank the many friends from Macalester College, the University of Minnesota and Engineers Without Borders I have met over the past 9 years who have made many cold MN winters just amazing. Finally, while my family has not been living near me for a long time, Mama, Papa, Andres, Lauri, Maria Noel, Clara have always been my biggest supporters and source of inspiration.

Dedicated to my parents,

Carlos Alfonzo and Stella Duarte

Abstract

This research presents the synthesis (by anionic polymerization and catalytic hydrogenation) and characterization of two types of block copolymers: CMC and XPX. In CMC, C is glassy poly(cyclohexylethylene) and M, the matrix, can be semicrystalline poly(ethylene) E, rubbery poly(ethylene-alt-propylene) P, or rubbery poly(ethylethylene) E_E, or a combination to yield: CPC, CE_EC, CEC, CPE_EC and CEPC, with $f_C \approx 0.18 - 0.30$. XPX materials have X = CEC, $f_C \approx f_E$, and $f_P \approx 0.40 - 0.60$. Block copolymer phase behavior and morphology were examined through a combination of DSC, rheology, SAXS, WAXS and TEM. CMC materials are melt-ordered due to block thermodynamic incompatibility with $T_{ODT} > T_g$ (C) ≈ 147 °C and show lamellar or C cylinder morphologies. The design of XPX yields melt disordered materials up to high M_n with microphase segregation induced by E crystallization. Two high M_n XPX polymers are melt ordered above T_m(E) and show two correlation lengths in SAXS assigned to the C – E and X – P length scales. TEM images indicate that all XPX materials, irrespective of melt segregation, are characterized by composite glassy and crystalline hard domains dispersed in rubbery P at room temperature.

Tensile and recovery testing at room temperature show that CMC and XPX materials, with the exception of plastic CEC, behave as thermoplastic elastomers with tunable properties. Interestingly, melt disordered XPX materials have competitive mechanical properties comparable to the strongest CMC polymers, but with advantageous processing. For melt ordered CMC, $T_{process} > T_{ODT}$, which is dependent

on M_n, while for melt disordered XPX, $T_{process} > T_m(E) \approx 100$ °C independent of M_n. The deformation of melt disordered XPX materials, probed by recovery studies and WAXS, suggests that deformation is first taken by P, then E and finally C, which causes ultimate failure, as agreed in the literature for conventional SBS and SIS thermoplastic elastomers. This implies that strain recovery in XPX materials can be comparable to that of CPC if materials contain low hard block content or are stretched to strains below the onset of E deformation.

Finally, a collection of data of mechanical properties, namely modulus *E*, strain at break ε_b, tensile strength σ_{TS} and tension set ε_s, obtained from CMC, XPX and previously reported materials were examined. Most notably, *E* and ε_s were found to be strongly correlated with the volume fractions of C and E, as properties increase with $(f_C + f_E)^{\delta}$, where $\delta = 1 – 2.4$. Ultimate properties such as σ_{TS} and ε_s are unaffected by changes in composition as failure is dictated by that of the hard domains and values are similar above a minimum amount of hard block. In addition, *E*, σ_{TS}, and ε_b are inversely correlated to rubber entanglement molecular weight M_e, which implies that modulus and ultimate properties are affected by the ability of the rubber network to redistribute stress by entanglement slippage. However, ε_s is unresponsive to M_e variations, which indicates that irrecoverable deformation in these materials results from deformation of the hard domains.

Table of Contents

List of Tables

List of Figures

1

Introductory Remarks

In this work, novel block copolymers were synthesized and characterized to find connections between the realm of phase behavior and structure with that of mechanical response as thermoplastic elastomers. After an introduction in Section 1.1, an overview of the fundamentals of block copolymer phase behavior is presented in Section 1.2, with an emphasis on the resulting structures. Section 1.3 reviews the mechanical properties of homopolymers, block copolymer thermoplastic elastomers and of comparable block copolymers. Finally, a synopsis of this manuscript is presented in Section 1.4.

1.1 Introduction

The development of polymer science in the last few decades has produced an array of polymer structures, which has in turn revolutionized the selection of materials for mechanical applications. Traditional materials (metals, ceramics, natural fibers) have been replaced by or combined with polymers, many times resulting in novel properties, for example as with carbon-reinforced plastics. This project deals with understanding the mechanical properties that arise from the combination of different polymers in order to produce innovative materials.

1.1.1 Block Copolymers and Mechanical Applications

Blending has been largely used to merge the mechanical properties of different polymers. However, this usually results in macroscopic separation, as most polymers are chemically incompatible. Block copolymers, which covalently connect two or more homopolymer subunits, will not undergo macroscopic segregation given the covalent bonds between blocks, and thus efficiently merge different polymers' mechanical behaviors. Block copolymers do experience segregation but on a molecular scale, which arises from the repulsive interaction forces between blocks of dissimilar chemical structures. This effect is countered by the entropic penalty of stretching the chains in this process of separation. The balance of these forces drives structural order into specific symmetries and periodicities, producing a variety of microstructures. For example, for a linear A-B diblock or A-B-A triblock, four morphologies have been observed to be thermodynamically stable: body-centered spheres, hexagonally packed cylinders, gyroid, and lamellae. According to Flory-Huggins theory, for these types of block copolymers, the enthalpic penalty can be described by a parameter χ_{AB}, which is inversely proportional to temperature. Thus, microphase separation, which is directly dependent on the degree of polymerization N, occurs at a certain value of χN, about 10.5 for AB symmetric diblocks. As a result, at constant M_n and composition, block copolymers disorder into a homogenous melt at a T_{ODT} or order-disorder temperature.[1]

1.1.2 Hydrogenated Thermoplastic Elastomers

Thermoplastic elastomers, or TPE's, based on block copolymers will contain, in their simplest form, a glassy or semicrystalline block A and a majority rubbery

block B in an A-B-A architecture and sufficient M_n to produce microphase segregated domains. This design yields elastomeric materials similar to vulcanized rubbers but with advantageous processing, as the thermoplastic blocks acting as crosslinks are thermally reversible above T_{ODT}. Typical block copolymer TPEs (bcTPEs) composed of polystyrene (S), polybutadiene (B) and polyisoprene (I) in the form SBS and SIS have tremendous practical applications in a variety of markets such as textiles, adhesives, roofing, road products, footwear, etc.[2]

However, there are important practical limitations when working with SBS and SIS, which can be improved with hydrogenation. An inexpensive Pt/Re on SiO_2 heterogeneous catalyst was developed which allows the hydrogenation of these polymers to produce four new molecules, as shown in Figure 1.1.[3-5]

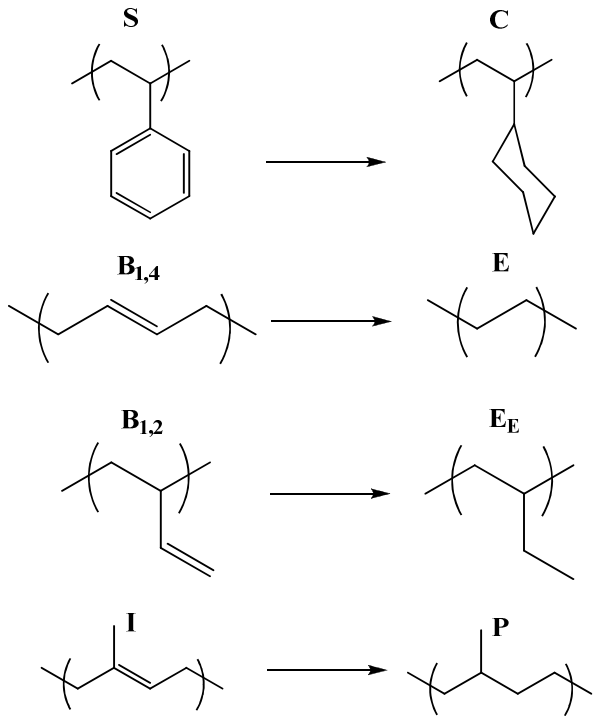

Figure 1.1: Homopolymers before (left) and after (right) hydrogenation.

Hydrogenation of glassy S, and of rubbery $B_{1,4}$, $B_{1,2}$ and $I_{1,4}$ yield glassy poly(cyclohexylethylene) (C), semicrystalline poly(ethylene) (E), rubbery poly(ethylethylene) (E_E) and rubbery poly(ethylene-alt-propylene) (P), respectively. Thus, hydrogenation of S, B and I can lead to three mechanically different polymers as opposed to two, given the introduction of the semicrystalline polymer E from $B_{1,4}$. Also, it yields homopolymers and block copolymers with enhanced oxidative and UC stability given the absence of double-bonds[6] as well as a higher upper service temperature as T_g(C) ≈ 147 °C while T_g(S) ≈ 100 °C.[7] Table 1.1 presents thermal transitions and density data for these homopolymers before and after saturation.

Table 1.1: Homopolymer physical properties

Homo-polymer	T_m [a] (°C)	T_g [a] (°C)	ρ [b] (g/cm^3)
S	-	100	0.969
$B_{1,2}$	-	-19	0.889
$B_{1,4}$	-	-97	0.826
I	-	-56	0.830
C	-	147	0.920
E	110	-80	0.784
E_E	-	-37	0.807
P	-	-60	0.790

[a] Thermal transitions.[7] [b] Densities at 140 °C ($B_{1,2}$ at 25 °C).[8]

In this project, block copolymers with glassy C endblocks, a combination of C, E, E_E and P as the matrix and different molecular characteristics have been synthesized through living anionic polymerization to yield CPC, CE_EC, CEC, CPE_EC, CEPC and CEC-P-CEC (XPX). Characterization of these materials and comparison

with previously developed ones has advanced the knowledge on the phase behavior, structure and mechanical properties of block copolymer thermoplastic elastomers (bcTPEs) which combine glassy, semicrystalline and elastomeric blocks.

1.2 Block Copolymer Phase Behavior

This section reviews the prevalent theories on block copolymer phase behavior, which dominates structure formation in block copolymers and thus affects their mechanical response. As mentioned in the introduction, block copolymers consist of different polymers chemically linked together, and while these cannot macroscopically phase separate, they can undergo microphase segregation. The balance of the enthalpic penalty of mixing repulsive structures and the entropic one from stretching the chains drives the organization of polymer domains into morphologies. An approach to understand and model this phenomenon is by using the Flory-Huggins theory, a modified version of regular solution theory. Flory-Huggins gives an expression for the free energy of mixing, ΔG_m, of polymer A and B, shown below, where k_B is the Boltzmann's constant, T is the absolute temperature, N is the number of repeat units, f is the volume fraction and χ_{AB} is the Flory-Huggins interaction parameter.[9]

$$\frac{\Delta G_m}{k_B T} = \frac{f_A}{N_A} \ln f_A + \frac{f_B}{N_B} \ln f_B + \chi_{AB} f_A f_B \qquad (1.1)$$

As χ_{AB} is a positive number for most hydrocarbon polymers, this expression gives a quantitative explanation as to why most polymer blends spontaneously phase separate macroscopically, which translates into microscopic phase separation for block copolymers. Moreover, it provides the three main parameters that affect

polymer phase behavior. For a specific block copolymer architecture, these are: the overall degree of polymerization *N*, the composition *f*, and the interaction parameter χ. Specifically, increasing the Flory Huggins parameter (χ) and/or the overall degree of polymerization (*N*) may cause microphase separation in block copolymers, while the opposite should lead the blocks to mix. Thus, for a given composition, the product χN effectively dictates the state of order in a block copolymer melt.[10] Finally, an inverse relationship between χ and temperature has been established and given by the formula below, where α and β are constants for a given composition.[11]

$$\chi \approx \alpha T^{-1} + \beta \qquad (1.2)$$

Because α is usually positive, an increase in temperature decreases χ and drives polymer blocks to mix and ultimately becoming disordered at a characteristic temperature defined as the order-disorder transition temperature or T_{ODT}. The degree of microphase separation in block copolymers is related to the concept of segregation limits. In the strong segregation limit (SSL), microdomains of nearly pure A and B are formed (equivalent to $\chi N >> 10$ *f*or a symmetric AB diblock). On the other end, in the weak segregation limit (WSL) ($\chi N \approx 10$), the composition profile of any one block follows a sinusoidal pattern moving across the domains. The intermediate segregation regime (ISR) lies in between these two.[11]

1.2.1 AB Diblock Copolymers

Theories of block copolymer phase behavior were constructed independently for the SSL and WSL and later unified to obtain the entire phase diagram. In essence, the theories are based on the idea of minimization of free energy, which is a function

of two competing contributions. One is the interfacial energy (related to χ) arising from the enthalpic repulsion between different polymers. The second contribution stems from the conformational entropic penalty derived from the perturbation of the Gaussian coils when chains are stretched to conform to a particular morphology.

Early theoretical models focused on the simplest architecture, that is symmetric diblock copolymers, extending the self-consistent mean field theory (SCMFT) developed earlier[12,13] in the SSL to predict domain spacing.[14] Later, in order to model the experimentally observed order-disorder transition, Leibler[15] combined the SCMFT with the random phase approximation (RPA) of de Gennes[16] in the WSL, and this work led to the theoretical phase diagram for diblock copolymers shown in Figure 1.2(a). The phase diagram is a plot of the segregation strength (χN) against the volume fraction (f) of one of the components. By including the effect of composition fluctuations (important because of finite chain lengths) Fredrickson and Helfand produced a phase diagram, shown in Figure 1.2(b), that allowed direct transitions from the disordered to lamellar and hexagonal phases, which agreed with experimental results but were not accounted by Leibler's result. [17,18]

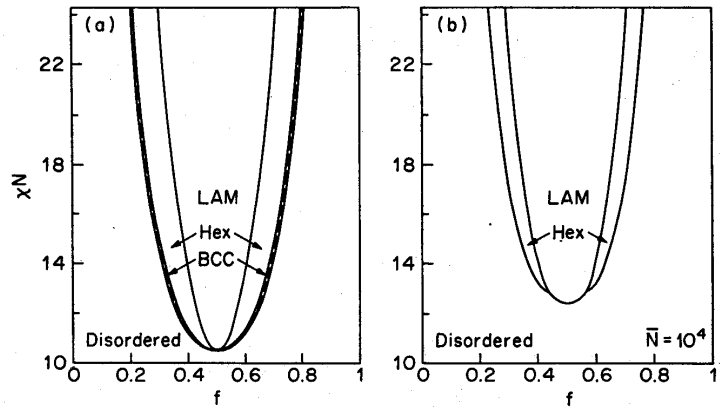

Figure 1.2: AB block copolymer phase diagrams in the WSL, based on (a) mean field and (b) fluctuation theories. Reproduced from Bates *et al.*[10]

These two phase diagrams do not include the experimentally observed bicontinuous morphology between lamellae and cylinders, which was first identified as the ordered bicontinuous double diamond[19,20] (OBDD, space group $Pn\bar{3}m$) but later shown to be the gyroid morphology, space group $Ia\bar{3}d$.[21,22] Matsen and Schick, by applying SCMFT to examine the stability of microphases of diblock copolymers in the WSL, found that the gyroid phase was stable, in addition to the classical lamellar, hexagonal and cubic phases.[23] Finally, Matsen and Bates extended this calculation to span all the segregation regimes to obtain a phase diagram that included all the phases observed in diblock copolymers.[24,25] The stable ordered structures included lamellae (L), hexagonally packed cylinders (H), BCC spheres (Q_{Im3m}), close packed spheres (CPS) and the gyroid (Q_{Ia3d}). Cohran *et al.*[26] produced a revised version of this phase diagram by proving the stability of the gryoid phase into the SSL, and this is shown in Figure 1.3(a).

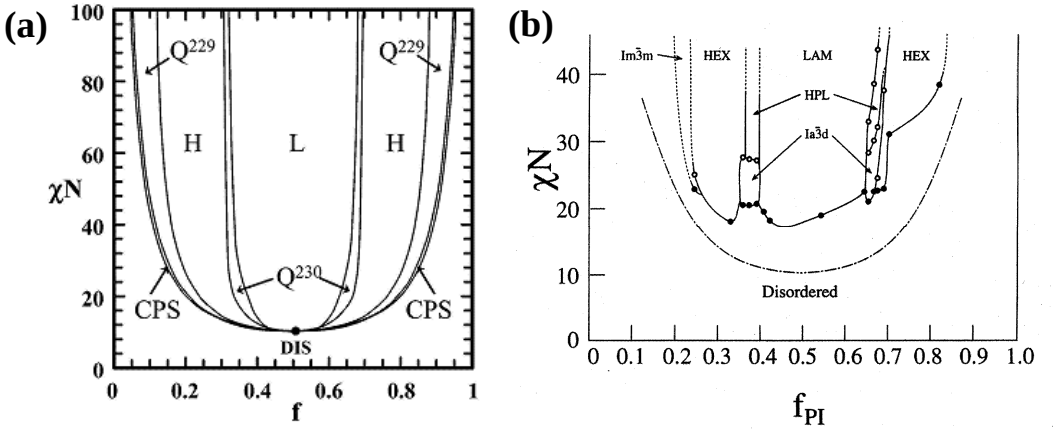

Figure 1.3: (a) Theoretical and (b) experimental phase diagrams for AB diblock copolymers. The dotted line in the experimental phase diagram represents theoretical results. Reproduced from Cochran *et al.*[26] and Khandpur *et al.*[27]

An experimental phase diagram for an S-I diblock copolymer melt was generated by Khandpur *et al.*[27] by experimentally determining ODT's and order-order transitions (OOTs) using rheology, TEM and scattering, shown in Figure 1.3(b). This diagram showed the success of the theoretical models in providing a generalized behavior, as both diagrams agree in terms of the phases observed and their relative locations along the volume fraction axis. The experimental phase diagram has hexagonally perforated layers (HPL) in narrow channels adjacent to the lamellar phase. This phase was predicted by theory to be metastable.

1.2.2 ABA Triblock Copolymers

In this work, three ABA-type triblock copolymers are presented: CPC, CE_EC, and CEC. If we think of a symmetric AB diblock as resulting from splitting a symmetric ABA triblock in half, the free energy of the two systems (diblock vs. triblock) in the SSL should not vary considerably. This is because the stretching of chains to reduce the AB interfacial area is minimized at the center of the B block, where the splitting would occur. After early theoretical results,[14,28,29] Matsen and Thompson[30] obtained the complete symmetric ABA phase diagram by applying SCMFT. The ABA and the homologous AB ($N_{AB} = 2N_{ABA}$) phase diagrams are shown in Figure 1.4.

Although the superposition of both diagrams clearly indicates that the phase behaviors are almost identical, there are some differences. Mainly, triblocks seem to remain ordered up to higher temperatures than diblocks, and this difference is greater

in the A abundant side of the diagram. This can be understood if one thinks that when triblocks are cut into two, it creates end segments out of the middle B segment. As a result, the B chains in diblock melts (half the size than in triblocks) are able to penetrate the A domains more easily, and thus disorder before triblocks. The above argument is more valid in the A-rich part of the phase diagram, which accounts for the observed skewing of the ABA phase diagram as opposed to the symmetric AB phase diagram.

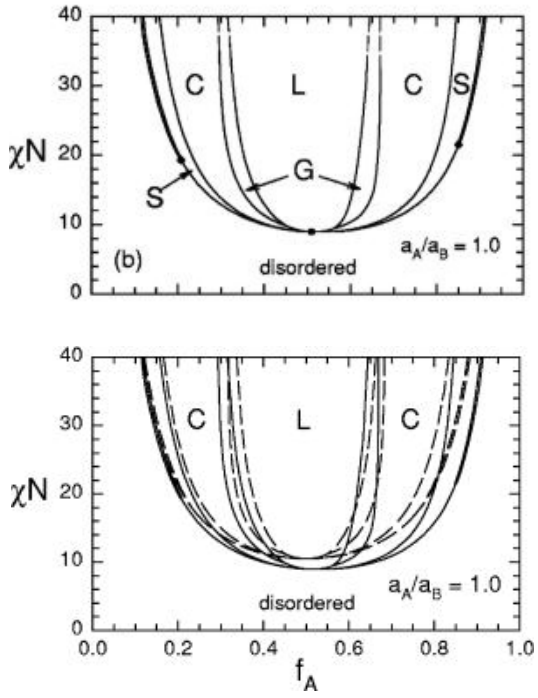

Figure 1.4: (Top) The ABA phase diagram (degree of polymerization 2N) and (bottom) the homologous AB phase diagram (degree of polymerization N) with the ABA one superposed as dotted lines. Figures reproduced from Matsen *et al*.[30]

Experimentally measured ODTs[31,32] and domain spacings[33,34] of matched diblock and triblock copolymers were found to be similar, confirming the predictions made by theory. Experiments also show the same classical phases (L, C and S) in

triblocks as shown in diblocks along with the gyroid (G) phase.[35,36] Figure 1.5 contains a schematic illustration of the shapes of these four phases.

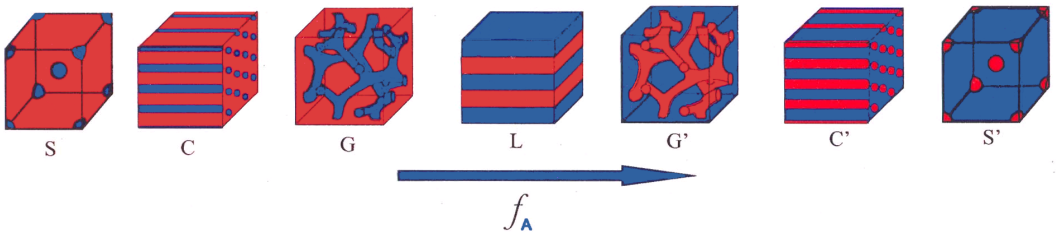

Figure 1.5: Schematic showing two-component (A & B) block copolymer morphologies as a function of volume fraction of component A, in blue. Reproduced from Bates *et al.*[1]

1.2.3 ABC Triblock Copolymers

In this project, three types of block terpolymers (with three different blocks) were produced, namely CEC-P-CEC, CEPC, and CE_EPC. While specific literature on these particular systems is not present, the study of the simplest ABC triblock copolymer provides important insights extendable to more complex architectures. For ABC triblock copolymers, three independent interaction parameters χ_{AB}, χ_{BC} and χ_{AC} as well as two independent volume fractions govern the thermodynamic behavior. As a result, block sequencing plays a key role and, for a given architecture, a much higher number of possible morphologies than for copolymers are expected. Consequently, theories which describe the phase behavior of simpler systems have proven inadequate. Therefore, the approach has been chiefly experimental, by looking at specific, simplified ABC systems obtained by placing certain restrictions on the volume fractions and/or interaction parameters. Some of the morphologies seen in ABC triblocks are shown in Figure 1.6.

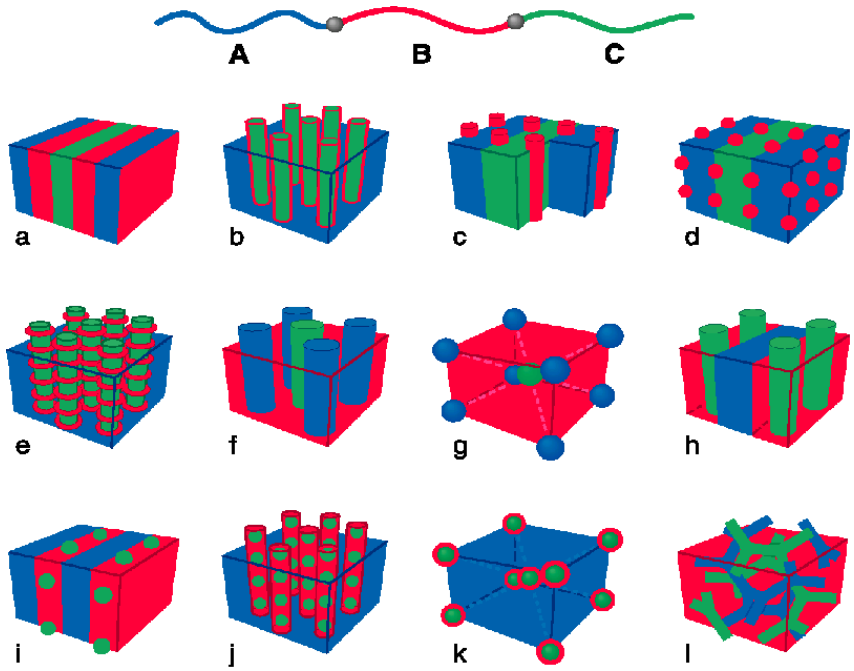

Figure 1.6: Some of the morphologies seen in ABC triblock copolymers. Reproduced from Bates *et al*.[1]

While these morphologies are hard to predict, they may be rationalized in terms of chain stretching, space filling and interfacial tension. A lamellar morphology is induced for triblocks when chain stretching is the dominant contribution to the free energy, which requires that blocks have similar compositions (i.e. $f_A \approx f_B \approx f_C$) and interaction parameters $\chi_{AB} \approx \chi_{BC} \approx \chi_{AC} > 0$ (Figure 1.6(a)). In this case, the repulsive interaction between two blocks will not be relieved by curving one interface, as this would cause an increase in the interfacial area between the other two blocks. However, if the interfacial tensions are not similar, then curvature may stabilize the system by reducing the interfacial area between the two most incompatible blocks. This would make cylindrical or spherical morphologies more stable, especially if the volume fractions are also dissimilar and the one or two minority blocks are incompatible with the matrix.

Core-shell structures have been observed when two adjacent blocks are strongly incompatible to minimize their interfacial contact, for instance between B and C when $\chi_{BC} > \chi_{AB}$. This example can lead to core-shell hexagonal cylindrical or spherical C cores (Figure 1.6 (b) and (k), respectively).[37] Other cylindrical and spherical structures may form, and can be classified dependent on whether the middle or the end block are the matrix. For instance, when B (middle block) forms the matrix, and $\chi_{AB} \approx \chi_{BC} < \chi_{AC}$ (AC interface is avoided), cylinders of A and C are pack in a tetragonal pattern (Figure 1.6 (f)).[38-41] For an endblock (C) matrix, there exist numerous configurations depending on f_A/f_B and χ parameters. For instance, when $f_B < f_A \approx f_C$ and $\chi_{AB} \approx \chi_{BC} > \chi_{AC}$ (A and C are compatible but incompatible with minority B), B cylinders or spheres will pack between A and C lamellae (Figure 1.6 (c) and (d), respectively) or hexagonally packed C cylinders will be encompassed by B rings in a matrix of A (Figure 1.6 (j)).[42-44] The gyroid phase has also been identified in two patterns, the pentacontinuous $Ia\bar{3}d$ core-shell structure (Figure 1.6 (l))[38-41] and the tricontinuous $I4_132$ structure.[45,46]

1.2.4 Crystallization Induced Microphase Segregation

Thus far, we have referred to block copolymer microphase separation as resulting from the chemical incompatibilities of the constituent blocks at a specific T_{ODT}, directly dependent on M_n. However, microphase segregation in disordered block copolymers can also be induced by crystallization. In this case, the transition from order to disorder would be dictated by the crystal melting point, T_m, which is independent of M_n, and thus provides a processing advantage. Different studies have

shown this effect or reported on the interplay between thermodynamic versus crystallization driven microphase segregation.[47-54] In some cases, when $T_{ODT} > T_c$, the melt-ordered structure can be disrupted by crystallization.[50] On the other hand, when $T_c > T_{ODT}$, the formation of crystal structure dictates the overall morphology. For example, Koo et al. developed $(EP)_n$ copolymers which, given a small χ_{EP}, were structured into a lamellar morphology as a result of E crystallization for M_n (EP) < 100 kg/mol.[51, 52]

1.3 Mechanical Properties of Polymeric Materials

This project presents block copolymers based on glassy C, semicrystalline E and rubbery E_E and P polymers to produce innovative bcTPEs and study their mechanical properties. This section reviews the mechanical response of these blocks as homopolymers, of other bcTPEs and of similar block copolymer materials. The reader is referred to Chapter 3 for the technical aspects of the experiments conducted, namely tensile and cyclic testing, and the procedures to measure the mechanical properties invoked in this work.

1.3.1 Homopolymers

Homopolymers usually show three distinct types of mechanical behavior at room temperature (besides viscoelastic): brittle, plastic and elastomeric, as shown in Figure 1.7. Brittle materials, such as glassy S or C homopolymers, are stiff and strong, that is they exhibit high modulus and tensile strength, respectively, but small elongations and toughness. Brittle failure in glassy polymers occurs through the formation and propagation of cracks. Crack propagation in highly entangled polymers

can take place in a particular mode called crazing. Briefly, crazes are local voids in the bulk material strung together by thin, lead-bearing extended polymer chains called fibrils. The fibrils are typically 10-20 nm thick and a typical craze is on the order of 100 nm in diameter.[55] Thus, crazing may accompany brittle failure as well as some plastic deformation.

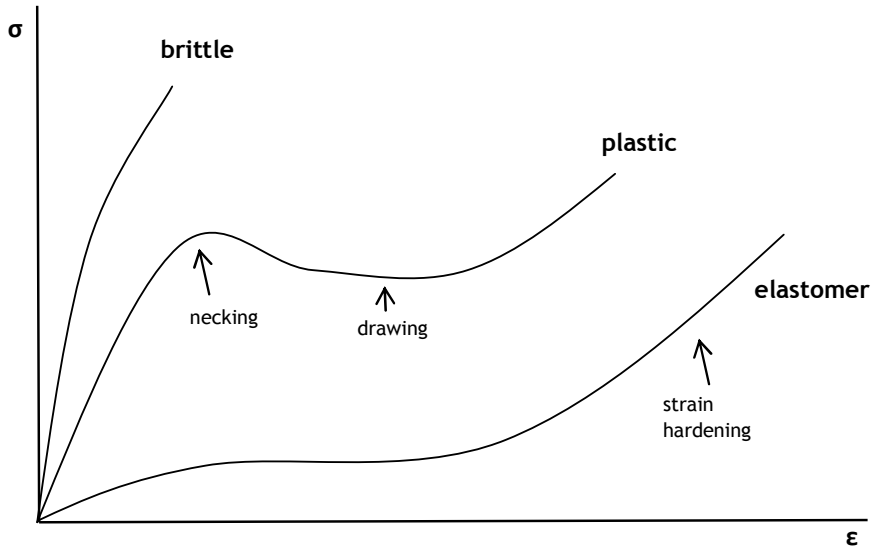

Figure 1.7: Schematic of mechanical response of brittle, plastic and elastomeric homopolymers. Three distinct behaviors are shown.

A plastic material, such as semicrystalline E, usually yields and deforms to a high strain and stress at failure. In the example shown in Figure 1.7, the plastic stress-strain curve exhibits a sharp yield point, followed by *necking* (narrowing of sample cross section and load drop on curve) and *drawing* (plastic deformation at a constant stress) and some *strain hardening* (the steep increase in stress at the end) leading to failure. On the molecular level, E shows lamellar crystals separated by a layer of amorphous polymer and held together by tie molecules through the

amorphous phase.[56] Since the amorphous regions are above the glass transition temperature, they have the smallest modulus and will deform first. The crystalline structure may then deform, often through crystallographic slip, when a critical shear stress in the direction of slip is attained.[57] Parallel slip planes may group together to form slip bands, which can be seen with an optical microscope. Crystal deformation in these materials will be accompanied with high permanent deformation.

Elastomeric materials, such as crosslinked B or I, as shown in Figure 1.7 as elastomer, show high extension, low modulus, diffuse yielding and pronounced strain hardening. Most importantly, their response is chiefly elastic, that is with high recoverability or little permanent deformation after unloading or failure. This hyper-elasticity derives from the change in entropy of the cross-linked flexible polymer molecules as opposed to the non-recoverable enthalpic change due to bond distortions through crazing or shear bands. The increased order achieved when the polymer chains are stretched guarantees their retraction to regain the initial high entropy unaligned state.

1.3.2 Block Copolymer Thermoplastic Elastomers

Block copolymers of glassy, semicrystalline and rubbery polymers can lead to the generation of bcTPEs, or tough and elastomeric materials. However, this is just one possible response. Block copolymers can show a wide spectrum of mechanical properties depending on their molecular characteristics. The literature points to certain important features of bcTPEs in terms of architecture, composition, molecular weight and morphology.

Chain architecture in bcTPEs usually involves having thermoplastic polymers as endblocks and rubbery blocks in the middle. This results in rubber molecules tied down on both ends by hard domains, which prevent rubber unraveling and act as effective crosslinks. As a result, SI and SB diblocks and ISI and BSB triblocks exhibit inferior ultimate mechanical properties (lower tensile strength and elongation) than SIS and SBS triblocks, respectively.[58,59]

Overall and block molecular weight have been shown to affect mechanical behavior of thermoplastic elastomers. Weakly segregated SBS and SIS materials of low overall M_n fail prematurely and for SBS, the load-bearing capacity of block copolymers at large strain appears to be enhanced with M_n at constant composition.[60-62] This stems from the fact that segregation of the thermoplastic domains is essential to create the crosslinked network. Furthermore, the molecular weight of the constituent blocks will control their degree of entanglement. This is important because, for example, for the case of S with a molecular weight smaller than its entanglement molecular weight, $M_e \approx 13{,}300$ g/mol at 413 K, pull out may occur at high strains, especially if the behavior of PS is viscoelastic.[63] Similarly, the molecular weight between rubber entanglements M_e has been shown to have an important effect on mechanical properties. This is because as rubber molecules are tethered on both ends, their entanglements cannot slip past each other and act as effective cross links. Thus, molecular weight between crosslinks $M_c \approx M_e$ in the Mooney-Rivlin equation, which implies that M_e will have a major impact on the low strain behavior of bcTPEs.[60] In addition, at high strains, higher M_e rubbers have been shown to produce materials with lower tensile strengths and higher elongations.[64]

As for composition, the relative amounts of thermoplastic versus rubbery material have a major effect on the overall mechanical properties. In a glassy-rubbery-glassy system, composition changes affect the mechanical behavior substantially, as illustrated in Figure 1.8 for an SBS triblock reported by Holden *et al.*[60] and reproduced here from Grady and Cooper.[65] Above 50% glass, the material's toughness and elongation is compromised and at high glass content it becomes brittle. If a rubbery matrix is maintained, the tough and elastic behavior dominates. Quirk and Morton obtained similar results for a semicrystalline thermoplastic block, such as for EBE triblocks, except for in this case the response at high E content is plastic as opposed to brittle.[61]

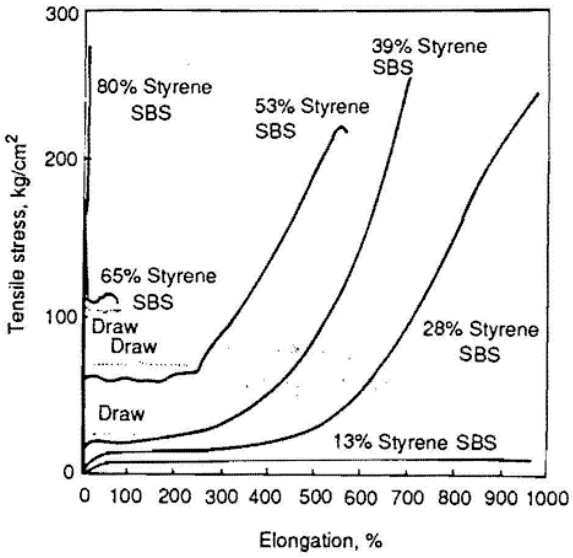

Figure 1.8: Typical stress-strain curves for SBS triblocks with varying S content. Reproduced from Grady and Cooper.[65]

Block copolymer morphology can also impact mechanical properties, especially at low strains. These effects can be explained by visualizing the morphology's space filling lattice. For a two component block copolymer, the gyroid

morphology gives both components continuity in all three directions while lamellar in two. The cylindrical morphology's matrix has continuity in all three directions while the cylinder domains only in one. Finally, spheres have a continuous matrix with discontinuous spherical domains. Qiao *et al.* isolated the effect of morphology on mechanical properties by studying SIS thin films of different morphologies but identical composition.[66] This was achieved by casting them with solvents of varying selectivity, which results in different "effective" volume fractions. It was found that morphology with higher continuity of the glassy domains (gyroid, then lamellar and finally glass cylinders) exhibit higher modulus and yield stress.

1.3.3 Glassy and Rubbery Block Copolymers

Much research has been conducted to understand the behavior of thermoplastic elastomers composed of glassy domains in a rubbery matrix, especially SBS and SIS. Holden et al. provide a general review on the mechanical properties of this type of materials.[60] Isotropic samples with different morphologies and compositions exhibit unique behaviors. Dair *et al.*[67] compared the tensile deformation of SIS with rubber majority in the double-gyroid (DG), lamellar (LAM), cylindrical (CYL) and spherical (SPH) morphologies, as shown in Figure 1.9. Samples with cylinders and spheres exhibit elastic behavior, with diffuse yielding and no necking. Lamellar and DG samples show a sharp yield point, but the DG sample is the only sample to exhibit necking and drawing. It was suggested that necking results from glass break-up in the stretching direction, as the DG's three-dimensional connectivity makes it the only one with glass continuity in an isotropic specimen.

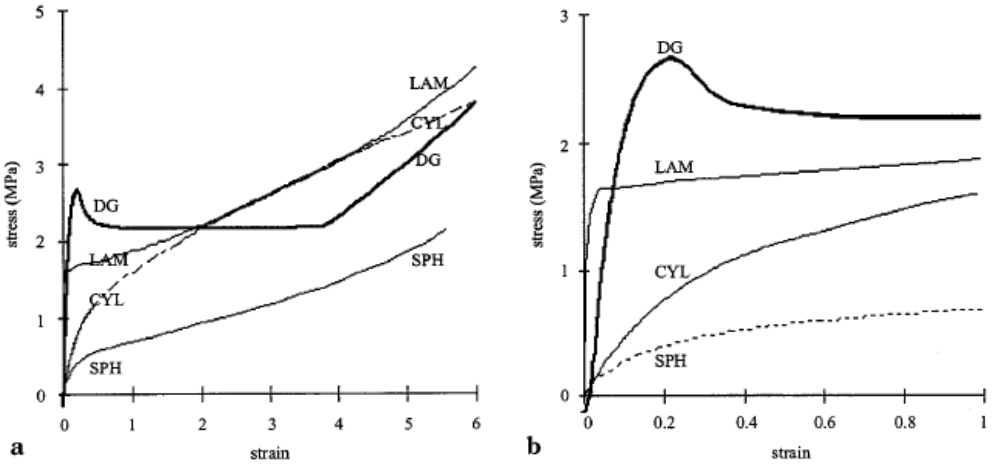

Figure 1.9: Stress-strain curves for SIS block copolymers with different morphologies up to (a) 600% strain (b) 100% strain. Reproduced from Dair *et al*.[67]

Deformation studies on thermoplastic elastomers with aligned lamellar morphologies support this argument. Stretching parallel to lamellar layers is expected to find much higher glass continuity than stretching perpendicularly to them. As shown in Figure 1.10, at small strains, stretching parallel to aligned lamellar SBS samples show sharp yielding and necking while perpendicular stretching exhibits diffusive yielding and absence of necking.[68] On the molecular level, parallel samples show glass crazing and subsequent plastic deformation, as the microfibrils stretch and draw glassy material into the crazes.[59,69] On the other hand, perpendicular samples were shown through TEM to plastically deform with lamellar shear banding into a zigzag structure. Kawai *et al.* also reported shear banding and plastic flow in isotropic SIS lamellae, postulating that it was induced by hydrostatic pressure due to the large difference in the Poisson's ratios of glass and rubber.[59] In the large strain limit, several studies suggest that lamellar bcTPEs' glassy domains in both the parallel and perpendicular orientations break up at high deformations by "kinking" or buckling to

eventually become homogenously dispersed particles.[59, 63,70,71] A deformation study on SBS by Fujimara *et al.* shows that glass break-up forms a chevron morphology at smaller deformations identified by SAXS as a four point pattern.[70] At higher deformations, a chaotic morphology of broken S domains is observed, identified by SAXS as diffuse scattering.

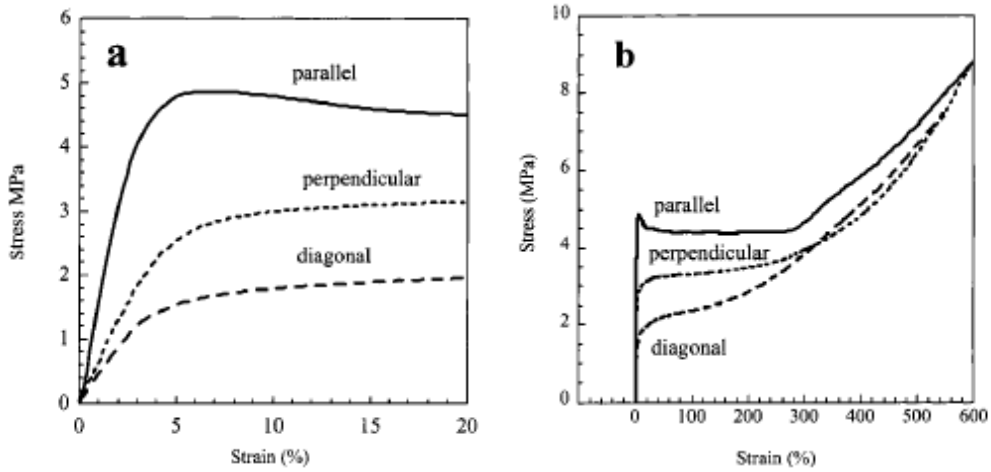

Figure 1.10: Stress-strain curves of SBS oriented lamellar samples with the lamellar normal oriented at three directions relative to the deformation axis: 90 degree (parallel), 0 degree (perpendicular) and 45 degree (diagonal). (a) low strain region (b) high strain to break. Reproduced from Cohen *et al.* [68]

SBS copolymers with oriented S cylinders have also been the subject of multiple studies. Odell and Keller showed that the deformation of an aligned cylindrical SBS sample (85 kg/mol and $w_S \approx 0.28$; w = weight fraction) was affine to a higher strain when stretching is perpendicular to the cylinder axes ($\leq$ 20%) versus parallel ($\leq$ 3%), at which point the material yielded, as shown in Figure 1.11.[72] Analogously to lamellar, a higher degree of glass continuity with parallel stretching leads to the observed sharper yield point and necking. This study also reported a high anisotropy in the elastic modulus, with a ratio of parallel to perpendicular of about

100, compared to the reported 3 for SBS lamellar[70] and 5 for SIS gyroid[63] (<111> direction versus its transverse).

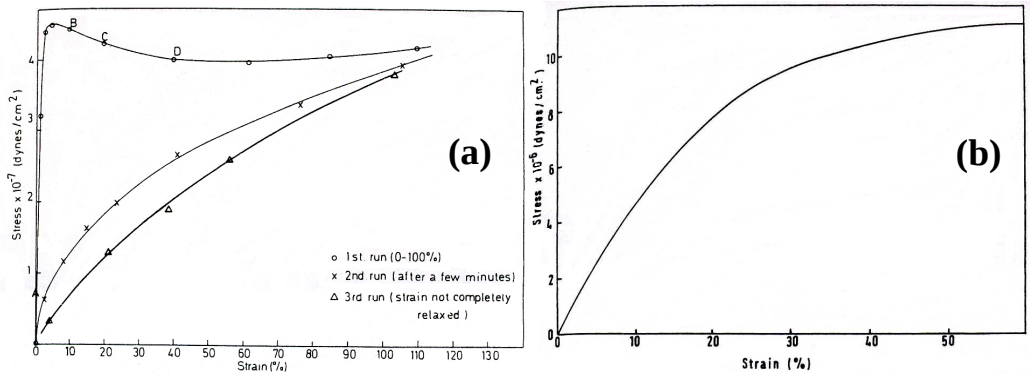

Figure 1.11: SBS stress-strain curves with strain applied (a) parallel to S cylinder direction and (b) perpendicular. Reproduced from Odell and Keller.[72]

Studies on large strain deformation of oriented cylinders demonstrate that while upon parallel stretching the broken glass rods stay aligned, perpendicular deformation breaks and aligns cylinders in the chevron structure, as shown in Figure 1.12.[73,74] Pakula *et al.* went on to show that in fact, at high enough deformations, deforming oriented cylinders in any direction results in the chevron structure.[75]

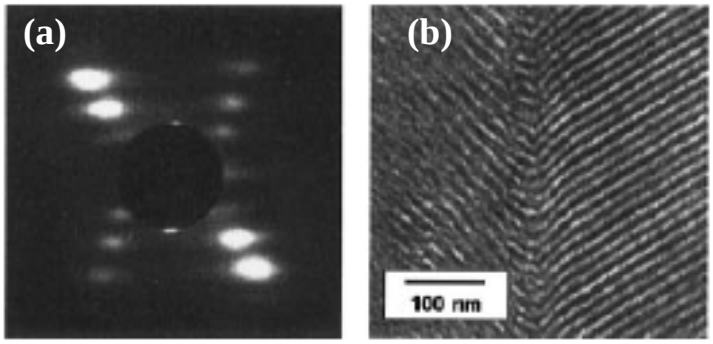

Figure 1.12: (a) SAXS pattern of an oriented SIS triblock deformed perpendicular to the S cylinders. The view direction is perpendicular to the cylinders axes. (b) TEM image of same polymer deformed up to ≈400% strain, cross-linked with high energy electrons and unloaded to 180% strain. The chevron structure in the transverse view generates the "X" pattern seen in (a). Reproduced from Honeker and Thomas.[73]

Thus, for cylinders, lamellar and gyroid forming glassy bcTPEs, while the low strain behavior is affected by morphology, the ultimate properties (tensile strength and elongation) are similar and dictated by the glassy domains. A series of experiments showed how the properties of the glassy domains directly affect the overall material's strength and elongation.[60, 61, 65,76] The rubber molecules, however, play an important role in delaying the ductile glass deformation until high strains. This is not the case, however, for TPEs with glassy spheres, where the deformation continues to be taken up by the rubber molecules up to rupture. A study by Inoue *et al.* on an SIS triblock with S spheres shows little disruption of the spherical domains as failure is caused by rubber micro-voids and subsequent cavitation.[77] As a result, this spherical forming SIS material has significant lower tensile strength than SIS materials of different morphologies.

1.3.4 Glassy and Semicrystalline Block Copolymers

Several articles examine the combination of glassy and semicrystalline polymers by creating block copolymers of C and E. Weiman produced CEC triblock copolymers and Figure 1.13 shows the tensile response of four of these, labeled VEV.[78] CEC triblocks are both stiff (high modulus) and tough (high elongation and tensile strength) when E is the majority component (Figure 1.13(a)), while they are brittle when E is minority (Figure 1.13(b)). Studies have analyzed CEC triblocks with a lamellar morphology ($f_C \approx 0.52$)[79] and with E cylinders in a C matrix ($f_C \approx 0.70$).[80] For these materials, if microdomains are aligned either randomly or parallel to the direction of applied strain, the block copolymer exhibits ductile behavior (especially if lamellar) while it is brittle if stretched perpendicular to the

microdomains. This is because the isotropic or parallel orientations are more effective in incorporating the ductile E in the craze fibril structure and hence in the path of the advancing crack.[79]

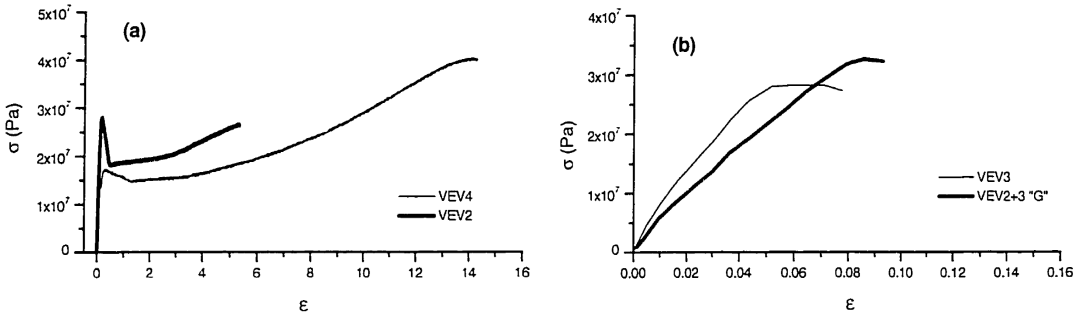

Figure 1.13: Typical strain-stress curves for CEC polymers, labeled VEV here, with different E volume fractions (f_E) and morphologies (C=cyl, L=lam & G= Gyr). Materials are: (a) VEV4 (C; $f_E \approx 0.70$) and VEV2 (L; $f_E \approx 0.51$) and (b) VEV3 (C; $f_E \approx 0.29$) and VEV2+3 (G; $f_E \approx 0.42$). Reproduced from Weiman.[78]

Moreover, for both microstructures (lamellar or E cylinders), a brittle-to-ductile transition, or an enhanced ductility, has been noted for aligned pentablocks CECEC versus triblocks CEC perpendicularly strained.[81] This striking difference is illustrated by Figure 1.14 for the lamellar case. For the CECEC pentablock, deformation was accompanied with E cavitation up to the yield point and lamellar buckling afterwards. For E-cylinder forming CEC and CECEC block copolymers with similar M_n and composition, the ductility of the pentablock is much higher also.[82] CEC deforms plastically by crazing but this leads to cracks at relatively small strains. Conversely, CECEC forms shear deformation zones and no significant craze or break down is observed up to ≈20% strains.

The reason behind this general enhanced ductility of CECEC versus CEC was assigned to its bridging C middle block, which provides a higher degree of anchoring of E chains and, subsequently, less E chain pull out.[81-83] Thus, for block copolymers composed of C and E blocks, differences in composition, morphology, architecture and orientation of aligned structures can lead to two mechanically distinct types of materials, either brittle or tough.

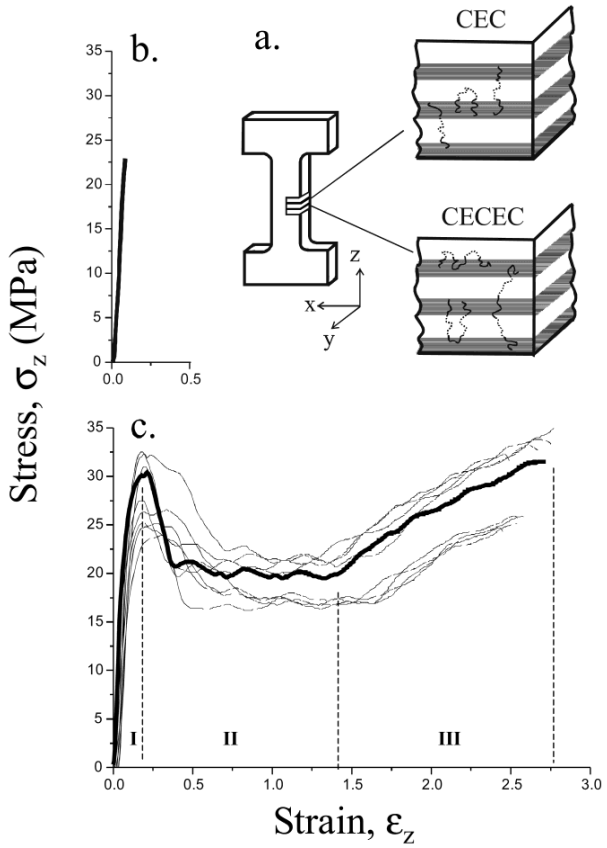

Figure 1.14: Stress-strain curves for lamellar (b) CEC versus (c) CECEC stretched in the direction perpendicular to the aligned lamellae, as shown by (a) schematic of a dog bone. CECEC is ductile while CEC is brittle. Reproduced from Hermel *et al*.[81]

1.3.5 Semicrystalline and Rubbery Block Copolymers

Studies have shown that thermoplastic elastomers can be produced with semicrystalline instead of glassy endblocks to anchor rubbery molecules.[51-54,84,85] Reports by Koo *et al*. provide a thorough examination of block copolymers of semicrystalline E and rubbery P.[51, 52] Block copolymers $(EP)_n$ were created, which contain two E endblocks, $f_E \approx f_P$ and the total number of blocks is equal to n+1. Thus, $(EP)_2$ is equivalent to EPE, $(EP)_4$ to EPEPE, etc. Stress-strain curves for $(EP)_2$ triblocks of varying M_n ($(EP)_2$-3 has M_n = 46 kg/mol while $(EP)_2$-8 has M_n = 372 kg/mol), are shown in Figure 1.15(a). $(EP)_n$ block copolymers with increasing number of blocks and similar M_n are shown in Figure 1.15(b). Materials are either weak with tensile strengths σ_{TS} < 10 MPa or are tough with σ_{TS} > 20 MPa and strain hardening. For the triblocks, tough materials were shown to be melt ordered, while weak polymers undergo crystallization induced microphase segregation. For higher order polymers, those with crystallization induced segregation were tough only if n > 10. It was concluded that reinforcing resulted from the orientation of the crystal lamellae for the melt ordered materials or the coupling effect from having a high number of blocks in the melt disordered ones.

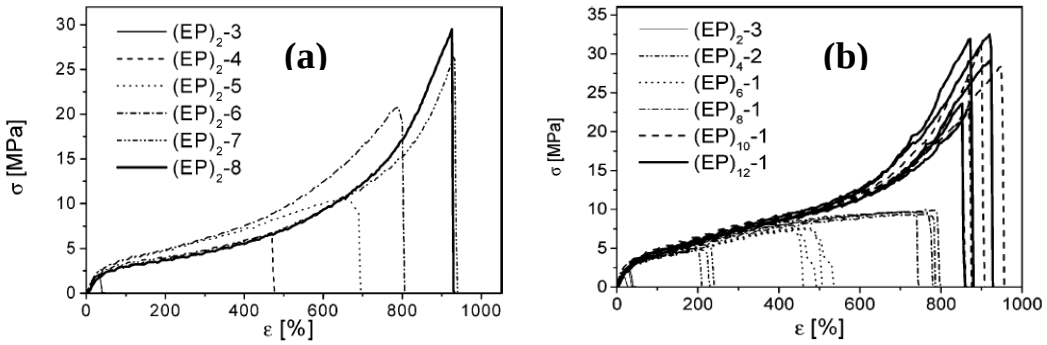

Figure 1.15: Stress-strain curves for (a) EPE triblocks of different M_n and (b) $(EP)_n$ with increasing number of n blocks and similar M_n. Reproduced from Koo *et al*.[52]

These and other results[53, 54, 84, 85] suggest that semicrystalline bcTPEs with high σ_{TS} values are only achieved through high M_n and high f_E to prevent crystallization induced segregation. This compromises processing as well as elastic recoverability, as E crystals are shown to incur high plastic deformation.

1.3.6 Glassy, Semicrystalline and Rubbery Block Terpolymers

Balsamo *et al.*[86] examined the properties of S-B-CL, where CL is semicrystalline poly(ϵ-caprolactone), with majority S. This material forms distorted core-shell cylinders of CL coaxially insulated from the S matrix by rubbery B blocks, which resembles the system in Figure 1.6(b) given that $\chi_{SCL} \approx \chi_{SB} < \chi_{BCL}$. Two triblocks, with $w_S \approx 0.51$ and 0.57, respectively, showed high elongations up to ≈900% strain. This represented an improvement in toughness as compared to S-CL,[87] which implies that the onset of failure is delayed by incorporation of the rubbery segment.

Schmalz *et al.*[88] compared the behavior of SPE triblock copolymers, in which S cylinders and E crystallites are embedded in a rubbery P matrix, with SPS triblock copolymers with S cylinders. As illustrated in Figure 1.16, the ultimate properties of these two types of materials are not significantly different. Note that SPE and SPS are labeled $S_xEP_yE_z^m$ and $S_xEP_yS_z^m$, respectively, where the subscripts give the block wt% and $m \approx M_n$ (kg/mol). The hysteresis curves in Figure 1.16 show that the SPE system is more recoverable than SPS at low strains, but the opposite is true at high strains. This difference was attributed to the ease of plastic deformation of the E

domains. The low strain behaviors are also different as SPS necks while SPE yields diffusively.

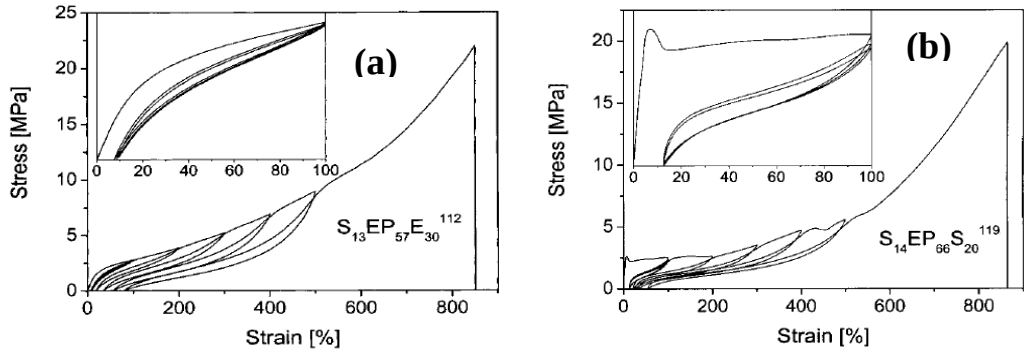

Figure 1.16: Hysteresis measurements on (a) SPE and (b) SPS. Insets show data only up to 100% strain. Reproduced from Schmalz *et al.*[88]

Finally, a recent study by Mahanthappa *et al.* examines the mechanical properties of block copolymers of C, E and P.[89] CPEPC pentablocks are compared to CEC and CPC triblocks and all materials have $f_C \approx 0.40$ and a lamellar morphology. For the pentablocks, the notation CPEPC-ξ is used as $\xi = w_E/(w_E + w_P)\times 100$ quantifies the proportion of E versus P. Thus, for CPEPC-50: $w_E \approx w_P \approx 0.3$. Figure 1.17 shows representative stress-strain curves for these materials.

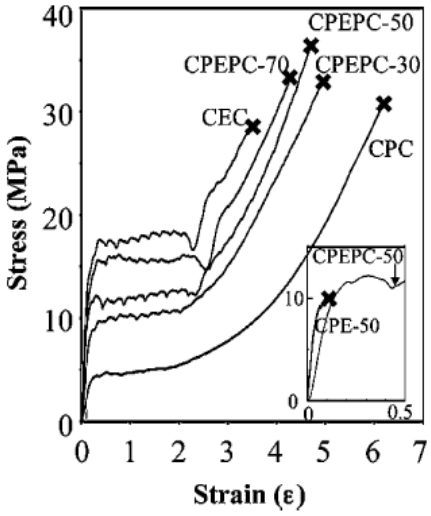

Figure 1.17: Representative stress vs. strain curves for undrawn CPEPC, CEC and CPC materials. The inset shows the brittle properties of CPE-50 relative to CPEPC-50. Reproduced from Mahanthappa *et al*.[89]

The tensile behavior indicates that a higher ξ, or E content, increases the modulus and yield stress while diminishing elongation and true stress at break. Also, a higher E content was associated with an increase in tension set, or the remaining strain after failure, which was attributed to E crystals' plastic deformation.

Cyclic elastic tests were performed on cold-drawn CEC, CPC, and CPEPC-50 ($w_E \approx w_P$) in which samples were cycled 15 times to 60% of their average breaking strain. The behavior asymptotically approaches a limiting mechanical response, as shown in Figure 1.18. A decrease in the maximum stress after the first cycle is observed for all samples. This phenomenon is known as the Mullins effect, or stress softening, and it is observed for many elastomers upon cyclic loading.[90,91] While the effect is more pronounced for materials with less E content, evidenced by the larger drop in stress for CPC in its second cycle, the recoverability of these polymers is also much greater. This suggests that E is able to delay the deformation of the C blocks,

which would greatly soften the material, but once E is deformed, it exhibits the least ability to recover.

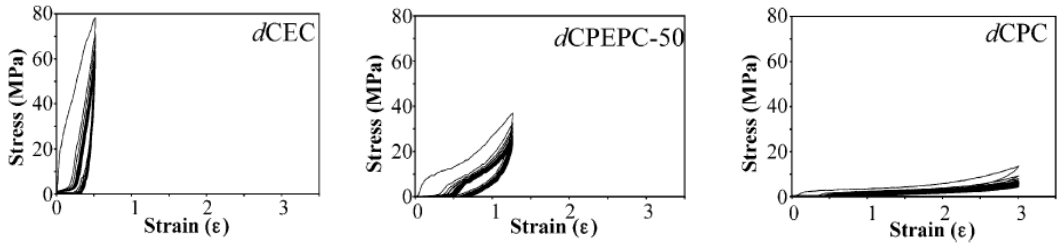

Figure 1.18: Stress vs. strain curves for drawn *d*CEC, *d*CPEPC-50 and *d*CPC in 15 cyclic tensile-compression tests. Reproduced from Mahanthappa *et al.*[89]

Thus, when combining glass and semicrystalline hard domains in rubbery networks, their reinforcing effects continue to apply but in a more complex way, as glass and crystals will deform at different times and affect properties to different extents. Also, most of the bcTPEs examples glass or semicrystalline blocks have a high content of thermoplastic domains, which may prevent the elastomeric response typical of TPEs.

1.4 Synopsis

This project presents the synthesis and characterization of block copolymers that expand the knowledge presented in the previous sections. Block polymers were created through living anionic polymerization and hydrogenation to yield the following types: CPC, CE_EC, CEC, CPE_EC, CEPC and CEC-P-CEC. Molecular properties were tested using SEC and NMR. Subsequently, block copolymer phase behavior and morphology were examined through a combination of DSC, rheology, SAXS, WAXS and TEM. Finally, mechanical testing, both uniaxial extension and cyclic testing, were conducted. The experimental techniques for polymer synthesis

and characterization are thoroughly described in Chapter 2, including the exact procedures employed. Also in this chapter, all polymers used in this work are presented to be revisited in the following ones.

Chapter 3, the first chapter to examine our findings, presents novel elastomeric heptablock terpolymers of the form CEC-P-CEC, or XPX, in comparison to CPC. Microphase segregation in XPX is induced by E crystallization and at room temperature these materials show a disorganized structure of composite hard C and E domains dispersed in rubbery P. On the other hand, microphase segregation in CPC triblocks is driven by thermodynamic incompatibility to form C cylinders in the melt. The tensile response of XPX, however, is equivalent to that of CPC, or other strong thermoplastic elastomers. This implies a benefit in processing, as for melt ordered CPC, or similar commercial glassy TPEs such as SBS or SIS, $T_{process} > T_{ODT}$, which is dependent on M_n. On the other hand, melt disordered XPX structure from a low viscosity homogenous melt, or $T_{process} > T_m(E) \approx 100$ °C, independent of M_n. Recovery in XPX is compromised when $f_X = f_C + f_E$ is high, but for $f_X < 0.39$, samples show equivalent or superior recovery than CPC with $f_C \approx 0.30$.

The second set of results, contained in Chapter 4, also relates to XPX polymers, but in this case, two XPX materials are presented which are melt ordered. Characterization of these materials allows us to understand the way structure develops in XPX and gives rise to the observed small angle x-ray scattering patterns. Finally, the deformation of these materials is studied by means of recovery tests as well as wide angle x-ray scattering. This shows that deformation is first taken by the rubbery P, then E starts to deform (at which point recovery decreases) and finally C

domains are ruptured and cause the material to fail. This agrees with the literature for glassy or semicrystalline thermoplastic elastomers which indicates that failure in hard domains is delayed by the straining of softer domains.

A comprehensive study on the mechanical properties of bcTPEs based on glassy, semicrystalline and rubbery blocks is presented in Chapter 5. Here, the synthesis and characterization of materials of the form CPC, CEC, CE_EC, CE_EPC, CEPC with different molecular characteristics are shown. The mechanical data obtained from these polymers is joined with those for materials with different characteristics and previously developed of the type CPC, CEC, CPEPC and XPX. This wide array of materials and properties allow us to draw some important conclusions by relating their mechanical properties to either glassy (C) or semicrystalline (E) content, or to rubber entanglements. Most notably, correlations were found for modulus E and tension set ε_s as a function of a combination of hard domain type and content, while tensile strength σ_{TS} and strain at break ε_b appear unrelated. In addition, for materials with constant $f_C = 0.30$, properties such as E, σ_{TS} and ε_b are inversely correlated to rubber entanglement molecular weight, or M_e, while tension set is unresponsive to M_e variations. These relationships allowed us to draw some important conclusions regarding the effects of molecular parameters f_C, f_E and M_e on the mechanical behavior of block copolymer TPEs. Finally, Chapter 6 provides a summary of our findings and proposes some areas of future investigation.

1. 5 References

[1] Bates, F. S.; Fredrickson, G. H. *Physics Today* **1999**, *52*, 32-40.

---

[2] Holden, G. In *Thermoplastic Elastomers*, 2nd ed.; Holden, G.; Legge, N. R.; Quirk, R. P.; Schroeder, H. E.; Eds.; Hanser Publishers: New York, 1996; 573-601.

[3] Hucul, D. A.; Hahn, S. F. *U.S. Patent* 5,612,422 **1977.**

[4] Hucul, D. A. *U.S. Patent6,090,359* **2000.**

[5] Hucul, D. A.; Hahn, S. F. *World Intellectual Property Organization* WO 96/34896 **1996.**

[6] Bates, F. S.; Fredrickson, G. H.; Hucul D. A.; Hahn S. F. *AIChe Journal* **2001**, *47*, 762.

[7] Brandrup, J. & Immergut, E. H. *Polymer Handbook*; Wiley-Interscience, New York, **1989**.

[8] Fetters, L. J.; Lohse, D. J.; Richter, D.; Witten, T. A.; Zirkel, A. *Macromolecules* **1995**, *27*, 4639-4646.

[9] Hiemenz, P.C.; Lodge, T.P. *Polymer Chemistry*, 2nd ed.; CRC Press: Boca Raton, FL, 2007.

[10] Bates, F. S.; Fredrickson, G. H. *Annu. Rev. Phys. Chem.* **1990**, *41*, 525-557.

[11] Bates, F. S.; Fredrickson, G. H. In *Thermoplastic Elastomers*, 2nd ed.; Holden, G.; Legge, N R.; Quirk, R. P.; Schroeder, H. E.; Eds.; Hanser Publishers: New York, 1996; 351-361.

[12] Helfand, E. *J. Chem. Phys.* **1975**, *56*, 999.

[13] Helfand, E.; Tagami, Y. *J. Chem. Phys.* **1971**, *56*, 3592.

[14] Helfand, E.; Wasserman, Z. R. *Macromolecules* **1976**, *9*, 879-888.

[15] Leibler, L. *Macromolecules* **1980**, *13*, 1602-1617.

[16] deGennes, P. G. *J. Phys. (Paris)* **1970**, *31*, 235.

[17] Fredrickson, G. H.; Helfand, E. *J. Chem. Phys* **1987**, *87*, 697-705.

[18] Bates, F. S.; Rosedale, J. H.; Fredrickson, G. H. *J. Chem. Phys.* **1990**, *92*, 6255-6270.

[19] Aggarwal, S. L. *Polymer* **1976**, *17*, 938.

[20] Thomas, E. L.; Alward, D. B.; Kinning, D. J.; Martin, D. C.; Handlin, D. L., Jr.; Fetters, L. J. *Macromolecules* **1986**, *19*, 2197-2202.

[21] Hajduk, D. A.; Harper, P. E.; Gruner, S. M.; Honeker, C. C.; Kim, G.; Thomas, E. L.; Fetters, L. J. *Macromolecules* **1994**, *27*, 4063-4075.

[22] Hajduk, D. A.; Harper, P. E.; Gruner, S. M.; Honeker, C. C.; Thomas, E. L.; Fetters, L. J. *Macromolecules* **1995**, *28*, 2570-2573.

[23] Matsen, M. W.; Schick, M. *Phys. Rev. Lett.* **1994**, *72*, 2660-2663.

[24] Matsen, M. W.; Bates, F. S. *Macromolecules* **1996**, *29*, 1091-1098.

[25] Matsen, M. W.; Bates, F. S. *J. Chem. Phys.* **1997**, *106*, 2436-2448.

[26] Cochran, E. W.; Garcia-Cervera, C. J.; Fredrickson, G. H. *Macromolecules* **2006**, *39*, 2449-2451.

[27] Khandpur, A. K.; Forster, S.; Bates, F. S.; Hamley, I. W.; Ryan, A. J.; Bras, W.; Almdal, K.; Mortensen, K. *Macromolecules* **1995**, *28*, 8796-8806.

[28] Matsen, M. W. *J. Chem. Phys.* **1995**, *102*, 3884-3887.

[29] Mayes, A. M.; delaCruz, M. O. *J. Chem. Phys.* **1989**, *91*, 7228-7235.

[30] Matsen, M. W.; Thompson, R. B. *J. Chem. Phys.* **1999**, *111*, 7139-7146.

[31] Ryu, C. Y.; Lee, M. S.; Hajduk, D. A.; Lodge, T. P. *J. Poly. Sci. B* **1997**, *35*, 2811-2823.

[32] Gehlsen, M. D.; Almdal, K.; Bates, F. S. *Macromolecules* **1992**, *25*, 939-943.

[33] Mai, S.-M.; Mingvanish, W.; Turner, S. C.; Chaibundit, C.; Fairclough, J. P. A.; Heatley, F.; Matsen, M. W.; Ryan, A. J.; Booth, C. *Macromolecules* **2000**, *33*, 5124-5130.

[34] Matsushita, Y.; Nomura, M.; Watanabe, J.; Mogi, Y.; Noda, I. *Macromolecules* **1995**, *28*, 6007-6013.

[35] Avgeropoulos, A.; Dair, B. J.; Hadjichristidis, N.; Thomas, E. L. *Macromolecules* **1997**, *30*, 5634-5642.

[36] Laurer, J. H.; Hajduk, D. A.; Fung, J. C.; Sedat, J. W.; Smith, S. D.; Gruner, S. M.; Agard, D. A.; Spontak, R. J. *Macromolecules* **1997**, *30*, 3938-3941.

[37] Stadler, R.; Auschra, C.; Beckmann, J.; Krappe, U.; Voight-Martin, I.; Leibler, L. *Macromolecules* **1995**, *28*, 3080-3097.

[38] Mogi, Y.; Kotsuji, H.; Kaneko, Y.; Mori, K.; Matsushita, Y.; Noda, I. *Macromolecules* **1992**, *25*, 5408-5411.

[39] Mogi, Y.; Mori, K.; Matsushita, Y.; Noda, I. *Macromolecules* **1992**, *25*, 5412-5415.

[40] Mogi, Y.; Mori, K.; Kotsuji, H.; Matsushita, Y.; Noda, I.; Han, C. C. *Macromolecules* **1993**, *26*, 5169-5173.

[41] Mogi, Y.; Nomura, M.; Kotsuji, H.; Ohnishi, K.; Matsushita, Y.; Noda, I. *Macromolecules* **1994**, *27*, 6755-6760.

[42] Beckmann, J.; Auschra, C.; Stadler, R. *Macromolecular Rapid Communications* **1994**, *15*, 67-72.

[43] Breiner, U.; Krappe, U.; Abetz, V.; Stadler, R. *Macromolecular Chemistry and Physics* **1997**, *198*, 1051-1083.

[44] Breiner, U.; Krappe, U.; Jakob, T.; Abetz, V.; Stadler, R. *Polymer Bulletin (Berlin)* **1998**, *40*, 219-226.

[45] Bailey, T. S.; Hardy, C. M.; Epps, T. H.,III; Bates, F. S. *Macromolecules* **2002**, *35*, 7007-7017.

[46] Epps, T. H.,III; Cochran, E. W.; Hardy, C. M.; Bailey, T. S.; Waletzko, R. S.; Bates, F. S. *Macromolecules* **2004**, *37*, 7085-7088.

[47] Seguela, R.; Prudhomme, J. *Polymer* **1989,** *30*, (8), 1446-1455.

[48] Cohen, R. E.; Cheng, P. L.; Douzinas, K.; Kofinas, P.; Berney, C. V. *Macromolecules* **1990,** *23*, 324-327.

[49] Rangarajan, P.; Register, R. A.; Fetters, L. J. *Macromolecules* **1993,** *26*, 4640-4645.

[50] Nandan, B.; Hsu, J. Y.; Chen, H. L. *Polymer Reviews* **2006,** *46*, (2), 143-172.

[51] Koo, C. M.; Wu, L. F.; Lim, L. S.; Mahanthappa, M. K.; Hillmyer, M. A.; Bates, F. S. *Macromolecules* **2005,** *38*, 6090-6098.

[52] Koo, C. M.; Hillmyer, M. A.; Bates, F. S. *Macromolecules* **2006,** *39*, 667-677.

[53] Hotta, A.; Cochran, E.; Ruokolainen, J.; Khanna, V.; Fredrickson, G. H.; Kramer, E. J.; Shin, Y. W.; Shimizu, F.; Cherian, A. E.; Hustad, P. D.; Rose, J. M.; Coates, G. W. *Proceedings of the National Academy of Sciences of the United States of America* **2006,** *103*, (42), 15327-15332.

[54] Wang, H. P.; Khariwala, D. U.; Cheung, W.; Chum, S. P.; Hiltner, A.; Baer, E. *Macromolecules* **2007,** *40*, (8), 2852-2862.

[55] Kramer, E. *J. Adv. Polym. Sci*. **2003**, *28*, 1643.

[56] Galeski, A. *Prog. Polym. Sci.* **2003**, *28*, 1643.

[57] Pope, D. P.; Keller, A. J.; *J. Polym. Sci. Polym. Phys*. **1975**, *12*, 533.

[58] Matsuo, M.; Ueno, T.; Horino, H.; Chujyo, S.; Asai, H. *Polymer* **1968**, *9*, 425-436.

[59] Kawai, H.; Hashimoto, T.; Miyoshi, K.; Uno, H.; Fujimura, M. *Journal of Macromolecular Science, Physics* **1980**, *B17*, 427-472.

[60] Holden, G.; Bishop, E. T.; Legge, N. R. *J. Polymer Sci., Part C* **1969,** *26*, 37-57.

[61] Quirk, R. P.; Morton, M. In *Thermoplastic Elastomers*, 2nd ed.; Holden, G.; Legge, N. R.; Quirk, R. P.; Schroeder, H. E.; Eds.; Hanser Publishers: New York, 1996; pp 71-100.

[62] Chen, Y. D. M.; Cohen, R. E. *J. Appl. Polym. Sci*. **1977**, *21*, 629-643.

[63] Dair, B. J.; Avgeropoulos, A.; Thomas, E. L.; *J. Mat. Sci.*, **2000**, *35*, 5207-5213.

[64] Tong, J. D.; Jerome, R. *Macromolecules* **2000**, *33*, 1479-1481.

[65] Grady, B. P.; Cooper, S. L. In *Science and Technology of Rubber*, 2nd ed.; Mark, J. E.; Erman, B.; Eirich, F. R.; Eds.; Academy Press: London, 1994; pp 601-674.

[66] Qiao, L.; Leibig, C.; Hahn, S. F.; Winey, K. I. *Industrial & Engineering Chemistry Research* **2006,** *45*, 5598-5602.

[67] Dair, B. J.; Honeker, C. C..; Alward, D. B.; Avgeropoulos A.; Hadjichristisdis N.; Fetters L. J.; Capel M.; Thomas E. L. *Macromolecules* **1999**, *32*, 8145-8152.

[68] Cohen, Y.; Albalak, R. J.; Dair, B. J.; Capel, M. S.; Thomas, E. L. *Macromolecules* **2000**, *33*, 6502-6516.

[69] Cochran, E. W. *PhD Dissertation*; University of Minnesota **2004.**

---

[70] Fujimura, M.; Hashimoto, T.; Kawai, H., *Rubber Chemistry and Technology* **1978**, *51*, 215.

[71] Hashimoto, T.; Fujimura, M.; Saijo H.; Kawai, H.; Diamant, J.; Shen, M. In *Multiphase Polymers*; Cooper, S. L.; Estes, G. M.; Eds.; ACS Advances in Chemistry Series, 1979; p 257.

[72] Odell, J. A.; Keller, A. *Polymer Engineering and Science* **1977**, *17*, 544.

[73] Honeker, C. C.; Thomas, E. L. *Chem. Mater*. **1996**, *8*, 1702-1714.

[74] Tarasov, S. G.; Tsvankin, D. Y.; Godovsky, Y. K.; *Polym. Sci. USSR* **1978**, *20*, 1728-1739.

[75] Pakula, T.; Saijo, K.; Kawai, H.; Hashimoto, T.; *Macromolecules* **1985**, *18*, 1294-1302.

[76] Morton, M.; Murphy, R. J.; Cheng, T. C. In *Le Reinforcement des Elastomers*; Centre National de la Recherche Scientifique: Paris, 1975; pp 33-40.

[77] Inoue, T.; Moritani, M.; Hashimoto, T.; Kawai, H. *Macromolecules* **1971,** *4*, 500-507.

[78] Weimann, P. A. *PhD Dissertation*; University of Minnesota **1998.**

[79] Khanna, V.; Ruokolainen, J.; Kramer, E. J.; Hahn, S. F. *Macromolecules* **2006**, *39*, 4480-4492.

[80] Ruokolainen, J.; Fredrickson, G. H.; Kramer, E. J. *Macromolecules* **2002**, *35*, 9391-9402.

[81] Hermel, T. J.; Hahn, S. F.; Chaffin, K. A.; Gerberich, W. W.; Bates, F. S. *Macromolecules* **2003**, *36*, 2190-2193.

[82] Ryu, C. Y.; Ruokolainen, J.; Fredrickson, G. H.; Kramer, E. J.; Hahn, S. F. *Macromolecules* **2002**, *35*, 2157-2166.

[83] Mori, Y.; Lim, L. S.; Bates, F. S. *Macromolecules* **2003**, *36*, 9879-9888.

[84] Mohajer, Y.; Wilkes, G. L.; Wang, I. C.; McGrath, J. E. *Polymer* **1982,** *23*, (10), 1523-1535.

[85] De Rosa, C.; Auriemma, F.; Ruiz de Ballesteros, O.; *Chem. Mater.* **2006**, *18*, (15), 3523–3530

---

[86] Balsamo, V.; von Gyldenfeldt, F.; Stadler, R. *Macromolecules* **1999**, *32*,1226-1232.

[87] Heuschen, J.; Vion, J. M.; Jerome, R.; Teyssie, P. *Macromolecules* **1989**, *22*, 2446-2451.

[88] Schmalz, H.; Boker, A.; Lange, R.; Krausch, G.; Abetz, V. *Macromolecules* **2001**, *34*, 8720-8729.

[89] Mahanthappa, M. K., Lim, L. S.; Hillmyer, M. A.; Bates, F. S. *Macromolecules* **2007**, *40*, 1585-1593.

[90] Mullins, L. *J. Phys. Chem.* **1950,** *54*, (2), 239-251.

[91] Trabelsi, S.; Albouy, P. A.; Rault, J. *Macromolecules* **2003**, *36*, 9093-9099.

2

Polymer Synthesis and Characterization

Block copolymers of poly(styrene) (S), 1,4-poly(butadiene) (B), 1,2-poly(butadiene) ($B_{1,2}$) and 1,4-polyisoprene (I) were synthesized and further hydrogenated to yield poly(cyclohexylethylene) (C), poly(ethylene) (E), poly(ethylethylene) (E_E) and poly(ethylene-alt-propylene) (P) (see structures in Chapter 1). The following type of block copolymers were synthesized: CPC, CE_EC, CEC, CEPC, CE_EPC and CEC-P-CEC (XPX). Materials were characterized using a variety of techniques for properties related to molecular structure (SEC and NMR), thermal and phase behavior (DSC and DMS), microstructure (SAXS, WAXS and TEM) and mechanical response (Tensile and Recovery Testing). The following sections describe both the principles and procedures behind the synthesis and characterization of the polymers produced.

As a way to introduce all the materials at once, Table 2.1 presents them together with molecular characterization data obtained through Size Exclusion Chromatography (SEC; see Section 2.3) and Nuclear Magnetic Resonance (NMR; see Section 2.4). In the next chapters, pertinent polymers are presented once again with this information and any further characterization performed.

Table 2.1: Molecular characterization data for all block copolymers

Sample	$B_{1,4}$[a] (%)	$I_{1,4}$[a] (%)	f_C[b]	$f_{E \text{ or } EE}$	f_P	N[c]	M_n[d] (kg/mol)	M_w/M_n[e]
CPC-1[f]	-	-	0.18	0.00	0.82	1193	90.0	1.04
CPC-2a	-	94	0.31	0.00	0.69	446	35.5	1.03
CPC-2	-	94	0.30	0.00	0.70	597	47.4	1.03
CPC-2b	-	93	0.30	0.00	0.70	746	59.3	1.07
CE_EC	18	-	0.30	0.70	0.00	911	60.7	1.03
CEC-1	93	-	0.31	0.69	0.00	341	22.9	1.06
CE_EPC	15	92	0.31	0.34	0.36	876	65.2	1.03
CEPC-1	91	94	0.17	0.21	0.62	866	61.7	1.04
CEPC-2	92	94	0.18	0.42	0.40	680	45.9	1.06
CEPC-3	89	93	0.30	0.16	0.54	828	63.3	1.05
XPX-1[g]	88	93	0.18	0.22	0.60	1450	103.4	1.11
XPX-2a	88	92	0.25	0.26	0.49	808	59.0	1.11
XPX-2b	90	92	0.25	0.26	0.49	1086	79.2	1.13
XPX-2c	90	92	0.25	0.26	0.49	1560	113.7	1.16
XPX-2d	87	91	0.27	0.25	0.48	1822	132.8	1.13
XPX-2e	87	92	0.26	0.25	0.49	2682	195.0	1.14
XPX-3	91	93	0.30	0.28	0.42	592	43.8	1.21

[a] % of 1,4 additions calculated from ^{1}H NMR.

[b] f values are volume fractions calculated from ^{1}H NMR of unsaturated precursors and bulk homopolymer densities from Fetters et al. with 118 Å^3 reference volume.

[c] Calculated from M_n of first block of unsaturated precursor by SEC with PS standards in THF at 30 °C and reaction stoichiometry.

[d] Overall molecular weight calculated from N.

[e] Determined for unsaturated precursors by SEC with PS standards in THF at 30 °C.

[f] Obtained from The Dow Chemical Company.

[g] XPX stands for block copolymer CEC-P-CEC.

2.1 Polymer Synthesis

Hydrocarbon block copolymers were synthesized by living anionic polymerization to produce polymers of narrow molecular weight distributions. The principles behind this technique as well as the exact procedures for the different types of polymers created are described in this section.

2.1.1 Living Anionic Polymerization

In order to correlate block copolymer behavior to molecular properties such as molecular weight and composition, materials with narrow molecular weight distributions are desired. Moreover, most polymer theories are constructed assuming all chains have the same length, and thus their predictions apply best for polymers with low polydispersity values.

Living anionic polymerization is a chain-growth polymerization mechanism which is able to achieve such narrow molecular weight distributions. An initiator, such as an alkyl lithium compound, is used to produce a negatively charged active chain center, through which the polymerization proceeds. These steps are shown below, where M represents the monomer:

Initiation: $$R^{-}Li^{+} + M \xrightarrow{k_i} RM^{-}Li^{+} \qquad (2.1)$$

Propagation: $$RM_x^{-}Li^{+} + M \xrightarrow{k_p} RM_{x+1}^{-}Li^{+} \qquad (2.2)$$

A “living” polymerization mechanism is one that lacks chain transfer and termination steps. This, compounded with a rate of initiation which is greater than the propagation rate ($k_i > k_p$), allows all chains to grow for essentially the same amount of time. As a result, chains have a similar molecular weight when all monomers are consumed.

Under ideal conditions, this type of polymerization yields a Poisson distribution of chain lengths, as described by the equation below, where N is the number average degree of polymerization and w_i is the weight fraction of the i-mer.[1]

$$w_i = \frac{iN^{i-1}e^{-N}}{(N+1)(i-1)!} \qquad (2.3)$$

The polydispersity index (PDI) associated with a Poisson molecular weight distribution is shown below, where M_N and M_W are the number-averaged and weight-averaged molecular weights, respectively.

$$PDI = \frac{M_W}{M_N} = 1 + \frac{N}{(N+1)^2} \approx 1 + \frac{1}{N} \qquad (2.4)$$

Thus, for even relatively small polymers, with $N \approx 100$, an ideal PDI of 1.01 is expected. In reality, experimental PDI range between 1.01 and 1.20 for a successful synthesis. After all the monomer is consumed, the chains can be end-functionalized as shown below.

$$RM_n^- Li^+ + X - Y \xrightarrow{k_t} RM_n X + LiY \qquad (2.5)$$

2.1.2 Monomers and Solvents

The range of monomers that are amenable to this chemistry is quite limited. For anionic polymerization to proceed successfully, the monomer must be able to stabilize the negative charge on the chain. This eliminates monomers that possess electrophilic substituent groups, such as hydroxyls, carboxyls or acetylenes while it validates monomers that have nucleophilic (electron withdrawing) groups such as phenyls, carbonyls, double bonds or nitro groups. However, the polar carbonyl and nitro groups are susceptible to side reactions that may be undesirable.[2] Styrene,

butadiene and isoprene, the monomers used in this project, satisfy these conditions, and thus are able to be polymerized through living anionic chemistry using alkyl lithium initiation.

When synthesizing block copolymers, *sequential* anionic polymerization is the most direct method. Polymerization of the first block proceeds until the complete conversion of the first monomer, at which point the second monomer is added to be polymerized by the living chains and this process can be continued up to the number of blocks desired. However, for this to occur, it is required that the polyanion formed from the conversion of one monomer be capable of initiating the polymerization of the next monomer. Given that the stabilities of the polyanions formed *before* and *after* the additions of S, B and I monomers are comparable,[2] the sequential polymerization of these monomers can be successfully done in any order.

The choice of solvent is limited by the requirement that it should be inert to the polyanion and should not take part in any chain transfer reactions. In our case, this implies that electrophilic or proton donating solvents cannot be used. For styrenes and dienes, this includes aromatic hydrocarbons, ethers, alkanes, and cycloalkanes. Aromatic solvents and polar solvents such as tetrahydrofuran (THF) enhance the initiation kinetics with alkyllithium initiators because they decrease their degree of aggregation. However, these are also somehow reactive toward the polyanion or the initiator, undergoing chain transfer reactions or deactivating the initiator (that is why polymerizations with THF are done at low temperatures).[2] Thus, the solvent of choice for this project was cyclohexane, with a reaction temperature of 40 °C. Solvents can also affect the microstructure of the polymer. When pure cyclohexane is

used, over 90% 1,4-poly(butadiene) is obtained. Addition of THF to cyclohexane increases the amount of 1,2- addition and when the reaction is carried out in pure THF, about 90% 1,2-poly(butadiene) is obtained.[3] This was the strategy used to increase the 1,2-poly(butadiene) addition to produce CE_EC and CE_EPC after polymerization of styrene or styrene and isoprene, respectively (see $B_{1,2}$ percentages in Table 2.1 and see procedures below).

2.1.3 Procedure

In order to attain a nearly monodisperse molecular weight distribution with living anionic polymerization, the reaction conditions have to be extremely pure. This is because of the high reactivity of the carbanion and the very small amount of initiator present in the reaction mixture. Even trace amounts of impurities like oxygen, carbon dioxide or moisture can inhibit the polymerization and cause side reactions. Any presence of impurities has to be thoroughly eliminated by rigorously purifying monomers and solvents and carrying out the reaction in an inert atmosphere.

Monomers, collected in round-bottom flasks, are deep frozen in liquid N_2 and then subjected to high vacuum (≈ 100 mTorr) to get rid of volatile impurities like oxygen.[4] Secondly, low pressure distillation into a flask containing excess dry purification agent and subsequent stirring removes the inhibitor added to commercially produced monomers as this initiates anions which react with monomer impurities. For styrene, stirring is done at room temperature and thus the less reactive dibutylmagnesium is used, as *n*-butyllithium would be able to initiate unfettered polymerization. For the dienes, because their large vapor pressure, purification is

carried out in an ice-water bath, using the more reactive *n*-butyllithium given the low temperature. The purified monomers are then distilled over to evacuated, flame-treated burettes. Cyclohexane is purified by passing through multiple columns of activated alumina and collected in an evacuated, flame-treated round-bottom flask.

Once all monomers and solvent have been purified and collected, and the initiator concentration determined, they are assembled into a heat-treated glass reactor, which is then subjected to six cycles of evacuation at high vacuum and subsequent pressurization to 3 psi with high purity grade Ar. The solvent is then added and allowed to reach the reaction temperature. The initiator is injected through a septum, which is followed by the addition of the first monomer. The volume of initiator, V_I (in ml), is calculated using the equation below, where m is the desired mass of block copolymer (in grams), M_N is the desired number averaged molecular weight (in g/mol) and C_I is the concentration of the initiator *sec*-butyllithium (in mol/L).

$$V_I = \frac{m}{M_N C_I} \tag{2.6}$$

Chemical routes with three sets of conditions were followed for the synthesis of the precursor materials (before hydrogenation) to the polymers presented in this thesis. Note that the names of the tetrablock copolymers, CEPC and CE_EPC, have the monomer letters in the reverse order to how the sequential addition occurred, or $SIB_{1,4}S$ and $SIB_{1,2}S$, respectively. This was done merely to facilitate labeling. Route 1 (Figure 2.1) was used to synthesize $SIB_{1,4}S$ (yields CEPC after hydrogenation) and it involves the sequential addition of S, I, $B_{1,4}$ and S in purified cyclohexane at 40 °C and initiation with *sec*-butyllithium.

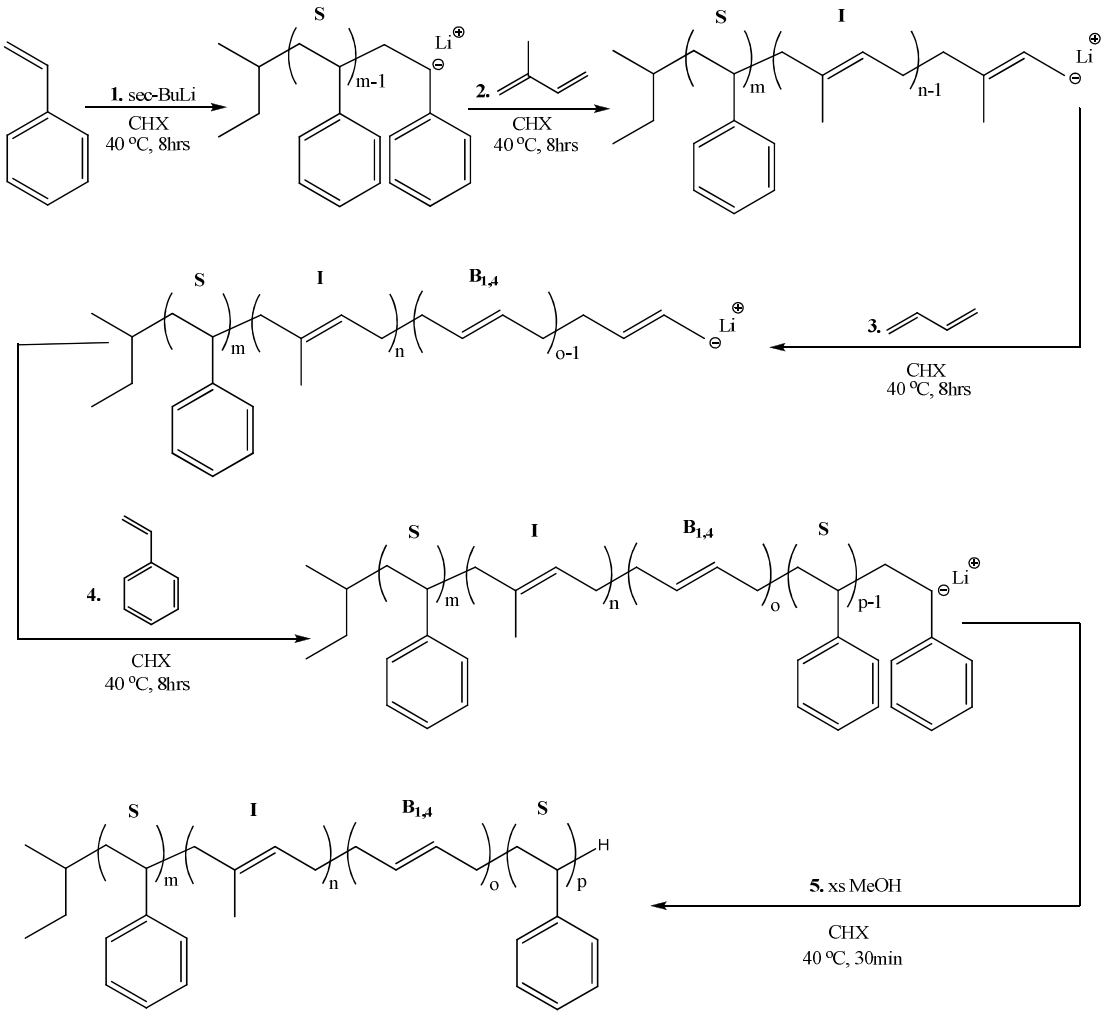

Figure 2.1: Synthesis route for $SIB_{1,4}S$, to yield CEPC upon hydrogenation. This is the same route to synthesize $SB_{1,4}S$ and SIS, which yield CEC and CPC after hydrogenation, except that one monomer is omitted for each.

These are the same conditions used to generate $SB_{1,4}S$ and SIS, which yield CEC and CPC after hydrogenation. Reaction times depend on the monomer. Styrene usually polymerizes in 4-6 hours, while butadiene and isoprene take 6-8 hours. The completion of the polymerizations of butadiene and isoprene is indicated by a drop of reactor pressure to the baseline value. The polymerization is terminated through the previously shown general end-capping reaction in Equation 2.5 with degassed

methanol as the terminating reagent. The polymer is recovered by precipitation into a 3:1 (volume ratio) mixture of methanol and isopropanol, filtered from the alcohol and dried under vacuum until constant mass.

Route 2 (Figure 2.2) shows the polymerization of $SIB_{1,2}S$ (yields CE_EPC after hydrogenation). This is identical to Route 1 with the exception of lowering the temperature to 10 °C and subsequently adding about 200:1 molar ratio of THF to active centers before B addition.

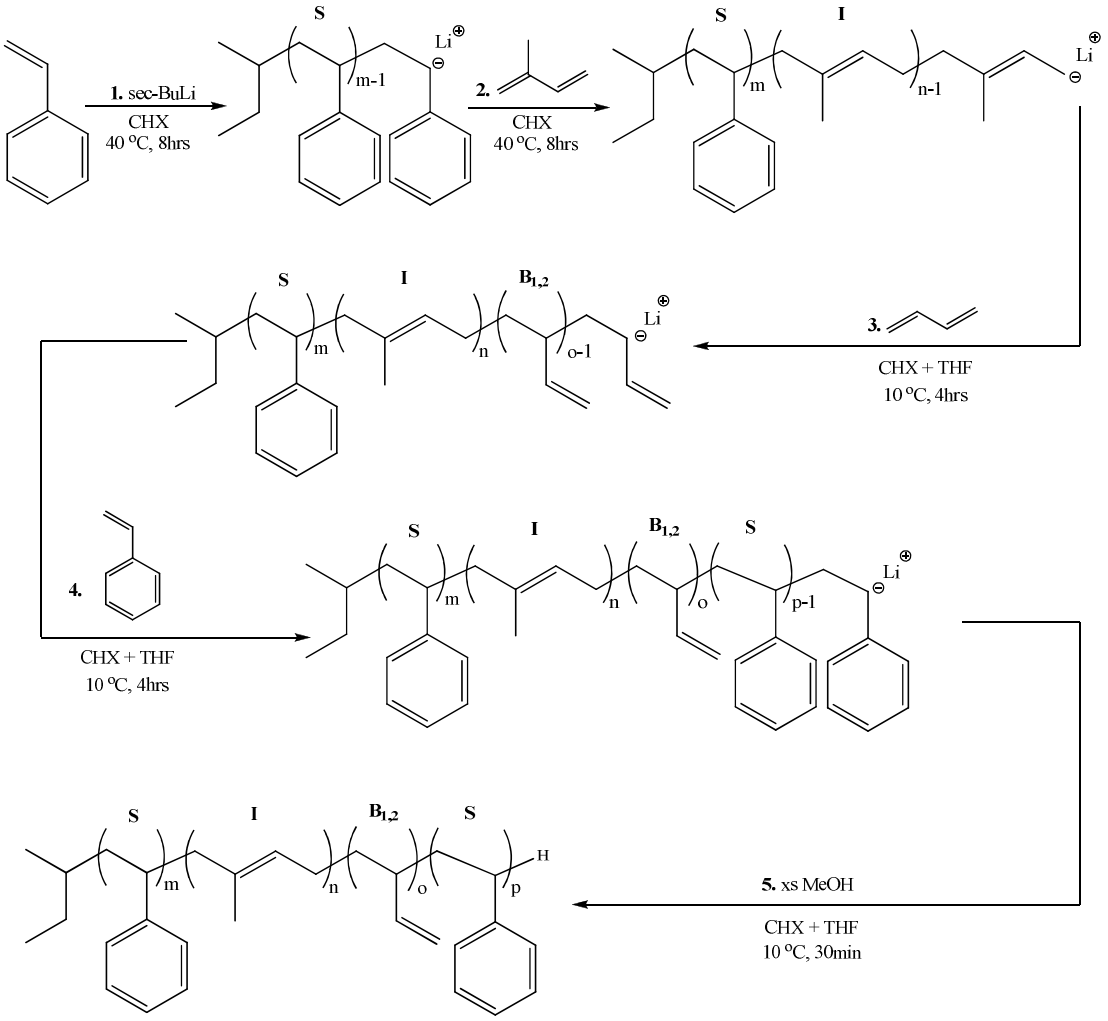

Figure 2.2: Synthesis route for $SIB_{1,2}S$, to yield CE_EPC upon hydrogenation. This is the same route to synthesize $SB_{1,2}S$, which yields CE_EC after hydrogenation, except for the exclusion of step 2 involving isoprene addition.

This THF addition elevates the fraction of 1,2-poly(butadiene) addition to almost 90%. Because a polar solvent such as THF accelerates the polymerization by promoting dissociation of the aggregated chains, the reaction times for B and S were shortened to about 4hrs. $SB_{1,2}S$ (CE_EC after hydrogenation) was polymerized in a similar fashion as route 2 but the addition of I was omitted. Termination and polymer recovery were done as in route 1. Finally, route 3 (Figure 2.3) was employed in synthesizing $SB_{1,4}S$-I-$SB_{1,4}S$ (XPX after hydrogenation)

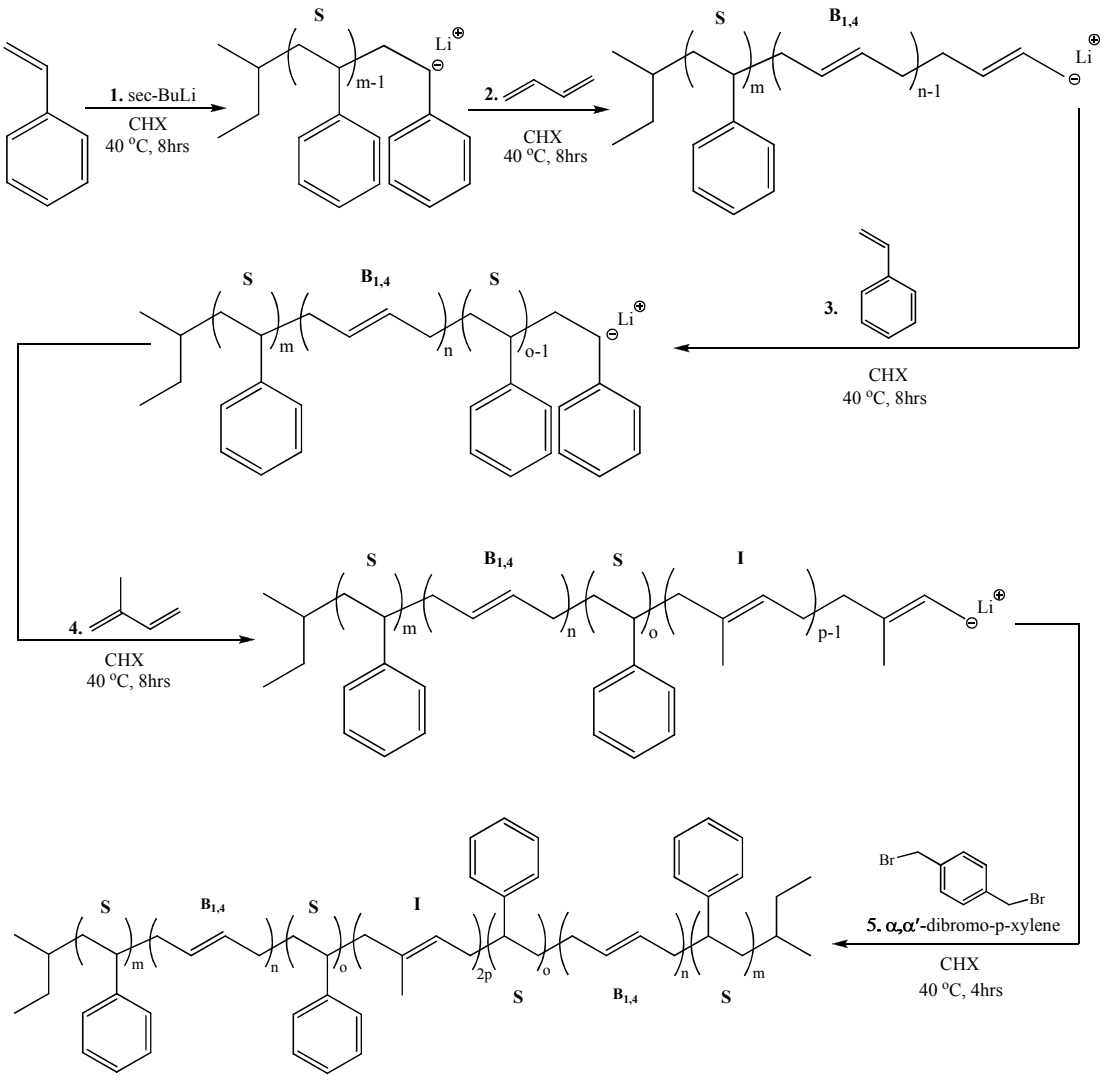

Figure 2.3: Synthesis route for $SB_{1,4}S$-I-$SB_{1,4}S$, to yield CEC-P-CEC (XPX) upon hydrogenation. Apart from sequential addition, this route employs a coupling agent on step 5.

This route has the same conditions as route 1 but follows a different sequential addition scheme, adding S, B, S and then I. Also, the reaction ends in the coupling of SBS-I$^-$ molecules with a stoichiometric amount of α,α'-dibromo-p-xylene added in a dropwise fashion until the solution becomes colorless (about 4 to 6 hours). Termination is not necessary in this case, and recovery is done as in the previous two routes.

2.2 Heterogeneous Catalytic Hydrogenation

As presented in Chapter 1 (see Figure 1.1), the block copolymers used in this project are prepared by hydrogenating block copolymers obtained from sequential living anionic polymerizations, as described in section 2.1. The recently developed ultra wide pore silica supported platinum/rhenium catalyst[5] (5% Pt/Re, Dow Chemicals Co.) is used in this study. This catalyst has been reported to saturate polystyrene (which is the hardest of the aforementioned unsaturated polymers to hydrogenate) at efficiencies up to 99.7 % in 6 hours and a catalyst to polymer weight ratio of only 1:0.27.[6] This is a significant improvement over hydrogenation procedures reported earlier, where this ratio was greater than 1:1.[7,8]

2.2.1 Procedure

About 10 grams of the precursor block copolymer is dissolved in 500 ml of cyclohexane and added to a high-pressure 1 L stainless steel reactor (Pressure Products, Inc). About 3 grams of the Dow catalyst is then added and the reactor is sealed. Nitrogen at around 50 psi is used to purge the reactor three times to remove any oxygen present. The vessel is then pressurized to 500 psi with hydrogen and the

reactor temperature is raised to 170 °C. This sequence is crucial because it gives the hydrogen enough time to diffuse to the surface of the catalyst and activate it. If the reactor is heated to the desired temperature prior to the addition of hydrogen, the polymer may diffuse to the catalyst surface before the hydrogen, thus preventing the catalyst from being activated. The reaction is allowed to proceed for 12 hours before the residual hydrogen is vented and the reactor is pressurized to 50 psi nitrogen. A 0.22 μm Millipore Durapore® membrane filter is used to remove the catalyst and the polymer is recovered by precipitation into a 1:1 mixture of methanol and isopropanol, followed by filtration and drying under vacuum until constant weight. The completion of the hydrogenation reaction is confirmed by the absence of ^{1}H NMR peaks corresponding to the unsaturated precursor block copolymers. Figure 2.4 shows the hydrogenation reaction with conditions to generate CEPC from $SIB_{1,4}S$. Hydrogenations of all other polymers followed the same conditions and the structures can be induced by comparison to Figure 2.4.

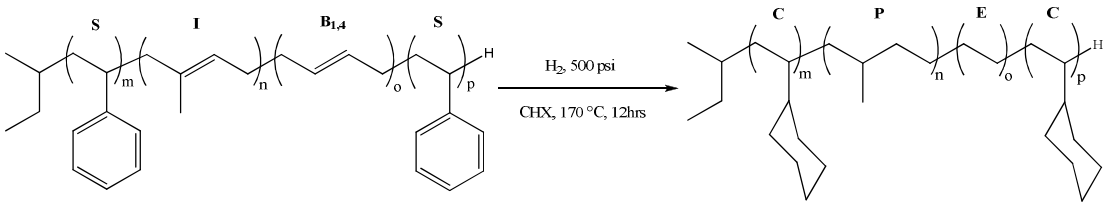

Figure 2.4: Hydrogenation reaction to produce CEPC, from $SIB_{1,4}S$. These conditions were used for all hydrogenations.

2.3 Size Exclusion Chromatography (SEC)

Size Exclusion Chromatography (SEC), or Gel Permeation Chromatography (GPC), as it is sometimes called, is used to obtain a polymer's molecular weight (M_W and M_N) and its distribution (or polydispersity index, PDI).[9] SEC essentially separates

polymer chains based on size as characterized by a hydrodynamic volume (V_R), which can be related to molecular weight. Thus, a separation of polymer chains by molecular weight is effectively achieved. A dilute solution of the polymer in a solvent (in this study THF was used at room temperature and TCB for high temperature SEC) is passed through a column packed with a porous material. Smaller polymer chains permeate the pores to a greater extent and thus are eluted at a later time.

The concentration of the eluting solution is detected (the detector signal is proportional to the concentration of the solution) and a plot of concentration versus V_R is obtained. This would represent the volume of solution having escaped the column before a chain of a particular molecular weight comes out of it. After performing column calibration to obtain a relationship between V_R and molecular weight, molecular weight distribution and molecular weight averages can be obtained as shown below. Here,c_i and M_i are the concentration and molecular weight of the polymer in the i^{th} slice of the chromatogram respectively.

$$M_N = \frac{\sum_{i=1}^{n} n_i M_i}{\sum_{i=1}^{n} n_i} = \frac{\sum_{i=1}^{n} c_i}{\sum_{i=1}^{n} (c_i / M_i)} \tag{2.7}$$

$$M_W = \frac{\sum_{i=1}^{n} n_i M_i^2}{\sum_{i=1}^{n} n_i M_i} = \frac{\sum_{i=1}^{n} c_i M_i}{\sum_{i=1}^{n} c_i} \tag{2.8}$$

For the block copolymer synthesized in this project, the molecular weight of the first S block $M_{n,S}$ (from extracted aliquot) and the molecular weight distribution

(M_w/M_n), or polydispersity, were determined from the SEC trace. A Waters 717 GPC fitted with three Polymer Laboratories Mixed-C columns and operated at 30 °C with tetrahydrofuran and calibrated with polystyrene standards was employed with the unsaturated polymers and with CPC, CE_EC and CE_EPC. The saturated E-containing materials, CEC, CEPC and XPX, were characterized with a PL-GPC 220 system operated at 135 °C with 1,2,4-trichlorobenzene. Figure 2.5 shows a SEC traces for CPC-2, which resembles those of all other materials as monomodal and relatively narrow distribution (M_w/M_n < 1.21) peaks were recorded in all cases. However, for the XPX-2 polymers some uncoupled chains are present but this will be discussed in Chapter 3 and 4. If the final saturated block copolymer maintains a narrow polydispersity index and the NMR data are consistent with the monomer ratios, then block and overall molecular weights can be calculated based on $M_{n,S}$ and the reaction stoichiometry.

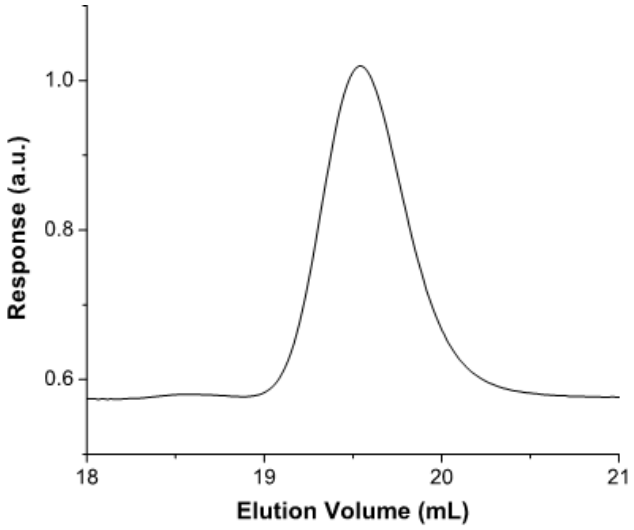

Figure 2.5: Size Exclusion Chromatograph for CPC-2 at 30 °C with THF and calibrated with polystyrene standards showing monomodal distribution.

2.4 Nuclear Magnetic Resonance (NMR)

Nuclear magnetic resonance (NMR) is a technique based on the existence of discreet spin states associated with the nuclei of a molecule.[10] Nuclei like ^{1}H and ^{13}C which have an odd number of protons or neutrons have a non-zero spin quantum number I and thus share similar properties to a spinning electric charge. These "spinning" nuclei generate a magnetic moment vector μ. Consider the ^{1}H atom, with spin I = ½. When an external magnetic field B_0 is applied two spin states exist +½ (lower energy) and -½ (higher energy), which can be pictured as arising from the moment aligning along B_0 (+½ state) versus opposite (-½ state). Lower energy nuclei can be excited by a specific value of frequency, known as the Larmor frequency, which is dependent on the applied magnetic field by the formula below, where h is Planck's constant. For example, ^{1}H has a Larmor frequency of roughly 300 MHz for a 7.05 Tesla field strength0.

$$\nu = \frac{\mu B_0}{hI} \tag{2.13}$$

The simplest way of obtaining an NMR spectrum is referred to as the continuous wave (CW) method. The idea is that if the sample is subjected to a specific magnetic field, and a range of frequencies are pulsed, a resonance peak will be observed at the Larmor frequency for ^{1}H. But protons don't exist by themselves. Rather, they are surrounded by electrons in covalent compounds or ions, and since these electrons are charged particles, they will move in response to the B_0 so as to generate a secondary field, which opposes the applied field. This phenomenon is referred to as "shielding", and accounts for the fact that the "felt" field shifts to higher

values than for a “naked” proton. Moreover, these values will be different depending on the specific chemical environment surrounding the proton. Hence, different types of protons (in different chemical environments) will resonate at different frequencies.

The NMR detector collects the energy released by all the protons in a compound as they return to the ground state, in what is called a free induction decay (FID) in the time domain, which is converted to a readable spectrum in the frequency domain via a Fourier transformation. A peak frequency will correspond to a specific type of proton and a peak’s intensity or integral will be proportional to the number of protons of that specific type. Because values of frequencies and magnetic fields will vary according to the instrument used, the concept of chemical shift δ was introduced to provide an unambiguous location for each type of proton. Given a certain magnetic field, the frequency shift is divided by the spectrometer frequency used to yield a parts per million (ppm) unit, as shown in Equation 2.14 below.

$$\delta = \frac{\nu^{sample} - \nu^{spectrometer}}{\nu^{spectrometer}} \qquad (2.14)$$

This is then compared to the ppm unit observed for the standard tetramethylsilane ($(CH_3)_4Si$ or TMS) with an assigned chemical shift of 0 ppm to produce the final δ. Table 2.2 lists the chemical shifts for some of the protons present in polymers S, B and I which can be clearly resolved from ^{1}H NMR. Based on the values in Table 2.2, peaks from the unsaturated block copolymers can be associated with different protons, as shown in Figure 2.6, which shows ^{1}H NMR spectra for SBS-I-SBS-3 and its hydrogenated version XPX-3.

Table 2.2: Chemical shifts for protons found in spectra of S, B and I

Polymer	Structure	δ (ppm)
1,4-Poly(butadiene)[11]	-CH_2-C***H***=***CH***-CH_2-	5.4*
1,2-Poly(butadiene)[11]	-CH_2-CH(C**H**=CH_2)-	5.4*
	-CH_2-CH(CH=C$\mathbf{H_2}$)-	4.9*
1,4-Poly(isoprene)[12]	-CH_2-C***H***=C(CH_3)-CH_2-	5.1$^{\Psi}$
3,4-Poly(isoprene)[12]	-CH_2-CH(C(CH_3)=C$\mathbf{H_2}$)-	4.7*
Poly(styrene)[13]	-CH_2-CH($C_6\mathbf{H_5}$)-	6.3-7.3$^{\Psi}$

* Multiple overlapping sharp peaks. $^{\Psi}$ Broad peaks.

For the unsaturated polymers, ^{1}H NMR spectra were collected in deuterated chloroform ($CDCl_3$) using a Varian Unity Inova 300 spectrometer. Monomer mole fractions were calculated by integrating resonances associated with S, B and I repeat units. These values were then converted to volume fractions for the saturated compounds using published polymer densities at 140 °C: ρ_C = 0.920 g/cm^3; ρ_E = 0.784 g/cm^3; ρ_P = 0.790 g/cm^{3}and ρ_{EE} = 0.866 g/cm^3[14] These spectra also allowed the calculation of the 1,4 versus 1,2 addition of both butadiene and isoprene, as shown in Table 2.1. As can be seen, for all polymers, the isoprene polymerizations resulted in predominantly 1,4-monomer addition, with 91-94 mol % $I_{1,4}$. On the other hand, the butadiene reactions resulted in 87-93 mol % $B_{1,4}$ for all polymers except for the precursors to CE_EC and CE_EPC, with 82 and 85 mol % $B_{1,2}$, respectively, as desired.

^{1}H NMR spectra were also recorded from the hydrogenated polymers in deuterated chloroform ($CDCl_3$) at room temperature for CPC, CE_EC and CE_EPC polymers, and in deuterated toluene (C_7D_8) at 70 °C for the E containing polymers

CEC, CEPC and XPX. The level of extinction of the unsaturated peaks was used to establish the extent of saturation for each polymer, which in every case was greater than 97%. For example, the spectrum for XPX-3 (Figure 2.6(b)) shows how the peaks previously present for its unsaturated precursor SBS-I-SBS-3 (Figure 2.6(a)) have disappeared.

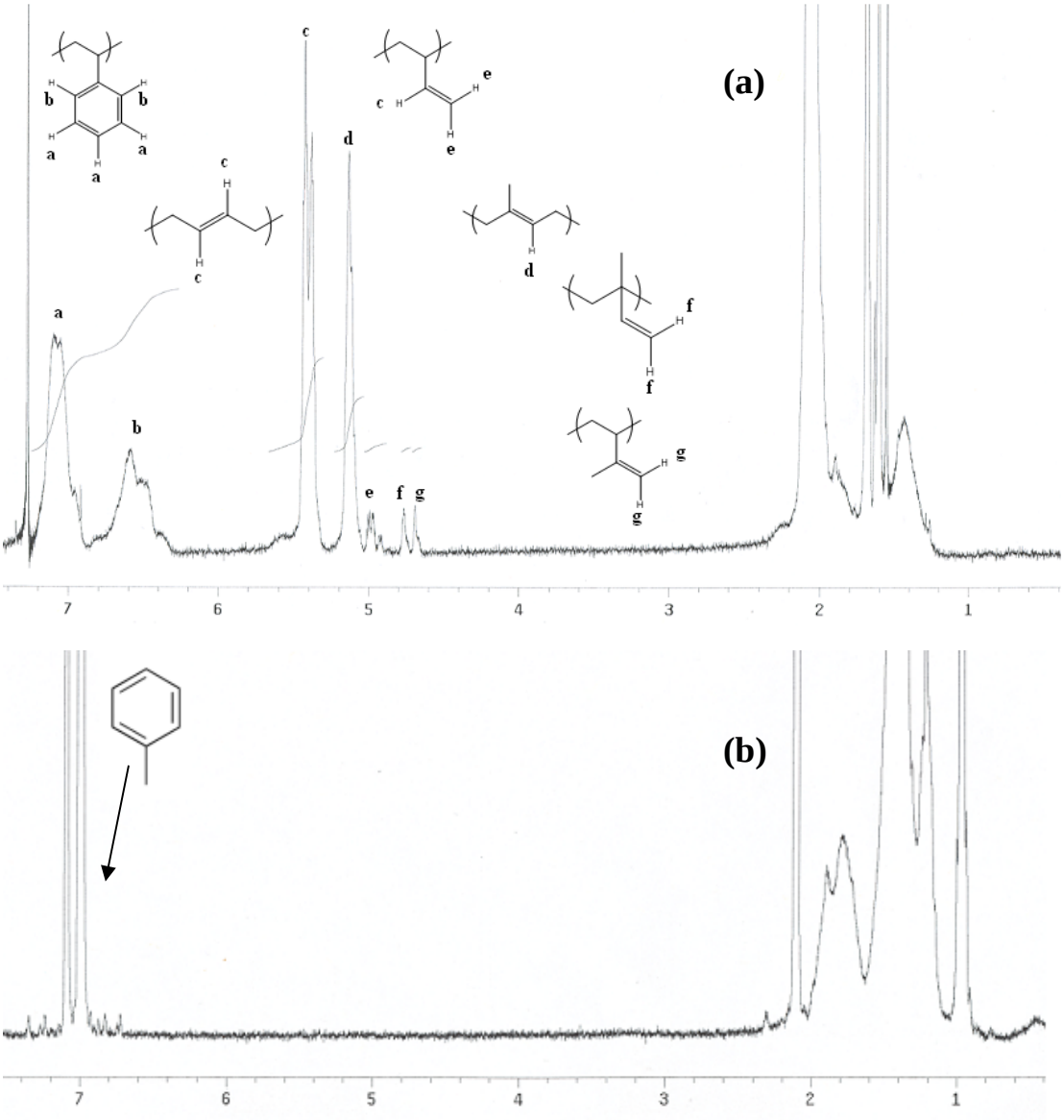

Figure 2.6: (a) ^{1}H NMR for SBS-I-SBS-3 at 25 °C in deuterated chloroform and (b) its homologous XPX-3 after hydrogenation in toluene. For the unsaturated polymer, peaks correspond to protons of the same letter. The disappearance of peaks for the saturated case indicates complete hydrogenation.

2.5 Differential Scanning Calorimetry (DSC)

DSC is able to detect thermal transitions by measuring heat flow in and out of a sample as the temperature is changed.[15] Specifically, the instrument records the difference in heat intake or outake to maintain two hermetic aluminum pans, one with 5 – 10 mg of specimen and a reference one with air, at the same temperature. Block copolymers specimens were heated in a TA Instruments Q1000 DSC to 160 °C to erase any thermal history and then transitions were measured upon cooling to -80 °C and heating back to 160 °C, all at 10 °C/min. Figure 2.7 shows a typical scan for this project, in this case polymer XPX-1 with f_C = 0.18, f_E = 0.22 and M_n = 103 kg/mol.

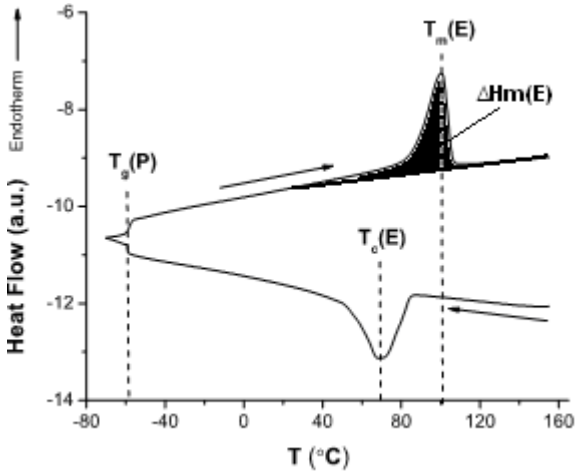

Figure 2.7: DSC trace of XPX-1 at 10 °C/min. T_g for P is evident -60 °C while melting and crystallization dominate at high temperatures. However, the glass transition for C is not identified.

A glass transition, in this case T_g(P) = -60 °C, is indicated by a change in the heat capacity of the material and is recorded at the inflection of the curve. E melting shows an endothermic peak at T_m(E) = 100 °C and E crystallization exhibits an exothermic peak at T_c(E) = 70 °C. T_g(C), about 147 °C for homopolymer C, was not

detected for any of the materials, which is probably due to a low f_C and the proximity to T_{ODT} and E melting. E fractional crystallinity, X_c, was calculated using expression 2.15 below, where w_E is the weight fraction of E and $H^\circ_{m,E}$ = 277 J.g^{-1} is the theoretical heat of melting for 100% crystalline poly(ethylene).[16] ΔH_m is the recorded heat of fusion from the DSC trace, or the area under the melting peak, shown shaded in black for XPX-1 in Figure 2.7.

$$X_c = \frac{\Delta H_m}{H^\circ_{m,E} \times w_E} \qquad (2.15)$$

2.6 Dynamic Mechanical Spectroscopy (DMS)

DMS is a rheological technique to study the viscoelastic behavior of polymers under sinusoidal shearing over a range of frequencies.[17] When a stress is applied to a solid, it stores the input energy and exhibits deformation, resulting in the relationship below, where σ is the shear stress, γ is the strain, and G is the shear modulus. When the stress is removed, the sample can return to its original size.

$$\sigma = G\gamma \qquad (2.16)$$

Conversely, when a stress is applied to a liquid, the energy is dissipated by friction through the motion of molecules and thus deformation is permanent. The stress σ follows the expression below, where η is the viscosity and $\dot{\gamma}$ is the strain rate.

$$\sigma = \eta\dot{\gamma} \qquad (2.17)$$

Polymer melts are known to be viscoelastic in nature, having deformation characteristics of a viscous liquid and an elastic solid. This behavior arises from the

length of the polymer molecules. The elastic response is mostly entropically driven through the stretching of the polymer chains when stressed. Upon removal of the stress, the chains relax back to their equilibrium conformation. The viscous response is due to the relaxation of the molecules within the moving fluid, which dissipates energy through friction.

Dynamic Mechanical Spectroscopy (DMS) can be used to probe the dynamics of polymer melts through the application of a sinusoidal strain γ, given by the expression below, with an amplitude γ_0, frequency ω as a function of time t.

$$\gamma = \gamma_0 \sin(\omega t) \tag{2.18}$$

The stress response, σ, is characterized by an in-phase elastic component (sine term) and an out-of-phase viscous component (cosine term) as given by the following equation, where G' is the elastic modulus and G'' is the viscous modulus.

$$\sigma = G'\gamma_0 \sin(\omega t) + G''\gamma_0 \cos(\omega t) \tag{2.19}$$

The elastic and viscous moduli can be combined into a complex modulus, G*, as indicated in the expression below.

$$G^* = G' + iG'' \tag{2.20}$$

The stress response for a viscoelastic fluid is dependent on the applied strain except at low strains in the regime called linear viscoelasticity. To ensure the moduli measured during DMS are characteristic of the material, all measurements were conducted within the linear viscoelastic regime.

The low frequency (long time) linear viscoelastic properties of block copolymers are governed by the underlying state of order while the high-frequency response (short time) is dominated by single chain dynamics. This is because in low frequency experiments, the time frame coincides with the longest relaxation times, or those associated with the large collection of polymer chains, as there is enough time for smaller molecular segments to relax. Thus, below a certain critical frequency ω_c the response is due to the long-range structure in the sample. As first reported by Chung and coworkers[18,19] and Gouinlock *et al.*,[20] who worked on SBS triblocks, the viscoelastic response of a block copolymer, in this low frequency limit, goes through an abrupt change at the order to disorder transition (ODT) temperature or T_{ODT}. Two experiments take advantage of this phenomenon in order to understand the phase behavior of block copolymers and to determine T_{ODT} values when accessible.

2.6.1 Isothermal Frequency Sweep

In this technique, the sinusoidal frequency is continuously varied at fixed temperature and strain amplitude, yielding the functions $G'(\omega)$ and $G''(\omega)$. Time temperature superposition (TTS) is used to horizontally shift and superpose rheological data obtained at different temperatures to obtain a master curve of $G'(\omega)$ and $G''(\omega)$ at a reference temperature. Below ω_c, the response will be different if the material is ordered or disordered. When disordered, polymers behave like liquids with $G' \sim \omega^2$ and $G'' \sim \omega^1$ as chains can completely relax. When ordered, the moduli dependence on ω in the low frequency or terminal regime changes.

As shown in Figure 2.8, the following dependences have been reported: $G' \sim G'' \sim \omega^{1/2}$ for lamellar samples,[21] $G' \sim G'' \sim \omega^{1/3}$ for hexagonally packed cylinders,[22], and $G' \sim G'' \sim \omega^{0}$ or solid like behavior for cubic phases.[21] This type of rheological characterization of morphology is not nearly as reliable as scattering or electron microscopy data. However, a master curve can be used to determine the T_{ODT} by detecting the temperature in the low frequency range at which the slope changes.

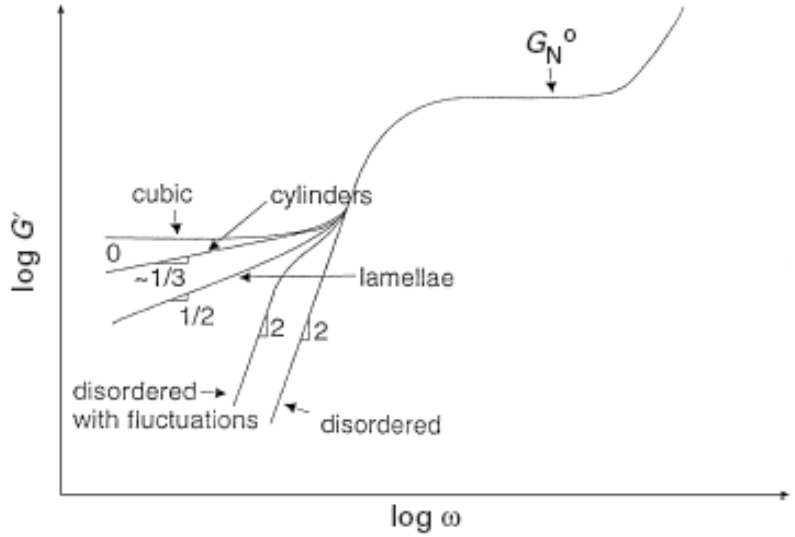

Figure 2.8: Schematic of time-temperature superposition (TTS) of dynamic elastic data showing the possible shapes for block copolymers in ordered and disordered states. Reproduced from Kossuth *et al.*[23]

An example of the detection of an approximate T_{ODT} is presented in Figure 2.9, which shows the mastercurve of G' for CPC-1, with $f_C \approx 0.18$ and $M_n \approx 90$ kg/mol. Temperatures were shifted to match the high frequency behavior at 145 °C. The low frequency response of G' shifts from $G' \sim \omega^{0.25}$ at T < 165 °C indicative of order to $G' \sim \omega^{2}$ for T > 175 °C indicative of disorder. This means the material has a

$T_{ODT} \approx 165 - 175$ °C. An isochronal temperature sweep is able to detect T_{ODT} more precisely, as shown next. .

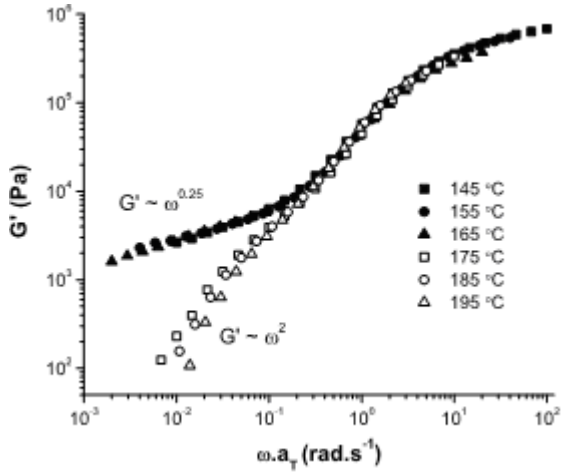

Figure 2.9: Superposition of G' versus reduced frequency, ωa_T, from isothermal frequency sweeps with T_{REF} = 145 °C for CPC-1 at 1% strain.

2.6.2 Isochronal Temperature Sweep

In this experiment, *G*' and *G''* are measured as the temperature is changed at a fixed rate and the sample is sheared at a small strain amplitude (linear viscoelastic regime) and in the terminal regime (low enough frequency). Block copolymer phase transformations, such as order-disorder and order-order transitions, result in sharp changes in response.[24] Most notably, a T_{ODT} is associated with a discontinuous drop in G' upon heating. This method has been supported by SANS and SAXS measurements.[21,25]

Figure 2.10 shows a temperature sweep for a material with $T_{ODT} \approx 210$ °C, where G' falls sharply upon heating. Cooling causes the modulus to sharply increase but at a slightly lower temperature. This hysteresis stems from the difference between

the nearly barrier-free disordering process versus ordering which is dependent on nucleation and growth kinetics.[26,27]

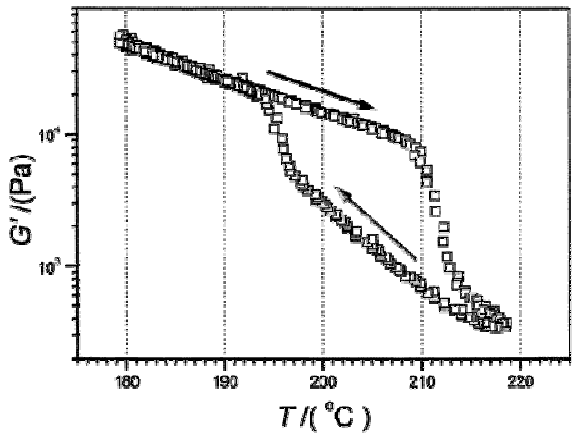

Figure 2.10: A typical isochronal temperature sweep used to determine T_{ODT} in block copolymer melts. Note the sudden drop in the modulus at T_{ODT}. Reproduced from Vigild *et al*.[24]

This technique was able to precisely detect a T_{ODT} = 168 °C for CPC-1 by heating the sample at a low rate and frequency, as illustrated in Figure 2.11. A diffuse T_g (C), undetectable by DSC, is observed at around 125 °C as G' drops.

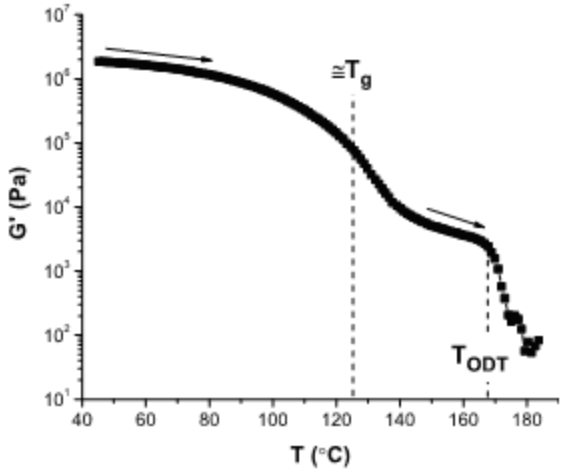

Figure 2.11: Temperature sweep at 0.1 rad/s, 0.5 °C/min and 1% strain for CPC-1. A T_{ODT} of 168 °C produces a change a discontinuity and T_g for C at around 125 °C is indicated by the decline in G'.

In general, in this project a Rheometrics Scientific ARES rheometer equipped with 25 or 8 mm diameter parallel plates was used to determine the elastic, G', and viscous, G'', dynamic moduli over the frequency range $0.01 \leq \omega \leq 100$ rad/s. All measurements were conducted at a strain of 1%, within the linear viscoelastic regime. Both types of tests described above, isothermal frequency sweeps and isochronal temperature sweeps, were used to probe the order-disorder transition at fixed heating or cooling rates of between 0.5 – 2 °C/min.

2.7 Large Amplitude Oscillatory Shear (LAOS)

Large Amplitude Oscillatory Shear (LAOS) is a technique that has been widely used to produce macroscopically aligned block copolymers.[28-31] In this project, a modified version of the reciprocating shear device built by Koppi[32] has been employed. The shearing device consists of channel cut aluminum plates with anodized rails. The aluminum plates are mounted on a slider, which is moved by a motor. The shear rate is given by the ratio between the velocity of the slider and sample thickness. The shearing procedure is carried out under Ar to prevent sample degradation. Figure 2.12 shows the coordinate system used to describe alignment.

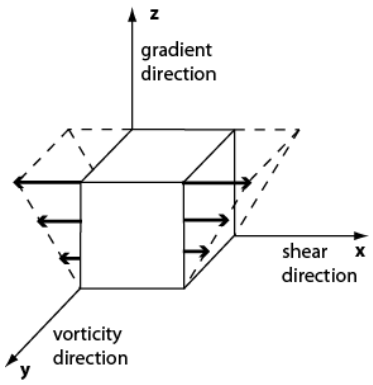

Figure 2.12: Diagram of coordinate system with shear direction (x-axis), vorticity direction (y-axis) and shear gradient direction (z-axis).

Shearing was done for 1 – 3 h, at a shear rate of 0.5 s^{-1} and a strain amplitude of 200% for all experiments. Samples were heated to T_{ODT} + 10 °C and held for about 10 min to anneal. Then, they were cooled down to about T_{ODT} - 30 °C, and once the temperature was equilibrated, shearing was started. This procedure has been described before and is called *shear from order*.[29] For this work, shear alignment has been used for several polymers mostly as a way to induce higher long range order. This may result in better scattering contrast and thus assist us in understanding morphology. Several samples were successfully aligned to produce more defined SAXS patterns, especially for cylinder forming polymers. For both lamellae and cylinders, the orientations are designated as parallel, perpendicular and transverse, as indicated in Figure 2.12(a) for lamellae and in Figure 2.12(b) for cylinders.

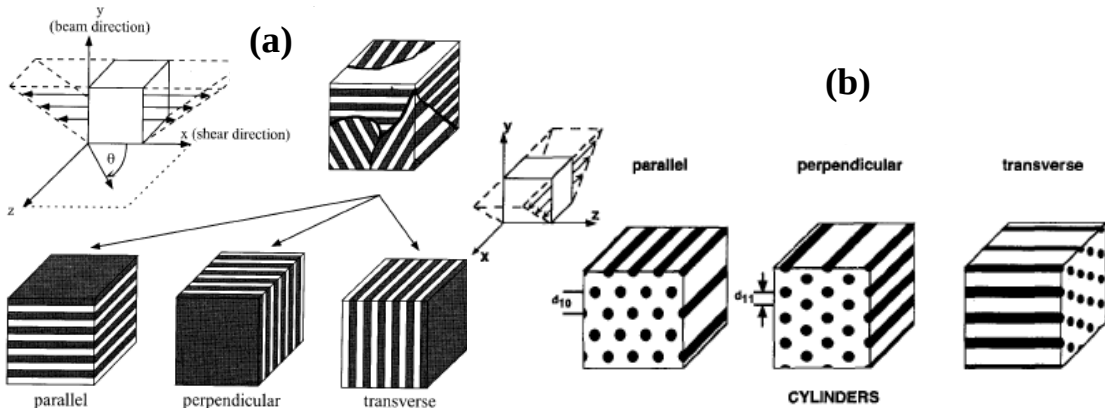

Figure 2.13: Illustration of three possible orthogonal orientations for (a) lamellar morphology, reproduced from Tepe *et al.*,[33] and (b) cylinder morphology, reproduced from Fredrickson and Bates.[34]

Figure 2.14(a) shows a 2D SAXS pattern for a shear aligned sample of CPC-2, with f_C = 0.30 and M_n = 47 kg/mol taken with the bam along the x shear direction. It shows a hexagonal arrangement characteristic of hexagonally packed cylinders

aligned along the shear direction, or in the parallel conformation (Figure 2.13(b)). This is in agreement with the expected morphology given the material's composition and molecular weight. By aligning this cylindrical morphology, contrast is improved for the 1D integration which is shown in Figure 2.14(b) which exhibits peaks at the expected positions for cylinders. The following section expands on SAXS and its use for morphology characterization.

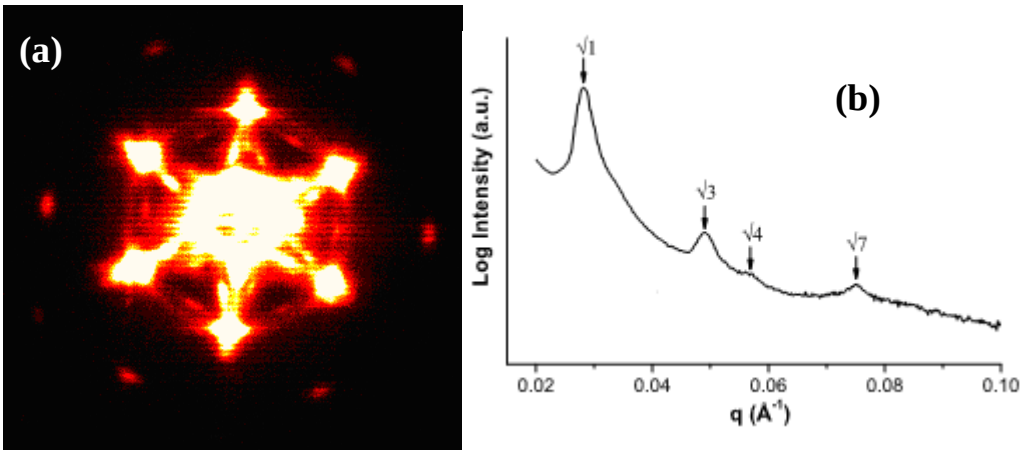

Figure 2.14: (a) 2D SAXS pattern in the shear direction for shear aligned CPC-2 at 150 °C and (b) 1D SAXS integrated data from (a). Arrows indicate peak positions, which suggest a hexagonally-packed cylindrical morphology.

2.8 Small Angle X-Ray (SAXS)

Light scattering experiments of polymer solutions are used to measure the weight average molecular weight M_W and radius of gyration R_g. In order to obtain information about morphology, smaller wavelength radiation sources such as X-rays and thermal neutrons are used.[9] Although X-ray and neutron scattering are based on the same physical principle, the origin of scattering is different. X-rays are scattered due to electron density differences, while neutron scattering occurs from the nuclei of

the samples. Small Angle X-ray Scattering (SAXS) was primarily used in this project to characterize the morphological structure of our block copolymers

It is a well-known phenomenon that wave-like particles interact with matter, causing a portion of the radiation to be scattered from the incident beam. Scattering may be classified as elastic or inelastic. In elastic scattering, only the direction of the particle's momentum is changed, or equivalently the wavelength of the incident and scattered beam are the same. The usual elastic scattering experiment involves shooting a well-collimated beam of monochromatic x-rays through a thin sample, where "thin" means that the sample should be much thinner than the scattering mean-free-path of the scattered radiation. Elastic scattering from a single object is illustrated in Figure 2.15.

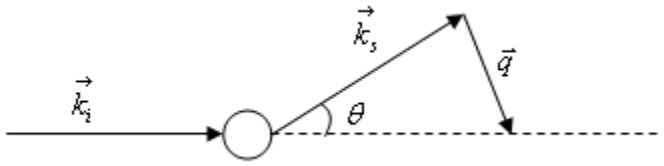

Figure 2.15: Elastic scattering from a single scattering object

The incident and scattering wavevectors are denoted $\vec{k}_i$ and $\vec{k}_s$, with equal magnitudes $2\pi/\lambda$, since this is an elastic event, and with directions at a scattering angle θ. The scattering vector $\vec{q}$ is defined as the difference between the incident and scattered wavevectors, $\vec{q} = \vec{k}_i - \vec{k}_s$. After some trigonometry, it is apparent that the magnitude of the scattering vector is given by the expression below.

$$|\vec{q}| = \frac{4\pi}{\lambda}\sin\left(\frac{\theta}{2}\right) \qquad (2.21)$$

We can relate this to the theory presented by Bragg for a bulk sample, with a series of scattering planes instead of just one scattering object, as shown in Figure 2.16. In SAXS experiments, the scattering planes are high electron density planes. In this case, the effective scattering intensity is the sum of the intensities from each plane.

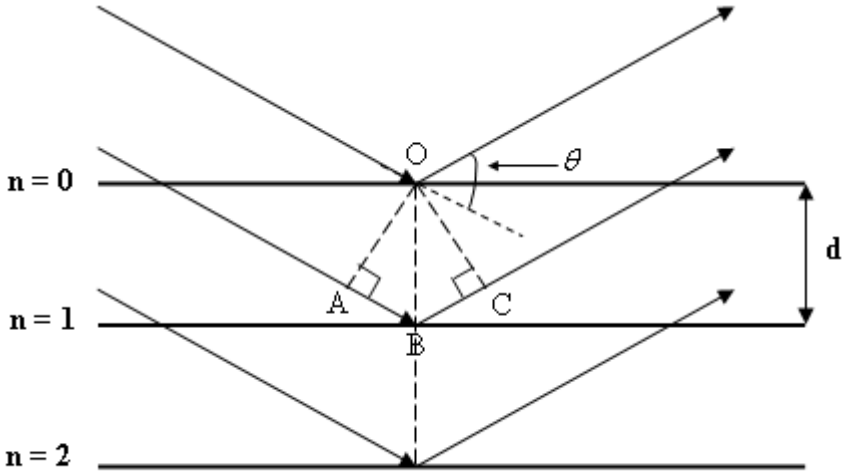

Figure 2.16: Scattering from a series of planes from Bragg's law

The basic idea is that the scattered waves will constructively interfere, and thus produce a diffraction spot, only when they are in phase with each other. In other words, the difference in the path lengths covered by the two rays must be an integral multiple of the radiation wavelength λ. In Figure 2.16, the extra distance traveled by the ray scattered from the first plane relative to the second plane is $\overline{AB} + \overline{BC}$. Thus, we can express the condition for constructive interference by the expression below, where n is an integer number.

$$\overline{AB} + \overline{BC} = n\lambda \qquad (2.22)$$

At the same time, the following relationship for $\overline{AB} + \overline{BC}$ can be derived from a geometrical analysis of Figure 2.16.

$$\hat{AOB} = \hat{BOC} = \frac{\theta}{2} \Rightarrow \overline{AB} + \overline{BC} = 2d \sin\frac{\theta}{2} \qquad (2.23)$$

Thus, the right sides of equation 2.22 and 2.23 are equal, and this gives us Bragg's Law, as expressed in the relationship below. Bragg's Law provides a physical representation of elastic scattering, stating that given a particular wavelength λ and structure of matter with interplanar distance *d*, scattering intensity will only be detected at certain θ values.

$$2d \sin\frac{\theta}{2} = n\lambda \qquad (2.24)$$

Moreover, it establishes a relationship between the magnitude of the reciprocal-space-defined scattering vector $\vec{q}$, and the real-space structural dimension, d, as shown below. Also, from the above treatment, it is clear that the wavelength λ used should be of the same magnitude as ($d \sin\frac{\theta}{2}$). So, for block copolymers, where dimensions are in the nanometer scale, if we use *Cu-*K_α x-rays, for which λ = 1.54 Å, the angle of observation should be 5° or less.

$$\left|\vec{q}\right| = q = \frac{2\pi n}{d} \qquad (2.25)$$

For perfect crystals, a scattering experiment would yield sharp peaks at specific magnitudes of *q* or θ, given the rigid and long range arrangement of atoms. Moreover, different arrangements as described by space group symmetries, will

produce specific scattering patterns. For instance, certain reflection orders (order is indicated by value of n in Bragg's Law) will be forbidden. Similarly, because block copolymer morphologies can be identified with specific space group symmetries, each morphology will produce a characteristic scattering pattern. This is revealed by the ratios of scattering vectors corresponding to higher order peaks (n > 1) relative to the 1st order peak (q^*, n = 1). Some of the seen reflections for the most common block copolymer morphologies are listed in Table 2.3.[35]

Table 2.3: Reflections for block copolymer morphologies

Block copolymer morphology	q/q^*
Lamellae	1, 2, 3, 4, 5, 6, …
BCC spheres	$\sqrt{1}, \sqrt{2}, \sqrt{3}, \sqrt{4}, \sqrt{5}, \sqrt{6}, \ldots$
$Ia3d$ gyroid	$\sqrt{3}, \sqrt{4}, \sqrt{7}, \sqrt{8}, \sqrt{10}, \ldots$
$Pn3m$ hexagonal cylinders	$\sqrt{1}, \sqrt{3}, \sqrt{4}, \sqrt{7}, \sqrt{9}, \sqrt{12}, \ldots$

Contrary to single crystals, isotropic block copolymers, typically melt processed, contain a polydomain structure. Thus, peaks are less sharp and the scattered intensity does not exhibit azymuthal dependence unless the sample has developed long-range order through alignment, as shown in Figure 2. 17 for both cases. Consequently, in this project, Two dimensional scattering data were azimuthally integrated to obtain plots of intensity I versus scattering wavevector modulus q ($q = (4\pi/\lambda) \sin(\theta/2)$, where θ is the scattering angle) as can be seen in Figure 2.14.

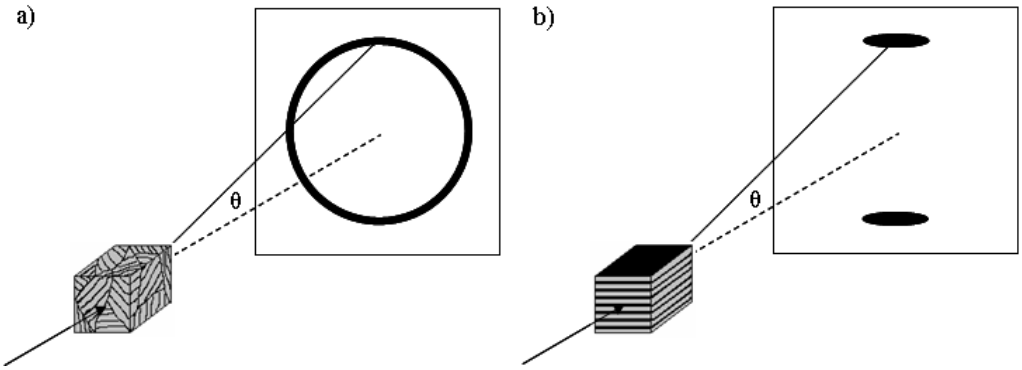

Figure 2. 17: Small angle x-ray scattering patterns for a) isotropic and b) aligned materials.

The discussion thus far assumed that block copolymers were in an ordered state, where morphologies are present, but the scattering of disordered polymer melts has also been the subject of much study. Chain dimensions in homogenous block copolymer melts are not affected by block-block interactions and follow Gaussian statistics.[36] However, the covalent connection between blocks and the incompressibility of the melt produce a fluctuating correlation between similar blocks of different chains in a length scale $d \sim R_g \sim N^{1/2}$. This gives rise to a so-called "correlation hole" peak in the scattering pattern at a q value such that $qR_g \approx 1$ whose intensity and narrowness increases with χ, as more segregation induces a more defined correlation or q value.[37-39]

Correlation hole has also been captured mathematically by an expression for the structure factor $S(q)$ of a disordered diblock copolymer shown below, where $F(x,f)$ is a function of the correlation functions of Gaussian chains dependent on $x = q^2R_g^2$ and composition f.

$$S(q) = \frac{N}{F(x, f) - 2\chi N} \qquad (2.29)$$

Figure 2.18 shows theoretically calculated scattering based on this expression of $S(q)$ versus $q^2R_g^2$ for a diblock with f = 0.25 for different χN values. The correlation hole peak becomes sharper and stronger with segregation strength.

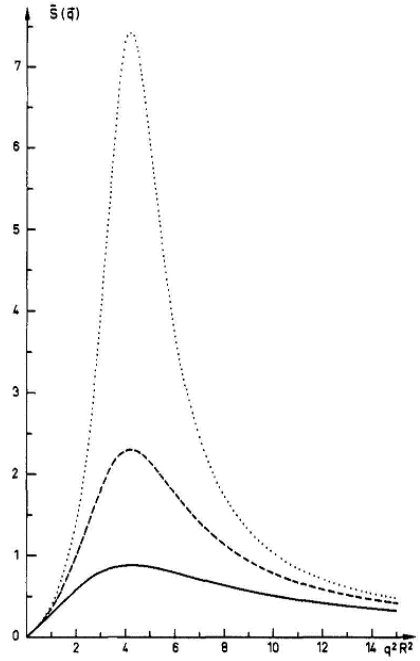

Figure 2.18: $S(q)$ versus $q^2R_g^2$ for diblock with f = 0.25 with χN values (—) 12.5 (--) 16.0 and (···) 17.5. Reproduced from Leibler.[38]

For large q, $qR_g >> 1$, $S(q)$ tends to 0 like $1/q^2$ and is independent of χ, as shown by the simplified expression below. This means that in the length scale of the entire polymer coils, Gaussian statistics dominate and the block correlations are unperturbed by repulsive interactions.

$$S(q) = \frac{2Nf(1-f)}{q^2R_g^2} \qquad (2.30)$$

At the other extreme, for $q \rightarrow 0$, $qR_g << 1$, $S(q)$ tends to 0 like q^2 and is again independent of χ, as indicated by the reduced equation below. At q = 0, scattering vanishes due to the incompressibility of the material. The power increase with q relates to correlation hole, as the probability of finding two A monomers from

different chains is reduced in this intermediate length regime because of the forced connection between A and B and the repulsion of polymer coils, not only due to χ but also because the material is incompressible.

$$S(q) = \frac{2Nf^2(1-f)^2 q^2 R_g^2}{3} \qquad (2.31)$$

The independence of correlation hole on χ is reinforced by that of the separate expressions for the asymptotic behaviors of $S(q)$. The scalings with q (direct and inverse) also imply that a maximum or peak exists in the intermediate range.

2.8.1 Procedure

SAXS experiments on the saturated block copolymers were conducted either at the University of Minnesota (Minneapolis, MN) or at Argonne National Laboratory (Argonne, IL) and this is indicated in each chapter where SAXS is presented. At the University of Minnesota, samples were run at the Institute of Technology Characterization Facility, with Cu K_α radiation from a Rigaku RU-200VBH rotating anode of wavelength λ = 0.1542 nm. The SAXS line is equipped with a Siemens area detector to collect two-dimensional diffraction data, with typical exposure times of between 3 to 5 minutes and area-to-detector distances of about 230 – 440 cm.

Synchrotron-source SAXS was performed at Argonne National Laboratory using the DuPont-Northwestern-Dow Collaborative Access Team (DND-CAT) facility with a beam wavelength of λ = 0.729 Å and a sample-to-detector distance of about 6.5 m. Calibration was achieved with silver behenate and data were collected on a Mar CCD area detector.

Experiments were performed on two types of samples. One was polydomain specimens that were molded at about 170 °C then cooled to room temperature. A second type were specimens molded in a similar fashion but then shear aligned before the SAXS experiments to improve the state of long-range. Alignment was achieved using the large amplitude reciprocating shear device described by Koppi and the procedure was explained in the previous section.[40]

2.9 Wide Angle X-ray Scatering (WAXS)

The previous section described the technique of Small Angle X-ray Scattering or SAXS, for which angles up to about 5° result in *q* values that are reciprocal to nanometer *d* spacings and thus can detect morphological structures. Wide Angle X-ray Scattering (WAXS) is based on the same principles described for SAXS but can detect scattering for angles up to 90°. This is used to elucidate structural information on the angstrom length scale, which is relevant to the crystallization of molecules. In this project, WAXS was used to probe the crystalline structure of the E block in the XPX polymers as these were subjected to controlled deformations.

Polyethylene molecules crystallize by folding into a lamellar structure, but only a fraction of monomers is included in the straight segments between folds and some of the polymer remains amorphous.[9] E's crystalline part has carbon atoms arranged in an orthorhombic unit cell, that is a parallelogram with 90° angles and three different lengths a, b and c. The structure factor confirms that there is systematic absence of peaks where h and k are mixed even and odd. Thus, the two lowest orders diffraction peaks are (110) and (200) and these are the ones we observe in our

experiments. Figure 2.19(a) shows 2D diffraction and Figure 2.19(b) shows the 1D azimuthally integrated plot for XPX-3, where an amorphous peak dominates the pattern but reflections (110) and (200) can be observed as sharp peaks off the main amorphous one.

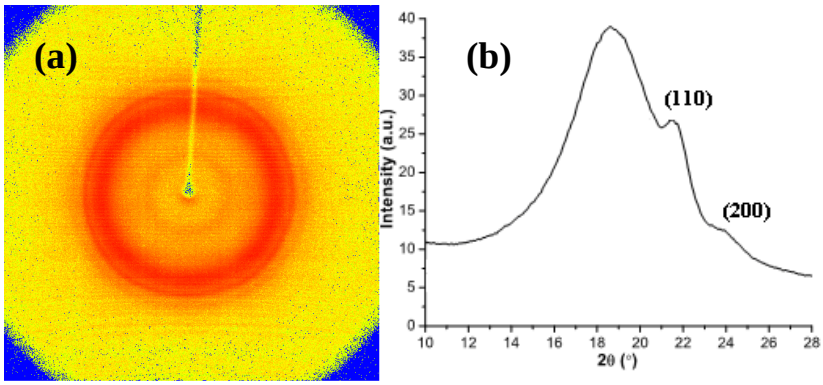

Figure 2.19: (a) 2D WAXS pattern and (b) 1D integration showing the amorphous scattering peak and the (110) and (200) peaks characteristic of polyethylene semicrystalline structure.

When the crystalline lamellae are aligned and diffraction is taken parallel to the lamellar faces, or along the c-axis, the (110) and (200) reflections appear as 4 and 2 spots, respectively, on the 2D pattern as shown in Figure 2.20 for an aligned lamellar CPEPC material.[41]

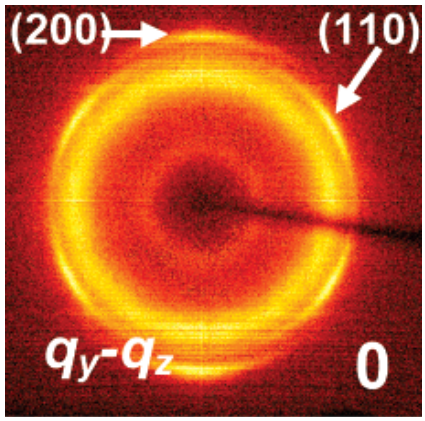

Figure 2.20: 2D WAXS for CPEPC-50 with $w_C \approx 0.44$, $w_E \approx 0.28$ and $w_P \approx 0.28$, with perpendicularly aligned lamellae of C and E/P and beam down the shear direction.Reproduced from Mahanthappa *et al.*[41]

When crystals are deformed, the lamellae break up and the molecules align in the deformation direction. This is reflected by the extinction of the (110) and (200) reflections and the formation of two spots perpendicular to the stretching direction on the 2D WAXS pattern, as shown in Figure 2.21(a) for undrawn XPX-3 and at 500% strain. This also produces two strong peaks in the 360° azymuthal integration and Figure 2.21(b) shows one of them in between angles 180-360° also for undrawn XPX-3 and at 500% strain. These types of patterns were collected in this work to monitor E deformation with XPX stretching.

Experiments were carried out at the Institute of Techonology's Characterization Facility at the University of Minnesota (Minneapolis, MN). Samples were stretched using the Minimat tensile tester (see next session) and the sample holder was fixed at a certain strain. The sample was then transferred and mounted with a specially fabricated holder that props the sample against the x-ray beam. 2D patterns were collected in transmission mode in a Bruker AXS Microdiffractometer at a distance of 5.92 cm. A 4XE short anode produced Cu Kα X-rays, which were monochromated with flat graphite and collimated through two 0.8 mm pinholes.

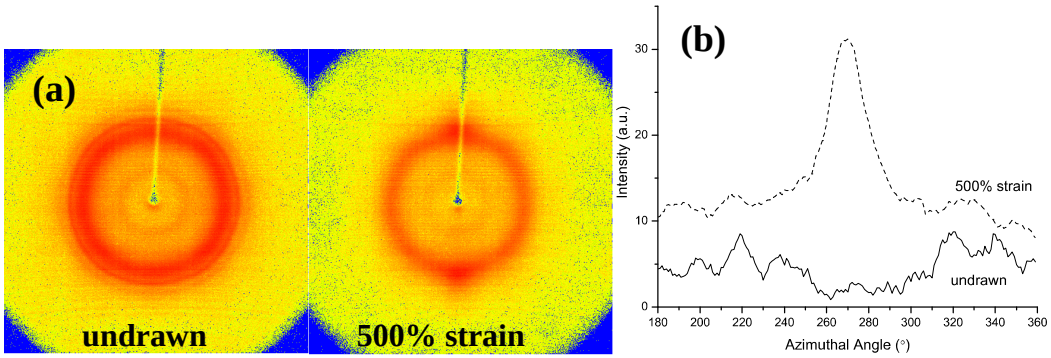

Figure 2.21: (a) 2D WAXS and (b) 1D azymuthal integrated patterns for undrawn XPX-3 (showing isotropic peaks) and at 500% strain (showing peak from crystal deformation).

2.10 Transmission Electron Microscopy (TEM)

TEM imaging is a powerful tool to obtain a real space picture of block copolymer structures. However, as it delivers a two dimensional image of a three dimensional arrangement, complementary techniques to assist in morphology determination should be used, as was SAXS in this project. TEM imaging is based on the collection of electrons after they interact with the atoms of a thin layer of material.[42] The most important type of interaction is electron scattering, which is highly dependent on the atomic number Z. Thus, images will present contrast that reflects the different atoms or chemical structures across the material.

To achieve this representation, nanometer scale thicknesses are of prime importance so that samples are electron transparent and show structural features along the surface. Also, image contrast is only observed for material containing high Z atoms. Because hydrogenated polymers consist of low electron density C and H atoms, little contrast can be observed between dissimilar polymers. To circumvent this issue, hydrogenated block copolymers are "stained" with high Z atom oxides, such as RuO_4 or OsO_4, which will preferentially diffuse into different type of monomers. Specifically, diffusion is best for rubbery polymers, then glassy ones and lastly through semicrystalline ones. Thus, rubbery polymer P will be stained heavily and greatly scatter electrons, appearing black on the image. On the other end, the crystalline areas of E, with the least free volume, will have negligible staining and appear white on the image. Glassy C has intermediate level of staining and thus will appear with a grey tone.

This tone grading was obtained for S-B-CL triblock copolymers developed by Balsamo *et al.*, where CL is semicrystalline poly(ε-caprolactone), stained with OsO_4.[43] Figure 2.22 shows a TEM image for S-B-CL with $f_S = 0.55$, $f_B = 0.30$, $f_{CL} = 0.15$ and $M_n = 137$ kg/mol, which shows core-shell cylinders of bright CL cores surrounded by a dark B shell in a matrix of S. For this image, the difference in tone between CL and S is not very clear, and this is the same issue encountered in this work to distinguish between E and C.

TEM experiments were performed on the XPX materials with a JEOL 1210 electron microscope in the bright field mode operating at 110 kV. Samples were cryo-microtomed at -120 °C with a diamond knife to produce a flat surface and subsequently stained with ruthenium oxide (RuO_4) for 4 h using reported procedures[44] to create contrast between chemically distinct domains. Stained samples were microtomed again at -120 °C and 70 – 100 nm thick specimens were collected for imaging.

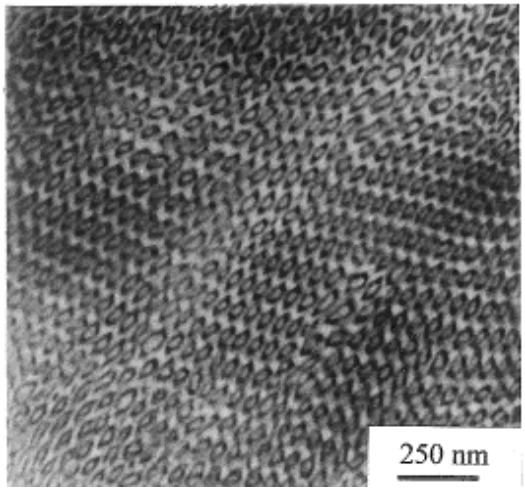

Figure 2.22: TEM of SBCL triblock copolymer shows core-shell cylinders of bright CL cores surrounded by a dark B shell in a matrix of S. Reproduced from Balsamo *et al.*[43]

2.11 Tensile Testing

In this project, mechanical properties are characterized through uniaxial tensile testing experiments and the resulting engineering stress versus nominal strain plots. Engineering stress, σ, is defined below in terms of force, F, and the specimen's initial cross sectional area, A_0.

$$\sigma = \frac{F}{A_0} \tag{2.32}$$

Nominal strain ε is calculated from the sample's displacement Δl defined in terms of final length l_f and original length l_0.

$$\varepsilon = \frac{l_f - l_0}{l_0} = \frac{\Delta l}{l_0} \tag{2.33}$$

Material properties are defined based on the shapes of the stress-strain curves and allow us to quantitatively compare mechanical responses. Figure 2.23 shows a representative stress-strain curve for CPC-2, similar to that of conventional thermoplastic elastomers, to illustrate the properties defined here. Some properties are defined for the low strain part of the curve. The slope of the curve in the linear elastic regime at low strains is defined as the elastic modulus E, given by the expression below. This is also shown in Figure 2.23 as the slope of the tangent line to the initial part of the curve, which is usually low for elastomeric systems E = 0.1 – 40 MPa.

$$E = \frac{\sigma}{\varepsilon} \tag{2.34}$$

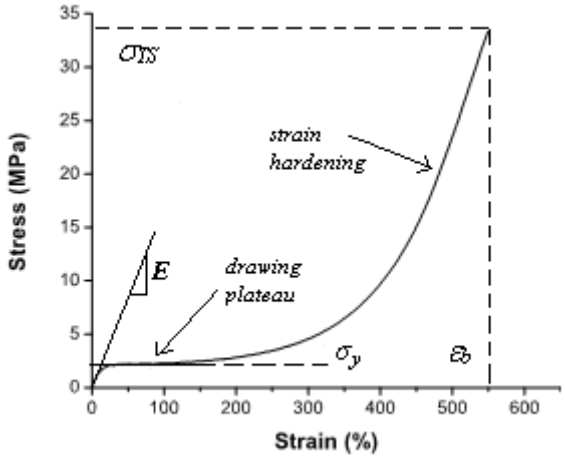

Figure 2.23: Representative stress-strain curve for CPC-2 with mechanical properties shown.

The stress at which the material is no longer elastic is the yield stress σ_y, which in Figure 2.23 is diffuse, as for most rubbery materials, and low $\sigma_y \approx 2$ MPa. After the yield point, materials usually go through irreversible deformation, either as plastic deformation or glass break up. Some materials may exhibit *necking* at yielding, indicated by a drop of stress and accompanied by narrowing of the sample cross section. However, since our materials are mostly elastomeric, this was not observed. The constant plateau after yielding is usually referred to as *drawing* and is typical of semicrystalline and rubbery materials as it involves high deformation at a constant stress (mostly reversible for rubbers and irreversible for crystals).

On the other end, ultimate mechanical properties apply to the large strain regime. Materials may exhibit *strain hardening*, especially rubbery ones, which is an increase in stress at the end of their elongation. This is usually due to an increased resistance to deformation with molecular alignment. The stress and strain at which the sample breaks determines ultimate tensile strength σ_{TS} and strain at break ε_b,

respectively. Both of these are usually high for thermoplastic elastomers as shown in Figure 2.23, where $\sigma_{TS} \approx 34$ MPa and $\varepsilon_b \approx 550\%$.

The quantitative parameters defined above give rise to qualitative descriptions of mechanical behavior. For example, higher modulus and yield stress are associated with the property of *stiffness*. Materials with high σ_{TS} are described as *strong* while those with high ε_b are said to achieve high *elongation* or *extensibility*. A material's *toughness*, or energy to break per volume, is determined by the area under the stress-strain curve. Increasing either the strength or the elongation of a material would result in an increase in toughness.

In this project, samples were drawn in tension up to the point of failure in a Rheometrics Scientific MINIMAT uniaxial tensile testing instrument fitted with a 200 N load cell. A picture with a top view of the instrument with information on dimensions is shown in Figure 2.24. All experiments were conducted at room temperature and at a constant rate of 200% strain per minute. Rectangular bars 11 mm long, 2 – 3 mm wide, and 0.8 – 1.2 mm thick were cut from pressed samples at T ≈ 170 °C, with a 5 – 7 mm gauge length (l_o) and a 2 – 3 mm^2 initial cross-sectional area (A_o). This geometry is the best one to avoid slipping and easily set up the sample in the instrument so that it can be stretched to high strains. The data reported here represent values averaged over at least 5 specimens tested per material. Appendix B presents all tensile curves for each material while Chapters 3, 4 and 5 show a representative curve for each material.

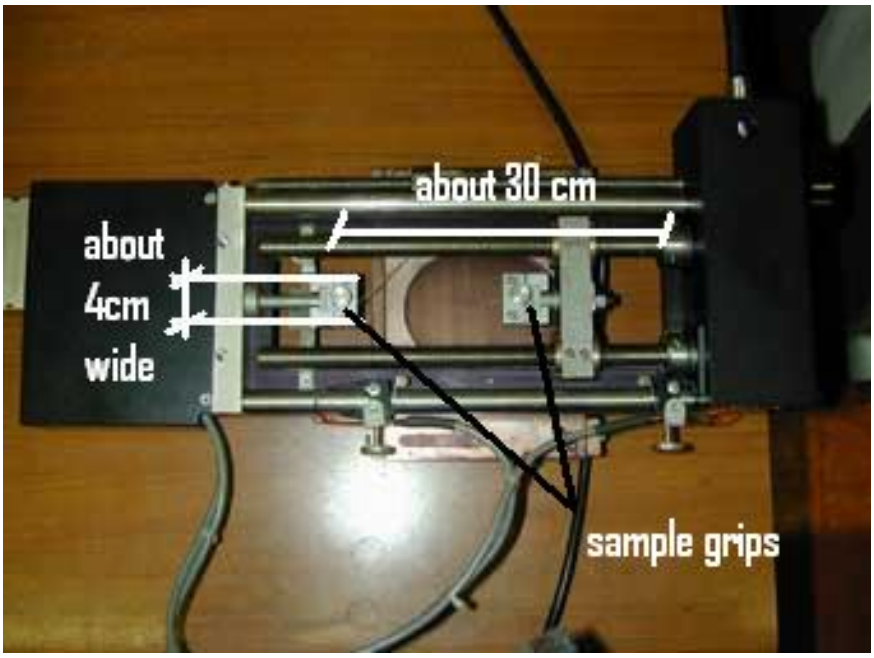

Figure 2.24: Top view of Minimat Uniaxial Tensile Tester.

2.12 Recovery Testing

In this project, strain recovery, or the capacity of the materials to recover from deformation was also studied. For all the materials in this project, the property defined as tension set ε_s (also sometimes called tensile set or permanent set) was measured. ε_s is the remaining strain after the material has failed and is calculated as (Final Gauge Length – l_o)/ l_o * 100. Tensile set provides an overall description of recoverability. In addition, selected materials were subjected to two types of cyclic extension-compression tests. These were also conducted with the same conditions (instrument, temperature, strain rate and geometry) as tensile testing. Figure 2.25 presents an example from each of these tests for CPC-2.

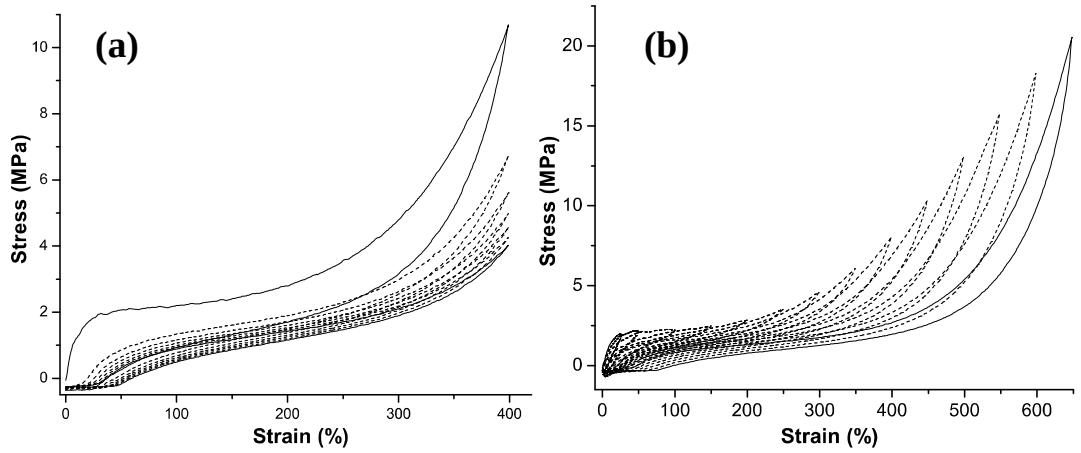

Figure 2.25: Cyclic tests for CPC-2 with (a) seven cycles up to 400% strain and (b) cycles of increasing strain up to failure. Residual strain, or the strain remaining at zero stress after compression, is recorded after each cycle.

The first type of test (Figure 2.25(a)) involved deformation in a series of seven cycles, each including application of a 400% strain followed by a return back to 0% strain. For this test, the property residual strain was defined as the strain remaining at zero stress following a sequence of extension and compression, and thus can be determined for each of the seven cycles. At least three specimens of each material were tested in this manner and each residual strain reflects the average of these three. Residual strain from this test is similar to tensile set in that it provides a quantity related to the large strain recovery. However, it is much more accurate than tensile set and it also sheds light on the material's resilience to deformation with constant cycling.

The second type of recovery test (Figure 2.25(b)) consisted of cycles of deformation, just like for the first test, but instead of up to a constant strain, each cycle imparted an increasing strain on the material. The fist strain was 25%, then 50%, 100% and so on in increments of 50% up to failure. Residual strain was once

again recorded after each cycle of deformation. Only one sample was run for this test as accuracy is not as important. Instead, the idea behind this tests is to look into how residual strain is generally dependent on deformation, which allows us to detect the strain at which the material becomes irrecoverable as opposed to the specific cycle.

2.13 References

[1] Flory, P. J. *J. Am. Chem. Soc.* **1940**, *62*, 1561-1565.

[2] Hsieh, H. I.; Quirk, R. P. *Anionic Polymerization: Principles and Practical Applications*; Marcel Dekker, Inc.: New York, 1996.

[3] Jones, T. *PhD Dissertation*, University of Minnesota **2000.**

[4] Perrin, D. D.; Armarego, W. L. F. *Purification of Laboratory Chemicals*, 3rd ed.; Permagon Press, 1988.

[5] Hucul, D. A.; Hahn, S. F. *Adv. Mater.* **2000**, *12*, 1855-1858.

[6] Hucul, D. A.: US Patent 6,399,538, 2000.

[7] Gehlsen, M. D.; Bates, F. S. *Macromolecules* **1993**, *26*, 4122-4127.

[8] Gehlsen, M. D.; Weimann, P. A.; Bates, F. S.; Harville, S.; Mays, J. W.; Wignall, G. D. *J. Polym. Sci. B* **1995**, *33*, 1527-1536.

[9] Hiemenz, P.C.; Lodge, T.P. *Polymer Chemistry*, 2nd ed.; CRC Press: Boca Raton, FL, 2007.

[10] Young, R. J.; Lovell, P. A. *Introduction to Polymers*, 2nd ed.; Stanley Thornes (Publishers) Ltd, 1991.

[11] Hillmyer, M. A.; Bates, F. S. *Macromolecules* **1996**, *29*, 6994-7002.

[12] Schmidt, S. C.; Hillmyer, M. A. *Macromolecules* **1999**, *32*, 4794-4801.

[13] Bailey, T. S. *Ph.D. Dissertation*; University of Minnesota: Minneapolis **2001**.

[14] Fetters, L. J.; Lohse, D. J.; Richter, D.; Witten, T. A.; Zirkel, A. *Macromolecules* **1994,** *27*, 4639-4647.

---

[15] Hiemenz, P.C.; Lodge, T.P. *Polymer Chemistry*, 2nd ed.; CRC Press: Boca Raton, FL, 2007; p 476.

[16] Brandrup, J.; Immergut, E. H., *Polymer Handbook*, 3rd ed.; John Wiley & Sons: New York, 1989.

[17] Macosko, C. W. *Rheology: Principles, Measurements and Applications;* Advances in Interfacial Engineering; Wiley-VCH: New York, 1994.

[18] Chung, C. I.; Gale, J. C. *J. Polym. Sci. B* **1976**, *14*, 1149-1156.

[19] Chung, C. I.; Lin, M. I. *J. Polym. Sci. B* **1978**, *16*, 545-553.

[20] Gouinlock, E. V.; Porter, R. S. *Polymer Engineering and Science* **1977**, *17*, 535-543

[21] Rosedale, J. H.; Bates, F. S.; Almdal, K.; Moretensen, K.; Wignall, G. D. *Macromolecules* **1995**, *28*, 1429-1443.

[22] Ryu, C. Y.; Lee, M. S.; Hajduk, D. A.; Lodge, T. P. *J. Poly. Sci. B* **1997**, *35*, 2811-2823.

[23] Kossuth, M. B.; Morse, D. C.; Bates, F. S. *Journal of Rheology* **1999**, *43*, 167-196.

[24] Vigild, M. E.; Chu, C.; Sugiyama, M.; Chaffin, K. A.; Bates, F. S. *Macromolecules* **2001**, *34*, 2533-2539.

[25] Winter, H. H.; Scott, D. B.; Gronski, W.; Okamoto, S.; Hashimoto, T. *Macromolecules* **1993**, *26*, 7236-7244.

[26] Morrison, F. A.; Winter, H. H.; Gronski, W.; Barnes, J. D. *Macromolecules* **1990**, *23*, 4200-4205.

[27] Ryu, C. Y.; Lee, M. S.; Hajduk, D. A.; Lodge, T. P. *J. Polym. Sci. Part B* **1997**, *35*, 2811-2823.

[28] Hadziioannou, G.; Mathis, A.; Skoulios, A. *Colloid and Polymer Sci.* **1979**, *257*, 136-139.

[29] Hermel, T. J.; Wu, L.; Hahn, S. F.; Lodge, T. P.; Bates, F. S. *Macromolecules* **2002**, *35*, 4685-4689.

[30] Koppi, K. A.; Tirrell, M.; Bates, F. S.; Almdal, K.; Colby, R. H. *J. Phys. II France* **1992**, *2*, 1941-1959.

---

[31] Tepe, T.; Hajduk, D. A.; Hillmyer, M. A.; Weimann, P. A.; Tirrell, M.; Bates, F. S.; Almdal, K.; Mortensen, K. *J. Rheol.* **1997**, *41*, 1147-1171.

[32] Koppi, K. A. *Ph.D. Dissertation*; University of Minnesota: Minneapolis **1993**.

[33] Tepe, T.; Hajduk, D. A.; Hillmyer, M. A.; Weimann, P. A.; Tirrell, M.; Bates, F. S.; Almdal, K.; Mortensen, K. *Journal of Rheology (New York)* **1997**, *41*, 1147-1171.

[34] Fredrickson, G. H.; Bates, F. S. *Annual Review of Materials Science* **1996**, *26*, 501-550.

[35] Hahn, T., Ed.; *International Tables for X-ray Crystallography;* Kluwer Academic Publishers: Boston, MA, 1992.

[36] Bates, F. S.; Fredrickson, G. H. *Annu. Rev. Phys. Chem.* **1990**, *41*, 525-557.

[37] Bates, F. S. *Macrmolecules* **1980**, *18*, 525-528.

[38] Leibler, L. *Macromolecules* **1980**, *13*, 1602-1617

[39] De Gennes, P. G. J. Phys. (Paris) **1970**, *31*, 235-238

[40] Koppi, K. A. *Ph.D. Dissertation*, University of Minnesota **1993**.

[41] Mahanthappa, M. K., Hillmyer, M. A., Bates, F. S. *Macromolecules* **2008**, *41*, 1341-1351.

[42] Williams, D. B. & Cater, C. B. *Transmission Electron Microscopy: Basics;* Plenum: New York, 1996.

[43] Balsamo, V.; Gil, G.; Urvina de Navarro, C.; Hamley, I. W.; von Gyldenfeldt, F.; Abetz, V.; Cañizales, E. *Macromolecules* **2003,** *36*, 4515-4525.

[44] Khandpur, A. K.; Macosko, C. W.; Bates, F. S. *Journal of Polymer Science Part B-Polymer Physics* **1995,** *33*, (2), 247-252.

3

Heptablock Terpolymers Structured by Crystallization as Novel Thermoplastic Elastomers*

3.1 Introduction

Block copolymers (BCPs) containing a matrix of rubbery blocks, anchored on both ends to thermodynamically incompatible and hard (glassy or semi-crystalline) blocks, are generally referred to as thermoplastic elastomers (TPEs).[1,2] Poly(styrene-*b*-isoprene-*b*-styrene) (SIS) triblock copolymers are the most familiar commercial products that fall into this category. Two temperatures control the properties and processing of these materials. Above the hard block glass transition temperature ($T_{g,S}$ ≈ 100 °C) the material softens and can be deformed irreversibly; in this temperature range the rheological properties are dominated by the microphase structure. Further heating the material can lead to a state of disorder and liquid-like rheological properties. However, the point at which this transition occurs, known as the order-disorder transition temperature (T_{ODT}), is directly dependent on the overall molecular weight for a given composition; increasing the molecular weight increases T_{ODT}.[3] Many applications of TPEs require tuning molecular weight to processing requirements that favor a low T_{ODT} (i.e., low processing temperature) in order to minimize polymer degradation and equipment needs. Choosing different block types

* This work is reproduced in part from: Alfonzo, C. G.; Fleury, G.; Chaffin, K. A.; Bates, F. S. *Macromolecules* **2010**, *43*, 5295-5305.

(e.g., hydrogenated poly(butadiene) instead of poly(isoprene)) necessitates a reevaluation of their impact on room temperature properties and processing, each dependent on the molecular weight. This publication describes a new approach to designing thermoplastic elastomers that decouples T_{ODT} from the overall block copolymer molecular weight.

Microphase separation of thermodynamically compatible block copolymers also can be induced by crystallization.[4-11] In this situation the transition from a state of microphase separation to disorder is determined by the crystal melting temperature (T_m) and does not depend on the block copolymer molecular weight. Several groups have demonstrated this effect, including Hotta *et al.*[10], who reported on poly(propylene)-based BPCs containing amorphous and rubbery mid-blocks and semicrystalline end-blocks, and Koo *et al.* who developed EPE triblock[8] and $(EP)_n$ multiblock copolymers,[9] where E is semicrystalline poly(ethylene) and P is rubbery poly(ethylene-*alt*-propylene). The $(EP)_n$ materials, which are produced by hydrogenating anionically polymerized poly(1,4-butadiene-*b*-1,4-isoprene)$_n$ multiblock copolymers, are characterized by a small Flory-Huggins χ parameter. Below a threshold block molecular weight ($M = M_E = M_P < 50$ kg/mol) these materials are disordered above T_m(E). Microphase separation is induced by crystallization upon cooling the homogeneous melt. Due to a finite, albeit small, segment-segment interaction parameter, increasing M above the critical value leads to ordering in the melt state. Koo et al. demonstrated two limiting types of mechanical properties in these block copolymers at room temperature. Crystallization induced segregation results in relatively weak materials with tensile strengths $\sigma_{TS} \leq 10$ MPa

(also reported for the poly(propylene) systems by Hotta et al.) while cooling and crystallizing higher molecular weight ($n > 8$) $(EP)_n$ polymers led to $\sigma_{TS} \approx 20 - 30$ MPa. The authors reasoned that these results could be traced to the orientation and inherent strength of the E crystals within the melt ordered morphologies and the reinforcing effect created by a large number of blocks even in the case of melt disorder. Thus, for crystalline and rubber block copolymers, crystallization-induced segregation tends to produce mechanically weak materials unless they are constructed with many blocks, which is often impractical. Also, regardless of the segregation mechanism, high strength values are only achieved with high volume fractions of E (> 50%), which compromises the low strain elastic response and results in significant irreversible plastic deformation.[11-14]

Another recently reported strategy for tailoring the mechanical properties of polyolefin block copolymers is to combine three basic physical states - rubbery, glassy and semi-crystalline - in a multiblock copolymer architecture. Mahanthappa et al.[14,15] produced CPEPC pentablock copolymers containing 40% by volume of glassy C, or poly(cyclohexylethylene), derived from hydrogenating polystyrene, and varying proportions of semicrystalline E and rubbery P. Despite relatively low overall molecular weights (30 to 40 kg/mol) these saturated terpolymers micro-phase separate into a lamellar structure at elevated temperatures, which is preserved upon cooling below $T_g(C) \approx 147$ °C, and subsequent crystallization of the E domains below 90 °C. These composite materials exhibit tensile strengths between 25 and 38 MPa accompanied by an elastic modulus intermediate to a rubber and plastic ($E \approx 50 - 100$ MPa). Balsamo et al.[16,17] and Schamlz et al.[13,18] have combined similar types of

monomers in producing ABC systems, where A is glassy, B is rubbery and C is semi-crystalline. These all have relatively high molecular weights (80 to 219 kg/mol) and are strongly segregated due to the chemical incompatibility between blocks. Although these polymers contain semicrystalline blocks, the ultimate processing conditions are governed by T_{ODT} which is coupled to the overall molecular weight.

Fleury and Bates[19] recently showed that an undecablock copolymer of the type CECEC-P-CECEC containing 50% P, 25% E and 25% C and a modest overall molecular weight of 87 kg/mol was disordered above the melting temperature of the E blocks. Yet this material displayed excellent elastic properties at room temperature (e.g., σ_{TS} = 32 MPa and a strain at break ε_b > 1,500%). This finding suggests that the synergistic combination of crystallization induced segregation and partial vitrification offers an attractive method of producing competitive thermoplastic elastomers that can be processed as homogeneous liquids at a temperature determined by the melting point of the semicrystalline blocks, i.e. independent of the overall molecular weight up to a limiting value.

This chapter expands on this idea, through an in-depth study of a basic hierarchical block copolymer architecture suitable for creating crystallization induced thermoplastic elastomers: CEC-P-CEC heptablock copolymers. Here we demonstrate that at modest molecular weights these multiblocks are homogenous (disordered) above about 100 °C, i.e. T_m of E, due to favorable mixing thermodynamics as defined by the three χ_{ij} parameters. Cooling below T_m(E) results in partial crystallization of E, which induces segregation and vitrification of C, leading to a class of microphase separated materials that have a common processing temperature, independent of

molecular weight for M ≤ 114 kg/mol. This combination of glassy (C) and semicrystalline (E) hard blocks results in thermoplastic elastomers with competitive strengths, and in certain limits excellent elastic recovery. Five CEC-P-CEC heptablock terpolymers were synthesized, each with equal volume fractions of C and E and between 40 and 60% P by volume. We have characterized the phase behavior of these specimens by differential scanning calorimetry (DSC) and dynamic mechanical spectroscopy (DMS), small angle x-ray scattering (SAXS) and transmission electron microscopy (TEM). The mechanical properties were measured in tension by simple extension and cyclic loading, and these results are compared with conventional CPC triblock copolymer elastomers prepared with similar C contents.

3.2 Experimental Section

Chapter 2 provided a comprehensive description of the techniques and procedures employed for all the materials analyzed in this project. This section presents the essential information regarding the procedures through which the materials of study in this chapter were synthesized and characterized.

3.2.1 Polymer Synthesis and Hydrogenation

Triblock copolymer CPC-1 was obtained from The Dow Chemical Company, while CPC-2 and the CEC-P-CEC heptablock copolymers were produced at the University of Minnesota. A SIS precursor triblock was synthesized by sequential living anionic polymerization of styrene (S) (Aldrich), isoprene (I) (Acros Organics)

and S in purified cyclohexane (Fischer Scientific) at 40 °C, initiated with *sec*-butyllithium (1.4M solution in cyclohexane, Aldrich), as described elsewhere.[20] For the heptablock copolymers, living SBS-I$^-$,Li$^+$ copolymers were prepared by sequential polymerization of S, butadiene (B) (Aldrich), S, and I as noted above and subsequently coupled using a stoichiometric amount of α,α'-dibromo-p-xylene (Aldrich) added in a dropwise fashion until solution became colorless (about 4 to 6 hours) to produce the precursor SBS-I-SBS materials. In all cases the overall fraction of S and B added to the reactor was held constant. An aliquot of the completed first S block was drawn after 8 hrs of reaction time and precipitated in degassed methanol (Aldrich) for further analysis.

SIS and SBS-I-SBS were hydrogenated to yield CPC and CEC-P-CEC, respectively. This was accomplished by reaction for 12 hrs over a Pt/Re catalyst supported on macroporous silica particles (Dow Chemical) in degassed cyclohexane at 170 °C under 500 psig of H_2.[21] Block copolymers were recovered from solution in all cases by precipitation in a 1:3 (volume ratio) mixture of isopropanol and methanol followed by drying at room temperature under vacuum to constant weight. We will refer to CEC-P-CEC as XPX based on the pseudo triblock geometry.

3.2.2 Molecular Characterization

Block copolymer compositions were determined from quantitative ^{1}H nuclear magnetic resonance (NMR) spectra collected on the unsaturated polymers in deuterated chloroform ($CDCl_3$) (99.8%, Aldrich) using a Varian Unity Inova 300 spectrometer. Monomer mole fractions were calculated by integrating resonances

associated with S, B and I repeat units; these values were then converted to volume fractions for the saturated compounds using the following published polymer densities at 140 °C [22]: ρ_C = 0.920 g/cm^3; ρ_E = 0.784 g/cm^3; ρ_P = 0.790 g/cm^3. These spectra also confirmed that the isoprene and butadiene polymerizations resulted in predominantly 1,4-monomer addition, with 6 – 8 mol % 4,3-I, and 10 – 12 mol % 1,2-B, respectively. ^{1}H NMR spectra were also recorded from the hydrogenated polymers in deuterated chloroform at room temperature for CPC and in deuterated toluene (C_7D_8) (99.6%, Aldrich) at 70 °C for XPX, to establish the extent of saturation for each polymer, which in every case was greater than 97%.

The number average molecular weight, $M_{n,S}$, of the first S block of each block copolymer and the molecular weight distribution (M_w/M_n), or polydispersity, of all polymers were determined by size exclusion chromatography (SEC). A Waters 717 GPC fitted with three Polymer Laboratories Mixed-C columns and operated at 30 °C with tetrahydrofuran (J.T. Baker) and calibrated with polystyrene standards was employed with the unsaturated polymers and with CPC. The saturated XPX polymers were characterized with a PL-GPC 220 system operated at 135 °C with 1,2,4-trichlorobenzene. Monomodal and relatively narrow distribution (M_w/M_n < 1.21) peaks were recorded in all cases. Saturated polymer molecular weights were calculated based on $M_{n,S}$ and the overall composition derived from the reaction stoichiometry and NMR results.

3.2.3 Dynamic Scanning Calorimetry (DSC)

Thermal transitions (glass transition and melting and crystallization temperatures) were determined using a TA Instruments Q1000 differential scanning calorimeter (DSC). Poly(ethylene) fractional crystallinity, X_c, was calculated using the expression $X_c = \Delta H_m / H°_{m,E} \times w_E$ where w_E is the weight fraction of E and $H°_{m,E}$ = 277 $J.g^{-1}$ is the theoretical heat of melting for the 100% crystalline poly(ethylene).[23] Samples were heated to 160 °C, cooled to -80 °C, and heated back to 160 °C, all at 10 °C/min.

3.2.4 Dynamic Mechanical Spectroscopy (DMS)

A Rheometrics Scientific ARES rheometer equipped with 25 or 8 mm diameter parallel plates was used to determine the elastic, G', and viscous, G'', dynamic moduli over the frequency range $0.01 \leq \omega \leq 100$ rad/s. All measurements were conducted at a strain of 1%, within the linear viscoelastic regime. Two types of tests were used to probe the order-disorder, melting and crystallization transitions: isothermal frequency sweeps and isochronal temperature sweeps at fixed heating or cooling rates of between 0.5 and 2 °C/min. [3,24]

3.2.5 Small Angle X-ray Scattering (SAXS)

Synchrotron-source SAXS was performed on the saturated block copolymers at Argonne National Laboratory (Argonne, IL) using the DuPont-Northwestern-Dow Collaborative Access Team (DND-CAT) facility with a beam wavelength of λ = 0.729 Å and a sample-to-detector distance of 6.53 m. Calibration was achieved with silver behenate and data were collected on a Mar CCD area detector. Experiments were performed on unaligned powder like XPX specimens that were molded at 170

°C then cooled to room temperature. XPX samples were heated to about 180 °C for 3 min to erase thermal history and then cooled at about 30 °C/min and held for 3 min at either 140 °C or 25 °C, where 2-D patterns were collected.

Laboratory source SAXS was performed at the Institute of Technology Characterization Facility at the University of Minnesota using Cu Kα X-rays from a Rigaku RU-200VBH rotating anode and a sample-to-detector distance of 4.41 m. CPC samples were shear aligned prior to the experiment to improve the state of long-range order and synchrotron SAXS data were collected at 25 °C for CPC-1 and laboratory SAXS data was collected at 150 °C for CPC-2 without any additional thermal treatment. Alignment of the cylindrical structures in the CPC copolymers was achieved using the large amplitude reciprocating shear device described by Koppi.[25] Compression molded samples 20 mm long by 10 mm wide by 1 mm thick were sheared under argon for about 2 h at T_{ODT} - 30 °C with a strain amplitude of 200% and a shear rate of 0.5 s^{-1}. Two dimensional scattering data were azimuthally integrated to obtain plots of intensity I versus scattering wavevector modulus q, ($q = (4\pi/\lambda) \sin(\theta/2)$, where θ is the scattering angle).

3.2.6 Transmission Electron Microscopy (TEM)

TEM experiments were performed at the Institute of Technology Characterization Facility at the University of Minnesota with a JEOL 1210 electron microscope in the bright field mode operating at 110 kV. Samples were cryo-microtomed at -120 °C with a diamond knife to produce a flat surface and subsequently stained with ruthenium oxide (RuO_4) for 4 hours using reported

procedures[26] to create contrast between chemically distinct domains. Stained samples were microtomed again at -120 °C and 70 – 100 nm thick specimens were collected for imaging.

3.2.7 Mechanical Testing

Samples were drawn in tension up to the point of failure in a Rheometrics Scientific MINIMAT uniaxial tensile testing instrument fitted with a 200 N load cell. All experiments were conducted at room temperature and at a constant rate of 200% strain per minute. Rectangular bars 11 mm long, 2 – 3 mm wide, and 0.8 – 1.2 mm thick were employed, with a 5 – 7 mm gauge length (l_o) and a 2 – 3 mm^2 initial cross-sectional area (A_o). This geometry is the best one to avoid slipping and easily set up the sample in the instrument so that it can be stretched to high strains. Engineering stress (σ) versus nominal strain (ε) curves were obtained from force (F) versus displacement (Δl) data, where $\sigma = F/A_o$ and $\varepsilon = \Delta l/l_o$. Young's modulus E was determined by fitting the linear regime of the stress-strain curve, below about 10% strain, with $\sigma = E \cdot \varepsilon$. The data reported here represent values averaged from at least 5 specimens tested per material.

Tension Set (%), ε_s, calculated as (Final Gauge Length – l_o)/ l_o * 100, was determined for each sample. Similar samples were used to run cyclic extension-compression tests at room temperature and at a rate of 200% strain/min. Seven cycles, each including application of a 400% strain followed by a return back to 0% strain, constituted a complete strain recovery experiment. Residual strain, reported for each cycle, is defined as the strain remaining at zero stress following a sequence of

extension and compression. At least three specimens of each material were tested in this manner.

3.2 Results and Analysis

3.2.1 Synthesis

Three types of CEC-P-CEC copolymers, abbreviated XPX and shown in Figure 3.1, were produced in this study, with C volume fractions f_C of 18%, 25% and 30% and similar corresponding volume fractions of E.

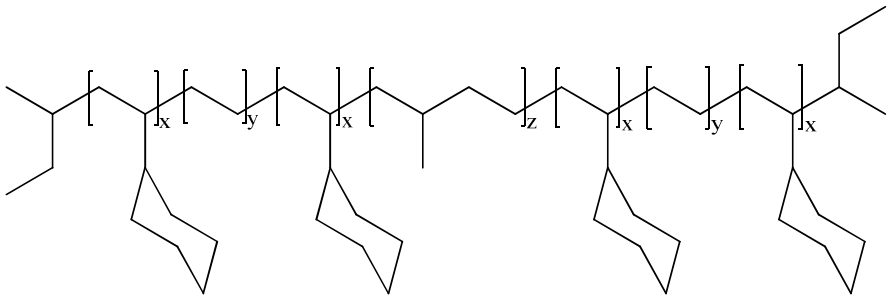

Figure 3.1: Molecular Structure of CEC-P-CEC Heptablock Copolymers

For $f_C \approx f_E \approx 25\%$, three materials were synthesized with molecular weights of 59, 79 and 114 kg/mol, in order to investigate the role of this parameter on properties. Two CPC materials with C volume fractions of 18% (obtained from Dow Chemical) and 30% (synthesized in our laboratory) were prepared for comparison. Table 3.1 summarizes the basic molecular characteristics of all block copolymers.

Table 3.1: Molecular characterization data for CPC and XPX copolymers

Sample	f_C	f_E	f_P	N [a]	M_n (kg/mol)	M_w/M_n [b]
CPC-1	0.18	0.00	0.82	1193	90.0	1.04
CPC-2	0.30	0.00	0.70	597	47.4	1.03
XPX-1	0.18	0.22	0.60	1450	103.4	1.11
XPX-2a	0.25	0.26	0.49	808	59.0	1.11
XPX-2b	0.25	0.26	0.49	1086	79.2	1.13
XPX-2c	0.25	0.26	0.49	1560	113.7	1.16
XPX-3	0.30	0.28	0.42	592	43.8	1.21

[a] Calculated using bulk homopolymer densities from Fetters et al.[22] with 118 $Å^3$ reference volume. [b] Determined for saturated CPC and for unsaturated precursors of XPX by SEC with PS standards in THF at 30 °C.

The final step in the polymerization of the SBS-I-SBS precursor copolymers was achieved by coupling "living" $SBSI^-,Li^+$ molecules. Figure 3.2 shows a size exclusion chromatograph (SEC) trace of the precursor materials associated with XPX-2b. Both the uncoupled ($SBSI^-$) and coupled (SBS-I-SBS) forms show monomodal molecular weight distributions with average molecular weights that differ by a factor of approximately two. A relatively small amount of uncoupled polymer is present in the coupled product. In all cases, at least 93% coupling was achieved through this reaction. Heptablock polydispersity indices are somewhat higher than those obtained with the CPC triblock which is attributed to the relatively slow addition of butadiene to poly(styryllithium). The molecular weight distribution was not affected by hydrogenation of the unsaturated heptablock copolymers.

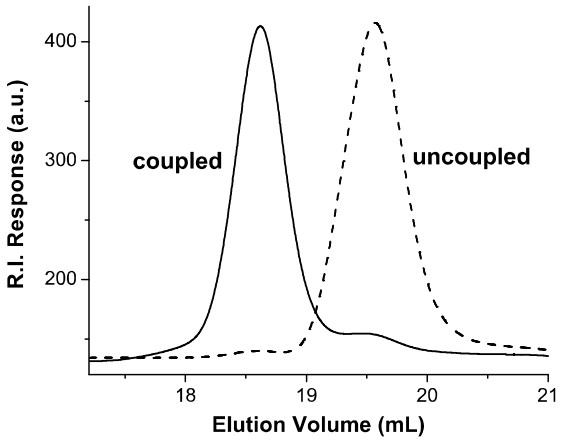

Figure 3.2: SEC trace for XPX-2b's precursor systems, in their uncoupled (SBSI) and coupled (SBS-I-SBS) forms, showing high coupling efficiency.

3.2.2 Thermal and Rheological Properties

DSC measurements provided information regarding the physical properties of the CPC and XPX materials. Figure 3.3 offers a comparison of the responses obtained from representative specimens, each containing 18% C (see Table 3.1). Evident in the thermal responses from CPC-1 (Figure 3.3a) and XPX-1 (Figure 3.3b) is a glass transition at -60 °C, which can be associated with the P domains.[27] We are not able to identify features in either DSC trace attributable to the glass transition of the C blocks; T_g for bulk C is about 147 °C. This may be a consequence of several factors. As shown below, XPX-1 is a homogeneous material above the E melting temperature $T_{m,E}$, hence there are no glassy domains above about 100 °C. While CPC-1 is microphase separated below 170 °C (see below), the combination of a minority of glassy domains (just 18%) and the proximity to T_{ODT} is most likely responsible for clearing any signature of T_g for C in the DSC trace from the material.

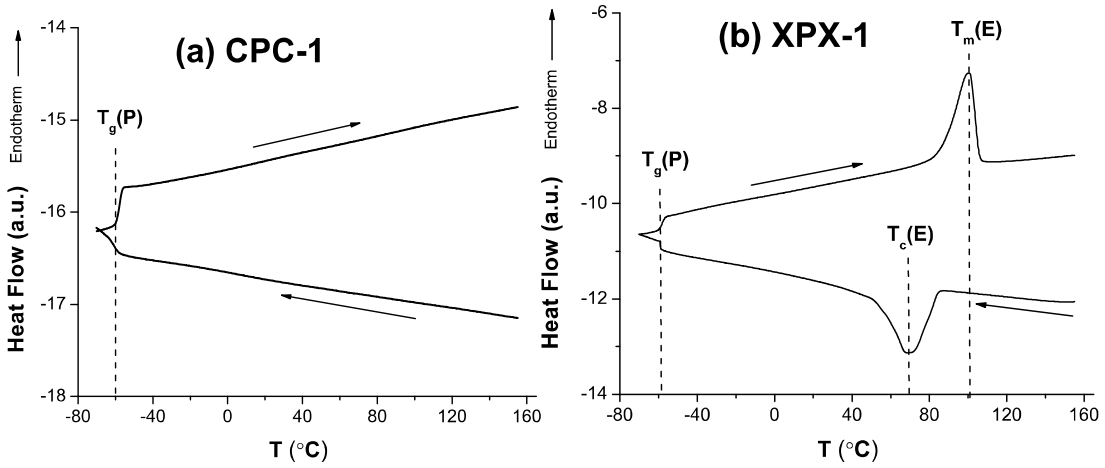

Figure 3.3: DSC traces obtained while heating and cooling (a) CPC-1 and (b) XPX-1 at 10 °C/min. T_g for P is evident in both specimens at about -60 °C. Melting and crystallization is apparent in XPX-1. However, the glass transition for C is not identified in either set of results.

The most prominent features in Figure 3.3b are the melting endotherm (T_m(E) = 100 °C) and crystallization exotherm (T_c(E) = 68 °C) found upon heating and cooling XPX-1, respectively. These thermal events, which derive from the partial local ordering of the poly(ethylene) blocks, play a primary role in driving the structural transitions that are responsible for the mechanical properties reported here. Table 3.2 summarizes the crystalline characteristics obtained by DSC for all the XPX heptablock copolymers considered in this article as well as the T_{ODT} values for the CPC materials. Consistent with previous work on block copolymers containing hydrogenated 1,4-poly(butadiene) with about 10% 1,2 additions we obtain melting temperatures between 93 and 100 °C and 23 to 36 % crystallinity (X_c) of the E blocks based on the area under the peak in the melting curve.[47,51,28] Cooling at 10 °C/min results in peak rates of crystallization between 54 and 68 °C; this degree of hysteresis between T_m(E) and T_c(E) is attributable to polymer crystal nucleation.

Table 3.2: Thermal properties of CPC and XPX copolymers

Sample	T_m (E) (°C)[a]	T_c (E) (°C)[b]	X_c (E) (%)[c]	T_{ODT} (°C)[d]
CPC-1	-	-	-	168
CPC-2	-	-	-	172
XPX-1	100	68	36	< T_m
XPX-2a	98	56	32	< T_m
XPX-2b	97	54	26	< T_m
XPX-2c	93	55	22	< T_m
XPX-3	93	54	23	< T_m

[a] Peak melting temperature determined by DSC. [b] Peak crystallinity temperature determined by DSC. [c] Percent crystallinity in E block determined by DSC. [d] Order-disorder transition temperature detected by DMS.

Thermal transitions also were determined using dynamic mechanical spectroscopy (DMS). Representative dynamic elastic moduli, G', obtained from CPC-1 are displayed in Figure 3.4 as a function of reduced frequency ($a_T\omega$ where a_T is a temperature dependent shift factor) at several temperatures and as a function of temperature at fixed frequency. The master curve obtained by time temperature superposition of isothermal data (Figure 3.4a) exhibits two branches at low reduced frequencies consistent with states of order and disorder below and above about 170 °C, respectively.[29-34] This apparent T_{ODT} also is reflected in the isochronal temperature scan (Figure 3.4b) as a nearly discontinuous drop in G' at 168 °C. Evidence of a glass transition between approximately 100 and 140 °C is apparent in the G'(T) curve as well. Similar DMS results were obtained from CPC-2, including a similar T_{ODT} at 172 °C (Table 3.2).

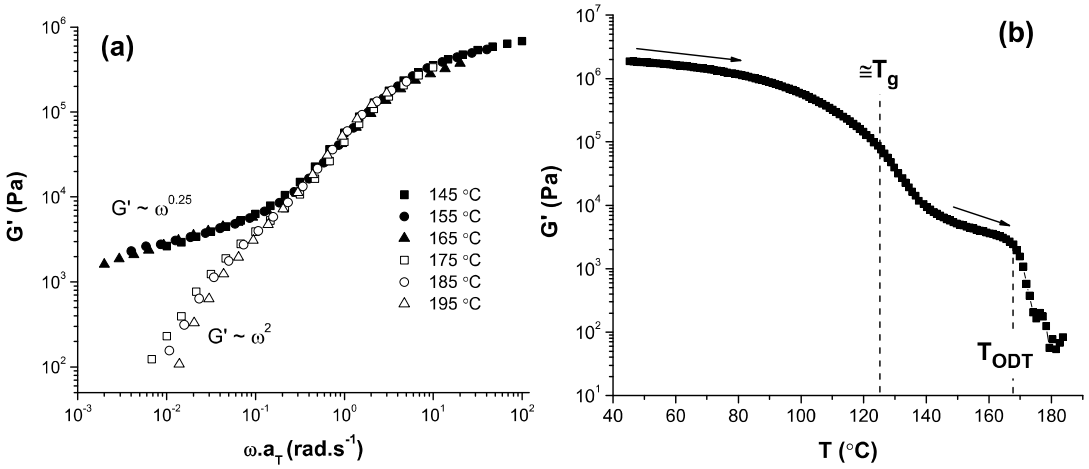

Figure 3.4: (a) Superposition of G' versus reduced frequency, ωa_T, from isothermal frequency sweeps with T_{REF} = 145 °C and (b) temperature sweep at 0.1 rad/s and 0.5 °C/min for CPC-1, both at 1% strain. A T_{ODT} of 168 °C produces a change of slopes in (a) and a discontinuity in (b) and T_g for C at around 125 °C is indicated by the decline in G' in (b).

DMS was also performed on the XPX materials, and Figure 3.5 shows a representative master curve and a typical set of temperature sweep data obtained at 0.1 rad/s and 2 °C/min for XPX-1. Above 100 °C the G'(ω) results (Figure 3.5a) superpose onto a single master curve with a terminal slope, G' ~ ω^2, consistent with liquid like behavior. Below 100 °C the low frequency portions of the G'(ω) curves depart from the high temperature master curve, indicative of a non-liquid like response. As shown, XPX-1 is semicrystalline at and below about 100 °C based on DSC measurements (see Figure 3.3b). Heating and cooling XPX-1 leads to hysteresis in G' (Figure 3.5b) with end points that match the exotherm and endotherm identified in the DSC measurements (Figure 3.3b). Similar results were obtained from the other XPX heptablock copolymers, as shown in Appendix A, leading us to conclude that all these materials are liquid like above T_m(E).

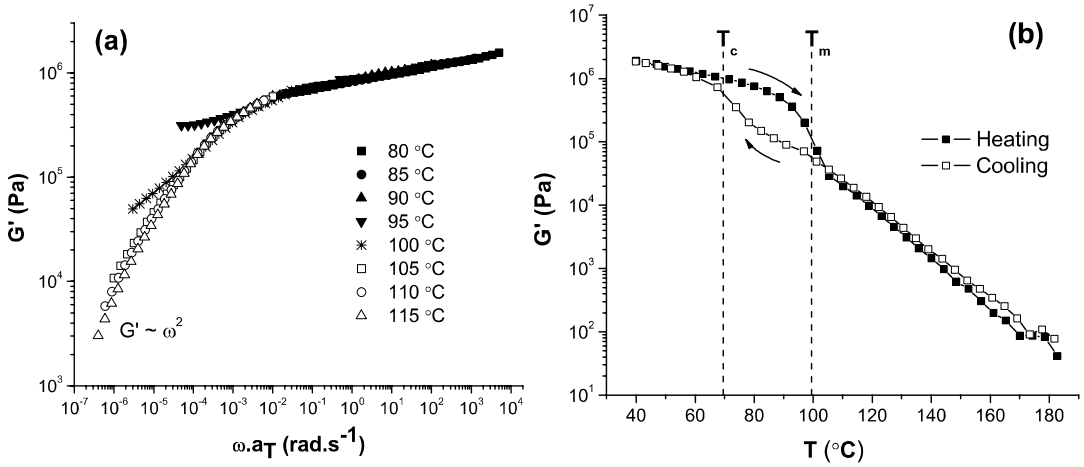

Figure 3.5: (a) Superposition of G' versus reduced frequency, ωa_T, from isothermal frequency sweeps with T_{REF} = 95 °C and (b) temperature sweep at 0.1 rad/s and 2 °C/min for XPX-1, both at 1% strain. Melting and crystallization dominate the thermal behavior of XPX.

3.2.3 Structural Analysis

The morphologies of the CPC and XPX materials were investigated using small angle X-ray scattering and transmission electron microscopy. The CPC triblocks were shear-aligned at about 160 °C using the procedures described by Koppi[40] and then analyzed by SAXS. Figure 3.6 shows a synchrotron SAXS pattern for CPC-1 at 25 °C and a laboratory source pattern for CPC-2 at 150 °C. CPC-1 and CPC-2 both produced SAXS patterns with multiple Bragg reflections at relative spacings $(q/q^*)^2$ = 1, 3, 4, 7, where q* is the position of the first order reflection. These results are consistent with a hexagonally ordered arrangement of C cylinders embedded in a matrix of P polymer.[35-37] The magnitude of the principal wave vectors are related to the spacing between domains, $d^* = 2\pi/q^*$, where d* corresponds to the

separation between (11) planes in a hexagonally ordered crystal. These values are listed for CPC-1 and CPC-2 in Table 3.3.

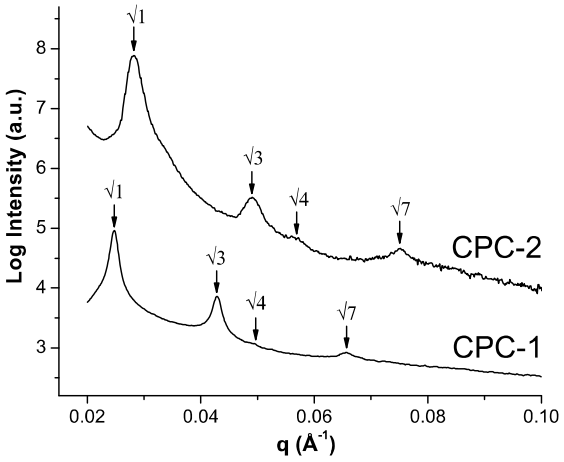

Figure 3.6: SAXS data acquired for shear aligned samples of CPC-1 (synchrotron, 25 °C) and CPC-2 (laboratory, 150 °C) in the shear direction. Arrows indicate peak positions, which suggest a hexagonally-packed cylindrical morphology for both materials below T_{ODT}. This structure is consistent with that expected for the block volume fractions.

Synchrotron SAXS data also were collected for the XPX systems at 140 and 25 °C, and the results are shown in Figure 3.7. In striking contrast to the SAXS patterns obtained from the CPC materials, every XPX heptablock displays only one rather broad peak at both temperatures, indicating that long range order is absent in these materials. Interestingly, the single broad peak is more intense at the higher temperature (consistent with earlier results),[14,28] which we assume reflects some degree of contrast matching in the microphase separated state at 25 °C. Since DMS measurements have established that the XPX polymers are liquid-like above about 100 °C, we associate the peak in I(q) at 140 °C with correlation hole scattering. Remarkably, q* varies only slightly between the three XPX-2 compounds (see Table

3.3) despite the fact that these polymers have the same composition profile but differ in molecular weight by nearly a factor of two. Moreover, q*, and thus d*, change very little from 140 °C to 25 °C for each material: d* values drop only about 0.9 nm on average with cooling. We return to these features in the discussion section.

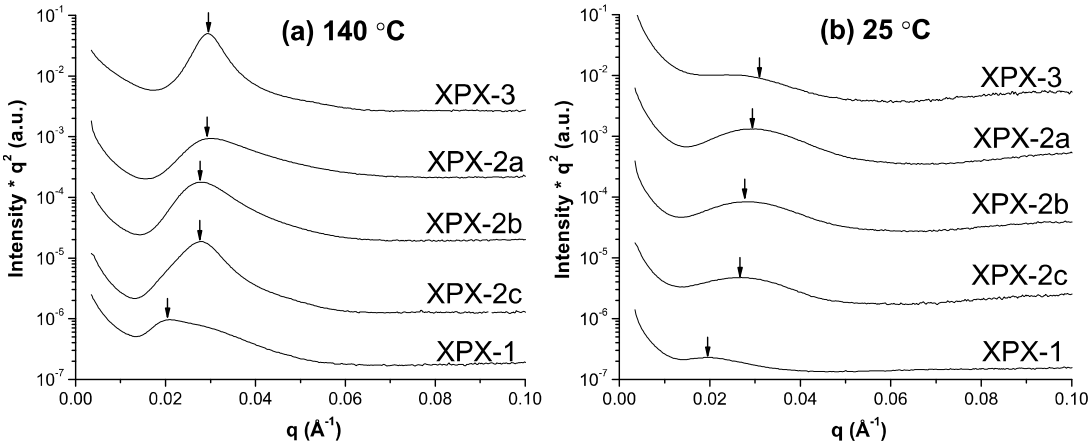

Figure 3.7: Synchrotron SAXS data acquired at (a) 140 °C and (b) 25 °C for XPX block copolymers. They each produce one relatively broad peak at both temperatures, which indicates the materials do not contain long range order.

Table 3.3 Domain spacings calculated from SAXS data

Sample	$q^*_{25\,°C}$ (Å^{-1})	$d^*_{25\,°C}$ (nm)	$q^*_{140\,°C}$ (Å^{-1})	$d^*_{140\,°C}$ (nm)
CPC-1	0.0249	25.2	-	-
CPC-2	-	-	0.0284[a]	22.1[a]
XPX-3	0.0305	20.6	0.0286	22.0
XPX-2a	0.0299	21.0	0.0284	22.1
XPX-2b	0.0291	21.7	0.0270	23.3
XPX-2c	0.0276	22.8	0.0268	23.4
XPX-1	0.0205	30.6	0.0199	31.6

[a] Measured at 150 °C.

TEM images were obtained from the XPX polymers to further delineate the microphase separated structures present at room temperature. Representative TEM images recorded from XPX-1, XPX-2b and XPX-3 are presented in Figure 3.8. Staining with RuO_4 creates contrast among the monomers resulting in images with black (P), gray (C) and white (E) regions.

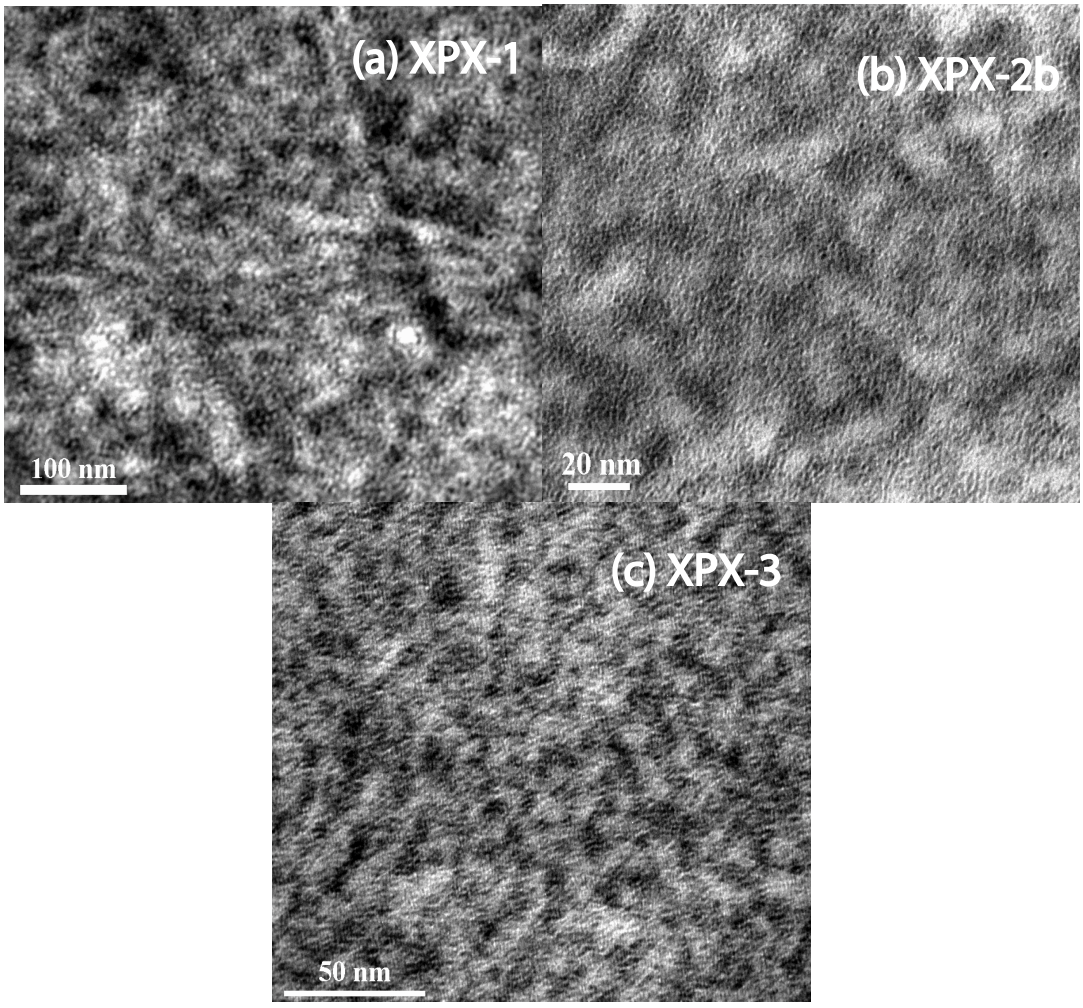

Figure 3.8: TEM images from (a) XPX-1, (b) XPX-2b and (c) XPX-3. All XPX materials show a disorganized morphology of C (gray), E (white) and P (black) domains.

All XPX images show rather disorganized structures with evidence of light and dark regions on a length scale that is compatible with the SAXS results (see Table 3.3). A combination of poor contrast, a lack of order, and ill-defined domain structure make it impossible to assign a specific shape or geometry to these features. Nevertheless, the TEM images indicate some form of microphase separation and confirm the state of disorder deduced from the SAXS data.

3.2.4 Tensile Properties

Rectangular samples were subjected to uniaxial tensile testing at a rate of 200% strain per minute at room temperature. Figure 3.9 compares representative tensile data (all data are presented in Appendix B) taken from each material evaluated in this study. Table 3.4 summarizes five measures of mechanical behavior for these materials, elastic modulus *E*, strain at break ε_b, tensile strength (stress at break) σ_{TS}, final residual strain ε_r, and tension set ε_s (see Strain Recovery section) extracted from each set of at least five measurements or three in the case of ε_r performed on each material. Here we note that our use of rectangular specimens, which almost always failed near the grips of the instrument, lead to conservative estimates of ε_b and σ_{TS}.

The CPC materials (Figure 3.9a) behave as typical thermoplastic elastomers, combining high elongation with low modulus and relatively high strength values. CPC-2 exhibits a higher modulus and tensile strength than CPC-1, which is attributable to a higher glass content.[1,2] Glassy domains act as cross-linkers and stiff filler particles, which can result in greater reinforcement (i.e., higher modulus and strength). All the XPX heptablock copolymers behave like strong thermoplastic

elastomers (Figure 3.9b). In fact, all the XPX materials are statistically as strong as CPC-2, with tensile strengths between 26 and 32 MPa.

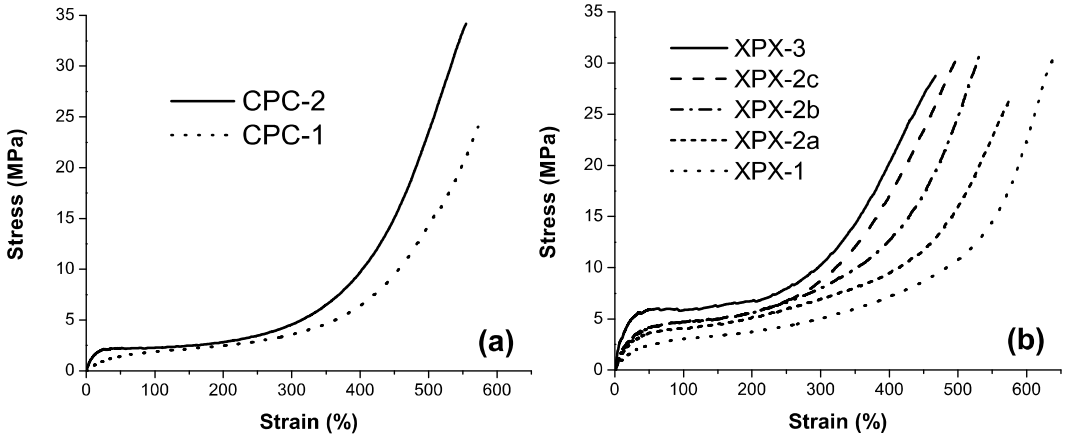

Figure 3.9 Representative engineering stress versus strain curves for (a) CPC copolymers and (b) XPX copolymers. XPX materials behave as strong thermoplastic elastomers with tensile strengths comparable to the strong CPC-2.

Table 3.4: Tensile properties of CPC and XPX block copolymers

Sample	*E* (MPa)	ε_b (%)	σ_{TS} (MPa)	ε_r (%)	ε_s (%)
CPC-1	5.5 ± 0.8	543 ± 33	22.2 ± 5.3	30 ± 5	11 ± 7
CPC-2	20.6 ± 5.0	552 ± 5	32.8 ± 2.2	44 ± 4	16 ± 6
XPX-1	10.0 ± 1.9	652 ± 23	26.9 ± 4.5	57 ± 3	31 ± 14
XPX-2a	19.2 ± 4.5	616 ± 32	25.8 ± 4.1	178 ± 3	84 ± 23
XPX-2b	21.9 ± 1.9	551 ± 11	30.5 ± 3.1	120 ± 11	64 ± 4
XPX-2c	24.0 ± 3.2	528 ± 19	32.1 ± 5.8	114 ± 3	80 ± 19
XPX-3	41.8 ± 6.3	509 ± 40	29.6 ± 2.8	198 ± 3	97 ± 20

Several interesting features emerge in comparing the XPX and CPC systems. The modulus (*E*) and stress plateau during drawing (strains up to about 200%) are higher for XPX than CPC at comparable glass contents due to the presence of the

semicrystalline E blocks; this effect resembles a previous comparison of melt-ordered CPEPC and CPC.[14] Both C and E content have an important effect on the magnitude of the modulus. With 67% higher C content the modulus *E* for CPC-2 is nearly four times that for CPC-1. Similarly, adding semicrystalline E to XPX also stiffens the material. Comparing XPX-1 to CPC-1 and XPX-3 to CPC-2, each pair having similar amounts of C, indicates that the semicrystalline blocks double the moduli.

However, this reinforcement of XPX at low strains does not translate into a higher strength. In general, tensile strengths in both CPC and XPX samples seem to have a maximum value of about 32 MPa. Nor do we find any statistical difference between XPX and CPC with respect to strain at break, which are about 550% for all materials, except for XPX-1 and XPX-2a, which extend to slightly higher elongation of 652% and 612%, respectively. However, this may stem from molecular weight differences, which are evident in the XPX-2 series. While all three XPX-2 materials have statistically similar moduli and tensile strengths, XPX-2a has a strain at break of 616%, modestly different than the average 540% for the two higher molecular weight systems. XPX heptablocks with lower molecular weight seem to produce “softer” materials that fail at significantly higher elongation.

3.2.5 Strain Recovery

Cyclic testing (strain and recovery) was performed on samples by stretching them to 400% strain (about 70% of their average strain at break) then compressing the specimen to 0% strain and repeating this sequence for a total of 7 cycles. Residual strain was identified after each cycle as the deformation (strain) at which the

measured stress disappeared (σ = 0 MPa) as the sample length was reduced back towards its original value.

Residual strain is plotted as a function of cycle number in Figure 3.10 for all the materials considered in this report. These measurements are remarkably reproducible as evidenced by the narrow range of values shown, about 5% variation. The final residual strains after 7 cycles, ε_r, are shown for each material in Table 3.4. Tension set values, ε_s, also presented in Table 3.4, are approximately half of ε_r for each material and show a similar trend of increasing irrecoverable deformations. However, these results have high uncertainty levels given the difficulty in manually measuring the final length of rubbery samples and thus our analysis is focused on the results of cyclic testing.

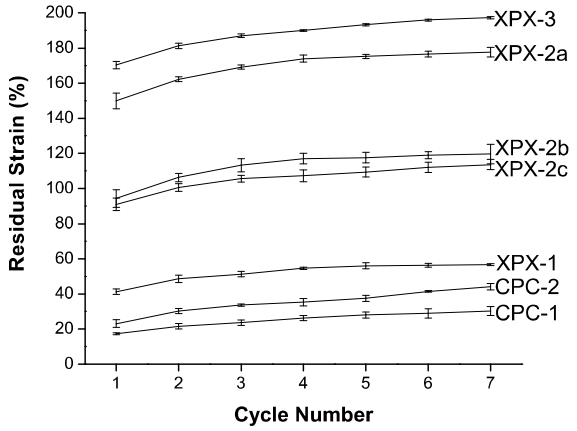

Figure 3.10: Residual strain after cyclic deformation up to 400% strain for CPC and XPX materials. Higher C and E content increases residual strain while an increase in molecular weight in the XPX-2 series improves recoverability.

All samples tend to reach a constant residual strain, especially the XPX compounds; after 4 cycles these materials add less than 5% additional residual strain

on average by the seventh cycle. The CPC copolymers show the least residual strains, which is readily explained by the hard glassy C domains, which offer little if any irreversible deformation.[13,14,18,37,38] Increasing the C content from 18% (CPC-1) to 30% (CPC-2) only elevates ε_r from 30% to just 44%.

Incorporation of semi-crystalline E blocks in the XPX materials has a significant impact on the elastic recovery of these specimens. Prior work with semicrystalline TPEs has led to the conclusion that plastic crystal deformation is responsible for non-recoverable strain.[4,10,12-14,18,19] Increasing the E content raises the amount of residual strain in the XPX compounds from 54% to 120% to 197% for 22% E (XPX-1) to 26% E (XPX-2b) to 28% E (XPX-3), respectively.

However, the C content also increases equally and the effects of the added crystallinity and glass can not be decoupled. Most importantly, the ill-defined morphology of the XPX elastomers may reorganize irreversibly during large strain extension, which could contribute to a larger residual strain, particularly as the C and E content increases. Figure 3.10 also shows the residual strain curves for the XPX-2 series, which have a constant composition but varying molecular weights. Here strain recovery increases as the overall molecular weight decreases. XPX-2a (M_n = 79 kg/mol) exhibits a 178% residual strain after seven cycles while XPX-2c (M_n = 114 kg/mol) recovers all but 114%. Thus, XPX materials seem to require a minimum molecular weight to achieve optimal recovery.

3.3 Discussion

3.3.1 Phase Behavior and Morphology

A combination of rheological measurements, SAXS and TEM revealed different types of phase behavior and different morphologies for the CPC versus the XPX systems. The CPC triblock copolymers produce classical, here hexagonally ordered, phases that go through a first-order transition to a disordered melt state at a temperature (T_{ODT}) that is determined by the overall polymer molecular weight (and composition). Microphase separation at low temperatures is driven by thermodynamic incompatibility between the C and P blocks, which is captured by the magnitude of the Flory-Huggins segment-segment interaction parameter, $\chi_{CP} = (V/RT)(\delta_C - \delta_P)^2$, where V is the segment volume and δ_C and δ_P are the solubility parameters of the C and P polymers, respectively. Despite chemical similarities most pairs of saturated hydrocarbon polymers such as C and P, C and E, and E and P are characterized by small but positive χ parameters. In fact, C and P have been shown to have nearly the same segment-segment interaction parameter as the unsaturated precursor polymers S and I, i.e., $\chi_{CP} \approx \chi_{SI}$.[33] This explains why CPC triblock copolymers order at modest molecular weights and CPC-1 and CPC-2 have $T_{ODT} \approx 170$ °C. Extensive investigations of numerous hydrogenated diblock copolymers have led to the following relative classifications: $\delta_C < \delta_P < \delta_E$ leading to $\chi_{EP} << \chi_{CP} < \chi_{CE}$.[39] These thermodynamic characteristics have been applied in designing the XPX heptablock copolymers.

The molecular arrangement of the XPX heptablocks creates terpolymers that are melt disordered, even at relatively high overall molecular weights. The molecular weights of the C and E blocks in the X portions of the molecules have been chosen to permit these polymers to mix above the melting point of the E blocks ($T_m \approx 100$ °C). A nearly symmetric (42% C) CEC triblock with $M_n = 30$ kg/mol has a T_{ODT} of about 220 °C.[14] Therefore, the CEC portions of the XPX molecules were kept below this critical value. XPX-2c has the largest X sequences, 28.5 kg/mol, which might be expected to induce segregation between the E and C blocks at a temperature above 100 °C. However, a second factor favors mixing of the C, E and P blocks above T_m. In the homogeneous state P segments can make contact with E and C segments and both these interactions are favored over C-E contacts. Alternatively, the mixed CEC portions of the heptablock copolymer present an average solubility parameter $(\delta_C\delta_E)^{1/2}$ that is close to δ_P, which promotes overall homogeneity.

Crystallization disrupts this delicate balance. C blocks will be ejected from the space close to the crystallizing E blocks, which will then propagate the segregation of P. We do not have a detailed understanding of either the dynamics of this process or the resulting structure. However, there is strong evidence to support our conclusion that the low temperature morphology contains largely separate E, C and P domains. DSC traces from XPX-1 (Figure 3.3b) evidence a sharp glass transition at about -60 °C, which is clearly associated with nearly pure poly(ethylene-*alt*-propylene). These thermal measurements also reveal poly(ethylene) melting temperatures and extents of crystallization (Table 3.2) that are typical of E-based diblock, triblock and multiblock copolymers.[4,8,9,28] There is little direct evidence for the presence of separate C

domains, although discrete E and P material makes this inevitable. We were not able to identify a glass transition temperature for poly(cyclohexylethylene) in any of the polymers examined by DSC, including the CPCs, for reasons discussed earlier. DMS experiments are complicated by crystallization and melting (Figure 3.5b) over the same range of temperatures where we expect to see the effects of vitrification. Unfortunately, the morphologies revealed in the TEM images are too disorganized to permit the reliable assignment of specific domain structures.

Above 100 °C mixing of C, E and P leads to a homogeneous viscoelastic fluid with a hypothetical glass transition temperature that is well below 100 °C, i.e., between that of pure C (ca. 140 °C) and amorphous E and P (< -50 °C). A liquid like low frequency rheological response (Figure 3.5 and Appendix A) supports this notion. Segregation of C blocks from E blocks during nucleation and growth of poly(ethylene) crystals are accompanied by C vitrification, which would arrest the development of equilibrium domain structures with long ranged order. The end result of these highly non-equilibrium processes are irregularly shaped microdomains with ill-defined internal placement of C and E, which are randomly distributed within the material. While crystallization triggers microphase separation we believe that the glassy portion of the resulting microdomains anchors the P blocks to the particles rendering high strength. Indeed, previous work with EPE triblock copolymers has shown that crystallization induced ordering from the disordered melt state results in rather weak elastomers.[4,8]

The scale of this structural development is controlled by the overall dimensions of the heptablock copolymer as shown by the SAXS measurements

obtained at 140 and 25 °C (Figure 3.7 and Table 3.3). Broad and low intensity SAXS peaks above T_m can be attributed to correlation hole scattering, which derives from a ≈ 15% melt density difference between poly(cyclohexylethylene) and poly(propylene); the melt densities of E and P are equal. Crystals of E will nucleate with dimensions significantly smaller than the overall molecular size but the sub-molecular arrangement of E and C domains will be immobilized by the vitrification of the C as it microphase separates before long range order can be established. Thus the morphology reflects the same average spacing as the correlation hole in the disordered melt.

Based on purely Gaussian statistics the Random Phase Approximation anticipates $d^* \sim N^{1/2}$ at constant composition. Despite composition differences, the values of $d^* = 2\pi/q^*$ for XPX-1 and XPX-3 follow this scaling. On the other hand, values for the XPX-2 polymers do not scale correctly with the rest of the data, especially as we increase M_n. Specifically, the peak position q^* for XPX-2a should appear at 1.39 times higher value than q^* for XPX-2c; clearly this is not the case. While we do not understand the exact origins of this experimental result, we should note that increasing N changes the segregation strength and may activate inhomogeneous composition fluctuations in the disordered melt (i.e., between C and E versus C and P versus E and P blocks), which are not accounted for in the simple scaling prediction. (Also puzzling is that disordered CECEC-P hexablocks exhibit two correlation hole peaks[19] while disordered CEC-P-CEC and CECEC-P-CECEC[19] multiblocks produce only one). This issue is taken up in the next chapter.

3.3.2 Tensile Properties

Tensile tests (Figure 3.9) show that all the block copolymers investigated in this study exhibit thermoplastic elastic behavior with certain similarities and differences. Any similarity is rather surprising given the dramatic difference in morphology between the CPC and XPX materials. While we have not been able to establish a detailed structure for the XPX compounds, TEM results suggest a random arrangement of X and P domains with an ill-defined state of connectivity. This contrasts sharply with the classical highly ordered cylindrical domain structure found with the CPC polymers (Figure 3.6).

In the small strain limit the linear elastic modulus E is correlated to the hard content or $f_X = f_C + f_E$ for both CPC and XPX, as illustrated in Figure 3.11. The X blocks are less effective at stiffening the material than the C cylinders. Most likely this is a combination of a morphological effect (hexagonally ordered cylinders versus disordered and possibly disconnected particles) and the composite nature of the X microdomains, i.e., softer semicrystalline E combined with glassy C. It takes roughly twice the volume fraction of X relative to C to obtain the same modulus in XPX as CPC. These data also suggest that the XPX materials are all continuous in rubbery P and most likely are not continuous in X. Prior reports have documented that the room temperature linear elastic modulus of nearly symmetric isotropic CEC triblock copolymers with $f_C \approx 0.42 - 0.61$ is $E \approx 156 - 410$ MPa.[14,40] A bicontinuous arrangement of this material with an equal volume fraction of rubbery P polymer would be expected to yield a modulus of roughly 80 – 200 MPa, an order of magnitude greater that what we measure. Therefore we conclude that the XPX

compounds contain largely disconnected hard particles composed of segregated semicrystalline E and glassy C.

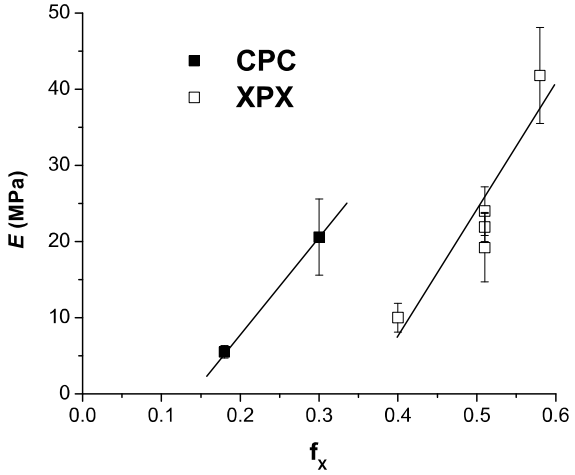

Figure 3.11: Elastic moduli of CPC and XPX materials versus $f_X = f_C + f_E$ shows that C cylinders stiffen the materials more than the X blocks.

All the block copolymers investigated in this study displayed similar tensile properties at large deformation with strain to break values falling between 500 and 650% and tensile strengths ranging from 22 to 33 MPa (Table 3.4). Similarity in ε_b and σ_{TS} suggests that the X particles in XPX are as effective at anchoring the P molecules as the C domains in CPC. Poly(ethylene-*alt*-propylene) (P) is a densely entangled polymer with a molecular weight between entanglements M_e = 1,475 g/mol at room temperature.[22] All the polymers under consideration in this work are highly entangled, containing more than 10 entanglements per center P block. The ultimate strength of an entangled rubber is controlled by the number of entanglements per rubbery chain and the strength of the anchors that restrain the chain ends. Although we are not aware of a quantitative theoretical treatment of this problem, the insensitivity of the measured tensile strengths to reinforcing particle type (C versus

X) offers strong evidence that the limits of particle mechanical integrity are similar for C and X, which may imply that either C and E are equally reinforcing or that failure occurs in both cases in C. This finding represents a significant accomplishment of our investigation. In summary, X nanoparticles containing C and E domains generated through crystallization induced microphase separation provide at least as much mechanical reinforcement to thermoplastic elastomers as conventional glassy microdomains.

3.3.3 Strain Recovery

In contrast to the single extension large strain properties discussed in the previous paragraph, there are significant differences in the strain recovery characteristics between CPC and XPX. Irreversible deformation in rubbery thermoplastic elastomers generally is correlated with the content and morphological connectivity of hard domains.[37,41-43] As with the modulus analysis (Figure 3.11), the residual strain after 7 cycles, as well as the tension set, are different for CPC versus XPX as a function of f_X (= f_C + f_E), as shown in Figure 3.12. Apparently changing f_X has a much more dramatic effect on the permanent deformation of the XPX elastomers than on the CPC materials. However, it is not possible to separate the effects of the brittle glassy C and plastic semicrystalline E components on strain recovery in XPX. Also, while we have documented a common hexagonal morphology for CPC-1 and CPC-2, we have not established how increasing f_X in the XPX materials influences the morphology, particularly the connectivity of the X domains, which is connected with irreversible distortion and breakup during extension.

An important implication of Figure 3.12a is that the residual strain in XPX materials will approach or exceed the performance of CPC when $f_X \leq 0.39$ even at a somewhat greater hard block content. This may be a consequence of morphological differences, i.e., glassy C cylinders versus isolated X domains. We expect most morphological changes to occur in a given material during the first 400% deformation cycle, which is supported by the result found in Figure 3.10. All the experimental curves in Figure 3.10 share a common form with the largest contribution to permanent set occurring in the first cycle followed by a more modest evolution of non-recoverable strain during subsequent extension and recovery cycles. Clearly the strain remaining after the first deformation cycle as well as the tension set values (Figure 3.12b) parallel the final residual strain plotted as a function of f_X in Figure 3.12a.

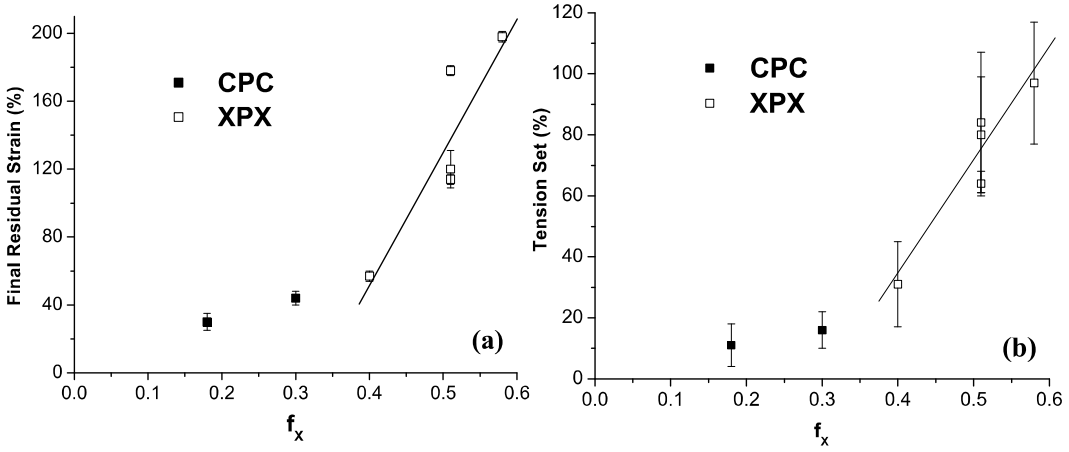

Figure 3.12: (a) Final residual strain after 7 cycles of deformation to 400% strain, and (b) tension set, versus $f_X = f_C + f_E$ for both CPC and XPX materials. XPX materials with residual strains comparable to CPC (about 44%) can be achieved when $f_X \leq 0.39$.

Thus, CPC and XPX experience maximum disruption of hard domains in the first extension where morphology and in particular its state of connectivity influence the type of deformation. Then, the random and more discreet (as evidenced by the values of modulus) arrangement of hard X particles in XPX may be able to produce materials as recoverable as CPC despite a higher composition of hard domains. Thus, generating XPX copolymers with $f_X \leq 0.39$ should yield materials as strong and recoverable as CPC but with the advantage of disordering at a fixed temperature given by $T_m(E)$, independent of molecular weight up to a limiting value, which allows for low temperature processing.

Finally, the XPX-2 series of polymers revealed that varying the molecular weight has important effects on tensile and recovery properties. The two higher molecular weight XPX-2 materials, XPX-2b and XPX-2c with M_n = 79 and 114 kg/mol, respectively, had similar values of ultimate tensile strength, strain at break and residual strain. On the other hand, the lowest molecular weight material, XPX-2a with M_n = 59 kg/mol, was statistically just as strong but failed at a higher extension and experienced a significantly higher residual strain. This suggests that for XPX with crystallization induced segregation a threshold value in M_n is necessary to achieve optimal properties. This resembles the requirement of a threshold M_n to create strongly segregated glassy domains in strong thermoplastic elastomers. However, in the case of XPX, properties that are affected are elongation and irrecoverable deformation but not strength, which suggests that a lower M_n in XPX will cause higher E deformation.

3.4 Conclusions

A new class of thermoplastic multiblock copolymer elastomers with a CEC-P-CEC heptablock molecular architecture, denoted XPX, was prepared and characterized for structure and tensile properties. XPX materials contained between 42 and 60% poly(ethylene-*alt*-propylene) (P) and all CEC block sequences combined equal fractions of poly(cyclohexylethylene) (C) and poly(ethylene) (E). CPC triblock elastomers with 18% and 30% C also were analyzed for comparison. Thermal analysis by DSC and DMS showed that the CPC compounds microphase separate in the melt with T_{ODT} at about 170 °C. The molecular configuration of the XPX terpolymers results in disordered materials above the melting temperature, T_m(E) of the E blocks for all specimens up to 114 kg/mol in molecular weight. Thermal, SAXS and TEM measurements indicate that the XPX materials microphase separate upon crystallization of the E blocks, resulting in a disordered arrangement of particles containing C and E domains dispersed in a rubbery P matrix. Both CPC specimens form conventional hexagonally packed (glassy) cylinders below T_{ODT}. Single extension and cyclic tensile tests were performed on all materials to assess and compare the mechanical properties of XPX and CPC. All the XPX materials were statistically as strong as the CPC elastomers with ultimate tensile strengths ranging from 26 to 32 MPa and strains at break between 500 and 650%. This indicates that microphase separated X particles, comprised of equal amounts of semicrystalline E and glassy C, are as reinforcing as C cylinders in CPC, notwithstanding crystallization induced segregation. Residual strain, following seven cycles of tensile deformation to 400% strain, was found to be dependent on both composition and

molecular weight. A relatively low elastic modulus for all XPX samples, 10 to 42 MPa, suggests a disconnected morphology of X regions, which may account for the substantial elastic recovery. Based on the extrapolation of this property we anticipate that XPX elastomers will exhibit equal or better recovery than the CPC compounds when the fraction of X domains, $f_X = f_C + f_E \leq 0.39$. Thus, CEC-P-CEC heptablock terpolymers provide strong and recoverable elastomeric materials with the advantage of possessing a common processing temperature dictated by $T_m(E)$ which is decoupled from molecular weight below a critical value.

Acknowledgement. I thank Dr. Guillaume Fleury for his assistance in the synthesis of the XPX block copolymers.

3.5 References

[1] Holden, G.; Bishop, E. T.; Legge, N. R. *J. Polymer Sci., Part C* **1969,** *26*, 37-57.

[2] Quirk, R. P.; Morton, M. In *Thermoplastic Elastomers*; 2nd ed.; Holden, G.; Legge, N. R.; Quirk, R. P.; Schroeder, H. E.; Eds.; Hanser Publishers: New York; 1996; pp 71-100.

[3] Fredrickson, G. H.; Bates, F. S. *Annual Review of Materials Science* **1996,** *26*, 501-550.

[4] Seguela, R.; Prudhomme, J. *Polymer* **1989,** *30*, (8), 1446-1455.

[5] Cohen, R. E.; Cheng, P. L.; Douzinas, K.; Kofinas, P.; Berney, C. V. *Macromolecules* **1990,** *23*, 324-327.

[6] Rangarajan, P.; Register, R. A.; Fetters, L. J. *Macromolecules* **1993,** *26*, 4640-4645.

[7] Nandan, B.; Hsu, J. Y.; Chen, H. L. *Polymer Reviews* **2006,** *46*, (2), 143-172.

[8] Koo, C. M.; Wu, L. F.; Lim, L. S.; Mahanthappa, M. K.; Hillmyer, M. A.; Bates, F. S. *Macromolecules* **2005,** *38*, 6090-6098.

[9] Koo, C. M.; Hillmyer, M. A.; Bates, F. S. *Macromolecules* **2006,** *39*, 667-677.

[10] Hotta, A.; Cochran, E.; Ruokolainen, J.; Khanna, V.; Fredrickson, G. H.; Kramer, E. J.; Shin, Y. W.; Shimizu, F.; Cherian, A. E.; Hustad, P. D.; Rose, J. M.; Coates, G. W. *Proceedings of the National Academy of Sciences of the United States of America* **2006,** *103*, (42), 15327-15332.

[11] Wang, H. P.; Khariwala, D. U.; Cheung, W.; Chum, S. P.; Hiltner, A.; Baer, E. *Macromolecules* **2007,** *40*, 2852-2862.

[12] Mohajer, Y.; Wilkes, G. L.; Wang, I. C.; McGrath, J. E. *Polymer* **1982,** *23*, (10), 1523-1535.

[13] Schmalz, H.; Boker, A.; Lange, R.; Krausch, G.; Abetz, V. *Macromolecules* **2001,** *34*, 8720-8729.

[14] Mahanthappa, M. K.; Lim, L. S.; Hillmyer, M. A.; Bates, F. S. *Macromolecules* **2007,** *40*, 1585-1593.

[15] Mahanthappa, M. K.; Hillmyer, M. A.; Bates, F. S. *Macromolecules* **2008,** *41*, 1341-1351.

[16] Balsamo, V.; Gil, G.; de Navarro, C. U.; Hamley, I. W.; von Gyldenfeldt, F.; Abetz, V.; Canizales, E. *Macromolecules* **2003,** *36*, 4515-4525.

[17] Balsamo, V.; de Navarro, C. U.; Gil, G. *Macromolecules* **2003,** *36*, 4507-4514.

[18] Schmalz, H.; Abetz, V.; Lange, R. *Composites Science and Technology* **2003,** *63*, (8), 1179-1186.

[19] Fleury, G.; Bates, F. S. *Macromolecules* **2009,** *42*, 3598-3610.

[20] Ndoni, S.; Papadakis, C. M.; Bates, F. S.; Almdal, K. *Review of Scientific Instruments* **1995,** *66*, (2), 1090-1095.

[21] Hucul, D. A.; Hahn, S. F. *Advanced Materials* **2000,** *12*, (23), 1855-1858.

[22] Fetters, L. J.; Lohse, D. J.; Richter, D.; Witten, T. A.; Zirkel, A. *Macromolecules* **1994,** *27*, 4639-4647.

[23] Brandrup, J.; Immergut, E. H., *Polymer Handbook*, 3rd ed.; John Wiley & Sons: New York, 1989.

[24] Rosedale, J.; Bates, F. S.; Almdal, K.; Mortensen, K.; Wignall, G. D. *Macromolecules* **1995,** *28*, 1429-1443.

[25] Koppi, K. A. *Ph.D. Dissertation*, University of Minnesota **1993**.

[26] Khandpur, A. K.; Macosko, C. W.; Bates, F. S. *Journal of Polymer Science Part B-Polymer Physics* **1995,** *33*, (2), 247-252.

[27] Gotro, J. T.; Graessley, W. W. *Macromolecules* **1984,** *17*, 2767-2775.

[28] Weimann, P. A.; Hajduk, D. A.; Chu, C.; Chaffin, K. A.; Brodil, J. C.; Bates, F. S. *Journal of Polymer Science Part B-Polymer Physics* **1999,** *37*, 2053-2068.

[29] Bates, F. S.; Rosedale, J. H.; Fredrickson, G. H.; Glinka, C. J. *Physical Review Letters* **1988,** *61*, (19), 2229-2232.

[30] Bates, F. S.; Rosedale, J. H.; Fredrickson, G. H. *Journal of Chemical Physics* **1990,** *92*, (10), 6255-6270.

[31] Rosedale, J. H.; Bates, F. S. *Macromolecules* **1990,** *23*, 2329-2338.

[32] Gehlsen, M. D.; Almdal, K.; Bates, F. S. *Macromolecules* **1992,** *25*, 939-943.

[33] Gehlsen, M. D.; Bates, F. S. *Macromolecules* **1993,** *26*, 4122-4127.

[34] Kossuth, M. B.; Morse, D. C.; Bates, F. S. *Journal of Rheology* **1999,** *43*, 167-196.

[35] Seguela, R.; Prudhomme, J. *Macromolecules* **1978,** *11*, 1007-1016.

[36] Bates, F. S.; Fredrickson, G. H. *Annual Review of Physical Chemistry* **1990,** *41*, 525-557.

[37] Honeker, C. C.; Thomas, E. L.; Albalak, R. J.; Hajduk, D. A.; Gruner, S. M.; Capel, M. C. *Macromolecules* **2000,** *33*, 9395-9406.

[38] Patel, R. M.; Hahn, S. F.; Esneault, C.; Bensason, S. *Advanced Materials* **2000,** *12*, (23), 1813-1817.

[39] Cochran, E. W.; Bates, F. S. *Macromolecules* **2002**, *35*, 7368-7374.

[40] Hermel, T. J. *Ph.D. Dissertation*. University of Minnesota **1993**, p 71.

[41] Odell, J. A.; Keller, A. *Polymer Engineering and Science* **1977,** *17*, (8), 544-559.

[42] Pakula, T.; Saijo, K.; Kawai, H.; Hashimoto, T. *Macromolecules* **1985,** *18*, 1294-1302.

[43] Honeker, C. C.; Thomas, E. L. *Chemistry of Materials* **1996,** *8*, (8), 1702-1714.

4

Structure Development and Deformation in Elastomeric Heptablock Terpolymers†

4.1 Introduction

Chapter 3 presented elastomeric heptablock terpolymers composed of glassy poly(cyclohexylethylene) (C), semicrystalline polye(ethylene) (E) and rubbery poly(ethylene-alt-propylene) (P) of the form CEC-P-CEC, or XPX. This molecular design matched with compositions $f_C \approx f_E$ and $f_P > 0.42$ (f = volume fraction) prevents melt ordering at modest M_n. Instead, E crystallization induces microphase segregation to yield strong thermoplastic elastomers[1] (TPEs). XPX materials show tensile properties similar to classic glassy TPEs such as CPC, but with a fixed processing temperature window. CPC polymers microphase separate due to thermodynamic incompatibility and, thus, the processing temperature $T_{process}$ is linked to the order-disorder temperature T_{ODT}, which is dependent on M_n. On the other hand, XPX polymers, which become structured upon E crystallization from a homogenous melt, have a fixed and accessible $T_{process} > T_m(E) \approx 100$ °C, independent of M_n up to a limiting value. Other materials with crystallization induced microphase segregation have been reported but, to the best of our knowledge, none show the combination of strength and recoverability of XPX.[2-9]

---

† This work was carried out in collaboration with Dr. Feng Zuo, Postdoctoral Researcher at the University of Minnesota.

The room temperature structure of XPX materials, formed by crystallization from the disordered melt, consists of randomly arranged composite CEC domains mostly insulated by P domains, as probed by SAXS and TEM. Fleury and Bates reported a similar bicontinuous morphology in CECEC-P and CECEC-P-CECEC polymers, with the same composition as the XPX-2 materials ($f_C \approx f_E \approx 0.25$), which also developed due to crystallization.[3] Room temperature SAXS measurements showed single broad peaks where $q^*(20°C) \approx q^*(T > T_m)$, where $q^* = 2\pi/d^*$ is the scattering wavevector associated with the spacing d^*. This suggests that crystallization locks in place the gross morphology present in the disordered melt, which was confirmed by SAXS and TEM. However, while SAXS in the melt presented two correlation hole peaks for melt disordered CECEC-P, the symmetric XPX and CECEC-P-CECEC materials exhibited only one. Also, for all specimens, peak positions resulted in domain spacings that scale as $d^* \sim N^{0.33 - 0.45}$ in contrast with the prediction for disordered Gaussian chains, $d^* \sim N^{1/2}$. Thus, while it is understood that crystallization drives microphase segregation in these materials, the origins of the scattering patterns and the precise development of structure are still unclear.

Melt ordered block terpolymers that combine glassy, rubbery and semicrystalline components have also been reported.[3,10-17] Most notably, the CECEC-P materials reported by Fleury and Bates transition from crystallization induced segregation to melt ordering for $M_n > 100$ kg/mol, where T_{ODT} increases beyond 300 °C; since optimal processing requires $T_{process} > T_{ODT}$ these polymers are rather intractable. Two CECEC-P materials with $M_n = 120$ and 150 kg/mol produced a doubly periodic structure in the melt with lamellar CECEC and P (long distance) and lamellar C and E

(short distance), which persists when cooled to room temperature. This is one of the few experimental observations of the coexistence of structures with different domain sizes in bulk block copolymers.[18-23] In this chapter, we investigate melt ordering in relatively high molecular weight XPX materials.

Although melt disordered CECEC-P and XPX materials form a similar crystallization-induced morphology, their mechanical properties are qualitatively different. XPX samples are tough with tensile strengths σ_{TS} > 30 MPa and strains at break ε_b > 550% whereas CECEC-P polymers achieve high elongations with σ_{TS} < 6 MPa. Higher strengths in XPX result from the moelcular architectural design, which anchors both ends of the rubbery P blocks with hard domains. This mechanical behavior is analogous to toughness exhibited by SIS and SBS with respect to SI or ISI and SB or BSB, respectively.[24,25] In addition, XPX shows lower tension set values (ε_s < 100%) than CECEC-P (ε_s > 200%). Examining the deformation mechanisms in XPX should prove useful in further understanding the distinct mechanical properties of these materials.

In this chapter, XPX-2d and XPX-2e were synthesized through living anionic polymerization followed by catalytic hydrogenation. These materials are similar to the set of XPX-2 compounds ($f_C \approx f_E \approx 0.25$) but with higher M_n (135 and 195 kg/mol, respectively). A comparison of the rheological responses of crystallization structured XPX-2 materials to the CPC materials reveals significant processing differences. SAXS data shows that XPX-2d and XPX-2e are melt ordered with two principal reflections, which sheds light on the origins of scattering for all XPX materials. SAXS from samples cooled at different rates and TEM images at room temperature

allowed us to probe the development of structure in XPX. Finally, WAXS at different deformations and cyclic testing of several XPX samples revealed important steps in the mechanism of deformation of these materials relative to CPC and CEC.

4.2 Experimental Section

Chapter 2 provided a comprehensive description of the techniques and procedures employed for all the materials analyzed in this project. This section presents the essential information regarding the procedures through which the materials of study in this chapter were synthesized and characterized.

4.2.1 Polymer Synthesis and Hydrogenation

All block copolymers presented in this chapter were produced at the University of Minnesota. An SIS precursor triblock was synthesized by sequential living anionic polymerization of styrene (S) (Aldrich), isoprene (I) (Acros Organics) and S in purified cyclohexane (Fischer Scientific) at 40 °C, initiated with *sec*-butyllithium (1.4M solution in cyclohexane, Aldrich), as described elsewhere.[26] An SBS precursor triblock was synthesized following the identical route as for SIS, except that addition of butadiene (B) replaced I addition. For the XPX heptablock copolymers, living SBS-I^-,Li^+ copolymers were prepared by sequential polymerization of S, butadiene (B) (Aldrich), S, and I as noted above and subsequently coupled using a stoichiometric amount of α,α'-dibromo-p-xylene (Aldrich) added in a dropwise fashion until the solution became colorless (about 4 to 6 h) to produce the precursor SBS-I-SBS materials. In all cases the overall fraction of

S and B added to the reactor was held constant. An aliquot of the completed first S block was drawn after 8 h of reaction time and precipitated in degassed methanol (Aldrich) for further analysis.

SIS, SBS and SBS-I-SBS were hydrogenated to yield CPC, CEC and CEC-P-CEC, respectively. This was accomplished by reaction for 12 h over a Pt/Re catalyst supported on macroporous silica particles (Dow Chemical) in degassed cyclohexane at 170 °C under 500 psig of H_2.[27] Block copolymers were recovered from solution in all cases by precipitation in a 1:3 (volume ratio) mixture of isopropanol and methanol followed by drying at room temperature under vacuum to constant weight. We will refer to CEC-P-CEC as XPX based on the pseudo triblock geometry.

4.2.2 Molecular Characterization

Block copolymer compositions were determined from quantitative ^{1}H nuclear magnetic resonance (NMR) spectra collected on the unsaturated polymers in deuterated chloroform ($CDCl_3$) (99.8%, Aldrich) using a Varian Unity Inova 300 spectrometer. Monomer mole fractions were calculated by integrating resonances associated with S, B and I repeat units; these values were then converted to volume fractions for the saturated compounds using the following published polymer densities at 140 °C: ρ_C = 0.920 g/cm^3; ρ_E = 0.784 g/cm^3; ρ_P = 0.790 g/cm^3.[28] These spectra also confirmed that the isoprene and butadiene polymerizations resulted in predominantly 1,4-monomer addition, with 6 – 9 mol % 3,4-I, and 10 – 13 mol % 1,2-B, respectively. ^{1}H NMR spectra were also recorded from the hydrogenated polymers in deuterated chloroform at room temperature for CPC and in deuterated

toluene (C_7D_8) (99.6%, Aldrich) at 70 °C for CEC and XPX, to establish the extent of saturation for each polymer, which in every case was greater than 97%.

The number average molecular weight, $M_{n,S}$, of the first S block of each block copolymer and the molecular weight distribution (M_w/M_n), or polydispersity, of all polymers were determined by size exclusion chromatography (SEC). A Waters 717 GPC fitted with three Polymer Laboratories Mixed-C columns and operated at 30 °C with tetrahydrofuran (J. T. Baker) and calibrated with polystyrene standards was employed with the unsaturated polymers and with CPC. The saturated CEC and XPX polymers were characterized with a PL-GPC 220 system operated at 135 °C with 1,2,4-trichlorobenzene. Monomodal and relatively narrow distribution (M_w/M_n < 1.21) peaks were recorded in all cases. Saturated polymer molecular weights were calculated based on $M_{n,S}$ and the overall composition derived from the reaction stoichiometry and NMR results.

4.2.3 Dynamic Scanning Calorimetry (DSC)

Thermal transitions (glass transition and melting and crystallization temperatures) were determined using a TA Instruments Q1000 differential scanning calorimeter (DSC). Poly(ethylene) fractional crystallinity, X_c, was calculated using the expression $X_c = \Delta H_m/H°_{m,E} \times w_E$ where $H^o_{m,E}$ = 277 J.g^{-1} is the theoretical heat of melting for the 100% crystalline poly(ethylene), w_E is the weight fraction of E, and ΔH_m is the area under the melting peak.[29] Samples were heated to 160 °C, cooled to -80 °C, and heated back to 160 °C, all at 10 °C/min.

4.2.4 Dynamic Mechanical Spectroscopy (DMS)

A Rheometrics Scientific ARES rheometer equipped with 25 or 8 mm diameter parallel plates was used to determine the elastic, G', and viscous, G'', dynamic moduli over the frequency range $0.01 \leq \omega \leq 100$ rad/s. All measurements were conducted at a strain of 1%, within the linear viscoelastic regime. Two types of tests were used to probe the order-disorder, melting and crystallization transitions: isothermal frequency sweeps and isochronal temperature sweeps at fixed heating or cooling rates of between 0.1 and 2 °C/min.[30,31]

4.2.5 Small Angle X-ray Scattering (SAXS)

Synchrotron-source SAXS was performed on the saturated block copolymers at Argonne National Laboratory (Argonne, IL) using the DuPont-Northwestern-Dow Collaborative Access Team (DND-CAT) facility with a beam wavelength of λ = 0.729 Å and a sample-to-detector distance of 6.11 m. Calibration was achieved with silver behenate and data were collected on a Mar CCD area detector. Experiments were performed on polydomain XPX specimens that were molded at about 170-200 °C for 15 min then cooled to room temperature in three different thermal treatments: slow cool (≈ 1 °C/min), fast cooled (≈ 20 – 30 °C/min) and quenched (≈ 100 °C/min). 2D SAXS collection was performed at room temperature for the three thermal profiles as well as on the fast cooled sample at 160 °C after 3 minutes of annealing. XPX-2d and XPX-2e, which are melt ordered below 230 – 270 °C and 270 – 310 °C, respectively, were subjected to a fourth thermal treatment procedure. Samples were pressed at 170 °C, annealed at high temperature (250 °C for XPX-2d and 310 °C for

XPX-2e), slowly cooled (≈ 1 °C/min) down to 140 °C stopping every 20 °C to anneal for about 8 h. Finally, they were slowly cooled to room temperature. SAXS was then performed in these samples at increasing temperatures of 25, 70, 110, 150, 190, 230, 270, 310 °C with 3 min annealing each in order to find an approximate T_{ODT}.

Laboratory source SAXS was performed at the Institute of Technology Characterization Facility at the University of Minnesota using Cu Kα X-rays from a Rigaku RU-200VBH rotating anode and a sample-to-detector distance of 4.41 m. CPC and CEC samples were shear aligned prior to the experiment to improve the state of long-range order. Laboratory SAXS data was collected at 150 °C for CEC-1 and CPC-2 without any additional thermal treatment. Alignment of the cylindrical structures in both copolymers was achieved using the large amplitude reciprocating shear device described by Koppi.[32] Compression molded samples 20 mm long by 10 mm wide by 1 mm thick were sheared under argon for about 2 h at T_{ODT} - 30 °C with a strain amplitude of 200% and a shear rate of 0.5 s^{-1}. Two dimensional scattering data were azimuthally integrated to obtain plots of intensity I versus scattering wavevector modulus q, ($q = (4\pi/\lambda) \sin(\theta/2)$, where θ is the scattering angle).

4.2.6 Transmission Electron Microscopy (TEM)

TEM experiments were performed at the Institute of Technology Characterization Facility at the University of Minnesota with a JEOL 1210 electron microscope in the bright field mode operating at 110 kV. Samples were cryo-microtomed at -120 °C with a diamond knife to produce a flat surface and subsequently stained with ruthenium oxide (RuO_4) for 4 hours using reported

procedures[33] to create contrast between chemically distinct domains. Stained samples were microtomed again at -120 °C and 70 – 100 nm thick specimens were collected for imaging.

4.2.7 Mechanical Testing

Samples were drawn in tension up to the point of failure in a Rheometrics Scientific MINIMAT uniaxial tensile testing instrument fitted with a 200 N load cell. All experiments were conducted at room temperature and at a constant rate of 200% strain per minute. Rectangular bars 11 mm long, 2 – 3 mm wide, and 0.8 – 1.2 mm thick were employed, with a 5 – 7 mm gauge length (l_o) and a 2 – 3 mm^2 initial cross-sectional area (A_o). This geometry is optimal for avoiding slipping in the grips and for setting up the sample in the instrument so that it can be stretched to high strains. Engineering stress (σ) versus nominal strain (ε) curves were obtained from force (F) versus displacement (Δl) data, where $\sigma = F/A_o$ and $\varepsilon = \Delta l/l_o$. Young's modulus E was determined by fitting the linear regime of the stress-strain curve, below about 10% strain, with $\sigma = E \cdot \varepsilon$. The data reported here represent values averaged from at least 5 specimens tested per material.

Tension Set (%), ε_s, calculated as (Final Gauge Length – l_o)/ l_o * 100, was determined for each sample. Cyclic extension-compression tests at room temperature were performed on one sample from each of polymers CPC-2, CEC-1, XPX-1, XPX-2b and XPX-3 at a rate of 200% strain/min. Cycles involved the application of an increasing strain, first 25%, then 50%, 100%, 150% and so on, followed by a return back to 0% strain, up to failure. Residual strain, reported for each cycle, is defined as

the strain remaining at zero stress following a sequence of extension and compression.

4.2.8 Wide Angle X-ray Scattering (WAXS)

Experiments were carried out at the Institute of Techonology's Characterization Facility at the University of Minnesota (Minneapolis, MN). 2D WAXS patterns were collected in transmission mode in a Bruker AXS Microdiffractometer at a distance of 5.92 cm. A 4XE short anode produced Cu Kα X-rays, which were monochromated with flat graphite and collimated through two 0.8 mm pinholes. Samples were stretched using the Minimat tensile tester and the sample holder was fixed at a certain strain. The specimen and holder were then transferred as a unit and mounted with a specially fabricated holder that props the sample against the x-ray beam.

4.3 Results and Analysis

4.3.1 Synthesis

Chapter 3 introduced the XPX polymers, which are structured by crystallization and behave as thermoplastic elastomers, and compared them to two melt ordered CPC materials. In this chapter, these XPX materials are compared to two melt ordered XPX materials with higher M_n as well as to melt ordered CEC and to melt ordered and disordered CPC materials of varying M_n. Polymers were synthesized by living anionic polymerization and catalytic hydrogenation, and the molecular characteristics are presented in Table 4.1 (see Chapter 2 for 1,2 versus 1,4 addition information).

The CPC-2 series of materials have f_C = 0.30 but increasing M_n = 36 – 59 kg/mol and the associated rheological properties will be compared to those of the XPX-2 polymers. CEC-1 is introduced as an all glass-semicrystalline material to compare to XPX in terms of strain recovery. The XPX materials have three different composition profiles with approximately equal f_C and f_E. The five XPX-2 series of materials have $f_C \approx f_E \approx 0.25$ and $f_P \approx 0.50$ and increasing M_n = 59 – 195 kg/mol. XPX-2d and XPX-2e are the only materials that show melt ordering and are thoroughly analyzed in this chapter.

Table 4.1: Molecular characterization data for all block copolymers

Sample	f_C	f_E	f_P	N [a]	M_n (kg/mol)	M_w/M_n [b]
CPC-2a	0.31	0.00	0.69	446	35.5	1.03
CPC-2	0.30	0.00	0.70	597	47.4	1.03
CPC-2b	0.30	0.00	0.70	746	59.3	1.07
CEC-1	0.31	0.69	0.00	610	22.9	1.06
XPX-1	0.18	0.22	0.60	1848	103.4	1.11
XPX-2a	0.25	0.26	0.49	1060	59.0	1.11
XPX-2b	0.25	0.26	0.49	1423	79.2	1.13
XPX-2c	0.25	0.26	0.49	2044	113.7	1.16
XPX-2d	0.27	0.25	0.48	2393	132.8	1.13
XPX-2e	0.26	0.25	0.49	3546	195.0	1.14
XPX-3	0.30	0.28	0.42	799	43.8	1.21

[a] Calculated using bulk homopolymer densities from Fetters et al.[28] with 118 Å^3 reference volume. [b] Determined for saturated CPC and for unsaturated precursors of CEC and XPX by SEC with PS standards in THF at 30 °C.

All the block copolymers listed in Table 4.1 have relatively narrow polydispersities. The XPX polymers show somewhat higher values, up to M_w/M_n =

1.21, which can be attributed to the slow addition of B to poly(styryllithium) in XPX. Figure 1 shows SEC traces for the unsaturated precursors of XPX-2d and XPX-2e with high M_n, which indicate the presence of lower M_n molecules, presumably SBS and SBSI, due to termination before coupling. However, the peaks represent less than 7% of the overall amount of material and thus we assume the effect on properties to be negligible.

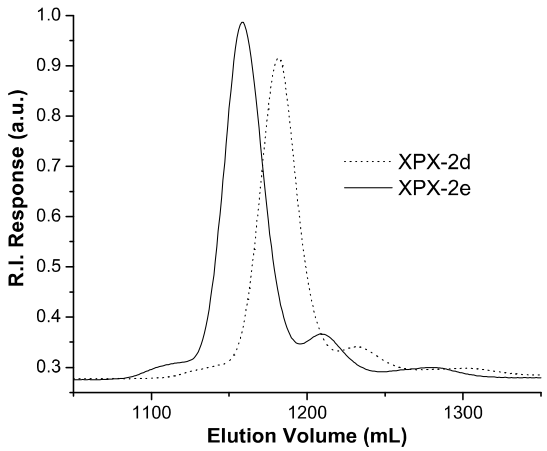

Figure 4.1: SEC traces for high molecular weight unsaturated precursors of XPX-2d and XPX-2e in their coupled (SBS-I-SBS) forms. Secondary peaks involve presence of uncoupled materials (SBS-I at ≈ 1,225 mL and SBS at ≈ 1,300 mL) but these are below 7% of the total material.

4.3.2 Thermal and Rheological Properties

Properties determined by DSC and rheology are summarized in Table 4.2 for CPC and Table 4.3 for CEC and XPX. Block copolymers showed three types of thermal responses by DSC, as represented by selected materials in Figure 4.2. In all cases, T_g for C, which lies at about 145 °C for homopolymer C,[34] was not detected for any of the materials. This is probably due to the low glass content and to its proximity to T_{ODT} in the case of CPC-2 and CEC-1 (≈ 170 °C; see rheology next). As shown in

Figure 4.2a for CPC-2 and consistent with previous results, the DSC traces for CPC polymers show a marked T_g for P between -55 and -57 °C. Also in Figure 4.2a, the high temperature regime of CEC-1 appears dominated by E melting and crystallization, with $T_m(E) \approx 107$ °C , $T_c(E) \approx 83$ °C and % crystallinity in E $X_c \approx$ 31%.

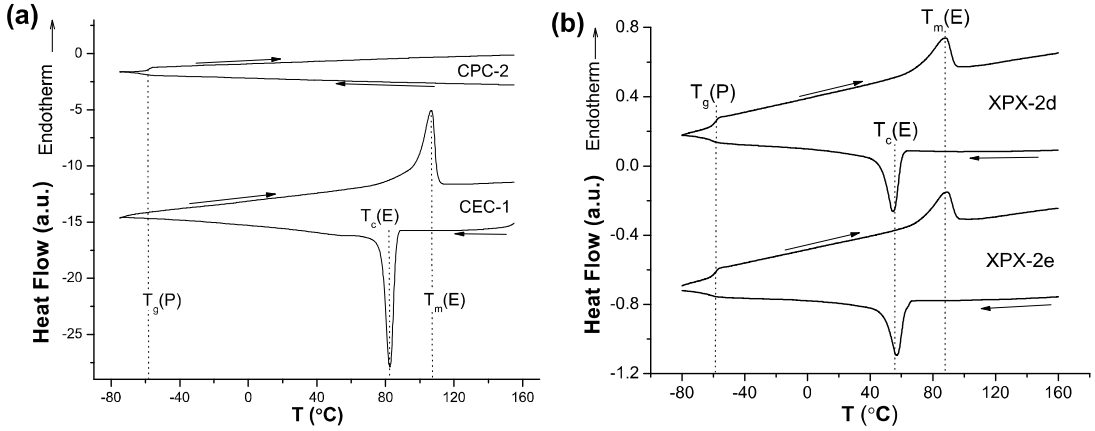

Figure 4.2: DSC traces for (a) CPC-2 and CEC-1 and (b) XPX-2d and XPX-2e. For all materials, T_g for C (145 °C) is undetected, T_g for P is observed at -57 °C, and crystallization and melting dominate thermal behavior of E containing polymers at high temperatures.

The XPX materials all showed a similar behavior in the DSC irrespective of the type of melt segregation (order or disorder) as illustrated by the traces for XPX-2d and XPX-2e in Figure 4.2b. In both cases, T_g(P) matches that from CPC at values between -57 and -59 °C. As summarized in Table 4.3, XPX crystallinity properties are similar to those for CEC, with a slight depression of both melting and crystallization temperatures. This probably stems from less architectural constraints and higher $f_E = 0.70$ in CEC versus $f_E = 0.22 – 0.28$ in XPX. Melting temperatures also decrease for higher M_n XPX-2, which may result from confinement with increased segregation strength, especially if melt ordering occurs.[35]

Table 4.2:Thermal properties of CPC-2 block copolymers

Sample	T_{ODT} (°C)[a]	T_g (P) (°C)[b]
CPC-2a	<140	-57
CPC-2	168	-57
CPC-2b	>300	-55

[a] Order-disorder transition temperature detected by DMS. [b] Glass transitions temperatures of the P block determined by DSC.

Table 4.3: Thermal properties of CEC and XPX block copolymers

Sample	T_{ODT} (°C)[a]	T_m (E) (°C)[b]	T_c (E) (°C)[c]	X_c (E) (%)[d]	T_g (P) (°C)[e]
CEC-1	165	107	83	31	-
XPX-1	$<T_m$	100	68	36	-58
XPX-2a	$<T_m$	98	56	32	-57
XPX-2b	$<T_m$	97	54	26	-58
XPX-2c	$<T_m$	93	55	22	-57
XPX-2d	230 – 270	87	55	34	-59
XPX-2e	270 – 310	87	57	32	-59
XPX-3	$<T_m$	93	54	23	-57

[a] Order-disorder transition temperature probed by DMS. [b] Peak melting temperature, [c] peak crystallinity temperature, [d] percent crystallinity in E block, and [e] glass transition temperature for P block, all determined by DSC.

Dynamic rheological measurements were performed on all block copolymers to probe the phase behavior and compare viscoelastic properties. Frequency and temperature sweeps for CEC and CPC materials are presented in Figure 4.3. Materials were tested at or above 140 °C, which is around the asymptotic T_g for high molecular weight C, and revealed three types of responses.

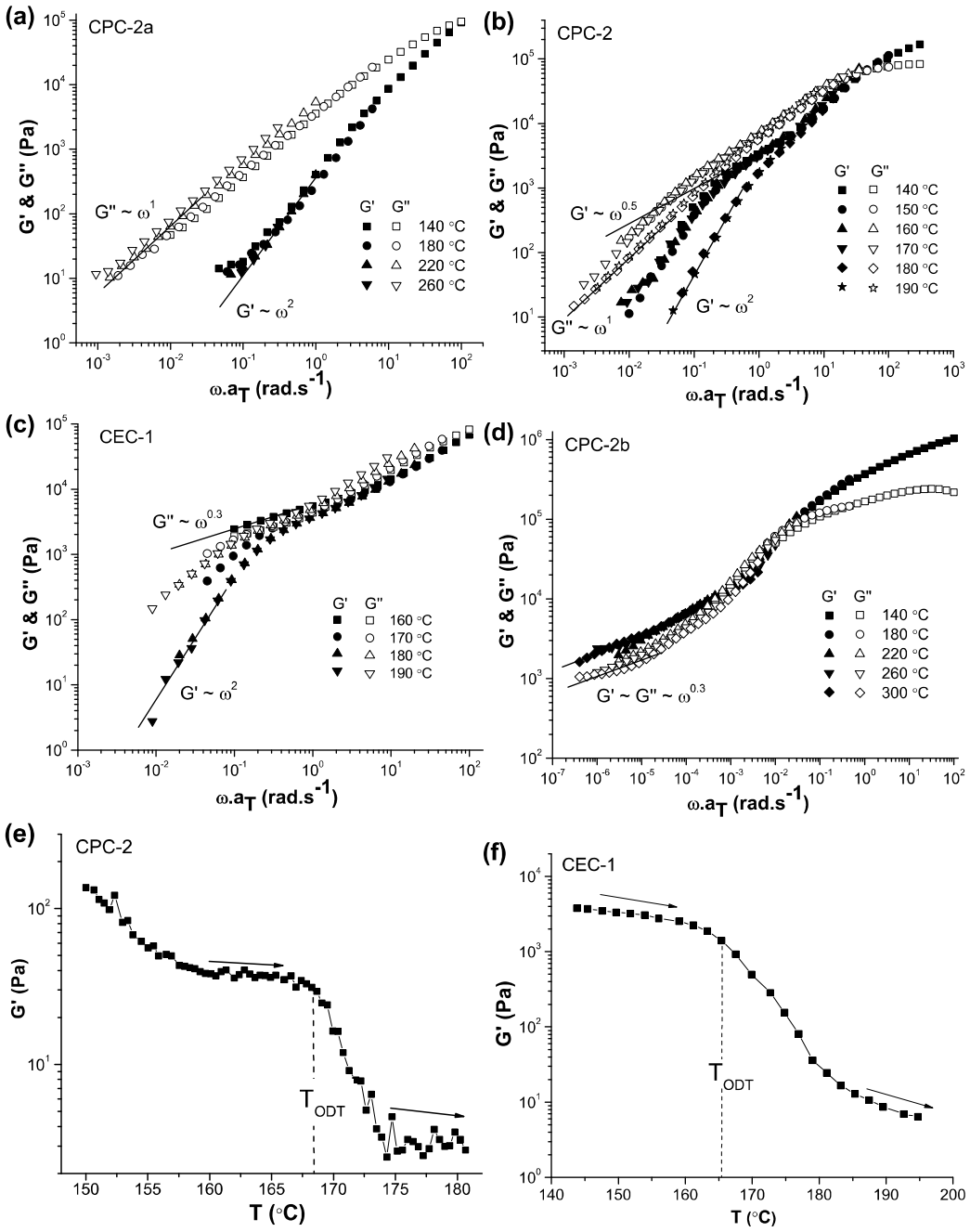

Figure 4.3: Master curves for (a) CPC-2a, (b) CPC-2, (c) CEC-1 and (d) CPC-2b with T_{REF} = 140 °C for CPC and 160 °C for CEC-1. Temperature sweeps for (e) CPC-2 (0.05 rad/s and 0.1 °C/min) and (f) CEC-1 (0.1 rad/s and 1 °C/min). CPC-2a appears disordered, CPC-2 and CEC-1 have $T_{ODT} \approx$ 170 °C and CPC-2b is ordered.

First, CPC-2a (Figure 4.3a) appears disordered at all temperatures above 140 °C, as the low frequency moduli in the master curve show a typical liquid-like

response with $G' \sim \omega^2$ and $G'' \sim \omega^1$.[30,31] On the other hand, frequency sweeps for CPC-2 and CEC-1 (Figure 4.3b and c, respectively) indicate a transition between ordered behavior with $G' \sim \omega^{0.3 - 0.5}$ to disorder with $G' \sim \omega^2$ indicative of $T_{ODT} \approx 170$ °C. However, for CPC-2 this transition is unclear; at 150 °C and above composition fluctuations appear to influence the low frequency rheological properties. Similar phenomena have been reported for E_EP diblocks (E_E is poly(ethylethylene)) especially after alignment of E_E cylinders.[31,36] Finally, the master curve for CPC-2b suggests this material is ordered at all temperatures, with $G' \sim G'' \sim \omega^{0.3}$, which is suggestive of a cylindrical morphology,[37] although in this work DMS was not employed to determine block copolymer morphology. Isochronal temperature sweeps performed on CPC-2 and CEC-1 are shown in Figure 4.3e and f, respectively, to corroborate the identification of $T_{ODT} \approx 170$ °C. Sharp drops in G' with heating, characteristic of T_{ODT}, are observed at 168 °C and 165 °C for CPC-2 and CEC-1, respectively. Temperature sweeps were conducted at low frequency and slow heating rates, namely 0.05 rad/s and 0.1 °C/min for CPC-2 and 0.1 rad/s and 1 °C/min for CEC-1. Melt ordering into cylindrical C domains for both of these materials below 170 °C was also confirmed by SAXS (see below).

Rheological characterization of the XPX-2d and XPX-2e materials proved challenging and inconclusive, attributable to the high molecular weights and associated high viscosities. Figure 4.4 presents frequency sweeps for both materials. Terminal responses are only observed above 220 °C for XPX-2d and 260 °C for XPX-2e; the materials appear disordered above these temperatures but at lower temperatures the states of order could not be established. However, SAXS was

performed (see below) on these materials and the T_{ODT} was narrowed down to the ranges 230 – 270 °C for XPX-2d and 270 – 310 °C for XPX-2e, as listed in Table 4.3. All other XPX materials, as discussed in Chapter 3, showed rheological behavior indicative of melt disorder above $T_m(E)$.

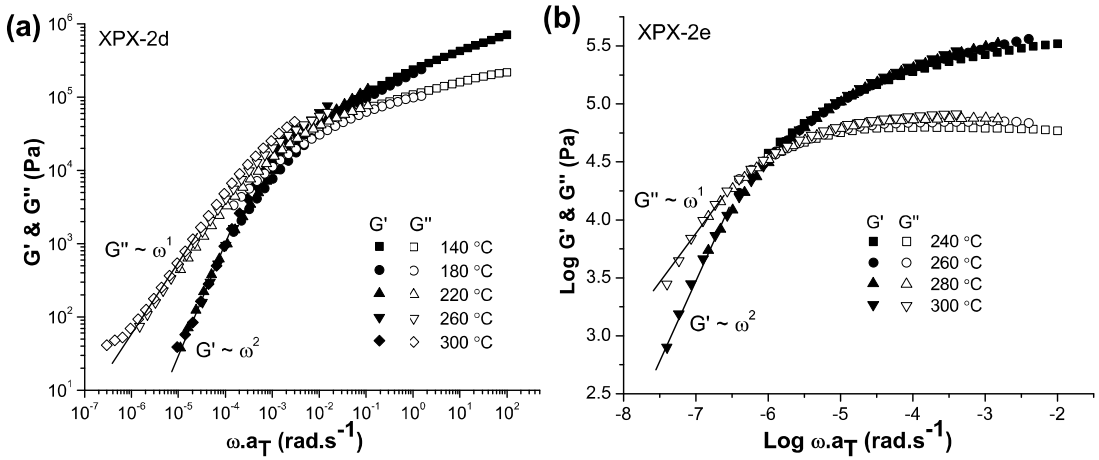

Figure 4.4: Superposition of G' and G'' against reduced frequency from isothermal frequency sweeps with T_{REF} = 140 °C for (a) XPX-2d and (b) XPX-2e. A disordered terminal behavior ($G' \sim \omega^1$ & $G'' \sim \omega^2$) is observed above 220 °C for XPX-2d and above 260 °C for XPX-2e. Below these temperatures their states are unknown.

As a way to indirectly compare the processing of these materials, Figure 4.5 exhibits complex viscosity η^* versus frequency ω for selected materials. Complex viscosities for polymers CPC and XPX-2a, 2b, 2c at 180 °C as well as for XPX-2e at 240 °C are displayed. Different temperatures were employed because the high viscosities of XPX-2d and XPX-2e at 180 °C made obtaining reliable values difficult as samples did not properly attach to the rheometer parallel plates. At 240 °C, sample XPX-2e could be melted and sandwiched between the plates. As observed in Figure 4.5a, CPC-2b (M_n = 59 kg/mol) shows a distinctly melt ordered response since the sample shear thins over all shear rates. On the other hand, CPC-2 (M_n = 47 kg/mol)

and CPC-2a (M_n = 36 kg/mol), which are expected to be disordered, behave as nearly Newtonian liquids, especially at low ω, with a rather constant complex viscosity over all frequencies.

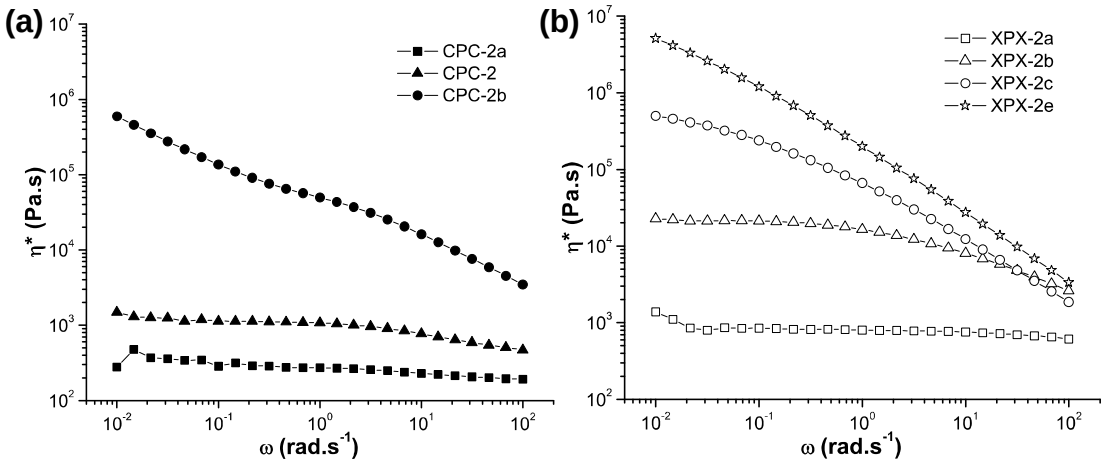

Figure 4.5: Complex viscosity versus frequency for (a) CPC at 180 °C and (b) melt disordered XPX-2a-c at 180 °C and melt ordered XPX-2e at 240 °C. XPX materials remain melt disordered, with low complex viscosities, up to higher M_n.

For the XPX-2 materials, shown in Figure 4.5b, XPX-2a (M_n = 59 kg/mol) and XPX-2b (M_n = 79 kg/mol) show a similar near Newtonian response as the disordered CPC materials at low ω, and XPX-2b shear thins above 1 rad/s. XPX-2c (M_n = 114 kg/mol) is close to order as η^* only plateaus at the lowest shear rates. The complex viscosities for the XPX-2b and XPX-2c materials converge at high frequency. This is the regime where the viscoelastic response is governed by entanglement dynamics, which should be similar for the entangled XPX-2 materials since $M_n(P) >> M_e(P)$ = 2,284 g/mol at 140 °C.[22] Finally, the response from XPX-2e resembles that of CPC-2b, suggestive of melt order at 240 °C, and shows the highest complex viscosity despite being measured at a significantly (60 °C) higher temperature. These results show that melt ordering of both CPC and XPX is

associated with a much greater η^*, a distinct disadvantage for melt processing. Melt ordering occurs at a significantly low overall M_n for CPC (59 kg/mol) while the crystallization structured XPX materials remain disordered up to much higher molecular weights (≈ 135 kg/mol).

4.3.3 SAXS in the Melt

The phase behavior and morphology of CEC, CPC and XPX polymers were probed by SAXS. Figure 4.6 shows SAXS patterns collected at the Characterization Facility at the University of Minnesota from shear aligned samples of CEC-1 and CPC-2 at 150 °C. Both materials appear to be melt ordered with a morphology of hexagonally packed C cylinders aligned along the shear direction. A small peak at a lower q than that of the main reflection is observed for each material. The origins of this reflection are unclear, but most likely result from the instrument optics or perhaps multiple scattering, and are not further considered.

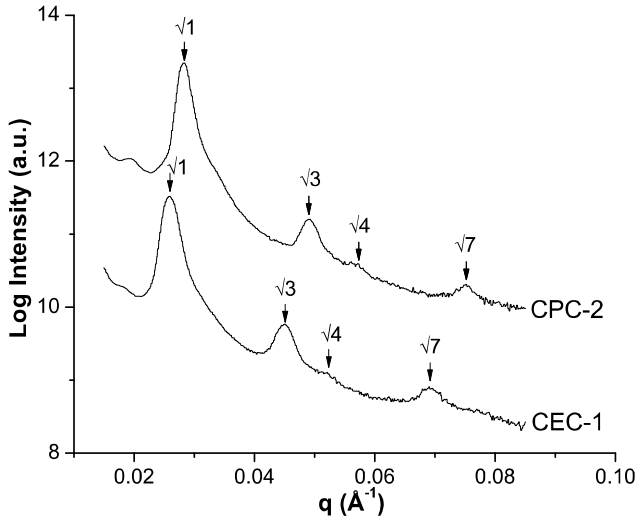

Figure 4.6: Laboratory SAXS data for shear aligned CEC-1 and CPC-2 at 150 °C and along the shear direction, showing hexagonally packed cylinders of C.

Figure 4.7 shows synchrotron-source scattering for XPX-2a, -2b and -2c at 160 °C collected at Argonne National Laboratory. Intensities are multiplied by q^2 in order to account for the angular dependence of the form factor from lamellae, the expected morphology given the compositions of XPX-2.[38] Consistent with the results from Chapter 3, these materials show one broad peak indicative of melt disorder. The q^* values and corresponding domain spacings are listed in Table 4.4.

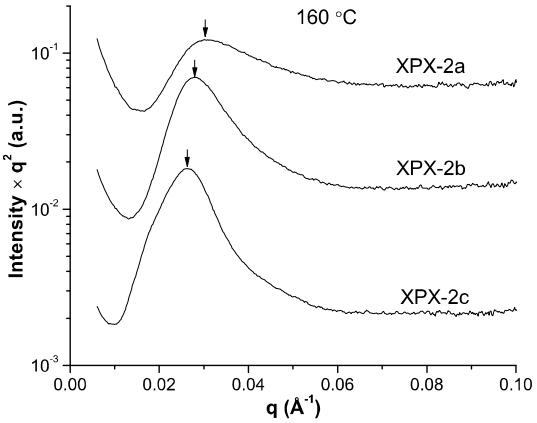

Figure 4.7: Synchrotron SAXS data for melt disordered XPX-2 materials at 160 °C.

Table 4.4: Domain spacings for XPX materials in the melt

Sample	q_1^* (Å^{-1})	d_1^* (nm)	q_2^* (Å^{-1})	d_2^* (nm)
XPX-2a[a]	-	-	0.0314	20.0
XPX-2b[a]	-	-	0.0283	22.2
XPX-2c[a]	-	-	0.0267	23.6
XPX-2d[b]	0.0170	37.5	0.0242	26.0
XPX-2e[b]	0.0138	45.5	0.0217	29.0

[a] At 160 °C. [b] At 110 °C.

SAXS data obtained from melt ordered XPX-2d and XPX-2e proved instrumental in understanding the origins of scattering from all of the XPX materials,

irrespective of the type of segregation. In order to induce the formation of equilibrium structures in XPX-2d and XPX-2e, specimens from these materials were subjected to the following annealing procedure. Specimens were heated to a high melt temperature (240 °C for XPX-2d and 310 °C for XPX-2e) and slowly cooled (≈ 1 °C/min) down to 140 °C stopping every 20 °C to anneal for about 8 h. Finally, they were slowly cooled down to room temperature. Figure 4.8 presents synchrotron-source SAXS data for annealed specimens of XPX-2d and XPX-2e. Data collection was first performed at room temperature and then at elevated temperatures 40 °C apart up to 310 °C.

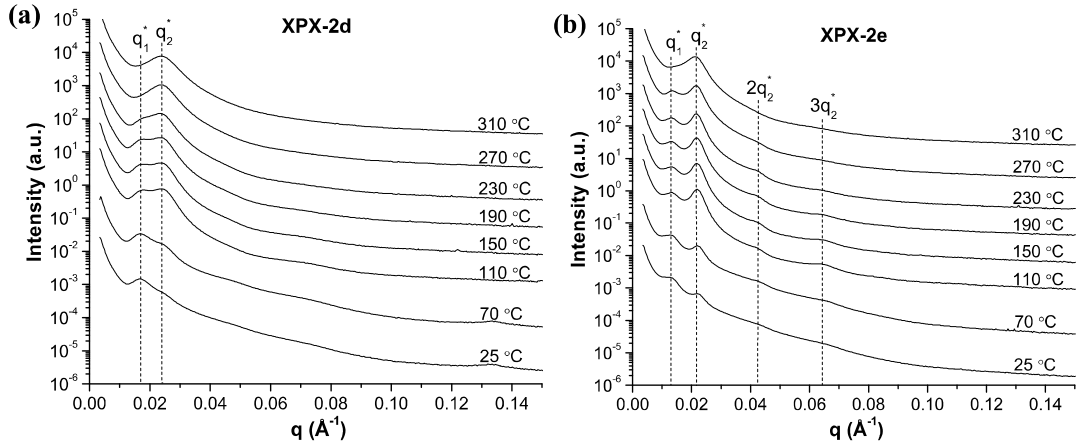

Figure 4.8: Synchrotron SAXS data for (a) XPX-2d and (b) XPX-2e at increasing temperatures after annealing and slow cooling (≈ 1°C/min) from the melt. Materials are ordered above $T_m(E)$ ≈ 100 °C and until high temperatures, showing two principal reflections involving two length scales.

Both materials show scattering with two principal reflections at room temperature, although the peaks for XPX-2e (higher M_n) are more clearly defined. As indicated in Figure 4.8, these patterns show a first peak at q_1^*, corresponding to a domain spacing $d_1^* = 2\pi/q_1^*$, and a second peak at q_2^*, associated with a second domain spacing $d_2^* = 2\pi/q_2^*$. For XPX-2e only, the second peak is associated with two

diffuse higher order peaks at $2q_2^*$ and $3q_2^*$, suggesting the formation of a weakly ordered lamellar morphology. As the temperature is elevated above $T_m(E) \approx 100$ °C, all the peaks are maintained at approximately the same q values. The q^* and associated d^* values from the two main reflections extracted at 110 °C are presented in Table 4.4 (see above). However, at high enough temperatures, 270 °C for XPX-2d and 310 °C for XPX-2e, only one broad peak is observed at $q^* = q_2^*$, which suggests the materials become melt disordered. These transitions provide an approximate range for T_{ODT} as reported in Table 4.3 (see above), and establish the molecular weight limit for XPX melt ordering at $M_n \approx M_n$ (XPX-2d) = 135 kg/mol.

The work by Fleury and Bates on CECEC-P and CECEC-P-CECEC (also named $(CECEC\text{-}P)_2$) block terpolymers with the same compositions as the XPX-2 materials affords a relevant comparison.[3] The melt disordered undecablock copolymer $(CECEC\text{-}P)_2$ shows one correlation hole peak in the melt, consistent with our results for XPX. Similarly, melt ordered CECEC-P materials produce SAXS patterns which resemble the 4 peak scattering observed for XPX-2e. Fleury and Bates matched the relative SAXS length scales to domain distances from TEM images of CECEC-P. Specifically, the first peak at q_1^* (larger domain spacing d_1^*) originates from the correlations between layers of (CECEC) and P while the peak at q_2^* (smaller length scale d_2^*) is related to lamellae of C and E within the CECEC domain. By analogy, we believe that for XPX, q_1^* reflects the X – P correlation, or the average distance between the middle of the CEC segments (X domains) and the P domains. The scattering intensity for this correlation is likely based on the average electron density of X versus P; note that E and P have nearly identical electron densities.

Similarly, the peak at q_2^* can be associated with the C – E spacing in CEC. Consistent with this assignment is the increase of the q_2^* peak upon melting, which is correlated with a reduction in the E domain density. In contrast, the intensity of the peak at q_1^*, associated with the X – P length scale, decreases with melting.[10,11]

Table 4.4 and Figure 4.8 (see above) show that the correlation hole dimensions of all melt disordered XPX-2 materials are comparable to the d_2^* values of the melt ordered XPX-2d and XPX-2e, which were associated with the C – E length scales. Thus, we can conclude that correlation hole scattering in melt disordered XPX polymers reflect the correlation between C and E blocks. However, d^* values for both melt disordered and ordered XPX materials, as well as for CECEC-P, do not scale with N as anticipated by theory. This suggests that the assignment of peak positions to specific block correlations may not be as straightforward as proposed. We return to this topic in the Discussion.

4.3.4 SAXS at Room Temperature

SAXS measurements allowed us to explore structure formation with cooling in XPX. Figure 4.9 shows scattering plots for the XPX-2 materials at room temperature after pressing the samples at 170 – 200 °C and subsequently cooling them at three rates: slow (≈ 1 °C/min), fast (≈ 20 °C/min) and quenching (≈ 100 °C/min). These patterns show relatively broad first-order peaks for all the materials, except for XPX-2e (which was shown to be melt ordered) after slow cooling. XPX-2e exhibits two main reflections and higher order peaks, resembling the melt ordered scattering shown in Figure 4.8b. However, these measurements establish that, even

for melt ordered samples, long range order in XPX generally does not develop when these materials are cooled down to room temperature.

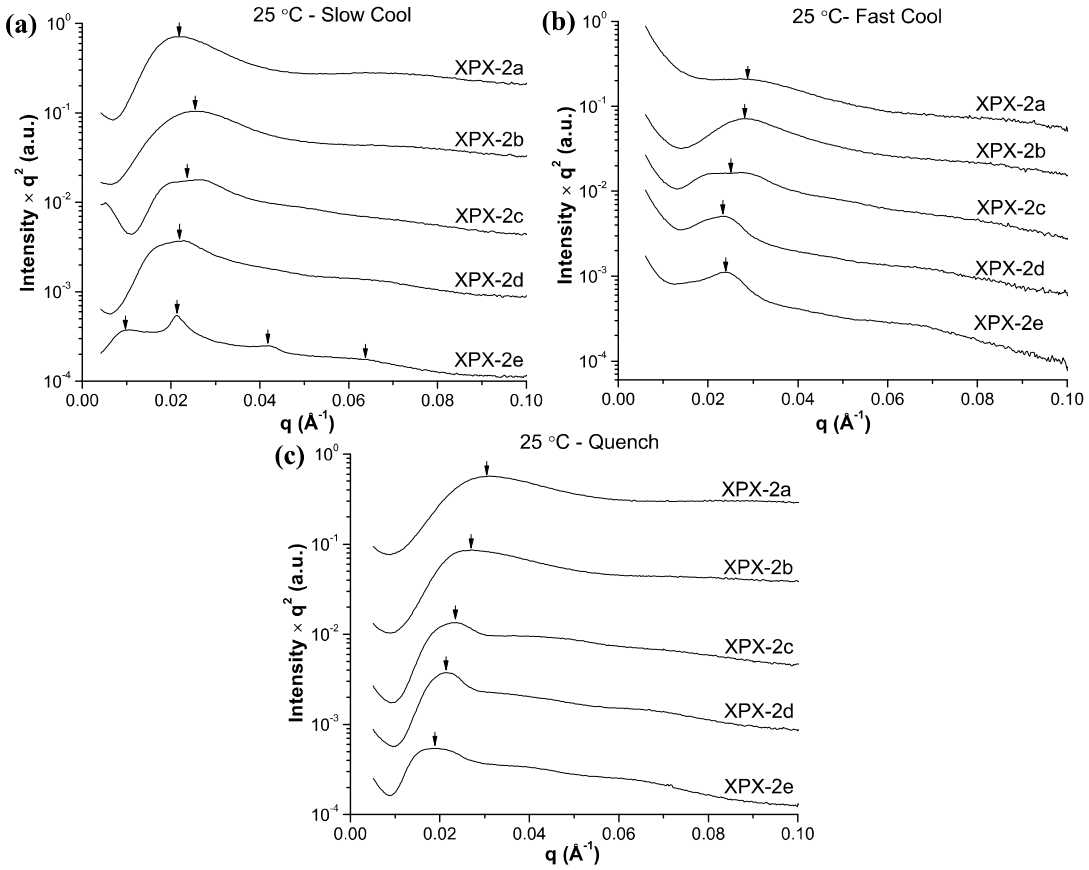

Figure 4.9: Synchrotron SAXS data for XPX-2 polymers at room temperature after three cooling treatments from the melt: (a) slow (≈ 1 °C/min), (b) fast (≈ 20 °C/min) and (c) quenched (≈ 100 °C/min). Relatively broad peaks are observed for all polymers, indicative of disorder, except for XPX-2e after slow cooling.

The domain sizes extracted from the main peaks of the room temperature SAXS patterns are reported in Table 4.5. The average spacings for the quenched samples increase steadily with M_n, which suggests that this cooling treatment may effectively lock in the gross disordered melt structure (obviously crystallinity greatly modifies the local E domain morphology). However, specimens cooled at lower rates have similar spacings. Also, the three highest M_n materials XPX-2c, -2d and -2e

exhibit broad principal reflections that appear to be close to splitting into two peaks, just like XPX-2e after slow cooling. In addition, scattering from these materials show diffuse higher q maxima, which indicate some type of form factor scattering, possibly deriving from the small E crystals. We believe that the absence of marked long range order, the similarity in d^* values, and the incomplete resolution of the two coexisting length scales at room temperature imply that structure formation in XPX is regulated by a complex process of E crystallization and C vitrification, even for the melt ordered materials. We address this further in the Discussion.

Table 4.5: XPX domain spacings from SAXS data at room temperature

Sample	$d^*_{25\,°C\ \text{Slow Cool}}$ (nm)	$d^*_{25\,°C\ \text{Fast Cooled}}$ (nm)	$d^*_{25\,°C\ \text{Quench}}$ (nm)
XPX-2a	28.9	21.2	20.2
XPX-2b	24.4	22.4	23.4
XPX-2c	27.0	26.7	27.1
XPX-2d	30.3	27.8	29.2
XPX-2e	29.0[a]	26.4	33.7

[a] d_2^* value

4.3.5 TEM images

TEM images of XPX-2d and XPX-2e, shown in Figure 4.10, were taken at room temperature after microtoming, staining with RuO_4 for about 12 h, and further microtoming into layers 50 – 100 nm thick. Staining renders the P regions dark, C grey and semicrystalline E white. Just as with the other XPX materials (see Chapter 3), it is clear that these polymers are microphase separated at room temperature. Furthermore, the morphologies are characterized by an irregular arrangement of CEC

and P domains with no particular long range order, in agreement with the absence of higher order peaks associated with the q_1^* peak in the SAXS data. Similarly, the C and E domains seem to produce composite domains without formation of the lamellar morphology associated with q_2^*, as suggested by the SAXS results for slowly cooled XPX-2e.

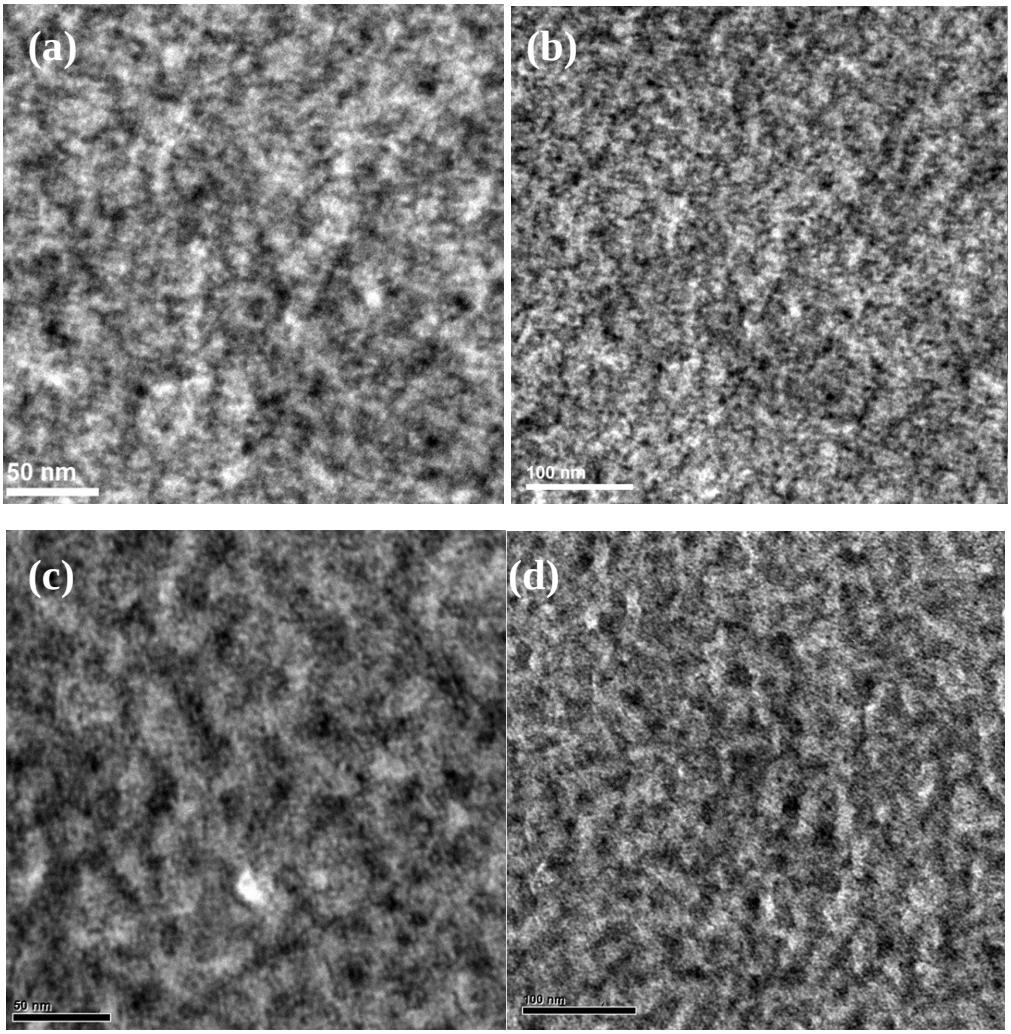

Figure 4.10: TEM images from slow cooled (a) & (b) XPX-2d and (c) & (d) XPX-2e at two different magnifications. These images suggest the presence of an irregular microstructure of C/E (gray and white) domains separated from P (dark) domains.

Scattering supported the co-existence of two length scales in XPX. The patterns for the melt ordered XPX-2 polymers indicated distances for X – P of 38 and 46 nm and for C – E of 26 and 29 nm, from XPX-2d and XPX-2e, respectively. The TEM images in Figure 4.10a and Figure 4.10c, with highest magnification, show that the lengths between dark areas separated by grey regions, or viceversa, are slightly below the 50 nm scale bar, thus matching the expected X – P length scale. On the other hand, the C – E distances determined by SAXS approximately fit the entire width of the grey (CEC) domains, which implies the C domains should be found at the boundaries, but lack of contrast and the general state of disorder between the domains complicates this analysis.

4.3.6 Tensile Properties

The mechanical behavior of two CPC materials and all of the XPX materials, except XPX-2d and XPX-2e, were presented in Chapter 3. Figure 4.11 compares representative stress-strain curves (all curves are presented in Appendix B) obtained from the highest molecular weight XPX heptablocks with those from the other XPX-2 materials; all these materials have the same composition. The responses of all XPX-2 materials resemble typical thermoplastic elastomers, with large elongations at break and relatively high tensile strengths. Table 4.6 summarizes the XPX-2 mechanical properties, which include modulus *E*, strain at break ε_b, tensile strength σ_{TS} and tension set ε_s (or the remaining irreversible strain after failure).

XPX-2d has the highest elastic modulus values, which may result from the combined effects of XPX-2d having an elevated processing temperature ($T_{ODT} \approx 250$

°C) and strongly segregated domains. In general, the mechanical properties of these five XPX-2 materials, with M_n = 59 – 195 kg/mol, are statistically indistinguishable, which emphasizes an advantage of using XPX as thermoplastic elastomers. XPX-2 polymers behave as strong TPEs which can be easily processed at $T_{process} > T_m \approx 100$ °C over all molecular weights up to 114 kg/mol. This is not possible with conventional glassy TPEs, as shown for CPC. The mechanical properties of crystallization structured XPX materials were reviewed in Chapter 3, including strain recovery, which is comparable to that of CPC when $f_X = f_C + f_E < 0.39$.

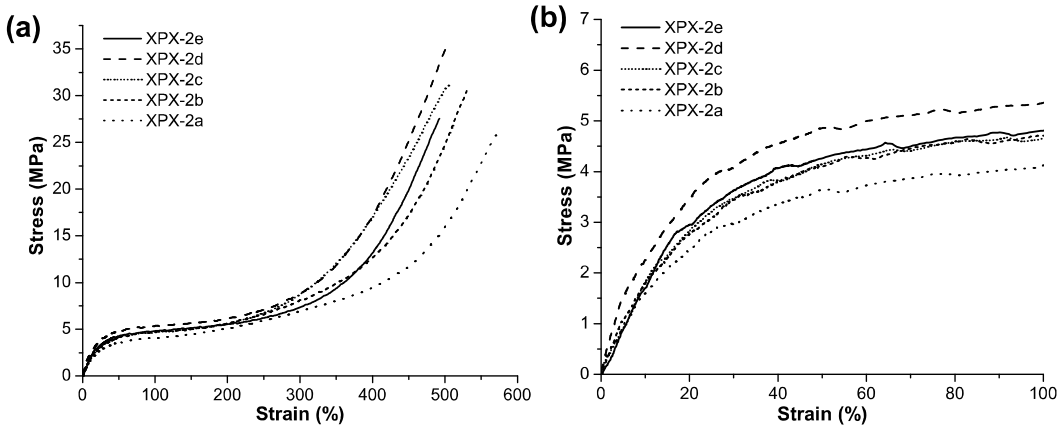

Figure 4.11: Representative engineering stress versus strain curves for the XPX-2 polymers (a) up to break and (b) up to 100% strain. Melt-ordered XPX-2d and XPX-2e behave in a similar fashion as its lower M_n counterparts.

Table 4.6: Tensile properties of selected block copolymers

Sample	*E* (MPa)	ε_b (%)	σ_{TS} (MPa)	ε_s (%)
XPX-2a	19.2 ± 4.5	616 ± 32	25.8 ± 4.1	84 ± 23
XPX-2b	21.9 ± 1.9	551 ± 11	30.5 ± 3.1	64 ± 4
XPX-2c	24.0 ± 3.2	528 ± 19	32.1 ± 5.8	80 ± 19
XPX-2d	33.6 ± 3.9	505 ± 20	34.0 ± 3.3	81 ± 6
XPX-2e	26.9 ± 6.6	482 ± 31	26.6 ± 6.9	72 ± 4

4.3.7 Structure Deformation

Mechanical deformation in XPX polymers with crystallization induced segregation was probed by a combination of cyclic tests and WAXS measurements. Samples were subjected to increasing cycles of deformation (to a desired strain and back to the original size) and the residual strains ε_r (strains remaining at zero load) were recorded. Figure 4.12 shows this cyclic test for CPC-2, XPX-1, XPX-2b, XPX-3 and CEC-1, which have increasing amounts of hard content $f_X = f_C + f_E$ = 0.30, 0.40, 0.50, 0.58 and 1.00, respectively, which should impact recovery. The arrows in Figure 4.12b (a magnified version of Figure 4.12a) indicate increasing ε_r with cycling. The strain recovery of these materials changes drastically with increasing hard content, achieving higher stress values (toughening) but also retaining higher residual strains after any given deformation.

Residual strains are plotted versus cycle strain (the maximum strain achieved at each cycle) for XPX, CPC and CEC materials in Figure 4.13. Non-recoverable deformation in TPEs has been directly related to the deformation of glassy domains (C) and semicrystalline domains (E); polymer crystals are particularly susceptible to plastic deformation.[39-45] As a result, CEC-1, deprived of rubbery blocks, shows the highest irreversible deformations, which increase linearly with deformation strain as the softer E matrix undergoes greater and greater deformation. CPC-2, with no crystallinity, shows the lowest residual strains, although these are comparable to those from XPX-1 at low deformation. The XPX materials have values that are intermediate between those from CEC-1 and CPC-2, which increase with $f_X = f_C + f_E$.

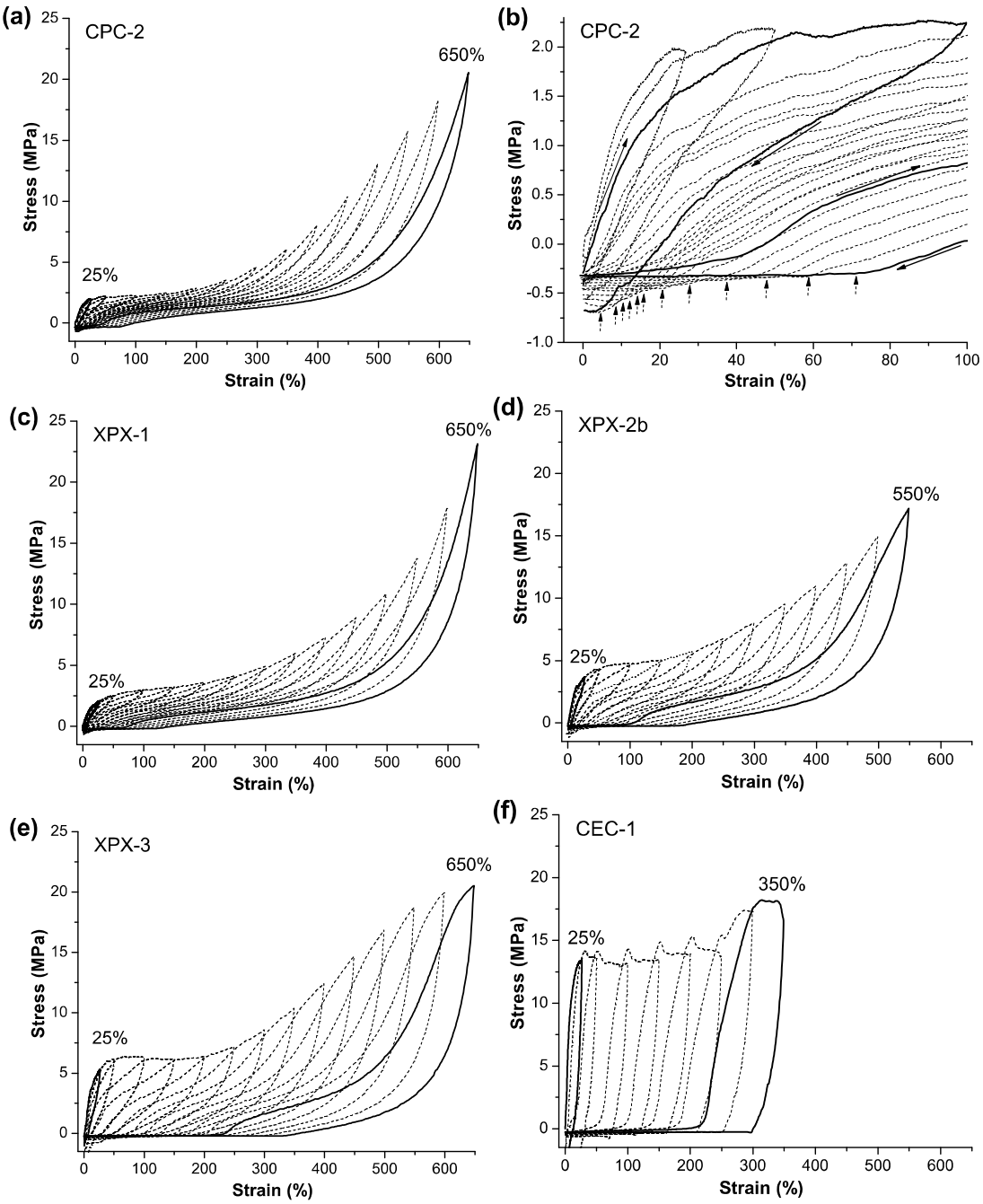

Figure 4.12: Cyclic testing up to increasing levels of strain (25%, 50%, 100%, etc) and back to 0% strain for (a) CPC-2, (b) CPC-2 up to 100%, (c) XPX-1, (d) XPX-2b, (e) XPX-3 and (f) CEC-1. Increasing residual strains ε_r are marked with arrows in (b). Strain recovery decreases as materials toughen with increasing $f_X = f_C + f_E$.

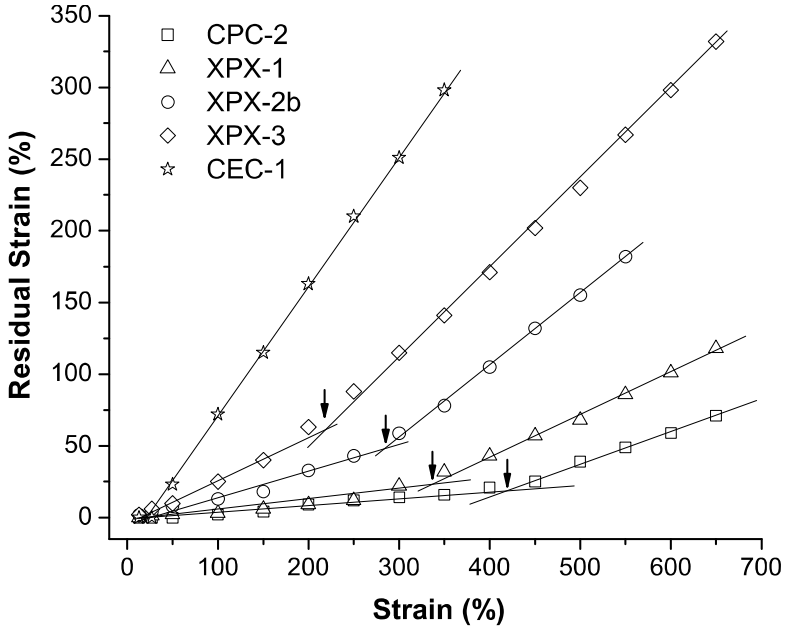

Figure 4.13: Residual strains ε_r versus cycle strain for selected CPC, CEC and XPX materials. In the case of CPC-2 and XPX, two rates of deformation are observed while residual strains for CEC-1 increase monotonically.

The mechanism of deformation for CPC-2 and the XPX materials changes above a specific strain value, which we define as a *transition strain* or ε_T. We believe that while hard content may undergo break-up from the beginning of stretching, ε_T represents the onset of major filler (C and E) disruption, which causes residual strains to increase dramatically. Table 4.7 lists the ε_T values for CPC-2 and XPX extrapolated from the intersection of two straight lines fitted to the data in Figure 4.13 (marked by arrows). As expected, transition strains are lower for materials with higher hard content. Note that these are crude approximations, as cyclic testing was performed only once for each sample and data points are separated by 50% in strain. These results underscore the competitive strain recovery of XPX, also noted in Chapter 3, which is comparable to that of CPC ($\varepsilon_r < 50\%$) for $\varepsilon < \varepsilon_T$.

Table 4.7: Recovery Tests Transition Strains

Sample	ε_T (%)
CPC-2	425
XPX-1	350
XPX-2b	300
XPX-3	225

The deformation of E crystals in XPX as a function of strain was also tracked by WAXS experiments. Samples were stretched and fixed at increasing strains at which WAXS data were collected at room temperature. Figure 4.14 shows 2D WAXS patterns at four increasing strains of 0%, 150%, 300% and 500% for XPX-3.

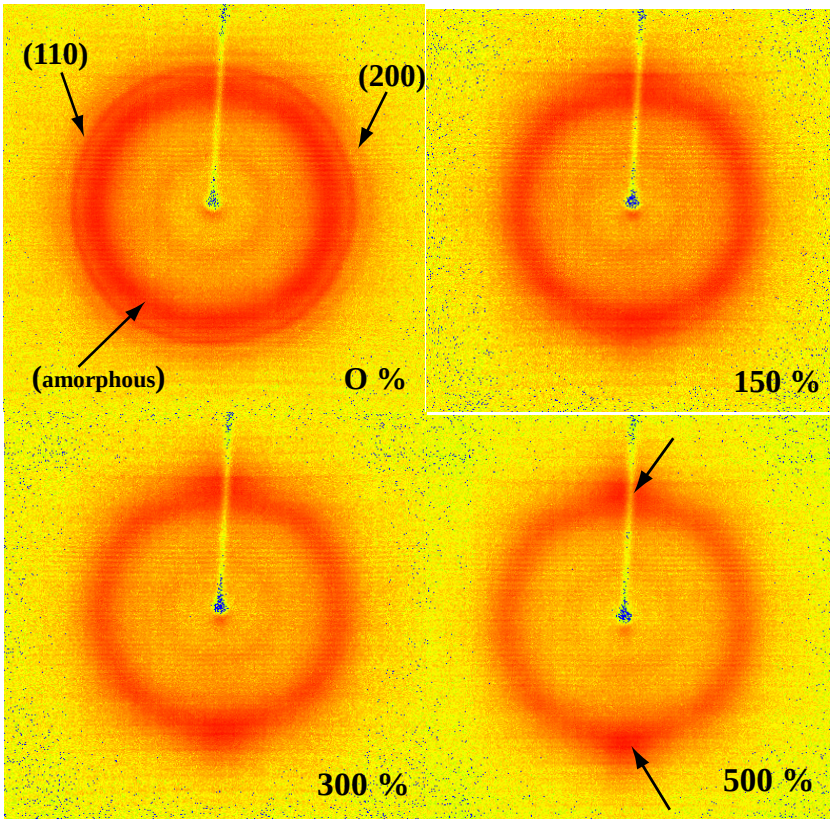

Figure 4.14: WAXS 2-D patterns for XPX-3 at increasing strains of deformation. Crystals deform and align along the deformation direction (horizontal) strain as evidenced by the appearance of spots vertically positioned.

At 0% strain, a broad isotropic ring can be observed associated with amorphous scattering as well as two rings from the (110) and (200) reflections, in that order from the beam stop.[11] As the specimen is stretched in the horizontal direction two spots appear along the vertical direction, indicative of deformed E crystal lamellae aligned along the stretching direction. Thus, the appearance of anisotropy in the scattering ring can be associated with E deformation. A similar behavior was observed for both XPX-1 and XPX-2b. Figure 4.15 shows the 1D azymuthal integration of the 2D WAXS patterns at increasing strains for XPX-1, XPX-2b and XPX-3.

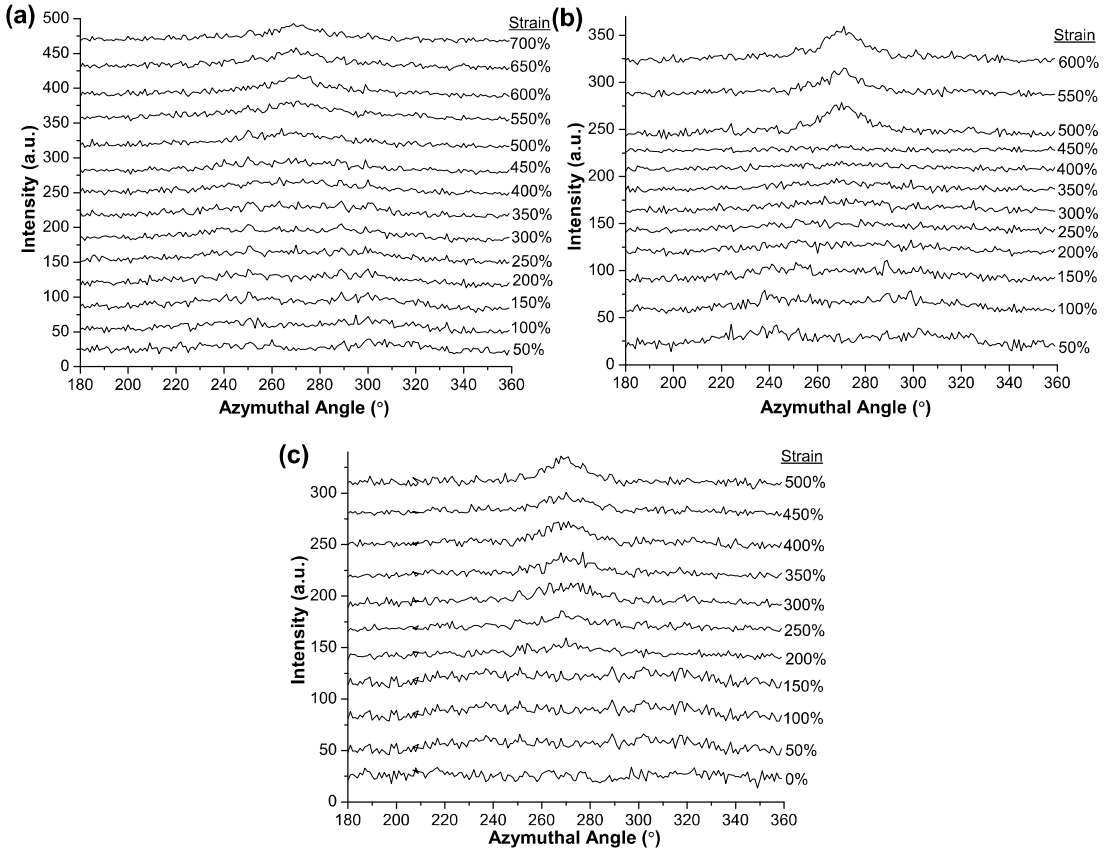

Figure 4.15: WAXS 1-D patterns integrated along the azymuthal angle taken at 25 °C and at increasing strains of deformation for (a) XPX-1 (b) XPX-2b and (c) XPX-3. A peak at around 270° implies crystal deformation and alignment.

This permits a more precise determination of the strain at which E crystals begin to irreversibly deform, as this corresponds to the emergence of a peak at 270°. These strains were determined to be 350% for XPX-1, 450% for XPX-2b and 200% for XPX-3, which are the same or close to the ε_T values detected for XPX by recovery testing. We believe that there is an approximate correspondence between ε_T for XPX, or the onset of high non-recoverable deformation, and the initiation of E deformation.

The tensile responses of the CPC-2 and XPX-1, -2b and -3 materials, first presented in Chapter 3, are shown in Figure 4.16 together with arrows indicating the ε_T values obtained from recovery testing. All curves feature a plateau at an approximately constant stress due to drawing and steep strain hardening at high strain before failure. While for CPC-2, high irreversible deformation is delayed until well into strain hardening, that for XPX coincides with the early onset of this regime.

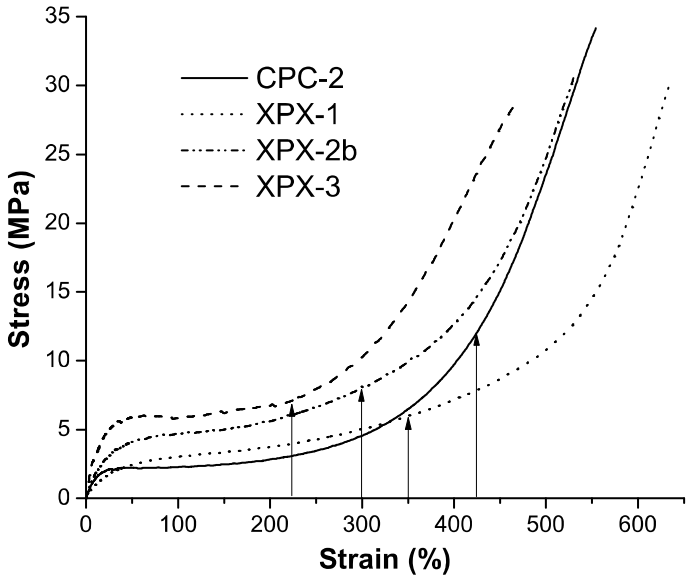

Figure 4.16: Representative engineering stress versus strain curves for (a) CPC-2 and (b) XPX copolymers. Arrows indicate each material's ε_T or the transition strain above which high irrecoverable deformation is onset, which is associated with hard content break up.

4.4 Discussion

4.4.1 Phase Behavior

The analysis of XPX-2 in this chapter suggests two types of XPX phase behavior. The first type, previously established in Chapter 3 and further investigated in this chapter, relates to moderate M_n XPX materials. Three XPX-2 samples (M_n < 115 kg/mol) as well as XPX-1 and XPX-3 are melt disordered based on rheological measurements and show correlation hole scattering with one broad peak at 160 °C (and at 140 °C as shown in Chapter 3) which persists when cooled down to room temperature. As TEM images present a heterogeneous morphology of domains at room temperature (see Chapter 3), we can conclude that crystallization represents the main driving force for microphase segregation.

In contrast, XPX-2d and XPX-2e with M_n = 135 and 195 kg/mol, respectively, are microphase segregated in the melt. For both polymers, scattering patterns indicate the formation of a doubly periodic structure in the melt and XPX-2e forms a lamellar morphology when annealed at elevated temperatures and slowly cooled. However, there was no evidence of long range order in TEM images. Rheological measurements could not access the ordered response at low frequency, making impossible the determination of T_{ODT} with this technique. However, SAXS experiments located T_{ODT} between 230 – 270 °C for XPX-2d and 270 – 310 °C for XPX-2e. Above these temperatures, these materials become disordered in the melt showing single peak scattering (Figure 4.8).

Scattering from melt ordered XPX-2e is similar to those of melt ordered CECEC-P materials (with the same compositions as XPX-2) developed by Fleury and Bates.[3] These SAXS patterns are among the few observations of hierarchical morphologies with double periodicity in block copolymers.[18-23] Based on SAXS and TEM images for CECEC-P, we believe that two correlations coexist belonging to the C – P length scale (q_1^*; longer distance) and the C – E length scale (q_2^*; shorter distance). Also, the proximity of the single reflections for all XPX to the melt ordered q_2^* suggests that the melt disordered peaks stem from C and E correlation hole scattering.[46-48]

Interestingly, while TEM images confirm long range order with two coexisting length scales for melt ordered CECEC-P, images for XPX are devoid of such features and show irregular morphologies. Also, two melt disordered CECEC-P materials showed two correlation hole peaks in the melt while XPX, just like $(CECEC\text{-}P)_2$ (the symmetric version of CECEC-P), shows only one in all cases. Finally, Fleury and Bates report that upon cooling CECEC separates from P *before* C and E segregate based on the presence of a q_1^* peak and associated lamellar higher peaks but not a peak at q_2^*. This result was treated theoretically by Subbotin *et al.*[49] In our case, both periodicities are observed simultaneously when melt ordered. Thus, despite the obvious similarities, the architectural symmetry variation seems to generate differences in segregation strength as well as in the expression of correlations by SAXS. We further investigate these correlations next.

4.4.2 Melt Length Scales

Figure 4.17 shows the domain spacings for melt ordered XPX-2d and -2e as well as the correlation hole dimensions for the XPX-2 materials in a state of melt disorder. These are plotted as a function of the total degree of polymerization N (for d_1^*, associated with X – P correlations) or that of the CEC segment N_{CEC} (for d_2^* or single peak d^*, associated with the C – E correlations). In addition, the d^* value of a symmetric CEC material, which melt orders into a lamellar morphology, is also graphed for comparison, and the associated theoretical scaling are shown with dashed lines.[50] For the melt ordered materials, the periodicities scale as $d_1^* \sim N^{0.49}$ and $d_2^* \sim N_{CEC}^{0.27}$ (Figure 4.17a). Similar trends ($d_1^* \sim N^{0.45 \pm 0.03}$ and $d_2^* \sim N_{CEC}^{0.33 \pm 0.05}$) were found by Fleury and Bates for the five CECEC-P materials, for which three were melt ordered.[3] These are significantly lower exponents than the expected $d \sim N^{2/3}$ predicted in the strong segregation limit.[51] Likewise, the melt disordered spacings scale as $d^* \sim N_{CEC}^{0.30 \pm 0.02}$ and thus also show a reduced exponent than that predicted by RPA theory, $d^* \sim N^{1/2}$, which was also reported in Chapter 3.[51]

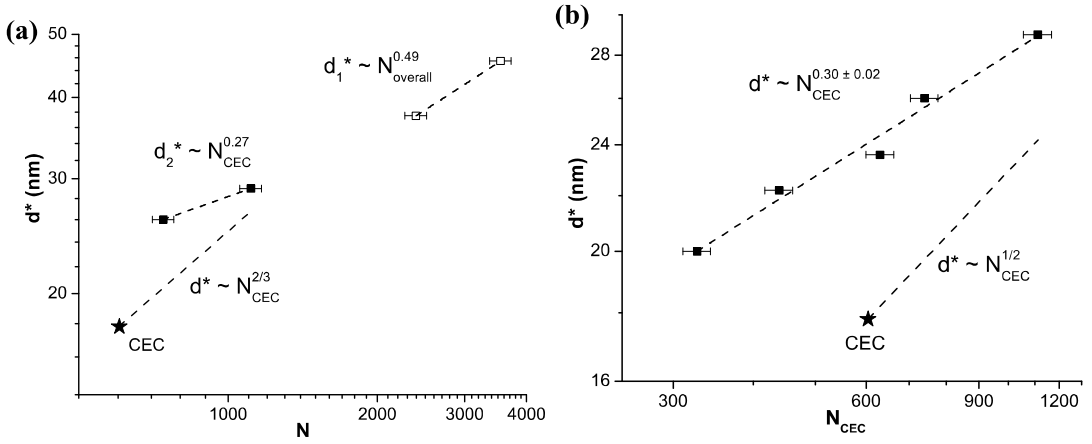

Figure 4.17: Domain spacings for (a) two periodicities in melt ordered XPX-2 and (b) melt disordered XPX-2 versus overall N or N_{CEC}. The spacing of a melt-ordered symmetric CEC and associated theoretical scalings are also plotted for comparison. The experimental scalings are lower than anticipated by theory.

For the melt ordered materials, or for CECEC-P with ordered and disordered materials, this low exponent may result from variations in segregation strength across the samples. For example, segregation was weaker for XPX-2d than for XPX-2e, as lamellar reflections were only apparent in XPX-2e. However, segregation strength should not appreciatively affect the *disordered* peak positions. A comparison between the XPX length scales and the CEC spacing plotted in Figure 4.17 may shed some light on this anomaly. Note that while d_1^*, or the X – P length scale is unique to the melt ordered XPX materials, d_2^* or melt disordered d^*, corresponding to the C – E spacing in X, should be comparable to the domain size of this symmetric CEC triblock. For both melt ordered and disordered XPX, the C – E correlations are larger than the ones predicted by scaling them with CEC and this difference increases with lower molecular weight. This comparison suggests that lower molecular weight XPX-2 materials have larger C – E length scale than anticipated. This is also supported by TEM images, which show that the SAXS length scales for C – E are relatively large compared to the grey CEC domains, matching the longest dimension. We do not understand the exact origins of this phenomenon. A possible explanation for this puzzling effect may be the favorable interactions between P and E, versus C and E, which could promote swelling of the E blocks. However, this interesting effect deserves a more detailed theoretical treatment than we can provide here or the collection of more experimental evidence.

4.4.3 Structure Formation with Cooling

Scattering at room temperature after different cooling treatments showed broad peaks indicative of the absence of long range order, except for slowly cooled

XPX-2e. The length scales associated with these peak positions are shown in Figure 4.18. Quenching produces domains which positively scale with N, as this treatment likely locks the melt structure, for which $d \sim N^{0.27 - 0.49}$. However, as cooling is slowed down, domain sizes become more uniform across the samples. Eventually, with slow cooling, specimens show similar length scales of about 28 nm.

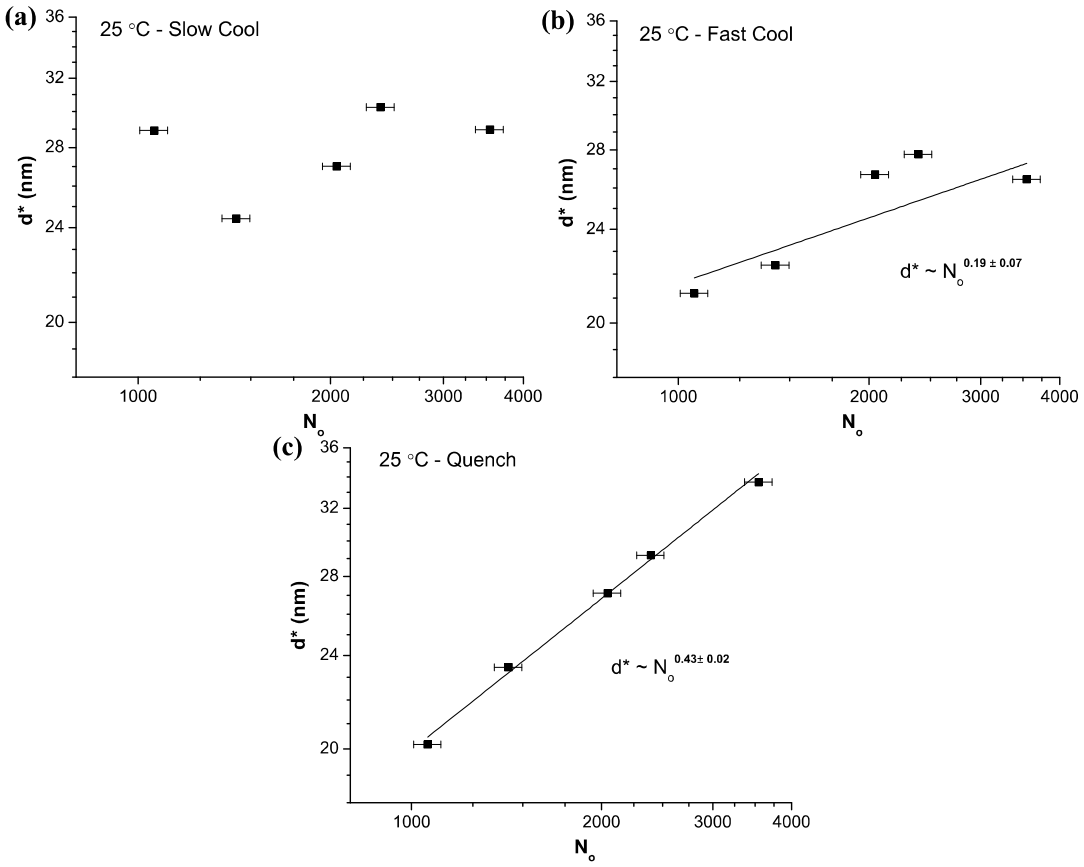

Figure 4.18: Principal domain spacings, d*, from SAXS data, for the XPX-2 series of materials versus degree of polymerization N at room temperature after being (a) slowy cooled, (b) fast cooled and (c) quenched. Domain scalings are inconsistent as they represent complex combinations of two correlations.

Slower cooling rates allow crystallization to further control structuring, with higher degrees of crystallinity and larger crystal sizes, especially for lower M_n materials. Koo *et al.* showed that for crystallization induced segregated EPE triblocks

$d \sim N^{0.22}$ and indicated that for the lowest M_n materials $d \sim N^0$, at room temperature.[7] In contrast, EPE microphase separated in the melt produced lamellar structures at room temperature with $d \sim N^{0.63}$, consistent with the scaling in the strong segregation limit.[51] This shows that E crystallization dominates structure formation in XPX, even for the melt ordered materials, producing similar domain sizes. This is in agreement with TEM images, which show similar structures for all XPX materials at room temperature, irrespective of the type of melt segregation. The unanticipated domain scaling with N may be related to the fact that the single peaks at room temperature represent a combination of the two length scales in these materials (C – E and X – P), as some peaks appeared to be close to splitting.

However, crystallization of rubbery and semicrystalline block copolymers from a homogenous melt usually leads to alternating amorphous and crystalline layers.[52] The fact that this morphology is not observed for any XPX material by SAXS (except for slowly cooled XPX-2e) or TEM may be attributed to the presence of a third polymer type, glassy C. Vitrification of this polymer should be inhibited in the melt disordered materials until spontaneously triggered by segregation at $T_c(E) = 54 – 68$ °C $< T_g(C) \approx 145$ °C (for homopolymer C). Figure 4.19 illustrates how melt disordered XPX at $T > T_m$ eventually microphase separates. Below T_c, the crystallization induced structuring into lamellae is arrested by C vitrification to produce the irregular morphologies observed by TEM at room temperature and the disordered peaks by SAXS. We believe that for the melt ordered materials, crystallization disrupts the melt separated domains, dominating structure development, but the glassy C domains also inhibit lamellar formation.

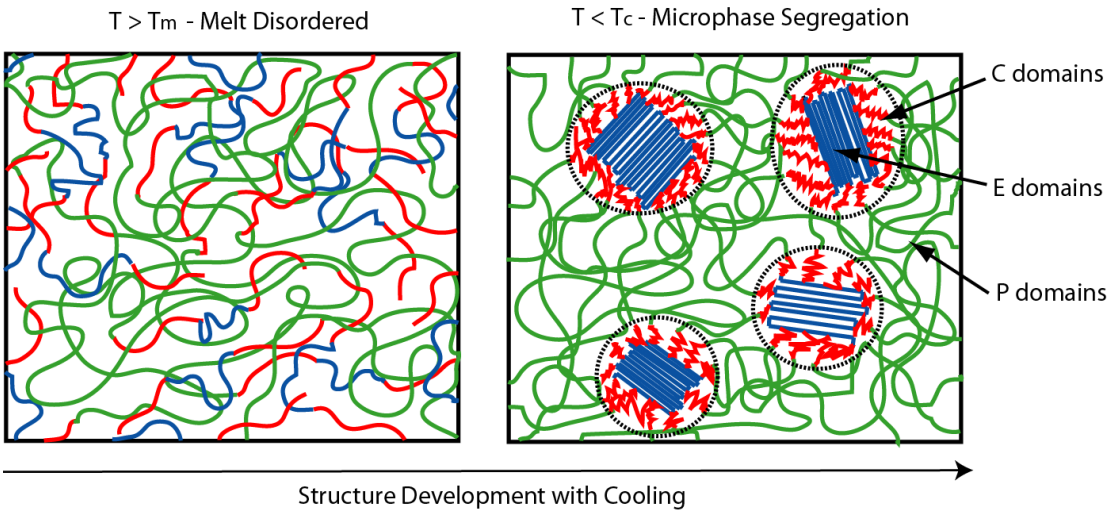

Figure 4.19: Structure development in melt disordered XPX with cooling. Structuring is dominated by E crystallization below T_c but lamellar formation is arrested by C vitrification to produce composite C/E domains insulated by P domains.

4.4.4 Mechanical Properties and Deformation

Melt ordered and disordered XPX materials show similar mechanical properties as strong thermoplastic elastomers (TPEs) as probed by tensile testing. This supports the idea that the XPX materials share a similar structure induced by crystallization. Recovery testing and WAXS experiments were used to identify transition strains ε_T corresponding to the onset of hard content (C and E) break-up, which results in high non-recoverable deformation. The literature supports the notion that glassy failure in TPEs is delayed by rubbery deformation and the results for CPC-2 confirm this and establish that C rupture does not start until the middle of the strain hardening regime.[53,54] On the other hand, the behavior of CEC-1 shows that the softer E domains also delay C break up, deforming prior to C resulting in higher residuals strains from the beginning of stretching. Finally, ε_T for the XPX materials, also associated with E deformation as in CEC-1, coincides with the early onset of strain

hardening. These facts suggest that in XPX, P deformation delays E deformation, which also occurs prior to C rupture.[55-57] This sequence is shown in a general deformation scheme for XPX in Figure 4.20.

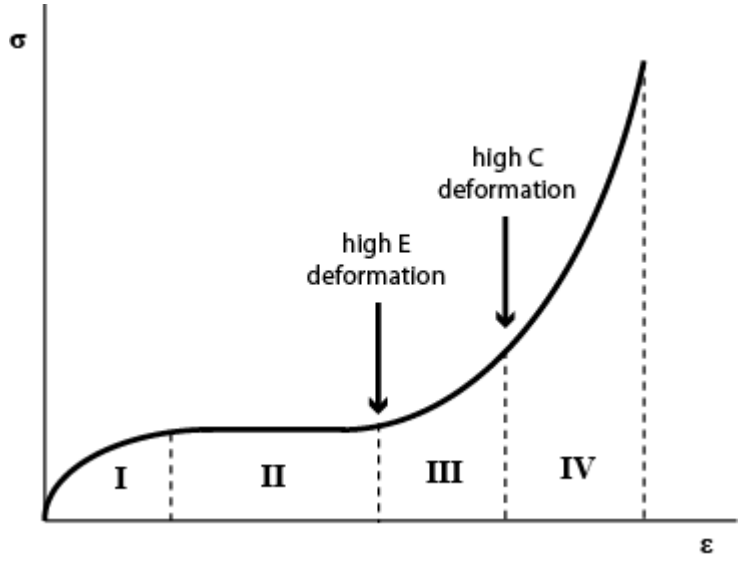

Figure 4.20: General XPX stress-strain curve showing the different regimes of monomer deformation based on recovery and WAXS experiments. The deformation of both hard domains is delayed in XPX by rubber deformation.

A recent publication by Bishop and Register reports on pentablock copolymers of the type *semicrystalline-glass-rubber-glass-semicrystalline*, where microphase segregation is also induced by crystallization.[2] However, these materials are comparable to previously reported polymers such as low M_n EPE or $(EP)_n$ with n < 10, which have tensile strengths σ_{TS} < 8 MPa.[3,6-9] In XPX, as shown in Figure 4.20, C deformation is delayed until close to failure first by P and then by E, rendering tough materials with σ_{TS} < 30 MPa. Also, the fact that E deformation, which produces high irrecoverable deformations as seen for CEC-1, is delayed in XPX until $\varepsilon > \varepsilon_T >$

200% yields materials with competitive recovery (ε_r < 50%), comparable to that of CPC.

Thus, the XPX design results in rather unique materials. XPX mechanical properties compare favorably to those of strong and recoverable TPEs such as commercially important SBS and SIS.[1] At the same time, for a large span of M_n (in XPX-2 from 59 to 195 kg/mol) they remain melt disordered or have accessible T_{ODT}, which is not conceivable with conventional TPEs (in CPC-2 M_n < 59 kg/mol). Thus, XPX materials share the processing benefit of low M_n EPE and similar materials, for which structuring through E crystallization occurs from a homogenous and easily processed melt, independent of M_n up to a high limiting value.

4.5 Conclusion

The thermal, phase and structural behavior of XPX materials were examined by focusing on a series of five XPX-2 polymers with increasing M_n = 59 – 195 kg/mol and the same composition profile $f_C \approx f_E \approx 0.25$ and $f_P \approx 0.50$. Materials with M_n < 115 kg/mol are melt disordered while those with M_n > 135 kg/mol appear melt ordered and produce a doubly periodic structure in the melt and at room temperature when slowly cooled and annealed by SAXS. Domain spacings exhibit the scaling $d \sim N^{\delta}$ with $0.19 \leq \delta \geq 0.49$ depending on the spacing regime and processing conditions. In all instances, δ is smaller than anticipated by theory. All XPX structures are similar at room temperature as shown by TEM, with randomly arranged C and E composite domains separated by P domains. This observation as well as the domain spacings at room temperature determined by SAXS, which resemble those reported for

crystallization induced structured EPE triblocks, suggests that crystallization plays a dominant role in structure formation even for melt ordered XPX. Avoidance of lamellar formation in these materials is attributed to the arresting effect of C segregation and vitrification upon cooling. All XPX materials behave as strong thermoplastic elastomers and have an accessible processing temperature over a wide range of M_n, which may be superior to conventional glassy TPEs such as SBS or SIS. Finally, deformation studies of these materials show that non-linear and irreversible deformation of E and C occurs in the strain hardening regime. This renders materials which are strong and have high elastic recovery after moderate strains.

4.6 References

[1] Holden, G.; Bishop, E. T.; Legge, N. R. *J. Polymer Sci., Part C* **1969,** *26*, 37-57.

[2] Bishop, J. P.; Register, R. A. *Macromolecules* **2010**, *43*, 4954-4960.

[3] Fleury, G.; Bates, F. S. *Macromolecules* **2009,** *42*, 3598-3610.

[4] Wang, H. P.; Khariwala, D. U.; Cheung, W.; Chum, S. P.; Hiltner, A.; Baer, E. *Macromolecules* **2007,** *40*, 2852-2862.

[5] Hotta, A.; Cochran, E.; Ruokolainen, J.; Khanna, V.; Fredrickson, G. H.; Kramer, E. J.; Shin, Y. W.; Shimizu, F.; Cherian, A. E.; Hustad, P. D.; Rose, J. M.; Coates, G. W. *Proceedings of the National Academy of Sciences of the United States of America* **2006,** *103*, (42), 15327-15332.

[6] Koo, C. M.; Hillmyer, M. A.; Bates, F. S. *Macromolecules* **2006,** *39*, 667-677.

[7] Koo, C. M.; Wu, L. F.; Lim, L. S.; Mahanthappa, M. K.; Hillmyer, M. A.; Bates, F. S. *Macromolecules* **2005,** *38*, 6090-6098.

[8] Seguela, R.; Prudhomme, J. *Polymer* **1989,** *30*, (8), 1446-1455.

[9] Mohajer, Y.; Wilkes, G. L.; Wang, I. C.; McGrath, J. E. *Polymer* **1982,** *23*, (10), 1523-1535.

[10] Mahanthappa, M. K.; Lim, L. S.; Hillmyer, M. A.; Bates, F. S. *Macromolecules* **2007,** *40*, 1585-1593.

[11] Mahanthappa, M. K.; Hillmyer, M. A.; Bates, F. S. *Macromolecules* **2008,** *41*, 1341-1351.

[12] Balsamo, V.; Gil, G.; de Navarro, C. U.; Hamley, I. W.; von Gyldenfeldt, F.; Abetz, V.; Canizales, E. *Macromolecules* **2003,** *36*, 4515-4525.

[13] Balsamo, V.; de Navarro, C. U.; Gil, G. *Macromolecules* **2003,** *36*, 4507-4514.

[14] Schmalz, H.; Abetz, V.; Lange, R. *Composites Science and Technology* **2003,** *63*, (8), 1179-1186.

[15] Schmalz, H.; Boker, A.; Lange, R.; Krausch, G.; Abetz, V. *Macromolecules* **2001,** *34*, 8720-8729.

[16] Balsamo, V.; von Gylendfeldt, F.; Stadler, R. *Macromolecules* **1999**, *32*, 1226-1232.

[17] Balsamo V.; Stadler, R. *Macromolecules* **1999**, *32*, 3994-3999.

[18] Ruokolainen, J.; Mäkinen, R.; Torkkeli, M.; Mäkelä, T.; Serimaa, R.; ten Brinke, G.; Ikkala, O. *Science* **1998**, *280*, (5363), 557-560

[19] Ikkala, O.; ten Brinke G.; *Science* **2002,** *295*, (5564), 2407-2409.

[20] Nap, R, J.; Kok, C.; ten Brinke, G.; Kuchanov, S. I. *Eur. Phys. J. E.* **2001**, *4*, 515-519.

[21] Nap, R.; Erukhimovich, I.; ten Brinke, G. *Macromolecules* **2004**, *37*, (11), 4296-4303

[22] Nagata, Y.; Masuda, J.; Noro, A.; Cho, D.; Takano, A.; Matsushita, Y. *Macromolecules* **2005**, *38*, 10220-10225.

[23] Masuda, J.; Takano, A.; Nagata, Y.; Noro, A.; Matsushita, Y. *Physical Review Letters* **2006**, *97*, 98301-98304.

[24] Matsuo, M.; Ueno, T.; Horino, H.; Chujyo, S.; Asai, H. *Polymer* **1968**, *9*, 425-436.

[25] Kawai, H.; Hashimoto, T.; Miyoshi, K.; Uno, H.; Fujimura, M. *Journal of Macromolecular Science, Physics* **1980**, *B17*, 427-472.

[26] Ndoni, S.; Papadakis, C. M.; Bates, F. S.; Almdal, K. *Review of Scientific*

Instruments **1995,** *66*, (2), 1090-1095.

[27] Hucul, D. A.; Hahn, S. F. *Advanced Materials* **2000,** 12, (23), 1855-1858.

[28] Fetters, L. J.; Lohse, D. J.; Richter, D.; Witten, T. A.; Zirkel, A. *Macromolecules* **1994,** *27*, (17), 4639-4647.

[29] Brandrup, J.; Immergut, E. H., Polymer Handbook. In 3rd ed.; John Wiley & Sons: New York, 1989.

[30] Fredrickson, G. H.; Bates, F. S. *Annual Review of Materials Science* **1996,** *26*, 501-550.

[31] Rosedale, J.; Bates, F. S.; Almdal, K.; Mortensen, K.; Wignall, G. D. *Macromolecules* **1995,** *28*, (5), 1429-1443.

[32] Koppi, K. A. *Ph.D. Dissertation*; University of Minnesota: Minneapolis **1993**.

[33] Khandpur, A. K.; Macosko, C. W.; Bates, F. S. *Journal of Polymer Science Part B-Polymer Physics* **1995,** *33*, (2), 247-252.

[34] Gehlsen, M. D.; Bates, F. S. *Macromolecules* **1993,** *26*, 4122-4127.

[35] Weimann, P. A.; Hajduk, D. A.; Chu, C.; Chaffin, K. A.; Brodil, J. C.; Bates, F. S. *Journal of Polymer Science Part B-Polymer Physics* **1999,** *37*, 2053-2068.

[36] Almdal, K.; Bates, F. S. Journal of Chemical Physics 1992, 96, (12), 9122-9132.

[37] Kossuth, M. B.; Morse, D. C.; Bates, F. S. *Journal of Rheology* **1999,** *43*, 167-196.

[38] Rangarajan, P.; Register, R. A. *Macromolecules* **1993**, *26*, 4640-4645.

[39] Odell, J. A.; Keller, A. *Polymer Engineering and Science* **1977,** *17*, (8), 544-559.

[40] Pakula, T.; Saijo, K.; Kawai, H.; Hashimoto, T. *Macromolecules* **1985,** *18*, 1294-1302.

[41] Honeker, C. C.; Thomas, E. L. *Chemistry of Materials* **1996,** *8*, (8), 1702-1714.

[42] Honeker, C. C.; Thomas, E. L.; Albalak, R. J.; Hajduk, D. A.; Gruner, S. M.; Capel, M. C. *Macromolecules* **2000,** *33*, 9395-9406.

[43] Oderkerk, J.; Groeninckx, G. *Macromolecules* **2002**, *35*, 3946-3954.

[44] De Rosa, C.; Auriemma, F.; Ruiz de Ballesteros, O.; *Chem. Mater.* **2006**, *18,* (15), 3523–3530

[45] Ikeda, Y.; Phinyocheep, P.; Kittipoom, S.; Ruancharoen, J.; Kokubo, Y.; Morita, Y.; Hijikata, K.; Kohjiya, S. *Polymers for Adavanced Technologies* **2008**, *19*, 1608-1615.

[46] deGennes, P. G. *J. Phys. (Paris)* **1970**, *31*, 235.

[47] Leibler, L. *Macromolecules* **1980**, *13*, 1602-1617.

[48] Bates, F. S. *Macromolecules* **1985**, *18*, 525-528.

[49] Subbotin, A.; Markov, V.; ten Brinke, G. *Journal of Physical Chemistry B* **2010**, *114*, 5250-5256.

[50] Weimann, P. A. *PhD Dissertation*; University of Minnesota **1998.**

[51] Almdal, K.; Rosedale, J. H.; Bates, F. S. *Physical Review Letters* **1990**, 65, 1112-1115.

[52] Rangarajan, P.; Register, R. A. *Macromolecules* **1993**, *26*, 4640-4645.

[53] Quirk, R. P.; Morton, M. In *Thermoplastic Elastomers*; 2nd ed.; Holden, G.; Legge, N. R.; Quirk, R. P.; Schroeder, H. E.; Eds.; Hanser Publishers: New York, **1996**; pp 71-100.

[54] Tong, J. D.; Jerome, R. *Macromolecules* **2000**, *33*, 1479-1481.

[55] Ryu, C. Y.; Ruokolainen, J.; Fredrickson, G. H.; Kramer, E. J.; Hahn, S. F. *Macromolecules* **2002**, *35*, 2157-2166.

[56] Hermel, T. J.; Hahn, S. F.; Chaffin, K. A.; Gerberich, W. W.; Bates, F. S. *Macromolecules* **2003**, *36*, 2190-2193.

[57] Mori, Y.; Lim, L. S.; Bates, F. S. *Macromolecules* **2003**, *36*, 9879-9888.

5

Hard Block Content and Rubber Entanglement Effects on the Mechanical Response of Elastomeric Block Copolymers

5.1 Introduction

Block copolymers based on glassy poly(styrene) (S) and rubbery poly(butadiene) (B) or poly(isoprene) (I) in the form SBS and SIS have tremendous commercial applications as thermoplastic elastomers (TPEs).[1] In general, block copolymer based TPEs (bcTPEs) consist of a matrix of rubbery blocks microphase separated from hard endblocks (glassy or semicrystalline), which act as both cross-links and reinforcing particles. Their mechanical behavior resembles that of vulcanized and filled rubbers but with superior processing, as cross-links are thermally reversible, i.e. hard domains may flow at high temperatures.[2-4] Catalytic hydrogenation of S, B and I yields saturated molecules with three types of mechanical behavior: glassy poly(cyclohexylethylene) (C) from S, semicrystalline poly(ethylene) (E) and rubbery poly(ethylethylene) from $B_{1,4}$ and $B_{1,2}$, respectively, and rubbery poly(ethylene-alt-proylene) (P) from $I_{1,4}$. Hydrogenated block copolymers have significant practical advantages over their precursors, such as enhanced oxidative and UV stability given the absence of double bonds as well as a higher upper service temperature based on the glass transitions T_g(C) ≈ 147 °C > T_g(S) ≈ 100 °C.[5]

The mechanical properties of bcTPEs have been explained by invoking the interaction between hard and soft blocks. A significant parameter is the overall

molecular weight M_n, which regulates the level of microphase segregation between domains. A weakly segregated bcTPE compromises the strength of the hard domains and thus fails at lower stresses, before the onset of strain hardening. On the other hand, if M_n is sufficient to drive microphase separation, additional increments do not considerably impact mechanical properties.[2,3]

For microphase segregated bcTPEs, changes in composition and, thus, morphology, can greatly impact mechanical behavior.[6,7] In ABA copolymers with glassy A and rubbery B blocks, increasing the glass volume fraction f_A elevates the modulus E and yield stress σ_y, eventually leading to necking. With further addition, strain at break ε_b is reduced, especially when $f_A > 0.50$, resulting in a brittle material at high glass content.[2-4,8] A similar trend is observed for analogous triblocks where A is semicrystalline, such as EBE materials[3] and syndiotactic poly(propylene) with degrees of crystallinity $X_c \approx 16 - 45\%$.[9] However, in this case, at high crystalline content the material's response is not brittle but instead shows high plasticity. Recovery, usually measured as tension set ε_s, or the permanent strain remaining after failure, is higher for semicrystalline TPEs after high deformations, which has been attributed to the plastic deformation of the crystalline component.[9-12]

A few articles have examined the mechanical properties of bcTPEs that combine both glass and semicrystalline polymers as hard phases.[10,11,13-21] Most notably, Mahanthappa *et al.* presented three CPEPC block terpolymers with $f_C \approx 0.4$ and $f_E = 0.30 - 0.70$[17] and the previous two chapters analyzed CEC-P-CEC block terpolymers with $f_C \approx f_E = 0.18 - 0.30$. The effects of C and E on the mechanical response in these materials are similar to the ones observed for the triblock

copolymers materials with only one type of hard block. However, it is difficult to separate the contribution of each component as only a few samples are presented in each work. This project brings together mechanical data from these two types of materials and from block copolymers of the type CEPC, CPC and CEC. All polymers (except CEC) have a typical TPE architecture where rubber blocks are anchored on both ends by hard domains to yield tough materials. Through this set of materials, we have secured a wide spectrum of compositions to investigate the relative effects of glassy C versus semicrystalline E on the mechanical properties of bcTPEs.

The rubber component in TPEs also plays a role in the tensile behavior. In particular, rubber entanglements are able to reinforce the elastomeric network by redistributing uneven stresses through the sliding of highly extended chains without disrupting the overall structure. Studies have reported higher modulus when M_e decreases[4] and Tong and Jerome have theoretically and experimentally established a direct relationship between tensile strength σ_{TS} and M_e^{-1} in bcTPEs made of poly(acrylates).[22] In this chapter, three block copolymers CPC, CE_EPC and CE_EC with $f_C \approx 0.30$ are presented. These materials represent glassy bcTPEs where the degree of entanglement changes considerably, as M_e (P) = 1,475 $gmol^{-1}$ and $M_e(E_E)$ = 4,510 $gmol^{-1}$.[22] E_E and P molecules in CE_EPC appear mixed at RT and we provide a crude estimate of the combined M_e, which is intermediate between that of P and E_E. This set of materials allowed the study of the effect of changing M_e on the mechanical response of bcTPEs.

Materials previously reported and introduced in this chapter were synthesized by living anionic polymerization and catalytic hydrogenation, which results in narrow

polydispersities. Polymers were characterized in terms of molecular structure by SEC and NMR, thermal transitions by DSC, phase behavior by DMS and structure by SAXS. In all cases, materials are micro-phase segregated at room temperature, which means that M_n should not considerably affect the mechanical properties. By examining this large array of polymers, which present different hard block and entanglement characteristics, we have expanded the understanding of the effect of glassy (C) versus semicrystalline (E) hard domains and of rubber entanglements on the mechanical properties of hydrogenated bcTPEs. In particular, we have found different strong positive nonlinear correlations for the modulus versus tension set with respect to the hard block volume fractions f_C and f_E. On the other hand, strain at break and tensile strength were minimally affected by changes in composition. Finally, M_e appears to have an important role in dictating the value of all properties except for tension set.

5.2 Experimental Section

Chapter 2 provided a comprehensive description of the techniques and procedures employed for all the materials analyzed in this project. This section presents the essential information regarding the procedures through which the materials of study in this chapter were synthesized and characterized.

5.2.1 Polymer Synthesis and Hydrogenation

All block copolymers presented in this chapter were produced at the University of Minnesota, except for CPC-1 provided by The Dow Chemical Company. Precursor triblock and tetrablock copolymers SIS, $SB_{1,4}S$, $SB_{1,2}S$, $SIB_{1,4}S$

and $SIB_{1,2}S$ were synthesized by sequential living anionic polymerization of styrene (S) (Aldrich), butadiene (B) and/or isoprene (I) (Acros Organics) and finally S in purified cyclohexane (Fischer Scientific). For those with predominant $B_{1,4}$ addition, the reaction was carried out at 40 °C and initiated with *sec*-butyllithium (1.4M solution in cyclohexane, Aldrich), as described elsewhere.[23] For those with predominant $B_{1,2}$, the reaction conditions were the same with the exception of lowering the temperature to 10 °C and subsequently adding about 200:1 molar ratio of THF to active centers before B addition. An aliquot of the completed first S block was drawn after 8 h of reaction time and precipitated in degassed methanol (Aldrich) for further analysis.

SIS, $SB_{1,4}S$, $SB_{1,2}S$, $SIB_{1,4}S$ and $SIB_{1,2}S$ were hydrogenated to yield CPC, CEC, CE_EC, CEPC and CE_EPC, respectively. This was accomplished by reaction for 12 h over a Pt/Re catalyst supported on macroporous silica particles (Dow Chemical) in degassed cyclohexane at 170 °C under 500 psig of H_2.[24] Block copolymers were recovered from solution in all cases by precipitation in a 1:3 (volume ratio) mixture of isopropanol and methanol followed by drying at room temperature under vacuum to constant weight.

5.2.2 Molecular Characterization

Block copolymer compositions were determined from quantitative ^1H nuclear magnetic resonance (NMR) spectra collected on the unsaturated polymers in deuterated chloroform ($CDCl_3$) (99.8%, Aldrich) using a Varian Unity Inova 300 spectrometer. Monomer mole fractions were calculated by integrating resonances

associated with S, B and I repeat units; these values were then converted to volume fractions for the saturated compounds using the following published polymer densities at 140 °C: ρ_C = 0.920 g/cm^3; ρ_E = 0.784 g/cm^3; ρ_P = 0.790 g/cm^3 and ρ_{EE} = 0.866 g/cm^3.[25] These spectra also allowed the determination of the proportions of 1,2 versus 1,4 additions in both isoprene and butadiene. ^{1}H NMR spectra were also recorded from the hydrogenated polymers in deuterated chloroform at room temperature for CPC, CE_EC and CE_EPC and in deuterated toluene (C_7D_8) (99.6%, Aldrich) at 70 °C for CEC and CEPC, to establish the extent of saturation for each polymer, which in every case was greater than 97%.

The number average molecular weight, $M_{n,S}$, of the first S block of each block copolymer and the molecular weight distribution (M_w/M_n), or polydispersity, of all polymers were determined by size exclusion chromatography (SEC). A Waters 717 GPC fitted with three Polymer Laboratories Mixed-C columns and operated at 30 °C with tetrahydrofuran (J. T. Baker) and calibrated with polystyrene standards was employed with the unsaturated polymers and with CPC, CE_EC and CE_EPC. The saturated CEC and CEPC polymers were characterized with a PL-GPC 220 system operated at 135 °C with 1,2,4-trichlorobenzene. Monomodal and relatively narrow distribution (M_w/M_n < 1.06) peaks were recorded in all cases. Saturated polymer molecular weights were calculated based on $M_{n,S}$ and the overall composition derived from the reaction stoichiometry and NMR results.

5.2.3 Dynamic Scanning Calorimetry (DSC)

Thermal transitions (glass transition and melting and crystallization temperatures) were determined using a TA Instruments Q1000 differential scanning calorimeter (DSC). Poly(ethylene) fractional crystallinity X_c was calculated using the expression $X_c = \Delta H_m / H°_{m,E} \times w_E$, where $H^o_{m,E}$ = 277 J.g^{-1} is the theoretical heat of melting for the 100% crystalline poly(ethylene), w_E is the weight fraction of E, and ΔH_m is the area under the melting peak.[26] Samples were heated to 160 °C, cooled to -80 °C, and heated back to 160 °C, all at 10 °C/min.

5.2.4 Dynamic Mechanical Spectroscopy (DMS)

A Rheometrics Scientific ARES rheometer equipped with 25 or 8 mm diameter parallel plates was used to determine the elastic, G', and viscous, G'', dynamic moduli over the frequency range $0.01 \leq \omega \leq 100$ rad/s. All measurements were conducted at a strain of 1%, within the linear viscoelastic regime. Two types of tests were used to probe the order-disorder, melting and crystallization transitions: isothermal frequency sweeps and isochronal temperature sweeps at fixed heating or cooling rates between 0.05 – 4 °C/min.[27,28]

5.2.5 Small Angle X-ray Scattering (SAXS)

Samples were shear aligned before SAXS collection as an attempt to improve the state of long-range order using the large amplitude reciprocating shear device described by Koppi.[29] Compression molded samples 20 mm long by 10 mm wide by 1 mm thick were sheared under argon for about 2 h at T_{ODT} - 20 °C (or at 250 °C for CEPC-3 where T_{ODT} > 290 °C) with a strain amplitude of 200% and a shear rate of

0.5 s^{-1}. Laboratory source SAXS was performed at the Institute of Technology Characterization Facility at the University of Minnesota using Cu Kα X-rays from a Rigaku RU-200VBH rotating anode and a sample-to-detector distance of 2.49 m. Laboratory SAXS data were collected along the shear direction at 150 °C for CEC-1, CPC-2, CE_EC, CE_EPC and CEPC-3. Synchrotron-source SAXS was performed on CPC-1 at 25 °C, and CEPC-1 at 80 °C and CEPC-2 at 140 °C along the shear direction at Argonne National Laboratory (Argonne, IL) using the DuPont-Northwestern-Dow Collaborative Access Team (DND-CAT) facility with a beam wavelength of λ = 0.729 Å and a sample-to-detector distance of 6.52 & 6.53 m, respectively. Calibration was achieved with silver behenate and data were collected on a Mar CCD area detector. Two dimensional scattering data were azimuthally integrated to obtain plots of intensity I versus scattering wavevector modulus q, ($q = (4\pi/\lambda)\sin(\theta/2)$, where θ is the scattering angle).

5.2.6 Mechanical Testing

Samples were drawn in tension up to the point of failure in a Rheometrics Scientific MINIMAT uniaxial tensile testing instrument fitted with a 200 N load cell. All experiments were conducted at room temperature and at a constant rate of 200% strain per minute. Rectangular bars 11 mm long, 2 – 3 mm wide, and 0.8 – 1.2 mm thick were employed, with a 5 – 7 mm gauge length (l_o) and a 2 – 3 mm^2 initial cross-sectional area (A_o). This geometry is the best one to avoid slipping and easily set up the sample in the instrument so that it can be stretched to high strains. Engineering stress (σ) versus nominal strain (ε) curves were obtained from force (F) versus

displacement (Δl) data, where $\sigma = F/A_o$ and $\varepsilon = \Delta l/l_o$. Young's modulus E was determined by fitting the linear regime of the stress-strain curve, below about 10% strain, with $\sigma = E \cdot \varepsilon$. The data reported here represent values averaged over at least 5 specimens tested per material. Tension Set (%) ε_s calculated as (Final Gauge Length – l_o)/ l_o * 100, was determined for each sample as a measure of strain recovery.

5.3 Results and Analysis

5.3.1 Synthesis

In this chapter, we present the complete characterization of the block copolymers listed in Table 5.1. In addition, we incorporate mechanical data from previously reported materials of the type CEC, CPEPC and CEC-P-CEC in the discussion. All polymers were synthesized at the University of Minnesota except for polymer CPC-1 obtained from The Dow Chemical Company.

Table 5.1: Molecular characterization data for block copolymers

Sample	f_C	f_E	f_{EE}	f_P	N[a]	M_n (kg/mol)	M_w/M_n [b]	$B_{1,2}$ [c] (%)	$I_{1,4}$ [c] (%)
CPC-1	0.18	0.00	0.00	0.82	1193	90.0	1.04	-	-
CPC-2	0.30	0.00	0.00	0.70	597	47.4	1.04	-	94
CE_EC	0.30	0.00	0.70	0.00	911	60.7	1.03	83	-
CE_EPC	0.31	0.00	0.34	0.36	876	65.2	1.03	85	92
CEC-1	0.31	0.69	0.00	0.00	341	22.9	1.06	7	-
CEPC-1	0.17	0.21	0.00	0.62	866	61.7	1.04	9	94
CEPC-2	0.18	0.42	0.00	0.40	680	45.9	1.06	8	94
CEPC-3	0.30	0.16	0.00	0.54	828	63.3	1.05	11	93

[a] Calculated using bulk homopolymer densities from Fetters *et al.*[22] with 118 Å^3 reference volume. [b] Determined for the unsaturated precursors by SEC with PS standards in THF at 30 °C. [c] Determined by ^{1}H NMR of the unsaturated precursors.

Materials CPC-2, CE_EC and CE_EPC share the same type and amount of hard phase, $f_C \approx 0.30$, but they differ in rubber content which permits a comparison on the effect of rubber entanglement molecular weight M_e on mechanical properties. On the other hand, block copolymers CEC, CPC and CEPC maintain the same type of rubber P (or have none for CEC) but contain different types of hard phase, either glassy C or semicrystalline E, and different contents, f_C = 0.18 and 0.30 and f_E = 0.18, 0.22, 0.42 and 0.70. The modest M_n of all polymers and their low architectural order (triblock and tetrablock) allowed sequential living anionic polymerization to yield materials with narrow polydispersities, $M_w/M_n < 1.06$. As shown in Table 5.1, all P containing materials had a high percentage of $I_{1,4}$ addition (above 92%) in the unsaturated versions. Similarly, materials containing E_E or E were generated from precursor systems with a majority of $B_{1,2}$ (above 82%) or $B_{1,4}$ (above 91%), respectively.

5.3.2 Thermal and Rheological Properties

The thermal properties of all materials were probed by DSC and traces are presented in Figure 5.1. As in the previous chapters, the glass transition T_g for C (145 °C for homopolymer[5]) is undetectable by DSC in all the materials, which may result from a combination of low content and proximity to the order-disorder transition T_{ODT} (150 – 170 °C). Consistent with previous results, the T_g for P is detected for the CPC and CEPC materials between -57 °C and -59 °C.[10,11] The T_g for E_E has been reported to vary depending on the amount of $B_{1,2}$. Graessley *et al.* detected transitions at -34 °C and -45 °C for homopolymer E_E with 88% and 78% $B_{1,2}$, respectively.[30] CE_EC with 83% 1,2 addition shows a transition at -31 °C, which approximately agrees with the observed values considering E_E is part of a segregated

triblock (see below). Notably, CE_EPC does not clearly show either transition. Instead, a diffuse inflection is observed at an intermediate temperature, which implies these polymers are mixed even at low temperatures. This is expected given the interaction parameter between these polymers and the specific combined molecular weight in CE_EPC.[31] For example, a symmetric E_EP diblock with T_{ODT} = 91 °C has a M_n = 50 kg/mol[32] while in CE_EPC $M_n(E_EP)$ = 43 kg/mol. For the CEC and CEPC materials, E melting and crystallization dominate the high temperature regime.

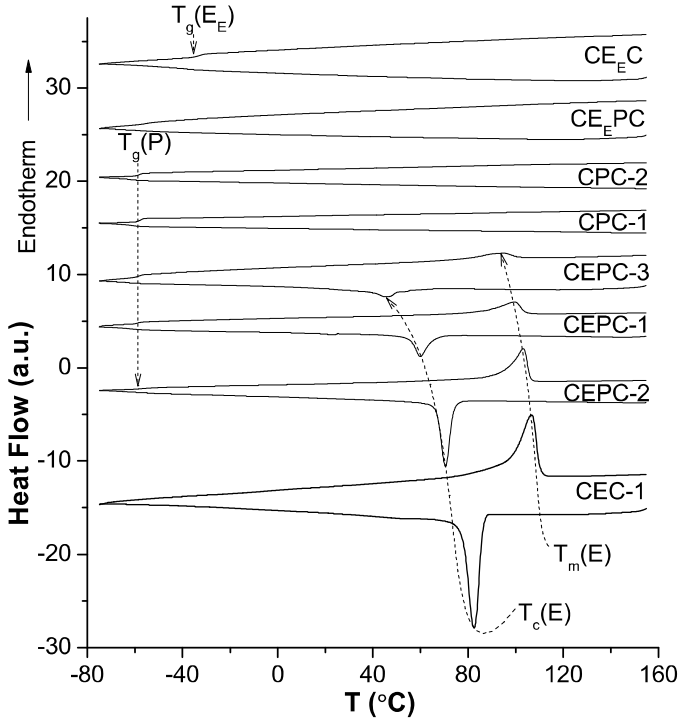

Figure 5.1: DSC traces obtained from heating and cooling all specimens at 10 °C/min. The glass transition for C (≈ 145 °C) is not detected. T_g for P is evident in CPC and CEPC at about -57 °C and for E_E in CE_EC at -31 °C. Melting and crystallization peaks are observed for CEC-1 and CEPC samples. A diffuse T_g between those for E_E and P for CE_EPC indicates the rubbery blocks are mixed.

Values for T_g, melting temperature T_m, crystallization temperature T_c, percent crystallinity X_c, as well as T_{ODT} (see below) are presented in Table 5.2 for the glass and rubber materials and in Table 5.3 for the polymers containing crystallinity. For

the materials that posses an E block, T_m and T_c are both depressed as E content decreases. On the other hand, X_c values extracted from the melting peak areas, do not follow a particular trend as crystallinity depends on parameters such as composition, M_n, architecture and segregation strength (T_{ODT}), which change in a non-trivial form across the samples. Instead, X_c averages about 32%, which is consistent with previously reported block copolymers with an E block.[33]

Table 5.2: Thermal properties of rubbery block copolymers

Sample	T_{ODT} (°C)[a]	T_g (P) (°C)[b]	T_g (E_E) (°C)[b]
CPC-1	172	-57	-
CPC-2	168	-57	-
CE_EC	149	-	-31
CE_EPC	163	-	-

[a] Order-disorder transition temperature detected by DMS. [b] Glass transitions temperatures for P and E_E blocks determined by DSC.

Table 5.3: Thermal properties of block copolymers with crystallinity

Sample	T_{ODT} (°C)[a]	T_m (E) (°C)[b]	T_c (E) (°C)[c]	X_c (E) (%)[d]	T_g (P) (°C)[e]
CEC-1	165	107	83	31.2	-
CEPC-2	≈165	103	70	33.0	-58
CEPC-1	≈180	99	60	38.4	-59
CEPC-3	>290	91	45	25.3	-57

[a] Order-disorder transition temperature detected by DMS. [b] Peak melting temperature, [c] peak crystallinity temperature, [d] percent crystallinity in E block and [e] glass transition temperature for P block, all determined by DSC.

Rheological measurements in the form of isothermal frequency sweeps and isochronal temperature ramps were performed on all materials to examine their phase behavior. For the triblocks and the CE_EPC tetrablock, distinct T_{ODT}s were detected through temperature ramps at low frequency as shown in Figure 5.2. In each case, T_{ODT} is marked by a line at the onset of the approximately discontinuous fall in G' upon heating. The transitions (listed in Table 5.2 and Table 5.3) vary between 149 °C and 172 °C, which should result in strongly segregated domains at room temperature and thus optimal mechanical properties representative of each material.

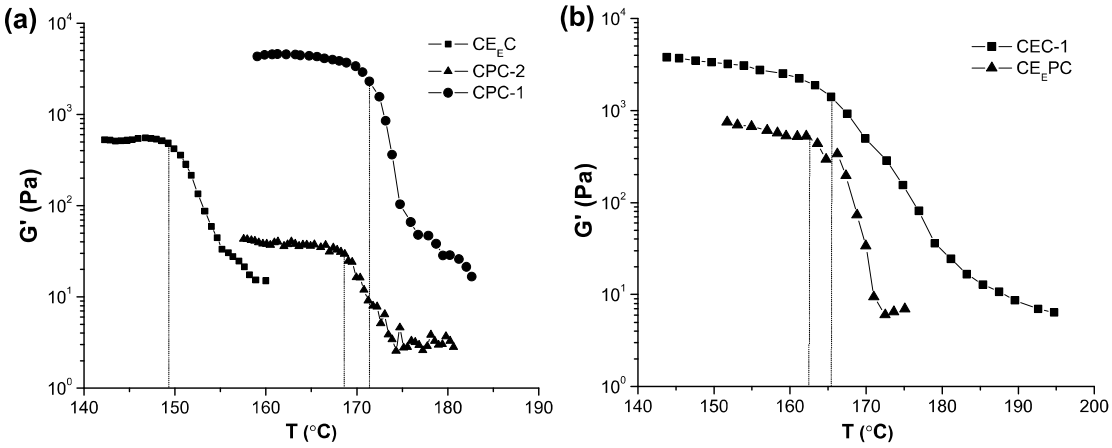

Figure 5.2: Temperature sweeps for (a) CE_EC (0.07 rad/s and 0.2 °C/min), CPC-2 (0.05 rad/s and 0.1 °C/min) and CPC-1 (0.01 rad/s and 0.05 °C/min), and (b) CEC-1 (0.1 rad/s and 1 °C/min) and CE_EPC (0.01 rad/s and 0.05 °C/min). T_{ODT} values are between 149 °C and 172 °C.

T_{ODT} determination for the CEPC-1 and CEPC-2 tetrablock materials was more subtle. Figure 5.3 shows three master curves from frequency sweeps at increasing melt temperatures for CEPC-1, -2 and -3. The master curve for CEPC-3 (Figure 5.3c) is conclusive in establishing a state of order at all melt temperatures, as both moduli plateau at low frequency, with $G' \sim G'' \sim \omega^{0.3}$. On the other hand, for the other two CEPC materials, fine changes in the slope of G' indicate a T_{ODT} between

140 – 160 °C for CEPC-1 (Figure 5.3a) and 120 – 180 °C for CEPC-2 (Figure 5.3b). However, it is difficult to ascertain that G' is not terminal for the lower temperatures and composition fluctuations affect the response at intermediate temperatures for CEPC-2. Nonetheless, isochronal temperature ramps for CEPC-1 and CEPC-2, when compared to the melt ordered CEPC-3 as shown in Figure 5.3d, present diffuse drops which support these transitions. Consequently, we can locate T_{ODT} at about 180 °C for CEPC-1 and 165 °C for CEPC-2 (listed in Table 5.3).

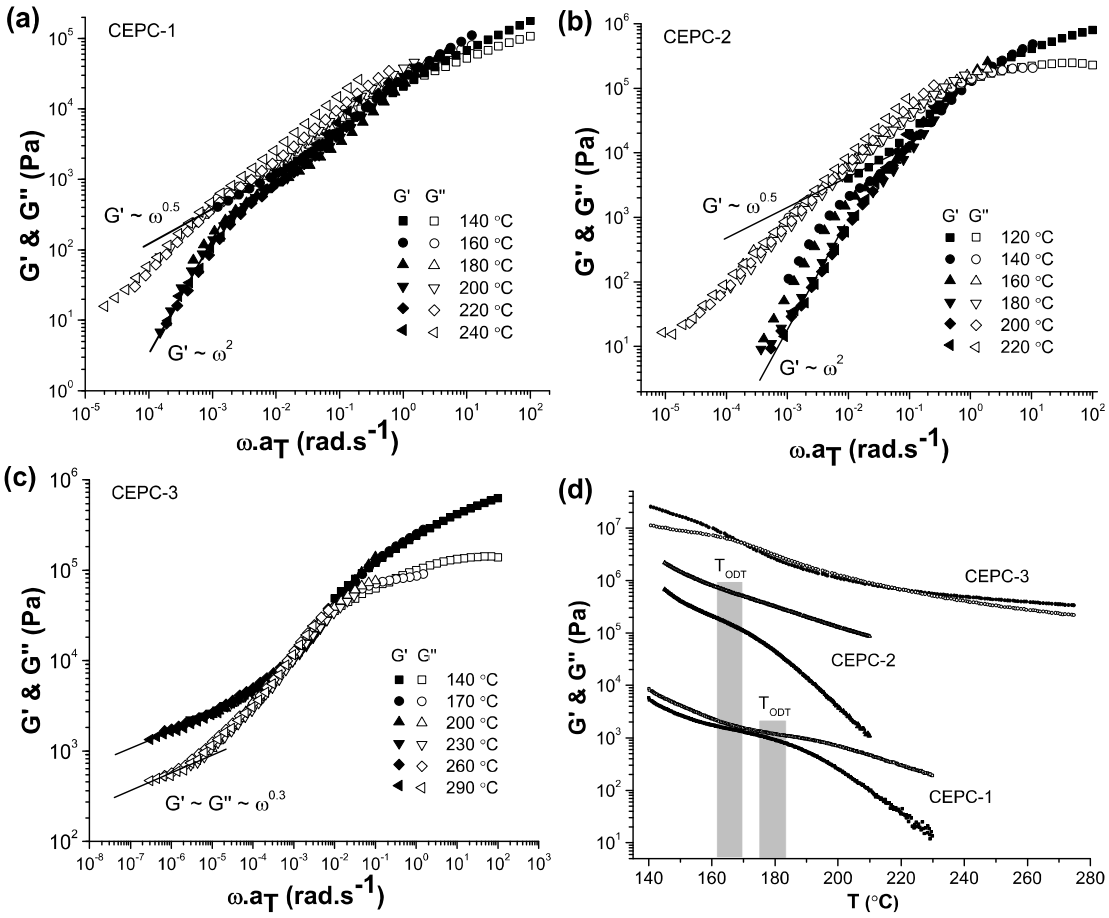

Figure 5.3: Master curves for (a) CEPC-1, (b) CEPC-2 and (c) CEPC-3, with T_{REF} = 140 °C. (d) Temperature sweeps for CEPC-1 (0.07 rad/s and 0.1 °C/min), CEPC-2 (1 rad/s and 1 °C/min) and CEPC-3 (1 rad/s and 4 °C/min). Moduli were vertically shifted by 70 °C for CEPC-2 and CEPC-3. CEPC-1 and CEPC-2 exhibit diffuse T_{ODT}s at about 180 °C and 165 °C, respectively, while CEPC-3 is ordered at all temperatures**.**

5.3.3 Structural Analysis

The structures of all polymers were deduced from SAXS experiments conducted at the Characterization Facility at the University of Minnesota or by synchrotron-source scattering at Argonne National Laboratory. All specimens were shear aligned at about T_{ODT} - 30° or at 250 °C for CEPC-3 with T_{ODT} > 290 °C in order to improve scattering contrast by creating macroscopically aligned structures. 2D SAXS data were collected along the shear direction at 140 °C and Figure 5.4 shows patterns for all materials except CEPC-1 and CEPC-2.

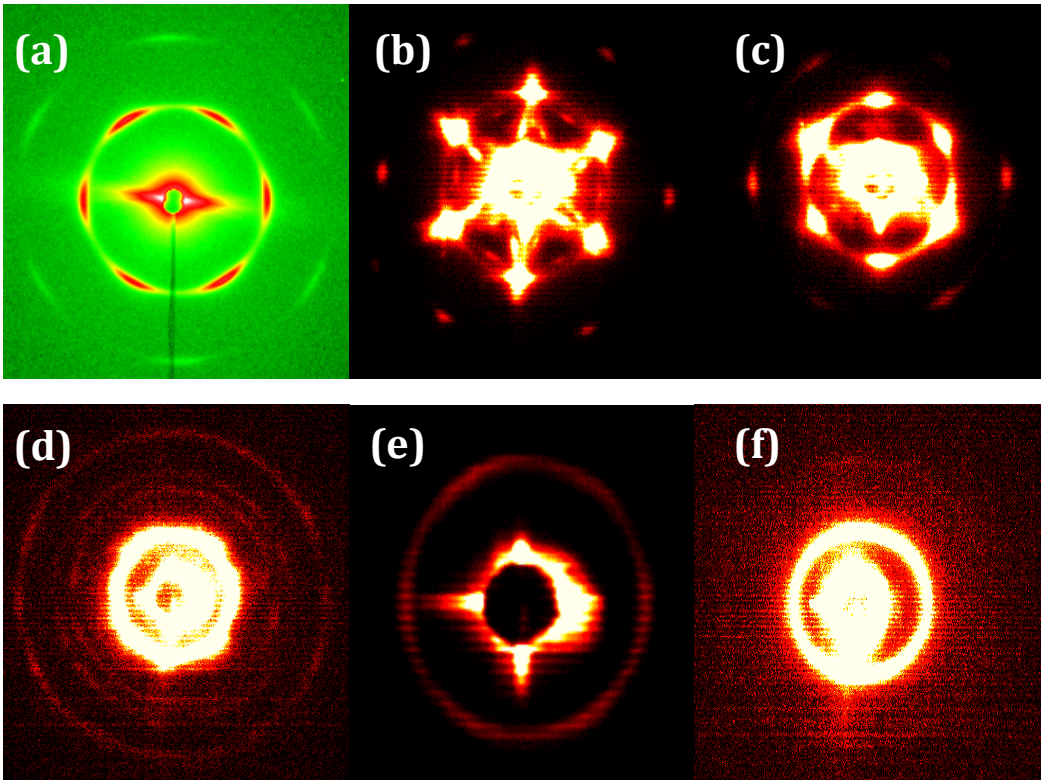

Figure 5.4: Two dimensional SAXS patterns in the shear direction for shear aligned samples of (a) CPC-1 at 25 °C with synchrotron source, (b) CPC-2, (c) CEC-1, (d) CEPC-3, (e) CE_EC and (f) CE_EPC at 140 °C with laboratory source. Except for CE_EPC, which shows two isotropic rings, materials exhibit hexagonal patterns indicative of a morphology of glassy cylinders oriented in the shear direction.

All materials apart from CE_EPC show anisotropic hexagonal scattering characteristic of a cylindrical morphology of C cylinders aligned along the shear direction. The levels of alignment and contrast, however, differ substantially among samples. Most notably, the pattern for CE_EC has low contrast and alignment as only weak peaks are seen and no higher order reflections are noticed. CEPC-3 shows strong contrast with several higher order reflections but alignment is poor and thus peaks are not restricted to a perfect hexagonal arrangement. Finally, CPC-1, CPC-2 and CEC-1 show good contrast and alignment with a neat pattern of six spots.

The 1-D integrations of 2D SAXS patterns from Figure 5.4 as well as those from CEPC-1 and CEPC-2 not shown are presented in Figure 5.5. The hexagonal 2D arrangements yield the expected peak positions for a cylindrical morphology for CEC-1, CPC-1, CPC-2 and CEPC-3. Interestingly, both CEC-1 and CPC-2 show a subtle peak below the principal reflections, at $q \approx q^*/1.7$, but the origins of these reflections are not clear to us at this time. The scattering pattern for CE_EC is devoid of any high order peaks, which we believe occurs due to the low electron density contrast between C and E_E.[31] However, the 2D pattern indicative of hexagonally arranged cylinders confirms this melt ordered arrangement. Similarly, contrast for CE_EPC is low and while we cannot conclusively establish its morphology, a faint peak at $2q^*$ confirms melt ordering at this temperature as suggested by rheology.

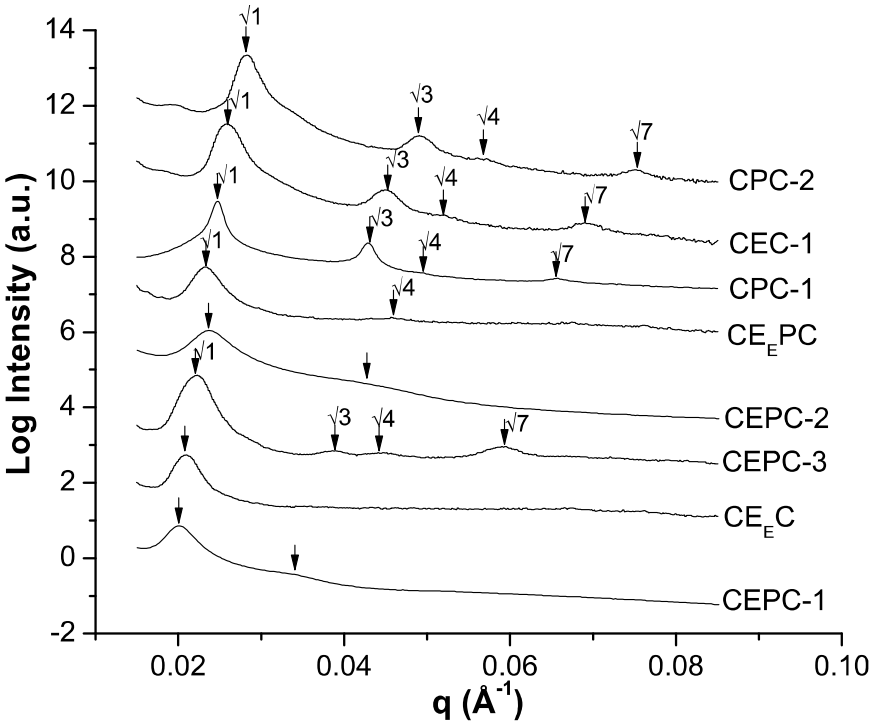

Figure 5.5: SAXS data of shear aligned samples in the shear direction at 140 °C with laboratory source and at 25 °C with synchrotron source for CPC-1. Most materials show patterns consistent with a cylindrical morphology. CE_EC shows no higher order reflections, CE_EPC has a faint $2q^*$ and CEPC-1 and -2 have diffuse maxima, which suggest melt ordering but not a specific morphology.

As with the rheological measurements, the structural characterization of CEPC-1 and CEPC-2 proved challenging. Alignment did not improve the scattering intensity or produce anisotropic 2D patterns. The 1D integrations do not exhibit resolved higher order peaks, and thus we are not capable of determining a specific morphology for either material. However, the patterns show relatively narrow first order peaks and maxima at higher q values for both materials, which confirm the rheological observation of melt ordering below 160 – 180 °C. Table 5.4 summarizes the morphologies determined by SAXS and lists the domain spacings extracted from the 1D patterns.

Table 5.4: Domain spacings calculated from SAXS data

Sample	N	q^* ($Å^{-1}$)	d^* (nm)	Morph[d]
CPC-1	1193	0.0249[a]	25.2	Cyl
CPC-2	597	0.0284[b]	22.1	Cyl
CE_EC	911	0.0211[c]	29.8	Cyl
CE_EPC	876	0.0235[c]	26.7	-
CEC-1	341	0.0259[b]	24.3	Cyl
CEPC-1	866	0.0199[c]	31.6	-
CEPC-2	680	0.0234[c]	26.8	-
CEPC-3	828	0.0226[c]	27.8	Cyl

[a] Measured at 20 °C. [b] Measured at 150 °C. [c] Measured at 140 °C. [d] Morphology by SAXS (Cyl = cylinders of C)

The similarity in length scales between triblock and tetrablocks support the notion that E_E and P are mixed in CE_EPC, as deduced from DSC and the molecular weight comparison to experimental evidence (see above). Similarly, we believe that E and P are mixed in the melt for all CEPC tetrablocks. This is based on the domain spacings as well as on the fact that the combined EP molecular weight in all CEPC materials does not exceed 51 kg/mol and a symmetric EP diblock with T_{ODT} = 114 °C has M_n = 145 kg/mol.[34] However, given the highly exothermic process of crystallization as shown by DSC, E and P should be segregated at room temperature. Consequently, we believe segregation is based on the repulsion between C and the other three blocks in all these materials.

5.3.4 Tensile Properties

The tensile responses of all materials are presented in Figure 5.6 through representative engineering stress-strain curves (all curves are presented in Appendix B). Materials with the same C content are plotted together generating a panel for materials with $f_C \approx 0.30$ (Figure 5.6a) and another one for $f_C \approx 0.18$ (Figure 5.6c). Two more plots are presented which are expanded versions of the previous ones up to 100% strain (Figure 5.6b & d). The behavior of CEC-1 is typically plastic with a clear yield point and drawing at high stress linked to extensive E ductile deformation. On the other hand, it is remarkable that all other materials, including CEPC-2 where f_P is only 0.40, show an elastomeric response. For these materials, the elastic modulus is low, yielding is diffusive, drawing happens at low stress and high strain hardening preambles failure.

Table 5.5 presents the mechanical properties of these block copolymers such as elastic modulus *E*, strain at break ε_b, tensile strength σ_{TS} and tension set ε_s. It also lists the approximate rubber entanglement molecular weight M_e of each material based on that of the rubber block or blocks they contain as determined by Fetters *et al.* at room temperature, where the mechanical response was evaluated.[22] Thus, CEC-1 shows no value, as crystallinity dominates its response at room temperature while CPC and CEPC materials show $M_e(P) = 1{,}475$ g/mol. For CE_EC with 83.3 mol% of $B_{1,2}$, the number of ethyl branches per 100 backbone carbon atoms is 35.8, and hence $M_e(E_E) \approx M_e(\text{PEB-39.3}) = 4{,}507$ g/mol, where PEB-39.3 is an analogous polymer in Fetters *et al.* with 39.3 branches.

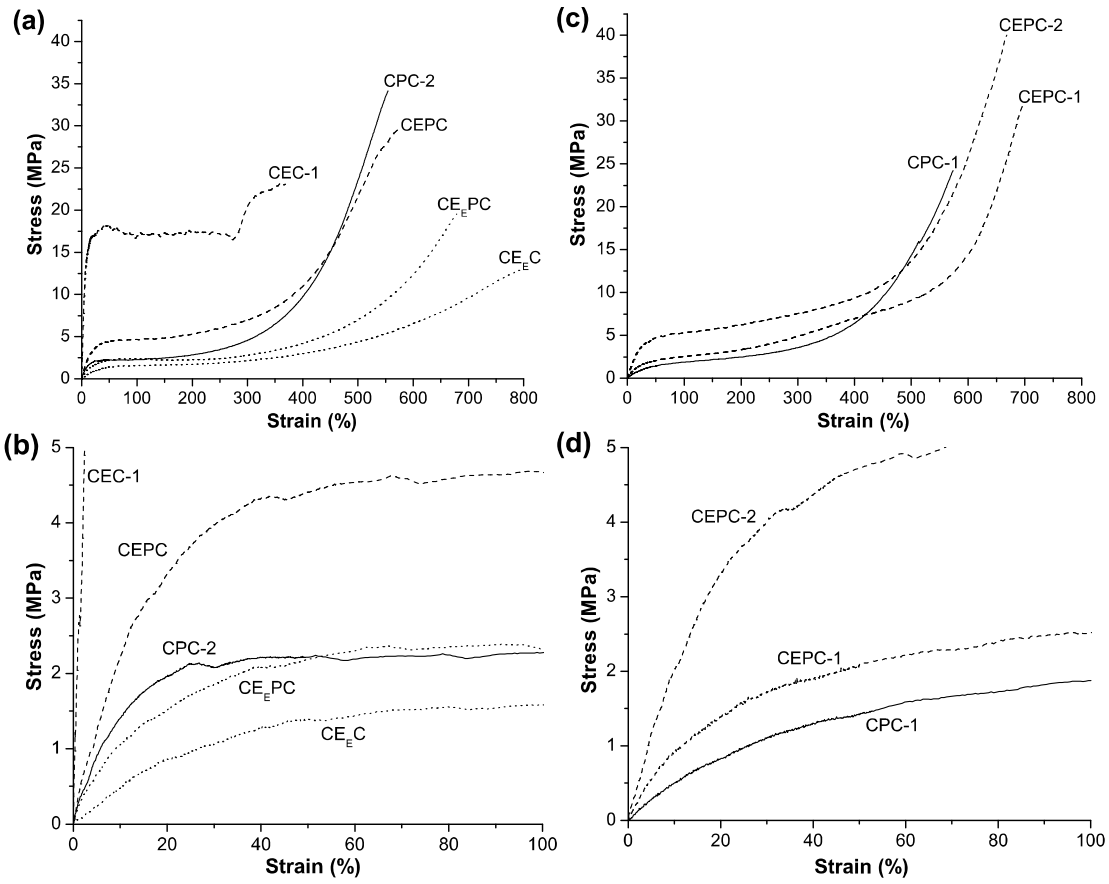

Figure 5.6: Representative engineering stress versus strain curves for block copolymers with $f_C \approx 0.30$ up to (a) failure and (b) 100% strain, and with $f_C \approx 0.18$ up to (c) failure and (d) 100% strain. With CPC samples as reference, the addition of E_E results in softer materials while semicrystalline E increases toughness and modulus.

Finally, the M_e for the tetrablock CE_EPC would be equivalent to that of a symmetric E_EP diblock but we are unaware of appropriate experimental data or of a direct theoretical approach to estimate its value based on those of E_E and P. An indirect method can be deduced from the combination of two relationships. First, the concept of entanglement density $d_e = 1/M_e$ as proposed by Rault *et al.*[35] Secondly, the assumption that total diblock density can be derived from the addition of the individual densities weighted by their mass fractions, since E_E and P are completely

mixed and are unreactive, or $d_e = (w_{E_E}/w_T) \times d_e(E_E) + (w_P/w_T) \times d_e(P)$, where $w_T = w_{E_E} + w_P$. This leads to Equation 5.1 below, which yields M_e (E_E-P) = 2,197 g/mol.

$$\frac{1}{M_e(E_E - P)} = \frac{w_{E_E}}{w_{E_E} + w_P}\frac{1}{M_e(E_E)} + \frac{w_P}{w_P + w_{E_E}}\frac{1}{M_e(P)} \qquad (5.1)$$

Table 5.5: Tensile properties of block copolymers

Sample	f_C	f_E	M_e[a] (g/mol)	E (MPa)	ε_b (%)	σ_{TS} (MPa)	ε_s (%)
CPC-1	0.18	0.00	1,475	5.5 ± 0.8	543 ± 33	22.2 ± 5.3	11 ± 7
CPC-2	0.30	0.00	1,475	20.6 ± 5.0	552 ± 30	32.8 ± 2.2	16 ± 6
CE_EPC	0.31	0.00	2,197[b]	11.3 ± 1.7	672 ± 35	20.3 ± 2.4	27 ± 7
CE_EC	0.30	0.00	4,507	4.0 ± 1.0	757 ± 60	13.2 ± 1.8	24 ± 6
CEPC-1	0.17	0.21	1,475	10 ± 1.6	687 ± 19	29.4 ± 3.4	34 ± 5
CEPC-2	0.18	0.42	1,475	18.4 ± 2.3	689 ± 42	39.0 ± 5.0	170 ± 30
CEPC-3	0.30	0.16	1,475	32.1 ± 7.9	529 ± 39	29.4 ± 5.8	52 ± 10
CEC-1	0.31	0.69	n/a	222 ± 21	356 ± 79	22.0 ± 2.9	232 ± 25

[a] From Fetters *et al.* at 298 K.[22] [b] Theoretical calculation.

Note that this value of M_e for E_E-P is much closer to the smallest M_e value of P than to that of E_E. This is supported by results by Han *et al.*, *who* created an SI diblock where $M_n(S) < M_e(S)$ and $M_n(I) < M_e(I)$ but the overall $M_n > M_e(I)$.[36] This diblock showed rheological properties consistent with an *entangled* polymer, which supports the idea that the combined M_e of two polymers is closer in value to the lowest M_e, as captured by expression 5.1. Thus, while we do not advocate for the

general validity of this approach, we do believe it predicts a correct estimate for this scenario.

In Table 5.5, rubber M_e seems to affect some of the properties of polymers CPC-2, CE_EPC and CE_EC with similar f_C. As M_e increases within these three materials, the modulus drops, the strain at break increases and tensile strength goes down. Based on these observations, a less entangled rubber seems to generate softer elastomeric block copolymers. On the other hand, tension set, or the level of irrecoverable deformation after failure, is statistically similar for all three materials, which indicates M_e might be unrelated to this property. Similarly, f_C and f_E also have an impact on the mechanical behavior of materials containing C, E and/or P blocks. Higher f_C and f_E values increase modulus but the effect of glassy content is more significant. For instance, CEPC-3, with a higher f_C but less total hard block content than CEPC-2, has a higher modulus. Also, a similar positive correlation is observed between the volume of hard blocks and tension set. However, in this case the effect of semicrystalline amount is more considerable than that of glass content. This can be concluded as an important increase in f_C between CPC-1 and CPC-2 only marginally lifts their tension sets whereas higher f_E values among materials with constant f_C results in larger irrecoverable deformations. On the other hand, changes in f_C or f_E seem to have no particular effect on the tensile strength or strain at break for these materials.

These results confirm the importance of f_C, f_E and M_e in controlling the mechanical properties of these materials. While we have been able to partially assess their general impact, it is clear that a larger pool of samples with differing

characteristics is needed in order to fully reveal their separate roles. In our discussion, we have incorporated the mechanical data from similar polymers of the type CPC, CEC, CPEPC and CEC-P-CEC, developed and characterized in our group, to those in Table 5.5 to expand the knowledge on the suggested correlations between these molecular parameters and mechanical properties.

5.4 Discussion

5.4.1 Phase Behavior and Morphology

This chapter introduced block copolymers which consist of hydrogenated polymers C, E, P and E_E with low glass content f_C = 0.18 – 0.30 to generate thermoplastic elastomers of the form CPC, CEC, CE_EC, CEPC and CE_EPC. For this class of materials, mechanical properties and processing are closely tied to the phase behavior and morphology. Specifically, the ability to control microphase segregation is desired given that microphase separated hard domains act as thermally reversible cross-links. For a given composition, microphase segregation will be dictated by the block-block interaction parameters $\chi_{CE} > \chi_{CP} > \chi_{CE_E} > \chi_{E_EP} > \chi_{EP}$ and the combined molecular weight.[31] When segregated, the resulting structures can be determined by SAXS, but peak intensity is dependent on the square of the electron density difference between polymers, which can be calculated based on the values $\rho_e(C) = 0.515 > \rho_e(E_E) = 0.461 > \rho_e(P) = 0.451 \approx \rho_e(E) = 0.448$.[31]

The triblock materials were shown to have optimal and similar values of $T_{ODT} \approx 170$ °C, as determined by rheological measurements, at different but modest

molecular weights that reflect the relative segregation strengths. Specifically, for those with $f_C = 0.30$, M_n (CEC) < M_n (CPC) < M_n (CE_EC), given that χ values scale in the opposite fashion. Consistent with the compositions of these materials, $f_C = 0.18 – 0.30$, materials show a cylindrical morphology by SAXS. However, the patterns at 140 °C for CE_EC have significantly reduced contrast relative to CPC and CEC, which we attribute to the lower electron density difference between C and E_E.

Tetrablock copolymers CEPC and CE_EPC represent novel materials with the favorable potential of combining the properties of two types of polymers in the TPE matrix. In both cases, rheological characterization and SAXS experiments confirmed that the materials were melt segregated. CEPC-3 showed an inaccessibly high T_{ODT} > 290 °C and strong contrast by SAXS suggestive of a cylindrical morphology. However, the other three tetrablocks appeared to be in a state of weak segregation in the melt. While rheology confirmed $T_{ODT} \approx 160 – 180$ °C and SAXS data were indicative of melt order at 140 °C, the exact morphologies were not revealed by scattering given the absence of resolved higher order peaks. In addition, we believe that the middle blocks are mixed in the melt for both types of materials. The domain sizes extracted from the SAXS data point to a significant similarity among domain spacings between tetrablocks and triblocks. Also, in case of CE_EPC, we showed that the combined M_n of E_E and P is modestly below a symmetric diblock with $T_{ODT} = 91$ °C. In fact, for this material, the middle blocks remain mixed below room temperature, as the DSC trace showed a diffuse intermediate T_g between that of E_E and P. Similarly, the combined M_n of E and P is largely below the required value to drive the microphase segregation of these polymers in the melt. However, in this case

we believe that E crystallization (T_c = 45 – 70 °C) must yield segregated E and P domains at room temperature. This importantly exothermic event has been repeatedly noted to drive microphase segregation in low M_n EPE[34], CPEPC[17] and CEC-P-CEC materials.[20] The thermodynamics of the CEPC tetrablock materials appear analogous to those reported by Mahanthappa *et al.* for CPEPC materials with higher $f_C \approx 0.45$ and moderate M_n, which showed lamellae of C and mixed E/P in the melt.[17] Thus, it appears that for materials that combine C, E, E_E and P and have modest M_n, melt microphase segregation is mostly dictated by the incompatibility of the C blocks.

5.4.2 Mechanical Properties

The materials presented in this chapter have a general design of glassy C endblocks and softer matrixes of E, E_E and P middle blocks. This results in materials which behave as thermoplastic elastomers given that the softer middle molecules are anchored on both ends by thermoplastic domains. Compared to commercially ubiquitous SBS and SIS thermoplastic elastomers, the materials in this chapter show a wider range of mechanical responses, which span across the stress-strain area on the basis of compositional and rubber entanglement differences. While we have identified some general correlations between these molecular and mechanical properties, this section introduces mechanical data from previously reported materials in order to draw more conclusive relationships.

Table 5.6 presents the compositions and mechanical characterization of reported materials CPC, CEC, CPEPC and CEC-P-CEC or XPX. Polymers CPC-3, CEC-2 and CPEPC are melt ordered with a lamellar morphology (E/P are mixed in

melt CPEPC). Representative stress-strain curves for these materials are shown in Chapter 1 (Section 1.3.6). In addition, data for XPX materials or CEC-P-CEC, characterized in Chapter 3 are shown. These materials are microphase separated at room temperature due to E crystallization and also behave as thermoplastic elastomers. In the following sections, we investigate E, ε_s, σ_{TS} and ε_b as a function of hard block content, $f_C + f_E$, for materials containing C, E and/or P blocks, and as a function of rubber M_e for CPC, CE_EC and CE_EPC with the same glass content, $f_C \approx 0.30$, but different rubber types.

Table 5.6: Composition and mechanical properties of reported materials

Sample	f_C	f_E	E (MPa)	ε_b (%)	σ_{TS} (MPa)	ε_s (%)
CPC-3[a]	0.36	0.00	28 ± 4	652 ± 65	29.6 ± 3.3	27 ± 4
CEC-2[a]	0.39	0.61	156 ± 20	376 ± 114	22.4 ± 3.5	205 ± 20
CPEPC-30[a]	0.36	0.20	53 ± 4	503 ± 20	29.3 ± 3.1	68 ± 5
CPEPC-50[a]	0.40	0.30	72 ± 6	486 ± 15	38.0 ± 4.3	133 ± 9
CPEPC-70[a]	0.37	0.44	106 ± 8	418 ± 28	29.8 ± 3.3	183 ± 5
XPX-1[b]	0.18	0.22	10.0 ± 1.9	652 ± 23	26.9 ± 4.5	31 ± 14
XPX-2c[b]	0.25	0.26	24.0 ± 3.2	528 ± 19	32.1 ± 5.8	80 ± 19
XPX-3[b]	0.30	0.28	41.8 ± 6.3	509 ± 40	29.6 ± 2.8	97 ± 20

Data reported by [a] Mahanthappa *et al.*[17] and [b] Alfonzo *et al.*[20]

5.4.3 Elastic Modulus

The mechanical characterization of materials presented in this chapter and in previous work affords a relatively large data set to investigate mechanical properties. Figure 5.7 plots the values of elastic modulus E versus hard block content and versus

M_e, both on a log-log scale. Figure 5.7a presents moduli versus overall hard block content $f_C + f_E$, where materials with the same f_C are grouped together. A general correlation for all the data is not evident. However, we have established power correlations which fit the values of the three CPC materials with increasing f_C as well as those for materials with constant f_C and increasing f_E. The value of CEC-1 does not follow the trend for f_C = 0.30, which implies properties change dramatically in the complete absence of rubbery P block.

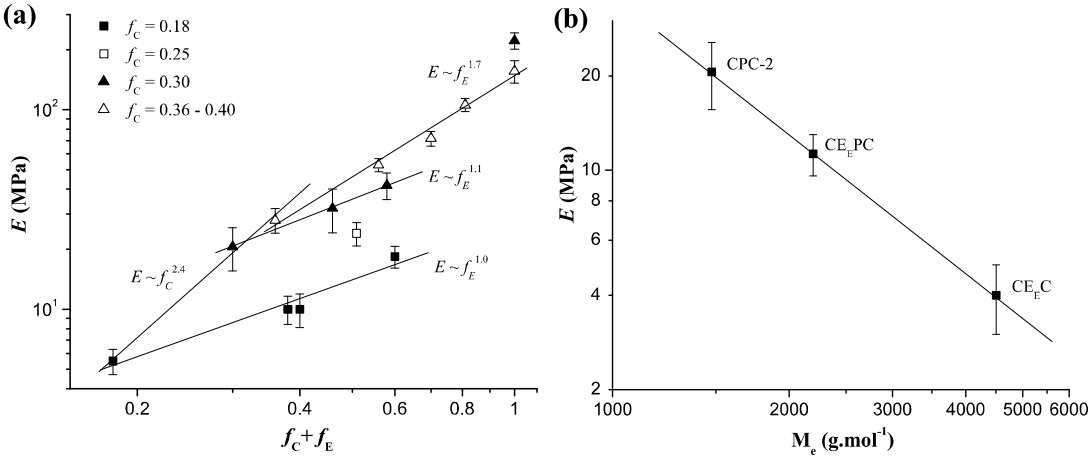

Figure 5.7: Elastic modulus versus (a) $f_C + f_E$ for polymers composed of C, E and P. (b) Modulus versus M_e for rubbery polymers with $f_C \approx 0.30$. Molecular parameters greatly impact E, especially f_C and M_e.

The choice of a power form to relate E to volume fraction derives from the Guth-Smallwood equation, which relates the moduli of a filled rubber E_f and the unfilled version E_u by a function of the filler volume fraction w_s as shown in Equation 5.2. [2,4]

$$\frac{E_f}{E_u} = \left(1 + 2.5w_s + 14.1w_s^{\,2}\right) \qquad (5.2)$$

The exponents found in our correlations vary about the power of 2 predicted by Equation 5.2. These power relationships point to the significant effect of substituting low modulus rubber content for hard blocks. In addition, they imply that moduli show a dependence on the specific type of hard block as well as on the combination of more than one type. Specifically, E appears more susceptible to changes in f_C ($E \sim f_C^{2.4}$) than in f_E ($E \sim f_E^{1.0 - 1.7}$) for all composition profiles. This is not surprising given the large difference ($\approx$ 25 – 37 times higher) in the moduli reported for homopolymer C ($E \approx$ 1.0 – 2.8 GPa)[24,37] versus for E ($E \approx$ 40 – 75 MPa).[37,38] However, the effect of E content is larger than this difference would predict, which suggests the effects of C and E content are coupled; for example, the effect of f_E increases for higher C amounts.

Similarly, the effect of M_e on modulus for the glass and rubbery polymers with $f_C \approx 0.30$ can be seen in Figure 5.7b. A perfect inverse power regression can be drawn between E and M_e, which implies that modulus falls at increasing rates with less rubber entanglement. This is in agreement with the similarly inverse relationship predicted by rubber elasticity. Specifically, the mechanical behavior of cross-linked rubbers at low strains is usually modeled by Equation 5.3, where σ is engineering stress, ρ is polymer density, R is the gas constant, T is temperature in K, M_c is the molecular weight between cross-links, C is an empirical constant and λ is the extension ratio.[2,4]

$$\sigma = \left(\frac{\rho \mathrm{RT}}{\mathrm{M_c}} + \frac{2C}{\lambda} \right) \left(\lambda - \frac{1}{\lambda^2} \right) \qquad (5.3)$$

In bcTPEs, hard domains act as rubber cross-links but experiments have shown that $M_c \neq M_{rubber}$ but instead $M_c \approx M_e$.[2-4] Rubber entanglements appear to function as effective cross-links, as they cannot come undone with extension given that both ends of the rubber chains are "tied down." In this way, entanglements are able to reinforce the rubbery network.

5.4.4 Strain Recovery

Available data on the strain recovery of TPEs is limited despite the superiority of these materials in this area of mechanical behavior. Figure 5.8 presents a large collection of values for tension set ε_s, or permanent deformation after tensile failure, of TPE block copolymers versus hard block content and versus M_e on log-log plots. Figure 5.8a presents ε_s as a function of $f_C + f_E$ for materials composed of C, E and P, grouped into materials with the same glass composition, as in the modulus analysis.

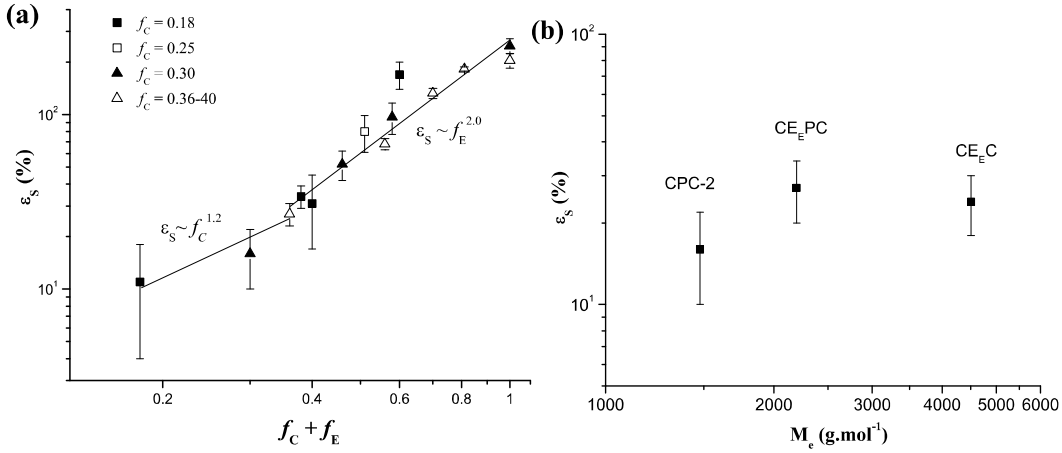

Figure 5.8: Tension set ε_s versus (a) $f_C + f_E$ for polymers composed of C, E and P, and (b) M_e for rubbery materials with $f_C \approx 0.30$. f_E impacts ε_s more than f_C and M_e seems to not have a major effect.

The values of ε_s for the CPC materials with increasing C content follow a power relationship, $\varepsilon_s \sim f_C^{1.2}$. On the other hand, the values of ε_s for materials containing E blocks follow a similar increasing power trend, $\varepsilon_s \sim f_E^{2.0}$. Thus, in contrast to the results for the elastic modulus, the data correlate more strongly with f_E than with f_C. This is supported by reports that show that after large deformations, materials with semicrystalline and glassy blocks have higher residual strains than those that only contain glassy blocks.[13,17,20] Moreover, because of the higher dependence of ε_s on f_E than on f_C and given the fact that all samples have a low f_C = 0.18 – 0.40, the entire data set can be represented approximately by one single trend dominated by $f_C + f_E$.

Figure 5.8c shows ε_s versus M_e for the rubbery samples with $f_C \approx 0.30$. While M_e had a clear effect on modulus, it appears unrelated to ε_s. Tension set has been directly connected to the deformation of the hard blocks in TPEs, especially in the presence of crystallinity.[3,9-11,17,20] As CPC, CE_EC and CE_EPC are devoid of the semicrystalline E block and have the same glass content, they produce similarly low tension sets.

5.4.5 Tensile Strength

Block copolymer thermoplastic elastomers are usually tougher than unfilled vulcanized rubbers, achieving higher tensile strengths σ_{TS}. In this section, the reinforcement of these materials is examined by graphing σ_{TS} as a function of $f_C + f_E$ for materials that consist of C, E and P blocks, and of M_e for the rubbery materials with $f_C \approx 0.30$ in Figure 5.9. A correlation cannot be established between σ_{TS} and hard block content $f_C + f_E$, as values seem to fluctuate about 30 MPa, as shown in Figure

5.9a. A slight increase up to about 40 MPa is noticed for intermediate compositions but these are not significantly higher than those at the extremes (about 20 MPa) given the large uncertainties. This agrees with widely researched SBS and SIS materials, for which tensile strengths do not change considerably with glass addition beyond a certain minimum.[2-4]

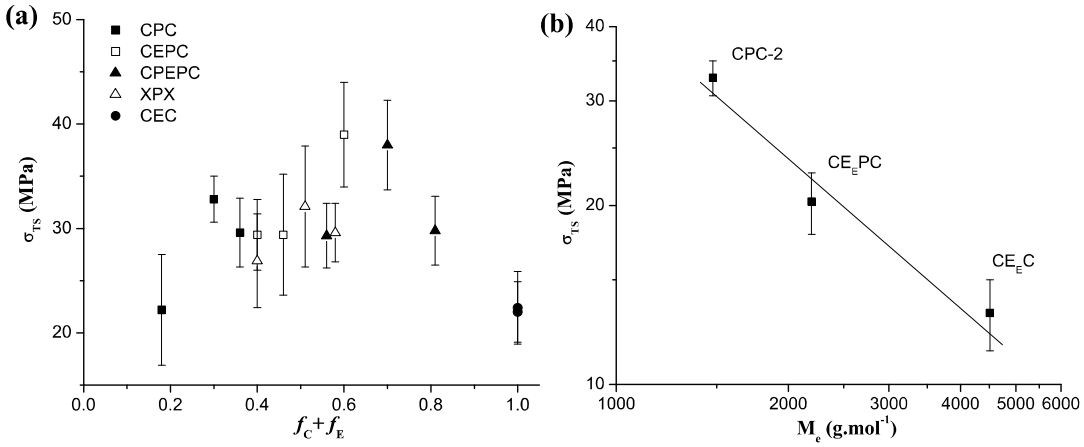

Figure 5.9: Tensile strength σ_{TS} versus (a) $f_C + f_E$ for polymers composed of C, E and P and (b) M_e for rubbery materials with $f_C \approx 0.30$. σ_{TS} is invariant to changes in hard block composition while M_e affects it significantly.

This result supports the accepted notion that failure in block copolymer TPEs occurs in the hard domains and thus is fixed at the strength of the hard particles. Mohajer *et al.* produced a homopolymer E ($M_n \approx 200$ kg/mol) in a similar fashion as in this study from the hydrogenation of $B_{1,4}$ and this materials shows $\sigma_{TS} \approx 20 – 25$ MPa.[38] Similarly, Weimann[37] reports a homopolymer C ($M_n \approx 113$ kg/mol) with $\sigma_{TS} \approx$ 40 MPa and Lim[39] indicates that a crazing stress $\sigma_{craze} \approx 20$ MPa (calculated based on E = 2.8 GPa[24] and ε_{craze} = 0.7% reported by Ryu *et al.*[40]) should be more representative of the load bearing capacity of C. Other experiments support this idea, such as the observed depression in σ_{TS} when the testing temperature of SBS and SIS

is increased towards $T_g(S) \approx 100$ °C.[3] Similarly, weakly segregated SIS samples[3] fail at lower $\sigma_{TS} \approx 10 – 15$ MPa and an SIS sample[41] with 20% glassy spheres failed with no signs of glass deformation at about 15 MPa. In this regard, it has been proposed that hard blocks act as large sinks for the energy released during rubber rupture, which delays failure of the hard domains.[2-4]

On the other hand, changes in M_e have an important impact on σ_{TS} for the rubbery materials with $f_C \approx 0.30$, as illustrated by the log-log plot in Figure 5.9b. Specifically, σ_{TS} shows a similar correlation with M_e as that exhibited by the modulus, decreasing dramatically as M_e is marginally lifted. Tong and Jerome found a similar inverse relationship between σ_{TS} and rubber M_e in MAM block copolymers where M is glassy poly(methylmethacrylate) (at 30% by weight) and A is one of four rubbery poly(acrylates) with $M_e = 11 – 60$ kg/mol.[22] Thus, while failure in TPEs may take place in the hard domains, it is also affected by the conditions of the rubber network. As rubber deformation delays the fracture of the hard blocks, rubber entanglement slippage distributes the force exerted on the material, maximizing the strength of the hard phase.[2-4]

5.4.6 Strain at Break

Another ultimate property analyzed is strain at break ε_b in terms of hard block content and rubber entanglements, as shown in Figure 5.10. While a general decreasing pattern is observed between ε_b and $f_C + f_E$ for the C, E and P containing block copolymers (Figure 5.10a), this is not significant ($\varepsilon_b \approx 400 – 600\%$). Also, the relationship does not reflect the behavior of materials with $f_C = 0.18$. For similar glassy TPEs, lower ε_b values with increasing hard block content derives from the

exchange between deformable rubber content and brittle glass.[2,3,8] This trade-off in extensibility may not hold between rubber and semicrystalline E, which can be plastically tensed to high strains.[3,9,13,17] In fact, EPE triblocks developed by Mohajer *et al.* with intermediate E contents (27 – 70%) show higher extensions (ε_b = 800 – 1200%) than all the materials in this report.[38] This explains why the materials with the lowest C content and significant amounts of E show higher strains at break.

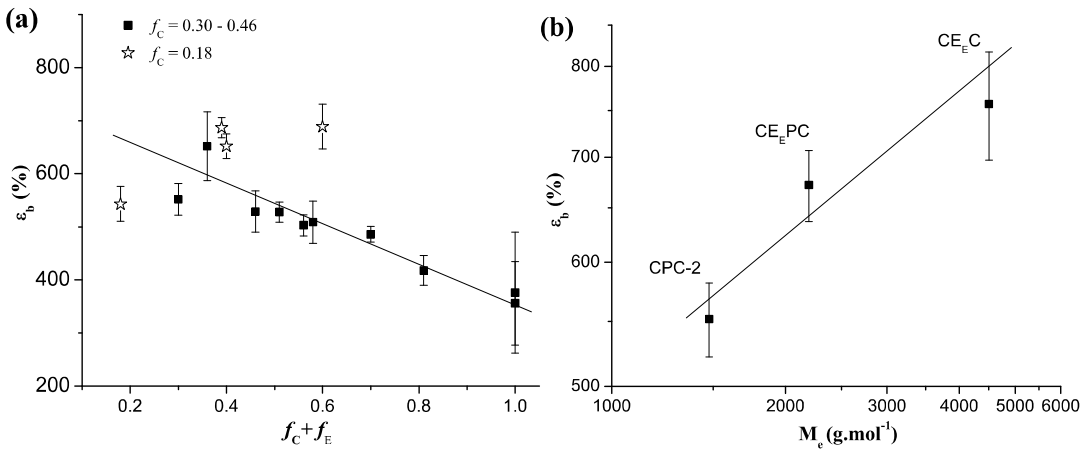

Figure 5.10: Strain at break versus (a) $f_C + f_E$ for polymers composed of C, E and P and (b) M_e for rubbery materials with $f_C \approx 0.30$. Only M_e has a clear impact on strain at break.

In contrast to the relationship between E and σ_{TS} versus M_e, Figure 5.10b shows how changes in ε_b are positively correlated with M_e for the rubbery materials with $f_C \approx 0.30$ on a log-log basis. This provides further evidence that entanglements in TPEs function as effective crosslinks, as rubber molecules are tied down on both ends by hard domains and thus cannot slip past each other.[2-4] Thus, $M_e \approx M_c$ for these block copolymers, which implies that M_e will dictate the highest level of deformation for the rubber blocks.

5.5 Conclusion

This chapter introduced a series of triblock and tetrablock copolymers composed of glassy C, semicrystalline E, and rubbery P and E_E of the type CEC, CPC, CE_EC, CEPC, CE_EPC, synthesized by living anionic polymerization and catalytic hydrogenation. All the materials are melt ordered with $T_{ODT} > T_g(C) \approx 147$ °C ($T_{ODT} \approx 170$ °C for all materials except CEPC-3 with $T_{ODT} > 290$ °C) as probed by rheological characterization and confirmed by SAXS experiments. However, in the case of the tetrablocks, P is mixed with E and E_E in the melt, and while crystallization drives the separation of E and P at room temperature, P and E_E remain mixed up to low temperatures, as shown by DSC and SAXS. We hence concluded that, in these materials, microphase segregation is driven primarily by the thermodynamic incompatibility of the C block. Scattering indicated that most polymers exhibit a morphology of hexagonally packed cylinders, consistent with the compositions. However, structure characterization of E_E containing polymers as well as CEPC with low $f_C \approx 0.18$ was inconclusive given states of weak segregation and low electron density difference between C and E_E.

Given the presence of glassy endblocks with $f_C = 0.18 – 0.30$, materials generate thermoplastic elastomers TPEs, as the softer middle blocks are anchored on both ends by hard domains. Also, the combination of C with three types of matrix components results in materials with a wider range of mechanical properties than conventional TPEs, such as SBS and SIS, especially for the tetrablocks. The mechanical data from reported materials CEC, CPEPC, CEC-P-CEC were incorporated to analyze mechanical properties in terms of hard block content $f_C + f_E$

and rubber M_e. We have found that both elastic modulus and tension set are greatly affected by composition, as properties increase with $(f_C + f_E)^{\delta}$, where $\delta = 1 - 2.4$. While C content has a larger impact on modulus than E content, the opposite is true for tension set. Modulus is affected by the inverse of M_e, as predicted by rubber elasticity, but tension set appears unrelated to M_e, which implies that strain recovery in these materials is mostly dictated by the irreversible deformation of the hard blocks. Ultimate properties such as tensile strength and strain at break show minor dependence on compositional changes but are greatly affected by M_e. Thus, while failure in TPEs occurs in the hard domains, it is greatly influenced by the conditions of the rubber network.

5.6 References

[1] Holden, G. In *Thermoplastic Elastomers*; 2nd ed.; Holden, G.; Legge, N. R.; Quirk, R. P.; Schroeder, H. E.; Eds.; Hanser Publishers: New York; 1996; pp 573-601.

[2] Holden, G.; Bishop, E. T.; Legge, N. R. *J. Polymer Sci., Part C* **1969,** *26*, 37-57.

[3] Quirk, R. P.; Morton, M. In *Thermoplastic Elastomers*; 2nd ed.; Holden, G.; Legge, N. R.; Quirk, R. P.; Schroeder, H. E.; Eds.; Hanser Publishers: New York, 1996; pp 71-100.

[4] Grady, B. P.; Cooper, S. L. In *Science and Technology of Rubber*; 2nd ed.; Mark, J. E.; Erman, B.; Eirich, F. R.; Eds.; Academy Press: London, 1994; pp 601-674.

[5] Bates, F. S.; Fredrickson, G. H.; Hucul, D.; Hahn, S. F. *AIChE Journal* **2001**, *47*, 762-765.

[6] Honeker, C. C.; Thomas, E. L. *Chem. Mater*. **1996**, *8*, 1702-1714.

[7] Qiao, L.; Leibig, C.; Hahn, S. F.; Winey, K. I. *Industrial & Engineering Chemistry Research* **2006,** *45*, 5598-5602.

[8] Tong, J. D.; Leclere, Ph. Doneux, C.; Bredas, J. L.; Lazzaroni, R.; Jerome, R. *Polymer* **2001**, *42*, 3503-3514.

[9] De Rosa, C.; Auriemma, F.; Ruiz de Ballesteros, O.; *Chem. Mater.* **2006**, *18*, (15), 3523–3530

[10] Schmalz, H.; Boker, A.; Lange, R.; Krausch, G.; Abetz, V. *Macromolecules* **2001,** *34*, 8720-8729.

[11] Schmalz, H.; Abetz, V.; Lange, R. *Composites Science and Technology* **2003,** *63*, (8), 1179-1186.

[12] Wang, H. P.; Chum, S. P.; Hiltner, A.; Baer, E. *Journal of Polymer Science: Part B: Polymer Physics* **2009**, *47*, 1313-1330.

[13] Balsamo, V.; Gil, G.; de Navarro, C. U.; Hamley, I. W.; von Gyldenfeldt, F.; Abetz, V.; Canizales, E. *Macromolecules* **2003,** *36*, 4515-4525.

[14] Balsamo, V.; de Navarro, C. U.; Gil, G. *Macromolecules* **2003,** *36*, 4507-4514.

[15] Balsamo, V.; von Gylendfeldt, F.; Stadler, R. *Macromolecules* **1999**, *32*, 1226-1232.

[16] Balsamo V.; Stadler, R. *Macromolecules* **1999**, *32*, 3994-3999.

[17] Mahanthappa, M. K.; Lim, L. S.; Hillmyer, M. A.; Bates, F. S. *Macromolecules* **2007,** *40*, 1585-1593.

[18] Mahanthappa, M. K.; Hillmyer, M. A.; Bates, F. S. *Macromolecules* **2008,** *41*, 1341-1351.

[19] Fleury, G.; Bates, F. S. *Macromolecules* **2009,** *42*, 3598-3610.

[20] Alfonzo, C. G.; Fleury, G.; Chaffin, K. A.; Bates, F. S. *Macromolecules* **2010**, *43*, 5295-5305.

[21] Bishop, J. P.; Register, R. A. *Macromolecules* **2010**, *43*, 4954-4960.

[22] Tong, J. D.; Jerome, R. *Macromolecules* **2000**, *33*, 1479-1481.

[23] Ndoni, S.; Papadakis, C. M.; Bates, F. S.; Almdal, K. *Review of Scientific Instruments* **1995,** *66*, (2), 1090-1095.

[24] Hucul, D. A.; Hahn, S. F. *Advanced Materials* **2000,** 12, (23), 1855-1858.

[25] Fetters, L. J.; Lohse, D. J.; Richter, D.; Witten, T. A.; Zirkel, A. *Macromolecules* **1994,** *27*, 4639-4647.

[26] Brandrup, J.; Immergut, E. H., *Polymer Handbook*. 3rd ed.; John Wiley & Sons: New York, **1989**.

[27] Fredrickson, G. H.; Bates, F. S. *Annual Review of Materials Science* **1996,** *26*, 501-550.

[28] Rosedale, J.; Bates, F. S.; Almdal, K.; Mortensen, K.; Wignall, G. D. *Macromolecules* **1995,** *28*, 1429-1443.

[29] Koppi, K. A. *Ph.D. Dissertation*; University of Minnesota: Minneapolis **1993**.

[30] Graessley, W. W.; Krishnamoorti, R.; Balsara, N. P.; Butera, R. J.; Fetters, L. J.; Lohse, D. J.; Schulz, D. N.; Sissano, J. A. *Macromolecules* **1994**, *27*, 3896-3901.

[31] Cochran, E. W.; Bates, F. S. *Macromolecules* **2002**, *35*, 7368-7374.

[32] Rosedale, J. H.; Bates, F. S. *Macromolecules* **1990**, *23*, 2329-2338.

[33] Weimann, P. A.; Hajduk, D. A.; Chu, C.; Chaffin, K. A.; Brodil, J. C.; Bates, F. S. *Journal of Polymer Science Part B-Polymer Physics* **1999,** *37*, 2053-2068.

[34] Koo, C. M.; Wu, L. F.; Lim, L. S.; Mahanthappa, M. K.; Hillmyer, M. A.; Bates, F. S. *Macromolecules* **2005,** *38*, 6090-6098.

[35] Rault, J.; Marchal, J.; Judeinstein, P.; Albouy, P. A. *Macromolecules* **2006**, *39*, 8356-8368.

[36] Han, C. D.; Baek, D. M.; Kim, J. K. *Macromolecules* **1995**, *28*, 5886-5896.

[37] Weimann, P. A. *PhD Dissertation*; University of Minnesota **1998.**

[38] Mohajer, Y.; Wilkes, G. L.; Wang, I. C.; McGrath, J. E. *Polymer* **1982,** *23*, (10), 1523-1535.

[39] Lim, L. S. *PhD Dissertation*; University of Minnesota **2005.**

[40] Ryu, C. Y.; Ruokolainen, J.; Fredrickson, G. H.; Kramer, E. J.; Hahn, S. F. *Macromolecules* **2002**, *35*, 2157-2166.

[41] Inoue, T.; Moritani, M.; Hashimoto, T.; Kawai, H. *Macromolecules* **1971,** *4*, 500-507.

6

Concluding Remarks

In this last chapter, we summarize the context of this project and the main findings as presented in each chapter. Subsequently, we provide some thoughts on potential routes of future investigation based on questions sparked by our research.

6.1 Summary

In this work, we have investigated novel block copolymer materials that can be applied as thermoplastic elastomers (TPEs). These are mechanically tough and elastomeric materials that resemble vulcanized and filled rubbers.[1,2] Most commercially important TPEs are block copolymers of glassy polystyrene (S) and rubbery polybutadiene (B) and polyisoprene (I) of the type SBS and SIS. When microphase separated, the triblock architecture renders a molecular arrangement where the rubbery blocks are tethered at the ends by hard domains, which act as thermally reversible crosslinks. Chapter 1 reviews the thermodynamics of block polymers as well as the mechanical properties of materials related to TPEs.

We have examined the way molecular and structural characteristics of block copolymer TPEs impact mechanical properties. Block copolymers are based on hydrogenated S, B and I, which results in glassy poly(cyclohexylethylene) (C) from S, semicrystalline poly(ethylene) (E) and rubbery poly(ethylethylene) from $B_{1,4}$ and $B_{1,2}$, respectively, and rubbery poly(ethylene-alt-propylene) (P) from $I_{1,4}$. Apart from

obtaining three mechanically distinct polymers, hydrogenated block copolymers have enhanced oxidative and UV stability given the absence of double bonds as well as a higher upper service temperature based on the glass transitions T_g (C) ≈ 147 °C > T_g (S) ≈ 100 °C.[3] Block copolymers were synthesized using sequential living anionic polymerization to create materials of the type CEC, CPC, CE_EC, CEPC, CE_EPC and CEC-P-CEC (XPX), with f_C = 0.18 – 0.30. These architectures generated TPE polymers, as they share the presence of glassy endblocks which anchor softer semicrystalline and/or rubbery blocks. In addition, both the tetrablock and heptablock materials represent new materials which attempt to combine three types of mechanical behavior. Polymers were subsequently characterized through SEC, NMR, DSC, DMS, SAXS, WAXS, TEM and mechanical testing. Chapter 2 presents a detailed description of the experimental techniques used in this work and some background theory in order to analyze the findings presented in Chapter 3, 4 and 5, which are briefly described next.

Chapter 3 introduces materials CEC-P-CEC, denoted XPX, with three composition profiles $f_C \approx f_E \approx$ 0.18, 0.25 and 0.30 and compares them to CPC materials with f_C = 0.18 and 0.30, which resemble conventional glassy TPEs such as SBS or SIS. The mixing thermodynamics of these blocks, given by $\chi_{CE} > \chi_{CP} >> \chi_{EP}$,[4] imply that in these materials segregation will be driven by the incompatibility of the C block. However, the XPX molecular design with four short C blocks produces materials with high melt compatibility. Thus, rheological and SAXS measurements show that the XPX materials are melt disordered up to high M_n. On the other hand, both CPC materials melt order at T_{ODT} ≈ 170 °C into a cylindrical morphology at

modest M_n. However, TEM images of XPX taken at room temperature show a randomly arranged morphology of microphase separated CEC and P domains. We conclude that segregation in XPX is thus driven by E crystallization upon cooling. This provides an advantage in terms of processability when compared to glassy TPEs, such as the melt ordered CPC materials. For melt ordered block copolymers, the processing temperature $T_{process}$ is equivalent to the order-disorder transition T_{ODT}, which is highly dependent on M_n. On the other hand, for melt disordered XPX, $T_{process} = T_m$ (E) ≈ 100 °C, which is independent of M_n, as shown by DSC.

Despite phase behavior and morphological differences, both CPC and XPX materials behave as strong TPE materials, with tensile strengths $\sigma_{TS} \approx 30$ MPa and strains at break $\varepsilon_b \approx 550\%$. Also, the elastic modulus for both materials $E = 5 – 42$ MPa and strain recovery were found to be highly dependent on hard content given by f_C and f_E. Specifically, both tension set ε_s (permanent strain after failure) and residual strain ε_r (permanent strain after cycles of deformation) after 7 cycles to 400% strain increase with hard content $f_X = f_C + f_E$. Interestingly, while this increase is more pronounced for XPX, which is attributed to the highly ductility of the E crystals, the correlation predicts XPX to exhibit $\varepsilon_r < 44\%$, which is comparable to CPC, for $f_X < 0.39$.

The analysis of XPX materials is continued in Chapter 4, which compares the melt disordered XPXs to a melt ordered CEC material with $f_C = 0.30$, CPC materials with $f_C = 0.30$ but different M_n and two high M_n (135 and 195 kg/mol) melt ordered XPX materials with $f_C \approx f_E \approx 0.25$. The rheological analysis of CPC versus XPX materials with constant compositions but increasing M_n shows how complex viscosity

remains advantageously nearly Newtonian for a wider range of molecular weights for XPX, as melt ordering only occurs at high M_n. SAXS patterns show that the two melt ordered XPX materials present two principal length scales corresponding to a short C – E correlation (for which a weakly ordered lamellar morphology is evident only for the highest M_n material) and a longer X – P one below $T_{ODT} \approx 260$ °C – 290 °C. Above these temperatures, both materials show one correlation hole peak associated with the C – E correlation, as these two blocks have the highest χ parameter and electron density difference. This is also the only correlation expressed in the melt for the lower M_n melt disordered XPX materials. However, the melt disordered peak positions do not scale as theory predicts, $d^* \sim N^{1/2}$, based on Gaussian statistics,[5] which we believe may involve the expression of a combination of C – E correlations. Despite different melt phase behavior, all XPX materials possess a similar structure at room temperature of randomly arranged CEC and P domains, as revealed by TEM. Thus, while materials may show differences in melt segregation, the highly exothermic process of E crystallization effectively dominates structure formation in all these cases.

Given the resemblance in structure in XPX, the mechanical responses of all these materials are similar and compare favorably with strong TPEs. The combination of cyclic mechanical testing up to increasing levels of deformation and WAXS data at such strains allowed us to track the deformation behavior in these materials as well as that in CPC and CEC for comparison. While E deformation starts immediately for CEC, in XPX this is delayed until the early onset of strain hardening, which makes these materials as recoverable as CPC after low deformations. Also, C fracture is

delayed in XPX by both P and E deformation until the end of the strain hardening regime, as P delays C fracture in CPC, which accounts for the observed strength and extensibility of XPX.

Finally, as opposed to Chapters 3 and 4, which mostly deal with melt disordered XPX materials, Chapter 5 presents melt ordered materials of the type CEC, CPC, CE_EC, CEPC and CE_EPC with f_C = 0.18 and 0.30 and f_E = 0.18 – 0.70. Given modest molecular weights, rheological measurements show optimal $T_{ODT} \approx$ 170 °C (except for one CEPC sample with T_{ODT} > 290 °C). SAXS shows that most materials are melt ordered into hexagonally packed C cylinders, while the assignment of structures for CEEPC and the CEPC with low f_C is complicated by weak segregation and low electron density differences in the melt. For the tetrablocks, the middle blocks appear mixed in the melt, as their combined molecular weights are two low for segregation. In fact, while E and P should microphase segregate at room temperature due to E crystallization, E_E and P appear to be mixed by DSC even below room temperature. These results support the idea, first presented for the XPX materials, that in all the materials in this project with modest M_n, C incompatibility dictates melt order or disorder.

The mechanical properties of these materials (except for plastic CEC) also resemble strong thermoplastic elastomers such as SBS and SIS. On the other hand, they have a wider range of mechanical properties given the presence of semicrystalline E, the use of two rubbers with different rubber entanglements (M_e(P) = 1,475 g/mol while $M_e(E_E)$ = 4,507 g/mol)[6] and compositional differences. In order to study the effect of hard block type (C versus E) and content as well as of rubber M_e

on mechanical properties, we incorporated data from the XPX polymers and from previously reported materials of the type CPC, CEC and CPEPC.[5,7,8] This afforded us data from a large set of materials that behave as thermoplastic elastomers but have a spectrum of compositions. We found that modulus E and tension set ε_s were strongly correlated with $f_C + f_E$. While the effects are coupled, C content impacts modulus more significantly than E content, while the opposite is true for strain recovery. In addition, elastic modulus is a function of the inverse of M_e as predicted by rubber elasticity theory. However, M_e does not affect ε_s, which supports the notion that strain recovery is mostly dictated by the irreversible deformation of the hard blocks.[2,7,9,10] Tensile strength and strain at break were minimally affected by changes in hard block content but instead reacted to M_e variations. We believe failure in block copolymer TPEs is dictated by the strength of the hard domains and thus is saturated at a maximum value of about 30 – 40 MPa.[1,2] However, M_e influences ultimate properties given that rubber entanglements redistribute stress, delaying the fracture of the hard domains and thus optimizing the strengthening effect.[11]

6.2 Future Work

The characterization of the CEC-P-CEC (XPX) materials and their comparison to similar CECEC-P and CECEC-P-CECEC materials prepared by Fleury and Bates[12] put forth questions related to the thermodynamics and scattering of multiblock copolymers that combine three types of blocks. In particular, despite similar compositions and molecular weights, CECEC-P materials were melt ordered at lower M_n, showed two correlation holes when disordered and produced a doubly

periodic lamellar morphology shown by SAXS and TEM. On the other hand, both XPX and CECEC-P-CECEC materials showed one correlation hole and were not able to show such order at room temperature. It is difficult to explain how architectural order and symmetry may influence phase behavior and scattering in these materials based on experimental or qualitative arguments alone. Instead, we believe that a more quantitative mathematical treatment is required. In fact, the thermodynamic behavior of CECEC-P has recently been explained by a simple free energy model developed by Subbotin *et al.*[13] We believe that a similar treatment or the use of the RPA method, as developed by Cochran *et al.*[14] for multiblock systems, might help explain the behavior of XPX and similar multiblock materials.

Another path of work related to multiblock copolymers with three components and large N (block length) differences relates to the formation of structures with multiple periodicities, which have only been observed on a few occasions.[15-20] As C incompatibility drives melt segregation, XPX materials with higher C compositions or with asymmetric C blocks (e.g. larger middle C blocks) may produce doubly periodic melt ordered morphologies which may not be disrupted by E crystallization. In addition, these variations as well as changes in the XPX architecture (e.g. producing CPC-E-CPC materials) may help us further understand the thermodynamics of combining C, E and P in multiblock copolymers as well as the origins of scattering in these materials.

Tetrablocks CEPC and CE_EPC shown in Chapter 5 represent a simple yet powerful strategy to produce materials with a wide range of mechanical properties while maintaining their identity as thermoplastic elastomers. The production of more

tetrablocks, or similar materials, with different combinations of E versus P and E_E versus P, as well as higher C compositions, would lead to an important spectrum of materials with tunable properties. Also, it would allow us to refine the suggested relationships between mechanical properties and molecular parameters such as f_C, f_E and M_e.

6.3 References

[1] Holden, G.; Bishop, E. T.; Legge, N. R. *J. Polymer Sci., Part C* **1969,** *26*, 37-57.

[2] Quirk, R. P.; Morton, M. In *Thermoplastic Elastomers*; 2nd ed.; Holden, G.; Legge, N. R.; Quirk, R. P.; Schroeder, H. E.; Eds.; Hanser Publishers: New York, **1996**; pp 71-100.

[3] Bates, F. S.; Fredrickson, G. H.; Hucul, D.; Hahn, S. F. *AIChE Journal* **2001**, *47*, 762-765.

[4] Cochran, E. W.; Bates, F. S. *Macromolecules* **2002**, *35*, 7368-7374.

[5] Almdal, K.; Rosedale, J. H.; Bates, F. S. *Physical Review Letters* **1990**, 65, 1112-1115.

[6] Fetters, L. J.; Lohse, D. J.; Richter, D.; Witten, T. A.; Zirkel, A. *Macromolecules* **1994,** *27*, (17), 4639-4647.

[7] Mahanthappa, M. K.; Lim, L. S.; Hillmyer, M. A.; Bates, F. S. *Macromolecules* **2007,** *40*, 1585-1593.

[8] Weimann, P. A. *PhD Dissertation*; University of Minnesota **1998.**

[9] Schmalz, H.; Boker, A.; Lange, R.; Krausch, G.; Abetz, V. *Macromolecules* **2001,** *34*, 8720-8729.

[10] De Rosa, C.; Auriemma, F.; Ruiz de Ballesteros, O.; *Chem. Mater.* **2006**, *18*, (15), 3523–3530

[11] Tong, J. D.; Jerome, R. *Macromolecules* **2000**, *33*, 1479-1481.

[12] Fleury, G.; Bates, F. S. *Macromolecules* **2009,** *42*, 3598-3610.

[13] Subbotin, A.; Markov, V.; ten Brinke, G. *Journal of Physical Chemistry B* **2010**, *114*, 5250-5256.

[14] Cochran, E. W.; Morse, D. C.; Bates, F. S. *Macromolecules* **2003**, *36*, 782-792.

[15] Ruokolainen, J.; Mäkinen, R.; Torkkeli, M.; Mäkelä, T.; Serimaa, R.; ten Brinke, G.; Ikkala, O. *Science* **1998**, *280*, (5363), 557-560.

[16] Ikkala, O.; ten Brinke G.; *Science* **2002,** *295*, (5564), 2407-2409.

[17] Nap, R, J.; Kok, C.; ten Brinke, G.; Kuchanov, S. I. *Eur. Phys. J. E.* **2001**, *4*, 515-519.

[18] Nap, R.; Erukhimovich, I.; ten Brinke, G. *Macromolecules* **2004**, *37*, (11), 4296-4303.

[19] Nagata, Y.; Masuda, J.; Noro, A.; Cho, D.; Takano, A.; Matsushita, Y. *Macromolecules* **2005**, *38*, 10220-10225.

[20] Masuda, J.; Takano, A.; Nagata, Y.; Noro, A.; Matsushita, Y. *Physical Review Letters* **2006**, *97*, 98301-98304.

Bibliography

- Aggarwal, S. L. *Polymer* **1976**, *17*, 938.
- Alfonzo, C. G.; Fleury, G.; Chaffin, K. A.; Bates, F. S. *Macromolecules* **2010**, *43*, 5295-5305.
- Almdal, K.; Bates, F. S. Journal of Chemical Physics **1992**, *96*, (12), 9122-9132.
- Almdal, K.; Rosedale, J. H.; Bates, F. S. *Physical Review Letters* **1990**, 65, 1112-1115.
- Avgeropoulos, A.; Dair, B. J.; Hadjichristidis, N.; Thomas, E. L. *Macromolecules* **1997**, *30*, 5634-5642.
- Bailey, T. S. *Ph.D. Dissertation*; University of Minnesota; **2001**.
- Bailey, T. S.; Hardy, C. M.; Epps, T. H.,III; Bates, F. S. *Macromolecules* **2002**, *35*, 7007-7017.
- Balsamo V.; Stadler, R. *Macromolecules* **1999**, *32*, 3994-3999.
- Balsamo, V.; de Navarro, C. U.; Gil, G. *Macromolecules* **2003,** *36*, 4507-4514.
- Balsamo, V.; Gil, G.; de Navarro, C. U.; Hamley, I. W.; von Gyldenfeldt, F.; Abetz, V.; Canizales, E. *Macromolecules* **2003,** *36*, 4515-4525.
- Balsamo, V.; von Gyldenfeldt, F.; Stadler, R. *Macromolecules* **1999**, *32*,1226-1232.
- Bates, F. S. *Macrmolecules* **1980**, *18*, 525-528.
- Bates, F. S. *Macromolecules* **1985**, *18*, 525-528.
- Bates, F. S.; Fredrickson, G. H. *Annual Review of Physical Chemistry* **1990,** *41*, 525-557.
- Bates, F. S.; Fredrickson, G. H. In *Thermoplastic Elastomers*, 2nd ed.; Holden, G.; Legge, N R.; Quirk, R. P.; Schroeder, H. E.; Eds.; Hanser Publishers: New York, 1996; pp. 351-361.

- Bates, F. S.; Fredrickson, G. H. *Physics Today* **1999**, *52*, 32-40.
- Bates, F. S.; Fredrickson, G. H.; Hucul, D.; Hahn, S. F. *AIChE Journal* **2001**, *47*, 762-765.
- Bates, F. S.; Rosedale, J. H.; Fredrickson, G. H. *Journal of Chemical Physics* **1990,** *92*, (10), 6255-6270.
- Bates, F. S.; Rosedale, J. H.; Fredrickson, G. H.; Glinka, C. J. *Physical Review Letters* **1988,** *61*, (19), 2229-2232.
- Beckmann, J.; Auschra, C.; Stadler, R. *Macromolecular Rapid Communications* **1994**, *15*, 67-72.
- Bishop, J. P.; Register, R. A. *Macromolecules* **2010**, *43*, 4954-4960.
- Brandrup, J.; Immergut, E. H., *Polymer Handbook*, 3rd ed.; John Wiley & Sons: New York, 1989.
- Breiner, U.; Krappe, U.; Abetz, V.; Stadler, R. *Macromolecular Chemistry and Physics* **1997**, *198*, 1051-1083.
- Breiner, U.; Krappe, U.; Jakob, T.; Abetz, V.; Stadler, R. *Polymer Bulletin (Berlin)* **1998**, *40*, 219-226.
- Chen, Y. D. M.; Cohen, R. E. *J. Appl. Polym. Sci.* **1977**, *21*, 629-643.
- Chung, C. I.; Gale, J. C. *J. Polym. Sci. B* **1976**, *14*, 1149-1156.
- Cochran, E. W. *PhD Dissertation*; University of Minnesota **2004.**
- Cochran, E. W.; Bates, F. S. *Macromolecules* **2002**, *35*, 7368-7374.
- Cochran, E. W.; Garcia-Cervera, C. J.; Fredrickson, G. H. *Macromolecules* **2006**, *39*, 2449-2451.
- Cochran, E. W.; Morse, D. C.; Bates, F. S. *Macromolecules* **2003**, *36*, 782-792.

- Cohen, R. E.; Cheng, P. L.; Douzinas, K.; Kofinas, P.; Berney, C. V. *Macromolecules* **1990,** *23*, 324-327.
- Cohen, Y.; Albalak, R. J.; Dair, B. J.; Capel, M. S.; Thomas, E. L. *Macromolecules* **2000**, *33*, 6502-6516.
- Dair, B. J.; Avgeropoulos, A.; Thomas, E. L.; *J. Mat. Sci.*, **2000**, *35*, 5207-5213.
- Dair, B. J.; Honeker, C. C..; Alward, D. B.; Avgeropoulos A.; Hadjichristisdis N.; Fetters L. J.; Capel M.; Thomas E. L. *Macromolecules* **1999**, *32*, 8145-8152.
- De Gennes, P. G. J. Phys. (Paris) **1970**, *31*, 235-238
- De Rosa, C.; Auriemma, F.; Ruiz de Ballesteros, O.; *Chem. Mater.* **2006**, *18*, (15), 3523–3530
- deGennes, P. G. *J. Phys. (Paris)* **1970**, *31*, 235.
- Epps, T. H.,III; Cochran, E. W.; Hardy, C. M.; Bailey, T. S.; Waletzko, R. S.; Bates, F. S. *Macromolecules* **2004**, *37*, 7085-7088.
- Fetters, L. J.; Lohse, D. J.; Richter, D.; Witten, T. A.; Zirkel, A. *Macromolecules* **1995**, *27*, 4639-4646.
- Fleury, G.; Bates, F. S. *Macromolecules* **2009,** *42*, 3598-3610.
- Flory, P. J. *J. Am. Chem. Soc.* **1940**, *62*, 1561-1565.
- Fredrickson, G. H.; Bates, F. S. *Annual Review of Materials Science* **1996**, *26*, 501-550.
- Fredrickson, G. H.; Helfand, E. *J. Chem. Phys* **1987**, *87*, 697-705.
- Fujimura, M.; Hashimoto, T.; Kawai, H., *Rubber Chemistry and Technology* **1978**, *51*, 215.
- Galeski, A. *Prog. Polym. Sci.* **2003**, *28*, 1643.
- Gehlsen, M. D.; Almdal, K.; Bates, F. S. *Macromolecules* **1992**, *25*, 939-943.

- Gehlsen, M. D.; Bates, F. S. *Macromolecules* **1993**, *26*, 4122-4127.
- Gehlsen, M. D.; Weimann, P. A.; Bates, F. S.; Harville, S.; Mays, J. W.; Wignall, G. D. *J. Polym. Sci. B* **1995**, *33*, 1527-1536.
- Gotro, J. T.; Graessley, W. W. *Macromolecules* **1984,** *17*, 2767-2775.
- Gouinlock, E. V.; Porter, R. S. *Polymer Engineering and Science* **1977**, *17*, 535-543
- Grady, B. P.; Cooper, S. L. In *Science and Technology of Rubber*, 2nd ed.; Mark, J. E.; Erman, B.; Eirich, F. R.; Eds.; Academy Press: London, 1994; pp 601-674.
- Graessley, W. W.; Krishnamoorti, R.; Balsara, N. P.; Butera, R. J.; Fetters, L. J.; Lohse, D. J.; Schulz, D. N.; Sissano, J. A. *Macromolecules* **1994**, *27*, 3896-3901.
- Hadziioannou, G.; Mathis, A.; Skoulios, A. *Colloid and Polymer Sci.* **1979**, *257*, 136-139.
- Hahn, T., Ed.; *International Tables for X-ray Crystallography;* Kluwer Academic Publishers: Boston, MA, 1992.
- Hajduk, D. A.; Harper, P. E.; Gruner, S. M.; Honeker, C. C.; Kim, G.; Thomas, E. L.; Fetters, L. J. *Macromolecules* **1994**, *27*, 4063-4075.
- Hajduk, D. A.; Harper, P. E.; Gruner, S. M.; Honeker, C. C.; Thomas, E. L.; Fetters, L. J. *Macromolecules* **1995**, *28*, 2570-2573.
- Han, C. D.; Baek, D. M.; Kim, J. K. *Macromolecules* **1995**, *28*, 5886-5896.
- Hashimoto, T.; Fujimura, M.; Saijo H.; Kawai, H.; Diamant, J.; Shen, M. In *Multiphase Polymers*; Cooper, S. L.; Estes, G. M.; Eds.; ACS Advances in Chemistry Series, 1979; p 257.
- Helfand, E. *J. Chem. Phys.* **1975**, *56*, 999.
- Helfand, E.; Tagami, Y. *J. Chem. Phys.* **1971**, *56*, 3592.
- Helfand, E.; Wasserman, Z. R. *Macromolecules* **1976**, *9*, 879-888.

- Hermel, T. J. *Ph.D. Dissertation*. University of Minnesota; **1993**.
- Hermel, T. J.; Wu, L.; Hahn, S. F.; Lodge, T. P.; Bates, F. S. *Macromolecules* **2002**, *35*, 4685-4689.
- Hermel, T. J.; Hahn, S. F.; Chaffin, K. A.; Gerberich, W. W.; Bates, F. S. *Macromolecules* **2003**, *36*, 2190-2193.
- Heuschen, J.; Vion, J. M.; Jerome, R.; Teyssie, P. *Macromolecules* **1989**, *22*, 2446-2451.
- Hiemenz, P.C.; Lodge, T.P. *Polymer Chemistry*, 2nd ed.; CRC Press: Boca Raton, FL, 2007.
- Hillmyer, M. A.; Bates, F. S. *Macromolecules* **1996**, *29*, 6994-7002.
- Holden, G. In *Thermoplastic Elastomers*, 2nd ed.; Holden, G.; Legge, N. R.; Quirk, R. P.; Schroeder, H. E.; Eds.; Hanser Publishers: New York, 1996; 573-601.
- Holden, G.; Bishop, E. T.; Legge, N. R. *J. Polymer Sci., Part C* **1969,** *26*, 37-57.
- Honeker, C. C.; Thomas, E. L. *Chemistry of Materials* **1996,** *8*, (8), 1702-1714.
- Honeker, C. C.; Thomas, E. L.; Albalak, R. J.; Hajduk, D. A.; Gruner, S. M.; Capel, M. C. *Macromolecules* **2000,** *33*, 9395-9406.
- Hotta, A.; Cochran, E.; Ruokolainen, J.; Khanna, V.; Fredrickson, G. H.; Kramer, E. J.; Shin, Y. W.; Shimizu, F.; Cherian, A. E.; Hustad, P. D.; Rose, J. M.; Coates, G. W. *Proceedings of the National Academy of Sciences of the United States of America* **2006,** *103*, (42), 15327-15332.
- Hsieh, H. I.; Quirk, R. P. *Anionic Polymerization: Principles and Practical Applications*; Marcel Dekker, Inc.: New York, 1996.
- Hucul, D. A.: *US Patent* 6,399,538; 2000.
- Hucul, D. A.; Hahn, S. F. *Advanced Materials* **2000,** *12*, (23), 1855-1858.
- Hucul, D. A.; Hahn, S. F. *U.S. Patent* 5,612,422; 1977**.**

- Hucul, D. A.; Hahn, S. F. *World Intellectual Property Organization* WO 96/34896 **1996.**
- Ikeda, Y.; Phinyocheep, P.; Kittipoom, S.; Ruancharoen, J.; Kokubo, Y.; Morita, Y.; Hijikata, K.; Kohjiya, S. *Polymers for Adavanced Technologies* **2008**, *19*, 1608-1615.
- Ikkala, O.; ten Brinke G.; *Science* **2002,** *295*, (5564), 2407-2409.
- Inoue, T.; Moritani, M.; Hashimoto, T.; Kawai, H. *Macromolecules* **1971,** *4*, 500-507.
- Jones, T. *PhD Dissertation*, University of Minnesota **2000.**
- Kawai, H.; Hashimoto, T.; Miyoshi, K.; Uno, H.; Fujimura, M. *Journal of Macromolecular Science, Physics* **1980**, *B17*, 427-472.
- Khandpur, A. K.; Forster, S.; Bates, F. S.; Hamley, I. W.; Ryan, A. J.; Bras, W.; Almdal, K.; Mortensen, K. *Macromolecules* **1995**, *28*, 8796-8806.
- Khandpur, A. K.; Macosko, C. W.; Bates, F. S. *Journal of Polymer Science Part B-Polymer Physics* **1995,** *33*, (2), 247-252.
- Khanna, V.; Ruokolainen, J.; Kramer, E. J.; Hahn, S. F. *Macromolecules* **2006**, *39*, 4480-4492.
- Koo, C. M.; Hillmyer, M. A.; Bates, F. S. *Macromolecules* **2006,** *39*, 667-677.
- Koo, C. M.; Wu, L. F.; Lim, L. S.; Mahanthappa, M. K.; Hillmyer, M. A.; Bates, F. S. *Macromolecules* **2005,** *38*, 6090-6098.
- Koppi, K. A. *Ph.D. Dissertation*, University of Minnesota **1993**.
- Koppi, K. A.; Tirrell, M.; Bates, F. S.; Almdal, K.; Colby, R. H. *J. Phys. II France* **1992**, *2*, 1941-1959.
- Kossuth, M. B.; Morse, D. C.; Bates, F. S. *Journal of Rheology* **1999**, *43*, 167-196.
- Kramer, E. *J. Adv. Polym. Sci*. **2003**, *28*, 1643.

- Laurer, J. H.; Hajduk, D. A.; Fung, J. C.; Sedat, J. W.; Smith, S. D.; Gruner, S. M.; Agard, D. A.; Spontak, R. J. *Macromolecules* **1997**, *30*, 3938-3941.
- Leibler, L. *Macromolecules* **1980**, *13*, 1602-1617.
- Lim, L. S. *PhD Dissertation*; University of Minnesota **2005.**
- Macosko, C. W. *Rheology: Principles, Measurements and Applications;* Advances in Interfacial Engineering; Wiley-VCH: New York, 1994.
- Mahanthappa, M. K., Hillmyer, M. A., Bates, F. S. *Macromolecules* **2008**, *41*, 1341-1351.
- Mahanthappa, M. K., Lim, L. S.; Hillmyer, M. A.; Bates, F. S. *Macromolecules* **2007**, *40*, 1585-1593.
- Mai, S.-M.; Mingvanish, W.; Turner, S. C.; Chaibundit, C.; Fairclough, J. P. A.; Heatley, F.; Matsen, M. W.; Ryan, A. J.; Booth, C. *Macromolecules* **2000**, *33*, 5124-5130.
- Masuda, J.; Takano, A.; Nagata, Y.; Noro, A.; Matsushita, Y. *Physical Review Letters* **2006**, *97*, 98301-98304.
- Matsen, M. W. *J. Chem. Phys.* **1995**, *102*, 3884-3887.
- Matsen, M. W.; Bates, F. S. *J. Chem. Phys.* **1997**, *106*, 2436-2448.
- Matsen, M. W.; Bates, F. S. *Macromolecules* **1996**, *29*, 1091-1098.
- Matsen, M. W.; Schick, M. *Phys. Rev. Lett.* **1994**, *72*, 2660-2663.
- Matsen, M. W.; Thompson, R. B. *J. Chem. Phys.* **1999**, *111*, 7139-7146.
- Matsuo, M.; Ueno, T.; Horino, H.; Chujyo, S.; Asai, H. *Polymer* **1968**, *9*, 425-436.
- Matsushita, Y.; Nomura, M.; Watanabe, J.; Mogi, Y.; Noda, I. *Macromolecules* **1995**, *28*, 6007-6013.

- Mayes, A. M.; delaCruz, M. O. *J. Chem. Phys.* **1989**, *91*, 7228-7235.
- Mogi, Y.; Kotsuji, H.; Kaneko, Y.; Mori, K.; Matsushita, Y.; Noda, I. *Macromolecules* **1992**, *25*, 5408-5411.
- Mogi, Y.; Mori, K.; Kotsuji, H.; Matsushita, Y.; Noda, I.; Han, C. C. *Macromolecules* **1993**, *26*, 5169-5173.
- Mogi, Y.; Mori, K.; Matsushita, Y.; Noda, I. *Macromolecules* **1992**, *25*, 5412-5415.
- Mogi, Y.; Nomura, M.; Kotsuji, H.; Ohnishi, K.; Matsushita, Y.; Noda, I. *Macromolecules* **1994**, *27*, 6755-6760.
- Mohajer, Y.; Wilkes, G. L.; Wang, I. C.; McGrath, J. E. *Polymer* **1982,** *23*, (10), 1523-1535.
- Mori, Y.; Lim, L. S.; Bates, F. S. *Macromolecules* **2003**, *36*, 9879-9888.
- Morrison, F. A.; Winter, H. H.; Gronski, W.; Barnes, J. D. *Macromolecules* **1990**, *23*, 4200-4205.
- Morton, M.; Murphy, R. J.; Cheng, T. C. In *Le Reinforcement des Elastomers*; Centre National de la Recherche Scientifique: Paris, 1975; pp 33-40.
- Mullins, L. *J. Phys. Chem.* **1950,** *54*, (2), 239-251.
- Nagata, Y.; Masuda, J.; Noro, A.; Cho, D.; Takano, A.; Matsushita, Y. *Macromolecules* **2005**, *38*, 10220-10225.
- Nandan, B.; Hsu, J. Y.; Chen, H. L. *Polymer Reviews* **2006,** *46*, (2), 143-172.
- Nap, R, J.; Kok, C.; ten Brinke, G.; Kuchanov, S. I. *Eur. Phys. J. E.* **2001**, *4*, 515-519.
- Nap, R.; Erukhimovich, I.; ten Brinke, G. *Macromolecules* **2004**, *37*, (11), 4296-4303.
- Ndoni, S.; Papadakis, C. M.; Bates, F. S.; Almdal, K. *Review of Scientific Instruments* **1995,** *66*, (2), 1090-1095.

- Odell, J. A.; Keller, A. *Polymer Engineering and Science* **1977,** *17*, (8), 544-559.
- Oderkerk, J.; Groeninckx, G. *Macromolecules* **2002**, *35*, 3946-3954.
- Pakula, T.; Saijo, K.; Kawai, H.; Hashimoto, T.; *Macromolecules* **1985**, *18*, 1294-1302.
- Patel, R. M.; Hahn, S. F.; Esneault, C.; Bensason, S. *Advanced Materials* **2000,** *12*, (23), 1813-1817.
- Perrin, D. D.; Armarego, W. L. F. *Purification of Laboratory Chemicals*, 3rd ed.; Permagon Press, 1988.
- Pope, D. P.; Keller, A. J.; *J. Polym. Sci. Polym. Phys*. **1975**, *12*, 533.
- Qiao, L.; Leibig, C.; Hahn, S. F.; Winey, K. I. *Industrial & Engineering Chemistry Research* **2006,** *45*, 5598-5602.
- Quirk, R. P.; Morton, M. In *Thermoplastic Elastomers*, 2nd ed.; Holden, G.; Legge, N. R.; Quirk, R. P.; Schroeder, H. E.; Eds.; Hanser Publishers: New York, 1996; pp 71-100.
- Rangarajan, P.; Register, R. A.; Fetters, L. J. *Macromolecules* **1993,** *26*, 4640-4645.
- Rault, J.; Marchal, J.; Judeinstein, P.; Albouy, P. A. *Macromolecules* **2006**, *39*, 8356-8368.
- Rosedale, J. H.; Bates, F. S. *Macromolecules* **1990**, *23*, 2329-2338.
- Rosedale, J. H.; Bates, F. S.; Almdal, K.; Moretensen, K.; Wignall, G. D. *Macromolecules* **1995**, *28*, 1429-1443.
- Ruokolainen, J.; Fredrickson, G. H.; Kramer, E. J. *Macromolecules* **2002**, *35*, 9391-9402.
- Ruokolainen, J.; Mäkinen, R.; Torkkeli, M.; Mäkelä, T.; Serimaa, R.; ten Brinke, G.; Ikkala, O. *Science* **1998**, *280*, (5363), 557-560
- Ryu, C. Y.; Lee, M. S.; Hajduk, D. A.; Lodge, T. P. *J. Poly. Sci. B* **1997**, *35*, 2811-2823.

- Ryu, C. Y.; Ruokolainen, J.; Fredrickson, G. H.; Kramer, E. J.; Hahn, S. F. *Macromolecules* **2002**, *35*, 2157-2166.
- Schmalz, H.; Abetz, V.; Lange, R. *Composites Science and Technology* **2003,** *63*, (8), 1179-1186.
- Schmalz, H.; Boker, A.; Lange, R.; Krausch, G.; Abetz, V. *Macromolecules* **2001**, *34*, 8720-8729.
- Schmidt, S. C.; Hillmyer, M. A. *Macromolecules* **1999**, *32*, 4794-4801.
- Seguela, R.; Prudhomme, J. *Macromolecules* **1978,** *11*, 1007-1016.
- Seguela, R.; Prudhomme, J. *Polymer* **1989,** *30*, (8), 1446-1455.
- Stadler, R.; Auschra, C.; Beckmann, J.; Krappe, U.; Voight-Martin, I.; Leibler, L. *Macromolecules* **1995**, *28*, 3080-3097.
- Subbotin, A.; Markov, V.; ten Brinke, G. *Journal of Physical Chemistry B* **2010**, *114*, 5250-5256.
- Tarasov, S. G.; Tsvankin, D. Y.; Godovsky, Y. K.; *Polym. Sci. USSR* **1978**, *20*, 1728-1739.
- Tepe, T.; Hajduk, D. A.; Hillmyer, M. A.; Weimann, P. A.; Tirrell, M.; Bates, F. S.; Almdal, K.; Mortensen, K. *Journal of Rheology (New York)* **1997**, *41*, 1147-1171.
- Thomas, E. L.; Alward, D. B.; Kinning, D. J.; Martin, D. C.; Handlin, D. L., Jr.; Fetters, L. J. *Macromolecules* **1986**, *19*, 2197-2202.
- Tong, J. D.; Jerome, R. *Macromolecules* **2000**, *33*, 1479-1481.
- Tong, J. D.; Leclere, Ph. Doneux, C.; Bredas, J. L.; Lazzaroni, R.; Jerome, R. *Polymer* **2001**, *42*, 3503-3514.
- Trabelsi, S.; Albouy, P. A.; Rault, J. *Macromolecules* **2003**, *36*, 9093-9099.

- Vigild, M. E.; Chu, C.; Sugiyama, M.; Chaffin, K. A.; Bates, F. S. *Macromolecules* **2001**, *34*, 2533-2539.
- Wang, H. P.; Chum, S. P.; Hiltner, A.; Baer, E. *Journal of Polymer Science: Part B: Polymer Physics* **2009**, *47*, 1313-1330.
- Wang, H. P.; Khariwala, D. U.; Cheung, W.; Chum, S. P.; Hiltner, A.; Baer, E. *Macromolecules* **2007,** *40*, (8), 2852-2862.
- Weimann, P. A. *PhD Dissertation*; University of Minnesota **1998.**
- Weimann, P. A.; Hajduk, D. A.; Chu, C.; Chaffin, K. A.; Brodil, J. C.; Bates, F. S. *Journal of Polymer Science Part B-Polymer Physics* **1999,** *37*, 2053-2068.
- Williams, D. B. & Cater, C. B. *Transmission Electron Microscopy: Basics;* Plenum: New York, 1996.
- Winter, H. H.; Scott, D. B.; Gronski, W.; Okamoto, S.; Hashimoto, T. *Macromolecules*, **1993**, *26*, 7236-7244.
- Young, R. J.; Lovell, P. A. *Introduction to Polymers*, 2nd ed.; Stanley Thornes (Publishers) Ltd, 1991.

Appendix A

Rheological Characterization of

XPX Block Copolymers

XPX materials, discussed in Chapter 3 and 4, appear to be melt disordered above $T_m(E)$ = 100 °C up to high molecular weights. In Chapter 3 we presented the rheological master curve of XPX-1 together with SAXS data for all materials in order to illustrate this point. This Appendix presents the master curves from frequency sweeps between 0.01 to 100 rad/s for XPX-2a, XPX-2b in Figure A.1 and for XPX-2c and XPX-3 in Figure A.2. As previously established, the low frequency response of all materials indicates that they are melt disordered. For XPX-2a and XPX-2b in Figure A.1, moduli show the expected liquid-like response at and above 140 °C.

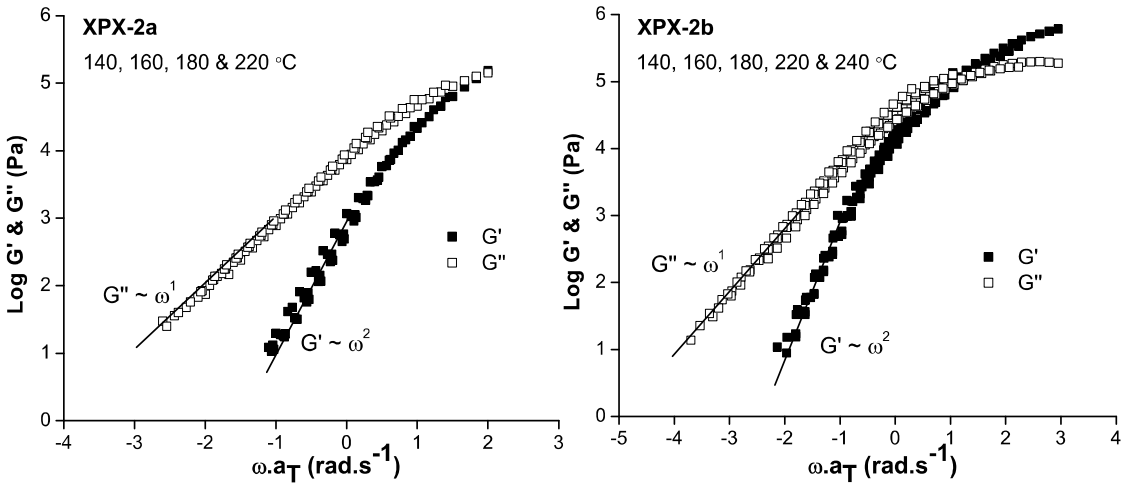

Figure A.1: Master curves between 0.01 – 100 rad/s for XPX-2a, XPX-2b, XPX-2c and XPX-3 showing disordered liquid-like response for both dynamic moduli at low frequency.

The response of XPX-2c and XPX-3 at 150 °C is inconclusive (neither disorder or order can be established) but above this temperature, the moduli are also liquid-like indicating melt disorder. However, SAXS data at 150 °C suggest a state of disorder for both materials.

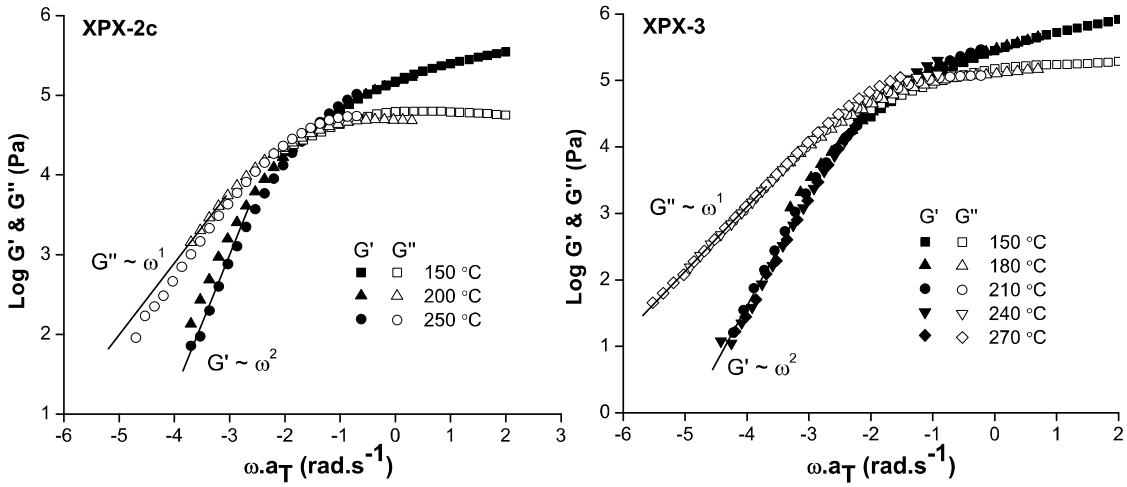

Figure A.2: Master curves between 0.01 – 100 rad/s for XPX-2c and XPX-3 showing melt disorder responses for both dynamic moduli at low frequency at temperatures above 150 °C. The response at 150 °C is inconclusive of the state of order or disorder, but SAXS data suggest disorder.

Appendix B

Block Copolymer Tensile Characterization

In this work, the mechanical properties of elastomeric block copolymers were averaged from the tensile testing of at least 5 samples. In the previous chapters, the stress-strain curve of a representative sample was presented to illustrate the mechanical response of each material. In this Appendix, Figure B.1 shows all the tensile curves obtained from the testing of each material. The representative curves presented in the body of this dissertation are highlighted as thicker lines within each plot.

As observed, for each material, the behavior of the different samples has good reproducibility. Also, sample slipping, or the motion of the sample out of the holder with stretching, which is very common in rubber testing, is avoided in most cases. This would be manifested on the tensile curves as drawings at constant stress or stress decreases especially in the strain hardening regime where the sample becomes highly stretched. Some of the samples of the CEPC-3 material exhibit slipping as the stress drops and then increases at the end of the curves. This material is also the only one that appears melt ordered at all temperatures, with an inaccessibly high T_{ODT}. This phenomenon underscores the importance of having easily processable materials to produce samples with consistent mechanical behaviors.

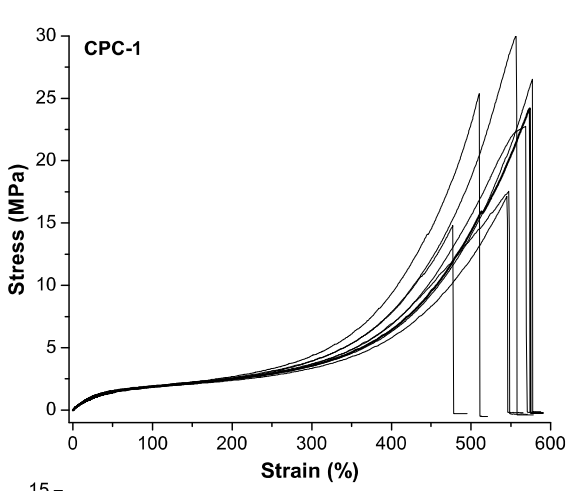
CPC-1
Stress (MPa)
Strain (%)

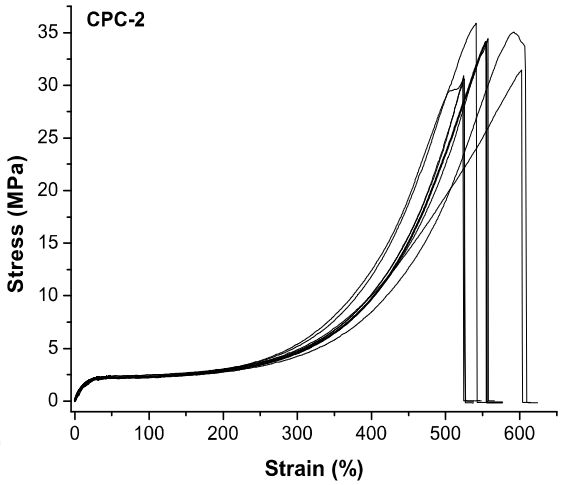
CPC-2
Stress (MPa)
Strain (%)

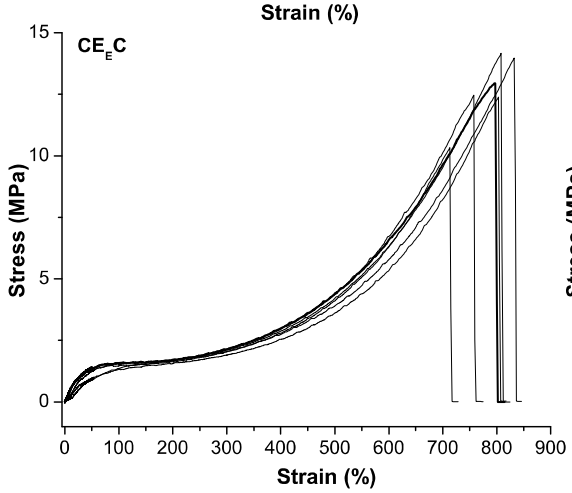
CE$_E$C
Stress (MPa)
Strain (%)

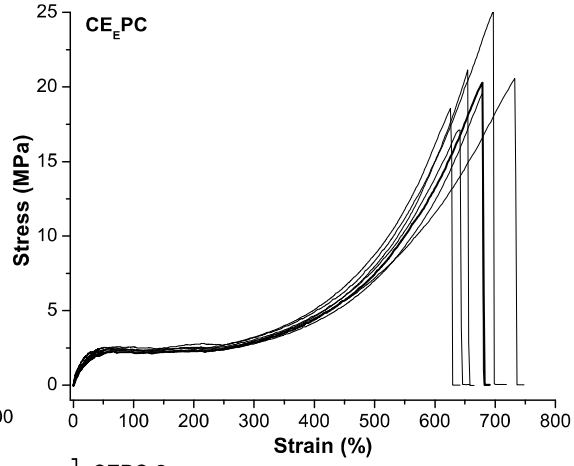
CE$_E$PC
Stress (MPa)
Strain (%)

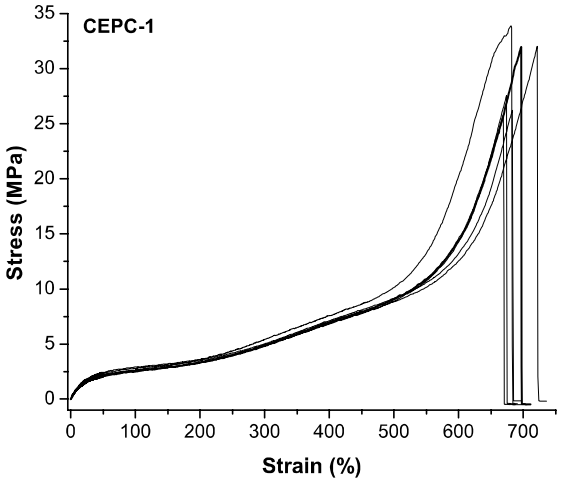
CEPC-1
Stress (MPa)
Strain (%)

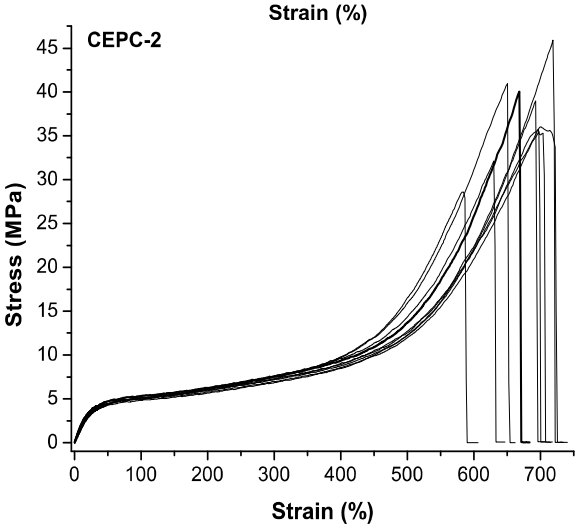
CEPC-2
Stress (MPa)
Strain (%)

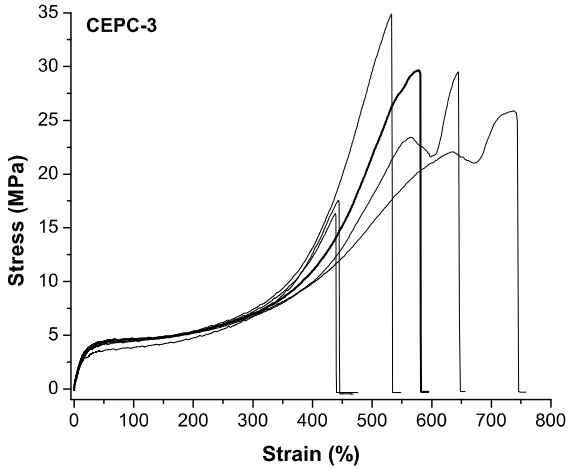
CEPC-3
Stress (MPa)
Strain (%)

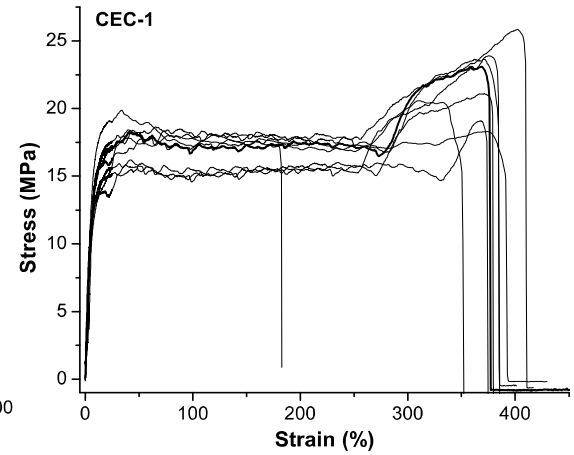
CEC-1
Stress (MPa)
Strain (%)

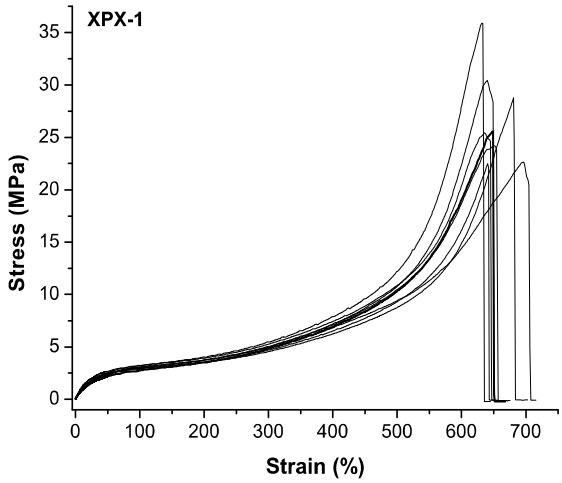
XPX-1
Stress (MPa)
Strain (%)

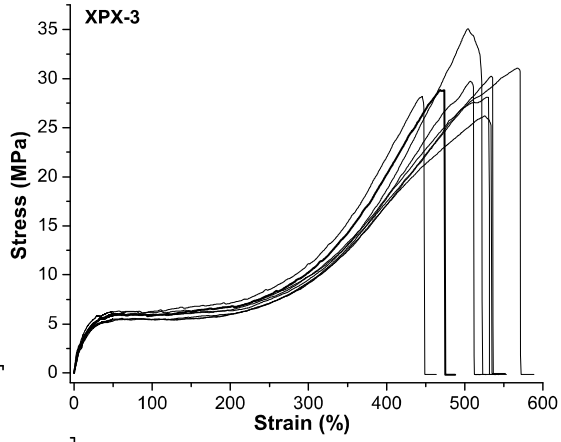
XPX-3
Stress (MPa)
Strain (%)

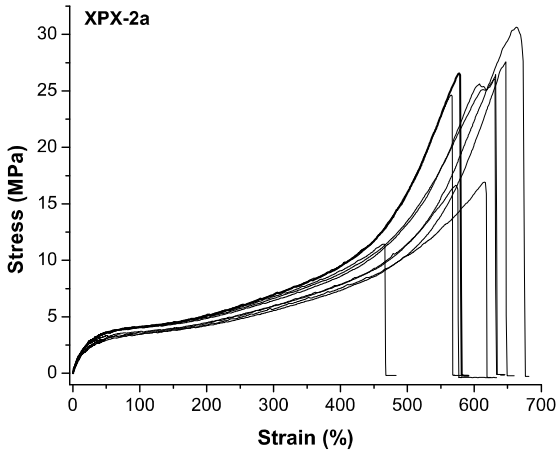
XPX-2a
Stress (MPa)
Strain (%)

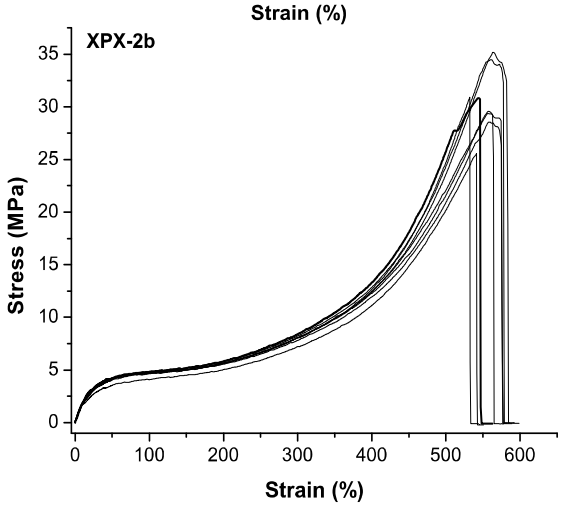
XPX-2b
Stress (MPa)
Strain (%)

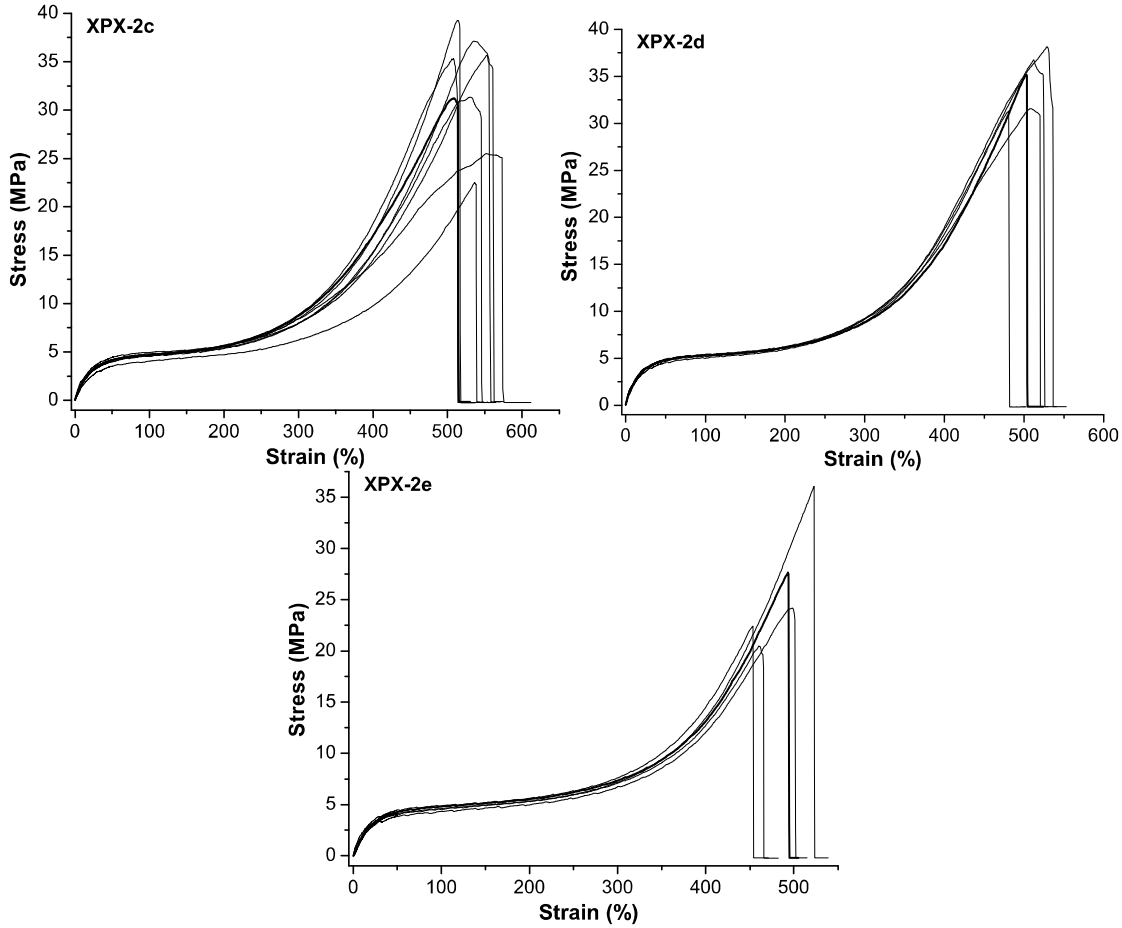

Figure B.1: Stress-strain curves for the block copolymers in this study that were characterized by tensile testing. The representative curves used in the previous chapters to illustrate the tensile response of each material are highlighted in each plot.